The University Of Sheffield.

Synaptic plasticity and visual tuning properties in the zebrafish optic tectum

Sandra Toledo-Rivera

A thesis submitted in partial fulfilment of the requirements for the degree of Doctor of Philosophy.

Supervisor:

Dr Anton Nikolaev

Avisors:

Dr Andrew Lin

Dr Mikko Juusola

Sep 2021

Abstract

The optic tectum (OT) is the structure in charge of processing vision which is one of the primary senses used for survival in non-mammalian vertebrates. Synaptic plasticity is the ability that allows the brain to learn and forget all the time while, for instance, you are reading this abstract. This thesis aims to contribute with the understanding of the mechanisms of neural plasticity in visual short-term memory such as adaptation and habituation, and how novel visual cues are processed in the zebrafish CNS, before deciding to trigger or not a response.

First, I reviewed different behavioural methods to assess memory formation in late-stage ZF larvae. These methods included the Novel object recognition (NOR) paradigm, with variants such as the visual lateralization NOR (VLNOR) tests. After excluding subjective bias using automatized analysis, I found that there is no statistically significant difference in the eye preferred to explore new objects. Thus, other parameters can be better used than those suggested in the literature, such as the distance kept from the novel object and exploration patterns.

Then, I used traditional and fluorescent in situ hybridization using *c-fos* to visualize the brain areas that activate when a novel object is presented. I found activation in the olfactory bulb and superficial tectal regions in fish exposed to a novelty compared with controls. Additionally, these protocols were optimized to match the latest larval stage of zebrafish suitable for calcium imaging (21 days post-fertilization).

Finally, I used calcium imaging *in vivo* to provide an initial characterization of how visual information is processed downstream of the visual system. We found that the processing mechanisms are multi-layered, and individual cells differ in degree and speed of adaptation and habituation to different stimuli. I demonstrate the diversity of tuning properties in the neuropil, broadly categorized into at least seven classes in relation with their selectivity towards different frequencies and contrasts: high-pass, band-pass, low-pass; high, medium, and low contrast sensitive, and contrast-suppressed cells.

Acknowledgements

The completion of this thesis was possible thanks to innumerable forms of support.

First, I would like to express my deepest gratitude to my supervisor Dr Anton Nikolaev, for luring me into this research, encouraging me to learn and improve every day. A debt of gratitude is also owed to my advisors Dr Andrew Lin and Miko Juusola, for their kind feedback and support during this project.

Special thanks to all my friends, which I am lucky to dare not naming individually here to avoid filling the page. Without any particular order, the ones from my childhood, C.F.P., C.N.M., U.A.M.N., my Social Service, and this University. Special thanks to Hector and Victor for keeping me cheerful despite any circumstance during my time in the UK.

To my family. Especially to my mom, dad, and brothers, who had always supported me with their existence and sometimes involuntary lessons.

To my dearest Poyito, Moka, and Polvoroncito, for their unconditional love and patience all this time. I won't ever be able to thank you enough.

Finally, I would like to thank you, dear reader, for making this work have a purpose. I hope you enjoy reading as much as I did during my PhD journey or at least find something worthy enough to remember and share. 😊

Disclaimer

This project would not have been possible without the financial assistance of the National Council for Science and Technology of Mexico (CONACYT) and The University of Sheffield joint grants and contributions made by the Faculty of Biomedical Sciences.

Declaration

I, Sandra Toledo-Rivera, confirm that the Thesis is my own work. I am aware of the University's Guidance on the Use of Unfair Means (www.sheffield.ac.uk/ssid/unfair-means). This work has not previously been presented for an award at this, or any other university.

Table of Contents

List of Figures

List of Tables

List of Abbreviations

A1	Primary auditory cortex
A2	Secondary auditory cortex
AC	Amacrine cells
AFs	Arborization fields
AI	Adaptation index
ALS	Amyotrophic Lateral Sclerosis
ANOVA	Analysis of variance
AMPARs	α-amino-3-hydroxy-5-methyl-4-isoxazole propionic acid receptors
AP	Action Potential
AUC	Area under the curve
BC	Bipolar cell
BCIP	5-bromo-4-chloro-3-indolyl phosphate
Bdnf	Brain-derived neurotrophic factor
BSA	Bovine serum albumin
CaM	Calmodulin
CaMKII	Calcium/calmodulin-dependent protein kinase II
cAMP	Cyclic Adenosine Monophosphate
CB	Cell bodies
cGMP	Cyclic GMP
CI	Confidence interval
CMV	Cytomegalovirus
CNII	Cranial Nerve II (optic nerve)
CNS	Central Nervous System
Cpd	Cycles per degree
CRE	cAMP response element
CREB	CRE binding protein
CS	Contrasts suppressed
CSF	Contrast sensitivity function

ΔF/F0 intensity	Representative change in Fluorescence relative to the resting signal
dH2O	Deionised water
Dpf	Days post-fertilization
dH2O	Deionised water
DIG	Digoxigenin
DNA	Deoxyribonucleic acid
DS	Direction selective/selectivity
EPSP	Excitatory postsynaptic potential
FISH	Fluorescent in situ hybridisation
FWISH	Fluorescence Whole-mount in situ hybridisation
GABA	Gamma-Aminobutyric Acid
GCaMP	Green fluorescent protein CaM
GDP	Guanosine diphosphate
GECI	Genetically encoded calcium indicator
GFP	Green Fluorescence protein
GMP	Guanosine monophosphate
G_t	Transducin
GTP	Guanosine triphosphate
HC	Horizontal cells
HCS	High contrast sensitive
HI	Habituation index
Hpf	Hours post-fertilization
IEG	Immediate early gene
iGluR	Ionotropic glutamate receptor
INL	Inner nuclear layer
IPL	Inner plexiform layer
IPSP	Inhibitory postsynaptic potential
IR	Infrared
ISH	In situ hybridisation

ISI	Interstimulus interval
ITNs	Inter-thalamic neurons
KARs	Kainate receptors
LCS	Low Contrast sensitive
LES	Left eye system
LGN	Lateral geniculate nucleus
LMP	Low-melting point
LTD	Long-term depression
LTM	Long-term memory
LTP	Long-term potentiation
MAGUKs	Membrane-associated guanylate kinases
MeOH	Methanol
MCS	Multiple cloning site
mGluR	Metabotropic G-protein coupled glutamate receptor
MT	Middle-temporal
NBT	Neural-specific beta tubulin / Nitro-blue tetrazolium
NF	Notch filter
NMDARs	N-methyl-d-aspartate receptors
NOR	Novel object recognition
NR	Normal raised
OE	Object-exposed (novel)
OKR	Optokinetic response
OMR	Optomotor response
OT	Optic tectum
ONL	Outer nuclear layer
OPL	Outer plexiform/pigmented layer
PBS	Phosphate buffered saline
PBT	PTW with 2% sheep or goat serum and 0.2% BSA (Table 10)
PDE	Phosphodiesterase
PFA	Paraformaldehyde

PI	Preference index
POD	Peroxidase conjugate
PR	Photoreceptor
PrPc	Cellular prion protein
PSD	Postsynaptic density
psi	Pounds per Square Inch
PTW	PBS with 0.1% Tween-20
PTZ	Pentylenetetrazole
PVN	Periventricular neuron
RES	Right eye system
RGC	Retinal ganglion cells
RF	Receptive field
ROI	Region of Interest
RNA	Ribonucleic acid
RPEL	Retinal pigment epithelial layer
RT	Room temperature
S1	Primary somatosensory area
S2	Secondary somatosensory area
SAC	*Stratum album central*
SACPV	*Stratum album central and periventricular*
SbC	Suppressed by contrast
SD	Standard deviation
SEM	Standard error of the mean
SF	Spatial frequency
SFGS	*Stratum fibrosus et griseum superficial*
SG	Show gratings (from the stimuli of moving sinusoidal gratings)
SO	*Stratum opticum*
SPV	*Stratum periventriculare*
SSC	Saline-sodium citrate buffer
STD	Short-Term depression

STDP	Spike-timing-dependent plasticity
STF	Short-term facilitation
Stxbp1	Syntaxin-binding protein 1
TBSTB	Solution of TNT with 0.5% Perkin-Elmer blocking powder (Table 15)
TL	*Torus longitudinalis*
TNT	Solution containing Tris, NaCl, and Tween20 used in FWISH (Table 14)
Tp1	Terminal protein 1
tRNA	Transfer Ribonucleic Nucleic Acid
UV	Ultraviolet
V1	Primary visual area
V2	Secondary visual area
VA	Visual angle
VF	Visual field
VLNOR	Visual lateralisation Novel object recognition
WISH	Whole-mount in situ hybridisation
WT	Wild type
ZF	Zebrafish
0CR	0% Contrast raised fish
100CR	100% Contrast raised fish
2-P	Two-photon
3D	Three-dimensional

Chapter 1. Introduction

1. Introduction

The central nervous system (CNS) can adapt, learn, and forget all the time while, for instance, you are reading this (Kitamura et al., 2017; Medina, 2018a; Nakai et al., 2017). These abilities are possible thanks to what we know as brain plasticity. Nowadays, there are many well-established molecular mechanisms around synaptic plasticity. However, many aspects of the physiological correlation remain unexplored, for instance, how different characteristics of sensory inputs are processed and filtered in the brain before triggering a specific behaviour, namely hunting or escape response (Baden, Euler, & Berens, 2020a; Schroeder, Oesterle, Berens, Yoshimatsu, & Baden, 2021).

Vision is one of the primary senses for survival, and even though the retina is the structure receiving the preliminary information in most species, in non-mammalian vertebrates, the optic tectum (OT) is the structure in charge of processing it. In other words, transforming the photons exciting the retinal ganglion cells into electrical impulses resulting in synapses, which will be either filtered and ignored or generate a behavioural response accordingly (Ueda, Sekoguchi, & Yanagisawa, 2021; Yin, Li, & Du, 2019a).

This research aimed to contribute with the definition of how visual synaptic plasticity occurs when presenting novel visual stimuli and how visual short-term memory is processed and filtered in the zebrafish CNS.

1 History of Synaptic Plasticity, Research and Theories

It is calculated that there are around one hundred billion (10^{11}) neurons in a human brain and that the synapses between them are much more (Landhuis, 2017). Numerous model systems have been developed over the past 50 years, to study mechanisms that might add knowledge to what we know about memory storage (Reviewed by Nicoll, 2017). The first approaches of *in vivo* models were made with the idea that simpler systems would be easier to address. The *Aplysia* -a sea snail with just around 20 thousand nerve cells- was the first model utilized for this purpose (Bailey & Chen, 1988), followed by other models such as the fruit fly *Drosophila melanogaster* (Jaiswal et al., 2012).

Ramon y Cajal proposed that in order to learn something new, there must be some change in the brain, such as new branches and contacts (Cajal, 1894a). This definition summarises what we now know as brain plasticity, which can be functional and structural. From that moment, researchers suggested possible mechanisms to establish how memory works. The first possibility is that there is indeed *neo-genesis* of a new set of neurons developing a new active network, the second possibility is the presence of structural plasticity, where new axons or dendrites are born, and with them, new connections and functionally new networks (Bailey & Chen, 1988). A third possibility is that the existing synapses gain strength of connectivity, and at the same time, this generates a new functional network –functional plasticity (Mayford et al., 2012).

In 1949 Donald Hebb postulated his now classic-Hebbian theory, which can be summarised in the phrase: "Neurons that fire together, wire together" and its counterpart: "Neurons that fire out of sync, lose their link". Since then, the ability of synapses to become strengthened or weakened is known as *synaptic plasticity* (Morris, 1999). Many experiments have been done in the last decades motivated by the Hebbian theory (Zylberberg & Strowbridge, 2017). One of the most relevant physiological correlations of this theory was the discovery of long term potentiation (LTP) and long term depression (LTD), which are indicators that the plasticity postulated by Hebb is indeed happening in hippocampal and cortical cells, showing the plasticity of synapses in response to the increment or decrease of activity (Reviewed by Keck et al., 2017).

1.1.1 Long Term Potentiation (LTP) and Long-Term Depression (LTD)

When an action potential (AP) reaches the end of a presynaptic cell, it causes the release of neurotransmitters, which pass through the synaptic gap and bind to the receptors available in the post-synaptic cell (Nikolaou et al., 2012). These can be metabotropic or ionotropic receptors (Zhu & Gouaux, 2017a). When a neurotransmitter stimulates a metabotropic receptor, it will produce a cascade of second messengers, modifying the number of proteins within the cell (Martin, Grimwood, & Morris, 2000). When an ion channel is stimulated, it may cause it to open or close, altering the flow of ions and producing a change of voltage in the post-synaptic cell.

Conventionally, there are two main types of synaptic plasticity. Long Term Potentiation (LTP) is when a synapse becomes strengthened. This definition was first described in

1973 (T V P Bliss & Gardner-Medwin, 1973a). Conversely, Long Term Depression (LTD) occurs when there is a synapse weakening (Buonomano & Merzenich, 2002). The precise molecular mechanisms by which each condition occurs and what we currently know about how it works and its relationship with glutamate receptors will be discussed in further detail.

1.1.2 Experimental triggering of LTP and LTD

The traditional *in vitro* experiment used to study LTP was through the preparation of brain slices from mice, the application of high-frequency tetanic stimulation, and direct depolarization of the presynaptic cell (Reviewed by Citri & Malenka, 2008). In addition, experiments using CA1 cells of the rat hippocampus showed that repeated presentation of short high-frequency stimuli of the presynaptic neuron would cause the release of neurotransmitters, which will lead to LTP (Bliss & Cooke, 2011).

LTD is evoked by prolonged low-frequency stimulation (Nakai et al., 2017). Different frequencies and oscillation variations have been tested among the studies performed with this basis (Grover, Kim, Cooke, & Holmes, 2009). The effects of high and low-frequency stimulation have been studied *in vivo,* mainly in tests with anaesthetized rats with electrode implantation (Staubli & Scafidi, 1997). These studies showed that the parameters of stimulation between *in vivo* and *in vitro* experiments highly differ depending on the protocol used, mainly when trying to achieve LTD (Gonzalez, Morales, Villarreal, & Derrick, 2014).

Another mechanism that determines if the synapse undergoes LTP or LTD is the so-called "spike-timing-dependent plasticity" (STDP) (Markram, Lübke, Frotscher, & Sakmann, 1997). According to this mechanism, there is a critical 20 milliseconds window for synaptic plasticity defining whether synapse undergoes LTP or LTD (Dan & Poo, 2006). If the presynaptic neuron fires 20ms before the post-synaptic cell, the cell will undergo LTP (the synapse will strengthen). If the presynaptic neuron fires after the post-synaptic neuron within the following 20ms, LTD occurs (See Fig. 1.1) (Grossberg, 2015; Martin et al., 2000; Mayford et al., 2012; Sgritta, Locatelli, Soda, Prestori, & D'Angelo, 2017). Molecular mechanisms that underlie this time-dependency seem to vary depending on the synapse specialization and the conditions of the experiments (Reviewed by Feldman, 2012).

Whether or not LTP and LTD are directly involved in memory formation is a subject of numerous studies (Grover et al., 2009; Gutierrez-Castellanos et al., 2017a; Malenka & Bear, 2004). For instance, various studies show that the block of NMDA receptor function leads to hippocampal memory impairment, modifying LTP (Reviewed by Martin et al., 2000).

1.1.3 Roles of AMPA and NMDA receptors in plasticity

Glutamate receptors have been identified in many synapses and are associated with memory formation and learning. As mentioned before, there are two main classes of glutamate receptors: metabotropic G-protein coupled receptor (mGluR) (Niswender & Conn, 2010) and ionotropic receptor (iGluR). Glutamate receptors have been identified in many synapses and are associated with memory formation and learning (Zhu & Gouaux, 2017b). The iGluRs allow the passage of positive ions into the post-synaptic cell. They are sub-classified into α-amino-3-hydroxy-5-methyl-4-isoxazole propionic acid receptors (AMPARs), N-methyl-d-aspartate receptors (NMDARs) –which are the first to appear in the post-synaptic neuron when a glutamatergic synapse first forms (Bear, Connors, & Paradiso, 2015)- or Kainate receptors (KARs). For this project, we will focus on the first two.

The main characteristic of the NMDA receptor is that in normal conditions, its channel is blocked by magnesium (Mg^{2+}) (Bear et al., 2015). The Mg^{2+} block is released when the post-synaptic cell becomes depolarised by electrostatic repulsion (Figure 1.1). The sodium and potassium flux also mediates this depolarisation through the AMPA receptors, which are permeable to these ions (Zhu et al., 2016). LTP occurs when a high concentration of calcium (Ca^{2+})enters the cell, and LTD when there is a low calcium entry (Buonomano & Merzenich, 2002; Zylberberg & Strowbridge, 2017).

Inside the neuron, there is a pool of AMPA receptors in constant recycling (Rathje et al., 2013). These will undergo exocytosis or endocytosis into the peri-synaptic sites depending on the volume of calcium influx to the post-synaptic cell (Malenka & Bear, 2004). High calcium concentrations also lead to the activation of kinases -such as calcium/calmodulin-dependent protein kinase II (CaMKII) - which will undergo phosphorylation, stimulating new AMPA receptors' exocytosis and increasing their permeability, resulting in a stronger synapse (See Fig 1.1-A). A low Ca2+ entry activates

protein phosphatases, which increase the endocytosis of AMPA receptors, decreasing the number of them available for the glutamate to bind. Therefore, the action potential change is reduced, leading to a weaker synapse (Fig 1.1-B) (Zhu et al., 2016).

Another molecular mechanism that regulates the endo- and exocytosis of the AMPARs is the role of the proteins from the membrane-associated guanylate kinases (MAGUKs), which are part of the post-synaptic density (PSD) (Malenka & Bear, 2004). Among these proteins, PSD-95 seems to be the most related to regulating the number of AMPARs, controlling the function and morphology of glutamatergic synapses (Ho, Lee, & Martin, 2011). In experiments with mice, overexpression of PSD-95 increases the synaptic strength, and the opposite occurs when PSD-95 is knocked out, and the expression of AMPARs is decreased in the PSD (Beique et al., 2006).

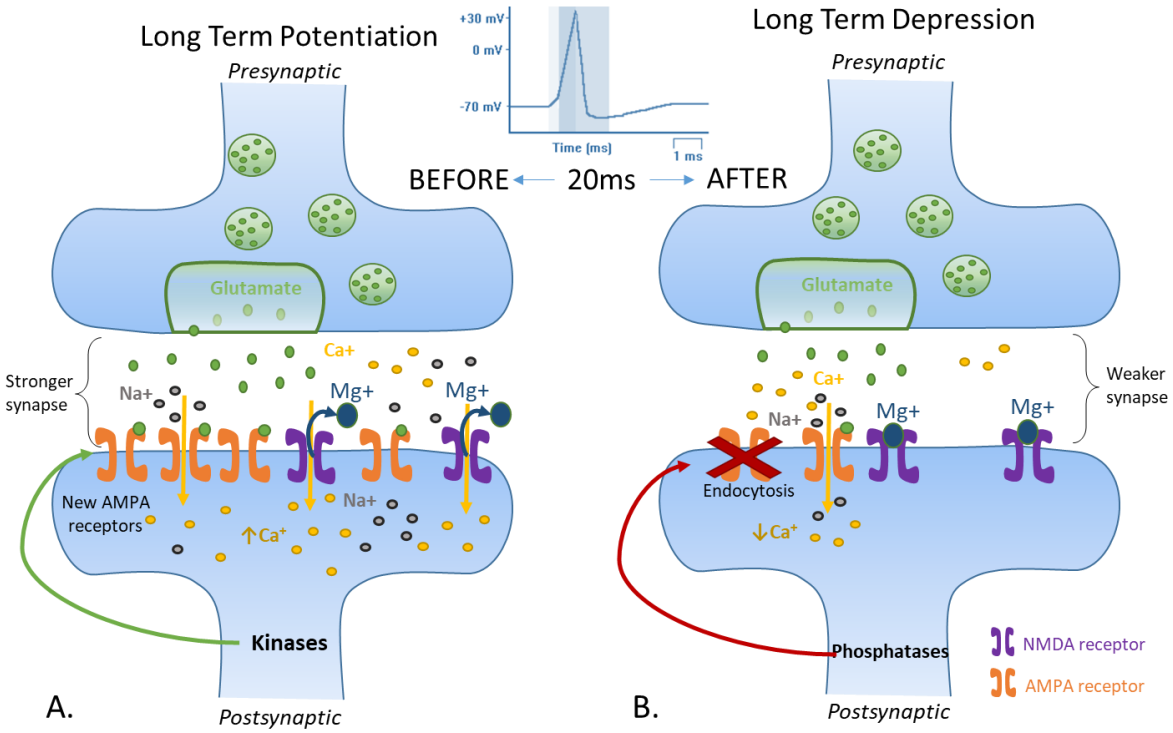

Figure 1.1 Summary of the basic mechanisms of LTP (A) and LTD (B) with spike-timing-dependent plasticity. (A) *If the presynaptic terminal produces an action potential (AP) ~20ms before the post-synaptic cell, it will become depolarised, and glutamate will be released, leading to LTP.* **(B)** *If the presynaptic cell fires and releases glutamate after, by this time, the post-synaptic cell will be already repolarising, and the NMDA receptors become blocked again by the Mg2+. (See main text)*

1.2 Updates in synaptic plasticity

The way we understand synaptic plasticity keeps evolving with every new study. For instance, it is common to assume that when a memory is formed, new synapses are created, and therefore LTP is directly related to memory development; meanwhile, LTD acts in a contrary way (Gutierrez-Castellanos et al., 2017b; Jia & Collingridge, 2017). However, LTD not necessarily means the loss of memory, and in fact, LTD could possibly enhance memory-gain functions by other sub-mechanisms such as preventing saturation of synapses, increasing their operating range, or refining the fidelity of such memories by adjusting synaptic weights (Connor & Wang, 2016).

Recent studies focus on the role of protein kinases and Long-Term Memory (LTM) mechanisms. One example is PKMζ, which is an unusual form of the protein kinase C present in LTP, and it is known to prevent the internalization of the glutamatergic receptor (AMPAR) if this contains the subunit GluA2 (Wright & Vissel, 2012). It is claimed that this mechanism keeps object recognition memory for around a week, suggesting that the synaptic removal of GluA2-dependent AMPARs in active synapses plays a significant role in forgetting during learning tasks, whereas inhibition of endocytosis results in memory preservation (Ashby, Rue, Ralph, Uney, & Graham, 2012; Migues et al., 2016). Moreover, we now know that memory storage is not only a job for cells from a single structure but one for a whole nervous system that can modify itself, aiming to adapt to new information (Grossberg, 2015).

The use of *in vivo* imaging techniques such as multiphoton or light-sheet microscopy has given us evidence regarding the size of the post-synaptic neuron, which is indeed growing or shrinking according to their specific activity (Keck et al., 2017). Within the research field of learning and memory formation, the biological process of the typical "active forgetting" is a topic that is getting attention. Forgetting also involves the activity of glutamatergic pathways and similar routes taken in memory gain, which should have the same level of importance (Medina, 2018b).

1.2.1 Behavioural tests regarding learning and memory

Processing new information requires that the brain passes through a series of changes first, to categorize it in a manner that will make the most sense to the subject

experiencing it and later discriminate if it is something worthy to keep "fresh" or forget (Medina et al., 2018; Randlett et al., 2019a).

A long the history of memory studies, it became clear that the pure act of remembering is not always an action that beings can decide voluntarily. Experimentally, the use of stress as stimuli for behavioural assays to impact synaptic plasticity have shown that it serves to enhance or decrease LTP and LTD mechanisms (Howland & Wang, 2008). The use of fear and stress has always been a subject of controversy, which has led to the exploration of other existing methods to convey this matter (deCarvalho, Akitake, Thisse, Thisse, & Halpern, 2013; Kitamura et al., 2017; Nakai et al., 2017). Nevertheless, behavioural experiments are in constant optimization and are frequently coupled with other approaches such as imaging or molecular detection tools.

1.2.2 Molecular tools to assess memory formation.

The use of molecular tools is acquiring importance in the field of memory research being optogenetics one of the most used approaches (Del Bene & Wyart, 2012; Repina, Rosenbloom, Mukherjee, Schaffer, & Kane, 2017). In optogenetics, neurons are modified to express light-sensitive ion channels, enabling them to be controlled using a specific light wavelength. For instance, with this approach it was found that there is a population of neurons in the mammalian brain that have continuous cellular changes and became activated during learning and recall, these are known as "engram cells" (Kitamura et al., 2017; Ramirez et al., 2013). Traditionally, it is thought that after receiving a stimulus or memory, the information is processed in the cortical region of the brain and eventually it gets stored in the hippocampus. Nevertheless, Kitamura et al. 2017, showed how engram cells in the rat brain hippocampus get weaker and might even become silent with time. Meanwhile, the synapses in neurons of the basolateral amygdala, a structure in the brain necessary for fear and memory, became stronger.

In addition, we currently count on techniques that allow us to find specific genes in a specific stage in development by targeting RNA and DNA through fluorescence such as in situ hybridization (ISH) (Aoki et al., 2013). Usually, in situ hybridization techniques are performed in slices of tissue. However, whole-mount version protocols (WISH) are in constant optimization (Sundquist & Nisenbaum, 2005; Wu, Luo, & Xiao, 2018). One of these approaches is the Fluorescence in situ hybridization (FISH), which allow us to

visualize the areas of labelled tissue with a more refined detail through confocal or multiphoton microscopy (Nelson & Guyer, 2013).

1.2.2.1 Immediate early genes as synaptic activity markers

Nowadays, over a hundred genes have been classified as an Immediate Early Gene (IEG). However, since the detection of these molecules in the brain, the functional role in neuronal activity has been a topic of ongoing investigation (Gallo et al., 2018a). The use of IEG as tools for studying brain activity, specifically learning and memory is gaining support from many reports that use them with different models. The coupling of these molecules with in situ hybridization techniques are some of the most common methods to define areas of brain activity (Minatohara, Akiyoshi, & Okuno, 2016a).

Examples of IEG found in the brain are *c-fos, Arc* and *Homer1a* which have seen to be expressed by high-frequency stimulation (Mayford et al., 2012), and have been widely used with in situ hybridization assays in brain slices of sacrificed rodents that were previously summited to behavioural tasks. Therefore, evidence of simple memory formation in zebrafish might be identified from this approach (Cruz, Javier Rubio, & Hope, 2015a). The use of WISH along with *c-fos* in zebrafish is commonly reported in fish up to 5dpf and it is usually induced by the use pentylenetetrazole (PTZ) (Baxendale et al., 2012a).

Despite the now extensive use of IEG as markers however, there are still some debates over their specific functionality. For instance, there are claims towards the hypothesis of serving just as a homeostatic maintenance; others suggest that its expression is dependent on plasticity-related activity changes, whereas others propose their role as integration of information. In any case, is agreed that there is no doubt their expression can be used as a marker for neuronal activity and creation study of new memories in several in vivo models which will be discussed below (Cruz et al., 2015a; Gallo et al., 2018a).

1.3 Understanding Vision and the Brain

The visual system provides us with an ideal approach to study other multiple general functions of the brain as well as vision itself (Dong, Gao, Lv, & Bao, 2016a). It is known that vision is given by the interaction of the light with our eyes; however, the process by which the light hitting the eyes is converted into neural signals is quite complex. Light can behave as a wave and as a particle (photon) (Karnieli, Rivera, Arie, & Kaminer, 2021; Rab et al., 2017). Even though we have an idea of the visual capabilities of several species, the limit range of the spectrum is not fully agreed upon since it depends on many factors such as the amount of light reaching the retina and the response of the observer's photoreceptors (Sliney, 2016).

In humans, the two limits of visible wavelength ranges between about 360-400 and 750-830 nanometres respectively. In this range, the specific wavelength determines the colour and intensity of light, determined by the brightness of the source. If the wavelength is a bit shorter -in the direction of the ultraviolet (UV) range- or a bit longer -towards infrared (IR) spectrum-, we (humans) would not be able to detect it. Other species have different wavelength sensitivities (Sliney, 2016; Wager, 2011).

Light passes through the pupil, which changes its size to adjust the amount of light that passes through (Timothy V P Bliss et al., 2017). Behind the pupil sits the lens, which focuses the light into the retina. In two-eyed species, the brain can interpret the binocular disparity, which is the difference in the position of an image on the two different retinas (Baden et al., 2020a). The higher the discrepancy, the closer the object is, and this is what gives us the perception of depth.

1.3.1 The "Net of light"; also known as the Retina.

The retina is a relatively thin net of cells structured in three primary layers built "upside-down", covering the interior of the posterior half of the eye (Figure 1.2). This organ receives its nutrition by diffusion through choroidal blood vessels (Kolb, 1995). When the light travels into the back of the eye, the photons move through the layers of the retina, reaching the photoreceptors. In mammals and other species, there are five layers made of different types of neurons: Photoreceptors (rods and cones depending on their shape), retinal ganglion cells (RGC), horizontal cells, bipolar cells (BC),

amacrine cells (AC) –the last three considered as interneurons- and the glial cells or Muller Glia. (Baden, Euler, & Berens, 2020b) These will be covered in more detail below (Figure 1.2).

Near the photoreceptors sits the outer pigmented layer (OPL) of the retina, also known as the retinal pigment epithelial layer (RPEL). This layer acts as a barrier between the choroid vessels and the neural retina. It consists of a specific type of cells containing melanin granules that absorb some light rays and prevent them from reflecting and scattering. Animals that specialise in nocturnal vision do not have black pigmented epithelium, so the light can reflect molecules in it to improve the ability to see. This feature allows them to activate their photoreceptors further when the photons bounce back (Luo-Li, Mazade, Zaidi, Alonso, & Freeman, 2018). Another element to notice is that all receptors, HC and BC, never give action potentials but graded potentials (Masland, 2012a).

PHOTORECEPTORS

The photoreceptors (PR), located at the back of the retina, are the first cells receiving the light input despite anatomically being located deeper (Figure 1.2). These cells hyperpolarise to light and depolarise in dark conditions. This depolarisation will trigger glutamate release from their synaptic terminals onto the dendrites of BC and HC. The resulting signal propagates towards the retinal ganglion cells (Baden et al., 2020b). There are two types of PRs named after their shape: cones and rods. Although there are functional differences between them, the transduction process, which will be discussed later, is the same (Repina et al., 2017; Schröder, Oesterle, Berens, Yoshimatsu, & Baden, 2021).

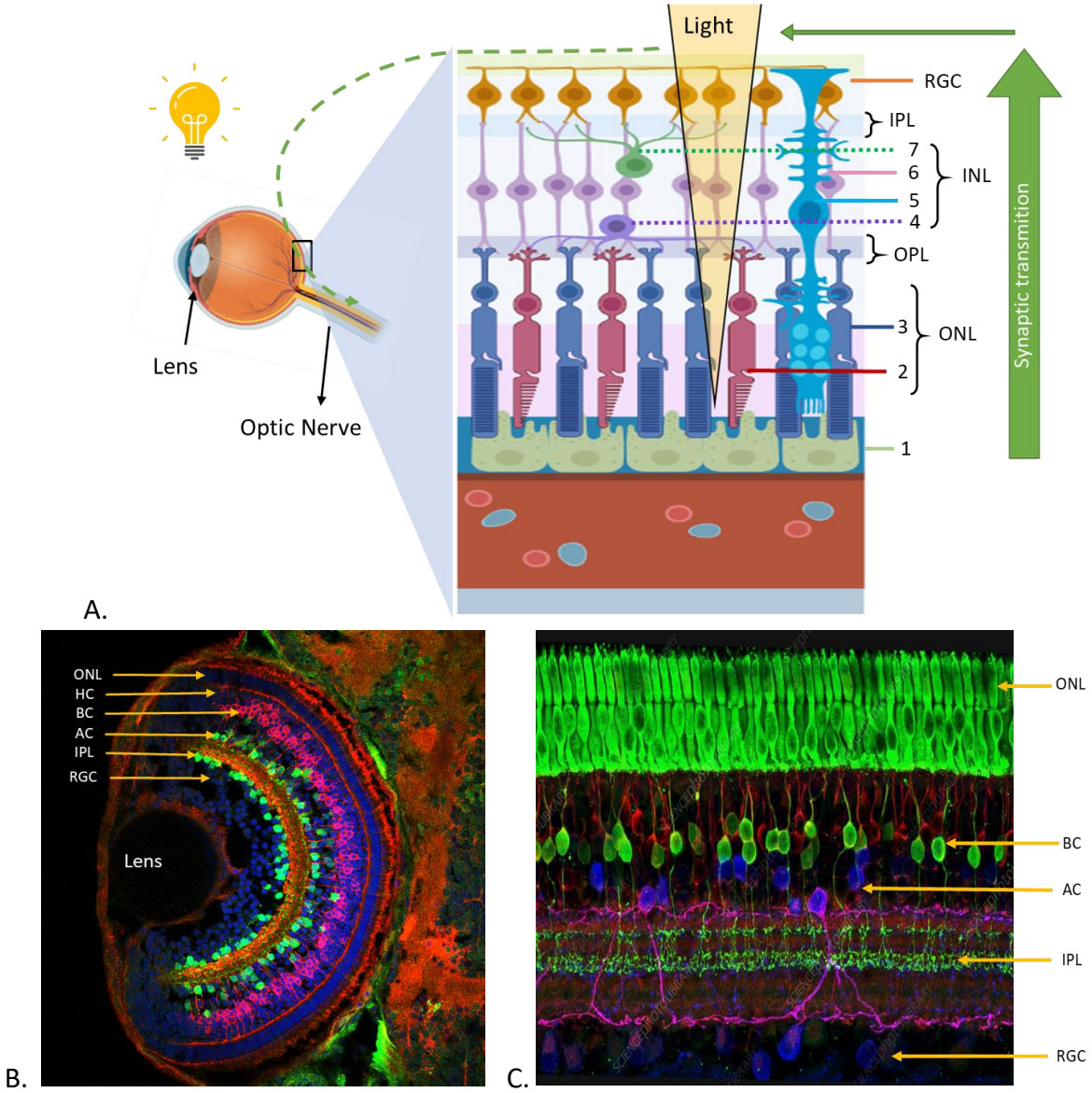

Figure 1.2 Structure of the retina. A. *Schematic of the layered organisation of the human retina. (Adapted from several sources, made using Bio Render) Left: Sagittal view of an eye showing general features including iris, lens, blood vessels and the optic nerve. Right: Overview of the layers of the retina. Bottom: Choroidal blood vessels supply oxygen to the retinal tissue. Light comes from the top and passes through the retinal layers until hitting the photoreceptors (PR).* **1.** *Retinal pigment epithelial layer (RPEL) containing melanocytes. This layer is followed by the outer nuclear layer (ONL) containing the nuclei of the PRs* **2.** *Cones and* **3.** *Rods. After the light hits these cells, phototransduction occurs towards the retinal ganglion cells (RGC).* **4.** *Horizontal cells (HC) and* **5.** *Müller glial cells help to keep the structure along with the layered organisation. The*

synaptic interaction continues through the outer plexiform layer (OPL) containing the synapses between the PRs, as well as **6.** *bipolar cells (BC). The inner nuclear layer (INL) containing the nuclei from the BC*. **7.** *Amacrine cells (AC) sit between the INL and the Inner plexiform layer (IPL). Before reaching the retinal ganglion cells (RGC), which continue the transduction through their axons to the rest of the brain, forming the optic nerve.* **B.** *Immunostaining of a zebrafish larvae retina. Amacrine cells (green), bipolar cells (red).* **C.** *Immunostaining of a mouse retina. Credit of images B and C from Wei Li, National Eye Institute, National Institutes of Health.*

1.3.2 Phototransduction

Phototransduction is the process of a cell absorbing light and creating a response. This response is a change in the amount of neurotransmitter (glutamate) that is being released on the target neurons (Sanes & Zipursky, 2010a; Schröder, Oesterle, Berens, & Yoshimatsu, 2021). All receptors hyperpolarise with light. Inside the PRs, there is a disk containing guanylyl cyclase, which converts GTP into cyclic cGMP, which is typically bounded to a particular type of channel in the rod cell membrane and, when this happens, allows the entrance of sodium, generating an excitatory post-synaptic potential (EPSP) (Masland, 2012b; Montague & Sejnowski, 1982).

The photopigments lie within the disk membrane of the outer membrane (Kolb, 1995). In rods, the photopigment is rhodopsin (Rh). When the photons reach the PRs, the light rays hit the outer membrane of the disk where the rhodopsin molecule is situated. The seven transmembrane domains of the protein portion of the molecule called opsin pass through the membrane bilayer (Figure 1.3). The opsin forms a pocket in which the light-absorbing portion of the photopigment (retinal) resides (Kolb, 1995; Li, Saha, & Alaimo, 2021). The photopigments in the rods and the three types of cones differ in the protein portion of the molecule, which transforms retinal to absorb a specific wavelength of light.

Retinal is in a conformation called 11-cis, where two hydrogen atoms sit on the same side of an important double bond. When the retinal absorbs a photon, a component of this double bond breaks, allowing a free rotation around the bond. This change in retinal to an all-trans shape triggers a series of alterations in the opsin component of the

molecule. Then, the changes in rhodopsin lead to activation of the G- protein (Schröder, Oesterle, Berens, & Yoshimatsu, 2021).

The next component in the cascade is a trimeric G-protein (alpha, beta, gamma) called Transducin (G_t) which in its inactive state is bounded to GDP. The active rhodopsin molecule activates transducin, allowing to exchange from GDP to GTP. The alpha subunit of G_t then activates a phosphodiesterase (PDE) in the disk membrane. PDE hydrolyses cGMP, thus lowering the concentration of cGMP throughout the outer segment. As the concentration of cGMP falls, these molecules no longer bind and therefore no longer hold to open the ion channels in the surface of the outer segment membrane of the PR. Thus, sodium and calcium will not come in but out by concentration gradient, making the cell more negative, therefore hyperpolarising the cell generating an inhibitory post-synaptic potential (IPSP). Once this happens, the overall number of Aps occurring will be very low or inexistent. Therefore, the voltage-gated calcium channels will be inhibited, and glutamate will not be released. However, a low concentration of glutamate stimulates the bipolar cells, producing an EPSP in these cells. This EPSP releases a high amount of glutamate, which enables the RGC to produce action potentials through the optic nerve.

Under dark conditions, subsequent elements in the retina will become activated. As mentioned before, photon absorption by the photo pigments results in the isomerisation of the chromophore from 11-cis to all-trans. This process causes hyperpolarisation, thereby reducing neurotransmitter release. On the other hand, if there is no light, the all-trans-retinal will go back to the 11-cis form. If this happens, opsin will come back and rebind; therefore, it will no longer activate the transducin. Hence, the PDE will be inhibited and will not be able to hydrolyse cGMP resulting in the opening of the ion channels in the dark, leading to the influx of the positively charged Na+ and Ca+ channels. Therefore, this decrease in illumination will cause depolarisation of the photoreceptors, which will generate glutamate release.

Additional to the ON, OFF and ON/OFF classification of BC in the IPL, there are two main categories: some of which mimic what the receptors do, known as sign-conserving synapses, given by the junction of OFF bipolar cells, and the so-called sign-inverting synapses which do the opposite and are mainly made from ON synaptic junctions.

The ON-bipolar receptor protagonist is mGluR6, which, when activated, leads to the closing of channels, causing hyperpolarisation (Walston, Chow, & Weiland, 2018). On the contrary, the OFF bipolar main receptors are mGluR1 and 2. Their activation leads to the opening of channels, causing depolarization (Niswender & Conn, 2010).

In the central retina, each cone connects with at least one bipolar cell. Therefore, there are many more BC than PRs. Usually, the ON and OFF signals are sent separately to the lateral geniculate nucleus (LGN), which is a set of ganglion cells within the pathway to send visual information to the visual cortex in mammals (Jaepel, Hübener, Bonhoeffer, & Rose, 2017). However, there are also ON/OFF (ON and OFF) cells projecting to the superior colliculus as well. This structure will be discussed in further detail below.

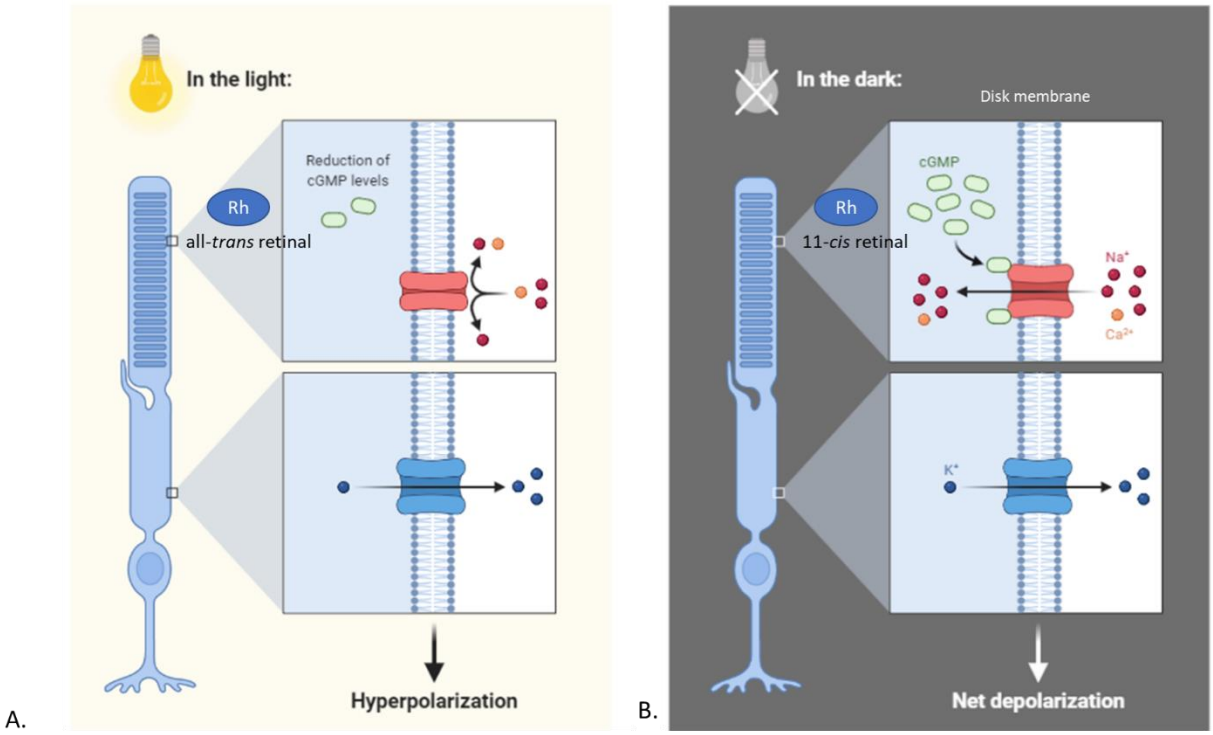

Figure 1.3 Phototransduction cascade. *(A) In blue a rod cell shows disks inside containing al-trans retinal rhodopsin in the presence of photon activation. (B) Phototransduction mechanisms in the absence of light.*

RETINAL GANGLION CELLS (RGC)

The RGC are the protagonist in the role of sending the previously filtered information by and from the retina to the rest of the brain (Khatib & Martin, 2017). They have a dendrite extension that connects with the bipolar cells, and their axons join to form the

optic nerve (CNII) (Kolb, 2005). The location where this union happens in the retina is called optic disk, and it is because of this disruption in the axon signal what results in a blackspot in our vision (Kolb, 1995; Preuss, Trivedi, Vom Berg-Maurer, Ryu, & Bollmann, 2014a; Sanes & Zipursky, 2010a).

Since the early 20th century, scientists have studied the activity of RGC. At that time, they recorded by dissecting one fibre of an optic nerve and applied a glass microelectrode electricity until they detected an AP (Hartline, 1938a). There are several types of RGC varying in size, morphology, and class. The traditional classification was made according to these characteristics. Using a flat whole mount cat-retina, they discovered three main types of cells depending on their phenotype. Perhaps being the densest of these classifications, the so-called midget (small) and parasol cells, named after their umbrella-like shape, respectively (Santon, Münch, & Michiels, 2019).

It was thought that prominent axons give faster conduction. Therefore, the conduction velocity in the optic nerve fibres might also differ: Rapid conduction comes from the parasol and the medium to slow conduction from the midget cells. Furthermore, they found out other vital differences among this broad classification. For instance, since the size of the midget cells is tiny, their input comes only from just a single PR. In fact, the excitatory centre of each class of midget cell has a different wavelength-sensitive cone; short, medium, and long-wavelength sensitive neurons or red, green, and blue. When the lights are turned off, the response is more sustained (adapts slower). Therefore, midget cells are more specific and can discriminate better details and colour.

On the other hand, parasol cells have larger receptor fields and are not specific. There is just a burst in response opposite to midget, which is more sustained; in other words, these cells adapt very quickly. In contrast with the midget cells, the parasol system has a mix of input both in the centre and the surround. Therefore, it is unlikely that parasol cells can discriminate or give any information about different wavelengths (C. Zhang, Kolodkin, Wong, & James, 2017a)

The receptive fields of the three major classes of RGC are considered to be ON cells, OFF cells and ON/OFF cells. However, it has been discovered that there are more cells apart from the ones that are excitatory in the surroundings and inhibitory in the surroundings. Nowadays, we know that there are more than 20 different classes of RGC

and that they perform other jobs accordingly. Currently, studies keep ongoing with the identification of subtypes, for instance, by looking at their transcriptional profiles (Langer et al., 2018).

1.3.3 Visual processing in mammals

The evolution of the visual system has been a complex process aiming to benefit each species for survival (Schroeder et al., 2021). It also seems that some sensory systems evolved in different manners according to their environmental needs (Bartel, Janiak, Osorio, & Baden, 2021). In this subchapter, I will refer to mammals in general. However, I will occasionally present it as perhaps a bit selfish "human" perspective so that it is easier to put all the information in a familiar context.

The need to relate sensory systems with other superior brain functions in highly evolved species like mammals has led to the development of a very complex sensory cortex (Trenholm & Krishnaswamy, 2020). Furthermore, we know that while in the auditory system, the morphological distance between the input (ears) is relatively close to the output (temporal lobe), in vision, the light input must cross from the eyes at the front of our heads, all the way to the posterior area of the brain in the occipital cortex (Figure 1.4) (Krubitzer, 2009). Interestingly, along this path, the information must do all kinds of complex loops and spread into other brain areas in the midbrain before reaching the visual cortex. Here I will describe how this process occurs.

First, we have the retina, already discussed in chapter 1.4.1, along with its fascinating molecular phototransduction mechanisms (Chapter 1.4.2). Now, what happens with the synaptic matter that was once converted from photons into electrical impulses? As mentioned before, the information is collected by the axons of the RGC, which in conjunction form the optic nerve (Hartline, 1938b; Kolb, 2005). Afterwards, the process in which this information arrives at the brain is complex and a summary of the history of discoveries regarding visual research is worth mentioning.

Background about research in mammalian vision

In the late 1700s, Francesco Gennari (1752-1797), a then medical student, was doing dissection practices when he noticed an extra layer of white matter in several slices of the brain, which was running only along the occipital cortex at the level of the calcarine sulcus (Paoletti, 1963). For this reason, this region of myelinated fibres is now called the

"stria of Gennari", and the visual cortex is also known as the striate cortex. Nowadays, it is thought to be related with multiple complex functions involved in vision despite being present in individuals that are blind from childbirth (Ide et al., 2012; Trampel, Ott, & Turner, 2011).

Over a century ago, it was already suspected the existence of different visual processing areas in the brain. Possibly some of the most famous evidence in this matter are the drawings from the Spanish histologist Ramon y Cajal (Buckner & Krienen, 2013). He followed the white and grey matter seen in many mouse-brain slices using the techniques from the Italian physician Camilo Golgi and reported his findings in a set of handmade illustrations as well as including valuable notations with his theories about the different synaptic pathways that might occur from his perspective (Fig 1.5-A) (Bentivoglio et al., 2019; Cajal, 1894b).

In the early 1960s, Hubel and Wiesel proposed a general classification for visual-related neurons. The first group comprised the cells, which are clearly defined as either an ON or OFF cell. This group of cells were called "simple cells" and included the RGC and LGN. The second group are the "complex cells", which, as its name suggests, consist of the cells which are harder to classify since from their RF there are not easily predictable (Hubel & Wiesel, 1962). Additionally, these scientists reported that some cells had a higher affinity to respond towards certain angles and directions. In their experiments, they conclude that whereas the LGN is not orientation-selective, this property may arise from these cells to the visual cortex.

Another example of early theories on visual processing is the reports about the lateral geniculate nucleus (LGN), a zone found in the ventral area of the brain, and it was thought to virtually contain the same receptive fields as the ones in the retina but with slight modifications, according to Hubel & Wiesel, 1962. For this reason, it was thought for many years that the LGN was acting just as a mere relay area to transfer information from the retina to the visual cortex. However, 15 years later, Sherman & Koch reported that, in fact, just 10-20% of these cells had originated from the retina (Sherman & Koch, 1986). Further studies demonstrated that around 50% of the cells in the LGN originate from cells from V1, and roughly about a third of them are GABAergic and hence, inhibitory.

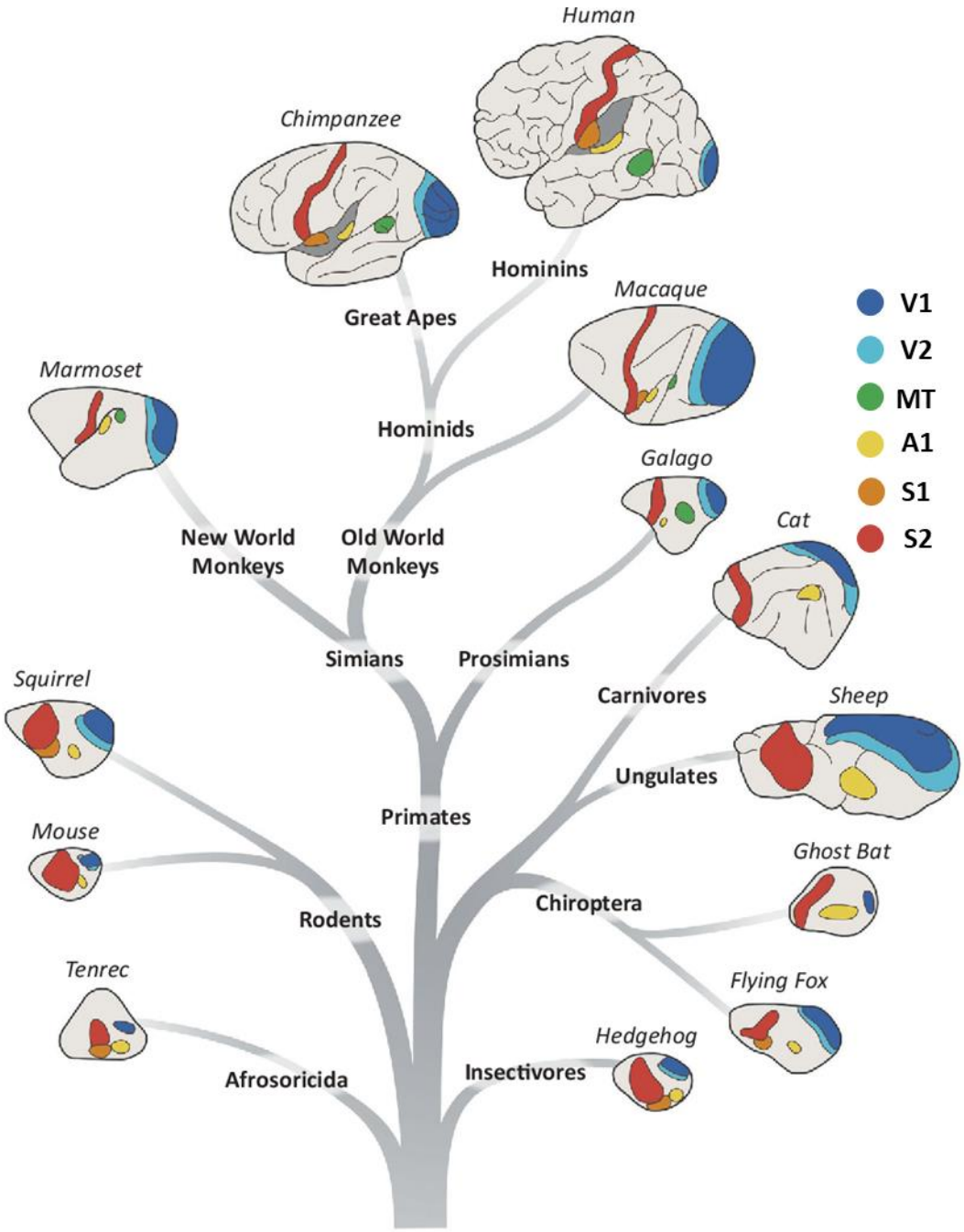

Figure 1.4 Sensory cortex brain areas from a phylogenic perspective. *Schematic of the evolution across mammals. Evident features to note include the enlargement of the neural volume and the preservation of the main sensory areas, which hint at the idea of common ancestors. The primary and secondary visual areas, V1 and V2, respectively, remain in the posterior side of the brain, later considered together as the visual cortex. MT: Middle temporal, A1: Primary auditory area. Finally, S1 and S2 identify primary and secondary somatosensory regions, respectively. Modified from (Buckner & Krienen, 2013; Krubitzer, 2009).*

Sherman & Koch, 1986 also reported that these GABAergic cells are derived from projections of cells near the LGN, and the remaining not-understood cells at that time, might possibly be noradrenergic, cholinergic or serotonergic projecting towards other geniculate nuclei (Jaepel et al., 2017).

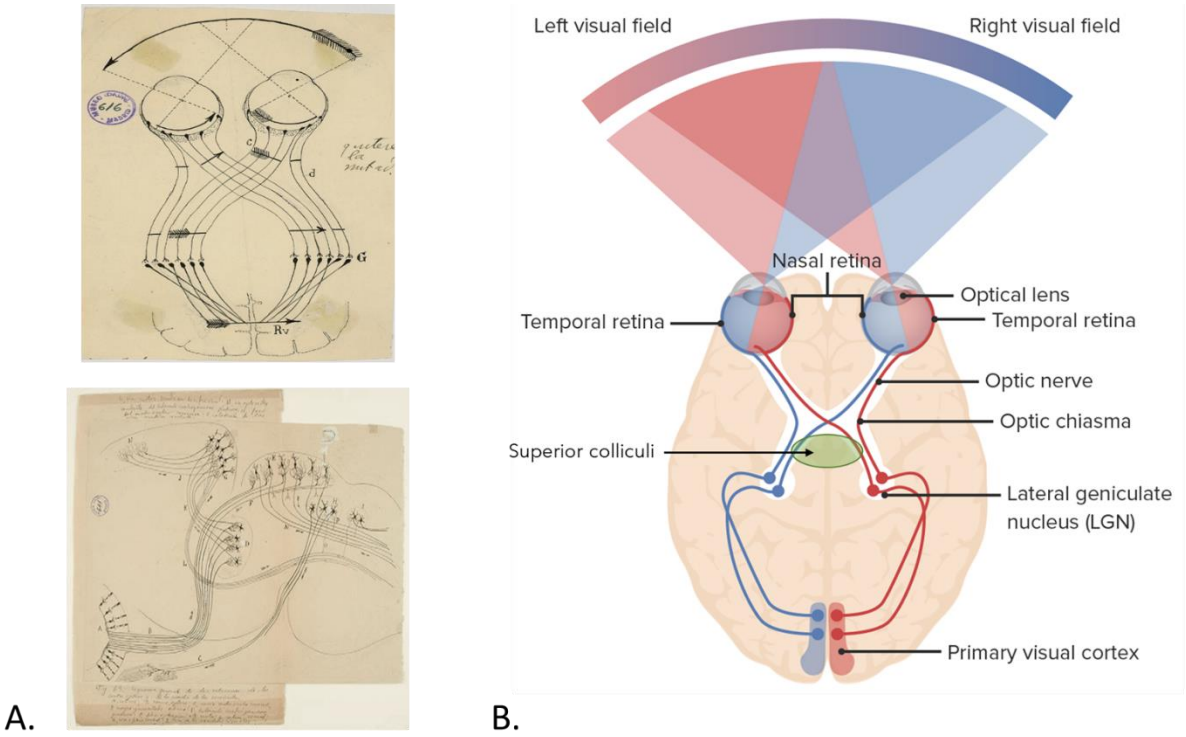

Figure 1.5 Basic understanding of the visual system in mammals. **(A)** *Drawings from Ramon y Cajal. Top: Schematic of the optic chiasm depicting the pathways followed by each left and right visual field. Notice the inclusion of the decussation of the optic chiasm already accurate with the modern knowledge. Bottom: Representation of the visual pathway from the retina to the occipital cortex in addition to other nuclei within the thalamus. This was inspired by the study of a rodent, and the description included the hypothesis of how this information is transmitted downstream. Some elements included are retinal projections, the LGN, superior colliculus, and thalamic neurons projecting to the visual cortex. Both images are public domain from Cajal circa 1902, courtesy of the Cajal Institute, "Cajal Legacy," Spanish National Research Council (CSIC), Madrid, Spain.* **(B)** *Modern schematic of a transversal view from a human brain illustrating the main components involved in the visual system pathway.*

From light to brain waves and visual disorders

When the light hits the lens, the images are received in the retina in an inverted form. Thus, the temporal visual fields from each eye will be projected to the nasal half of the retina and vice versa. Then, this synaptic information will be gathered in the optic nerves in each eye, where the first station is the *chiasma opticum* or optic chiasm. This structure is a crossing of myelinated fibres from the optic nerve. Interestingly, however, only the information coming from the nasal half of the visual fields from each eye will cross over and be processed into the contralateral lobe in the brain. The temporal visual fields continue their trajectory ipsilaterally (Figure 1.5-B). Subsequently, lesions at the level of the optic chiasm will generate a loss of vision in the nasal area of the visual field or bipolar temporal hemianopia, a common sign in patients with pituitary tumours.

After this crossed-over journey, the synapses will continue through the optic tracts, and here, some projections will reach the superior colliculi (Helmbrecht, dal Maschio, Donovan, Koutsouli, & Baier, 2018). These tiny structures at the posterior side of the thalamus are primarily involved in visual reflexes. Hence for instance, when you see any fast-speed element passing in your gaze, the superior colliculi are the individuals responsible for making your head turn around towards that flash-sight moving object. Lesions by pressure at the level of one optic tract, such as aneurysms, will produce blindness in half of the contralateral visual field, in other words, a left or right homonymous hemianopia.

Up to this level, we discussed only how the visual field information from the left and right sides is transmitted; however, the upper and lower halves are involved in the following stages of the pathway towards V1. The LGN follows many myelinated radiations, also named geniculate-calcarine tracts, broadly classified as upper or parietal confining the posterior Baum's loop, and a lower or temporal, containing the so-called Meyer's loop (Figure 1.5-B). The information from the upper half of the visual fields is transmitted through the temporal loop, whereas the data from the bottom half will be processed through the superior loop. Depending on the specific site, lesions at a particular level of these loops will cause a different type of quadrantanopia or loss of vision in just one quadrant of the visual fields. Other particulars of how vision is coded

in the mammalian CNS are far more complex and exciting; however, I will not get far into them since this work is based on ZF only.

1.4 Use of *in vivo* models to study visual memory formation

Memory paradigms are tangible methods for studying synaptic plasticity. Memory can be classified in two main types: explicit or declarative, and implicit or non-declarative memory (Nicoll, 2017). The first one is related with objects, events, places and other beings, and is known to be mainly associated with activity in the hippocampus and cerebral cortex being considered a complex approach in humans since need full consciousness (Kandel, Dudai, & Mayford, 2014). Meanwhile, the non-declarative memory, which is maintained among the species and is linked with simple motor responses and does not requires full mind awareness is located in other neural pathways such as the cerebellum, the striatum, the amygdala and even simple reflex systems in invertebrate animals (Best et al., 2008). In humans, the hippocampus and the cerebral cortex are currently recognized as the most studied structures that enable learning and have been the most studied regions in the context of memory (T V P Bliss & Gardner-Medwin, 1973b; Citri & Malenka, 2008a; Medina, 2018a). For this reason, *in vivo* models are ideal to study these functional characteristics (R. W. Zhang, Li, Kawakami, & Du, 2016; Zhou et al., 2020).

Researchers have selected many different *in vivo* models aiming to study how memory works. The fruit fly *Drosophila melanogaster* and its variants are perhaps the most used model among invertebrates, followed by a variety of bees since these insects possess a very suitable olfactory system (J. Akerboom et al., 2012a; Kaschula & Salecker, 2016a). Among other advantages, these models allow us to perform odour and visual memory assays, analyze, and measure responses via imaging (Kaschula & Salecker, 2016b). Another still widely used invertebrate is the giant mollusc *Aplysia* due to the simplicity of its neural system. For instance, this model revealed mechanisms of neuronal growing and an increase of the learning-related neurotransmitter cAMP by sensitization from its gill-withdrawal reflex (Mayford et al., 2012).

In regard of vertebrates there are studies using many approaches, from mice -which are perhaps the most common mammalian model- to cats, guinea pigs, among other widely used species such as zebrafish (Kandel et al., 2014), which will be discussed in the following section. The study of the visual process across the species has given us tools to answer questions such as to how and why vision is computed in different environments, which might not be possible otherwise (Baden et al., 2020a).

1.4.1 Zebrafish as a model for memory formation.

The use of zebrafish in neuroscience has become one of the most relevant approaches in the last decades. This model offers many advantages, such as the relatively high homology with the human genome, sharing approximately 70%, and around 84% of genes related with human diseases have zebrafish homologues (Kalueff, Stewart, Gerlai, & Court, 2014). Other advantages are the relatively low cost in terms of maintenance and fast development (Roberts, Bill, & Glanzman, 2013). They are translucent in the early stages of their lives, allowing us to see through its scales thus, to use different novel imaging techniques such as calcium imaging -which will be discussed below-, light sheet microscopy, among others (Ahrens, Orger, Robson, Li, & Keller, 2013a; J. Akerboom et al., 2012b; Portugues, Severi, Wyart, & Ahrens, 2013). Regarding memory research, zebrafish presents the advantageous feature of having a brain morphology and neurochemistry that is similar to mammals, since these characteristics are highly conserved across vertebrates (Drapeau et al., 2002).

1.4.2 Behavioural experiments in ZF

Although the absence of limbs in fish might difficult a fair comparison of motor learning with humans, a large number of behavioural phenotypes had already been described (Keatinge et al., 2015; May et al., 2016a).

Nowadays, there is a broad set of independent studies in which zebrafish has been compared with some human neurodegenerative disorders related to memory loss, both functionally and anatomically (See Fig 1.2). However, although particular sets of neurons have been identified as neurotransmitter regulation areas (dopamine,

serotonin, histamine, among others), the precise roles and interactions within other systems are still far from being well understood (Panula et al., 2010). Thus, despite the complexity of behavioural assays, these are becoming essential tools to uncover these mechanisms.

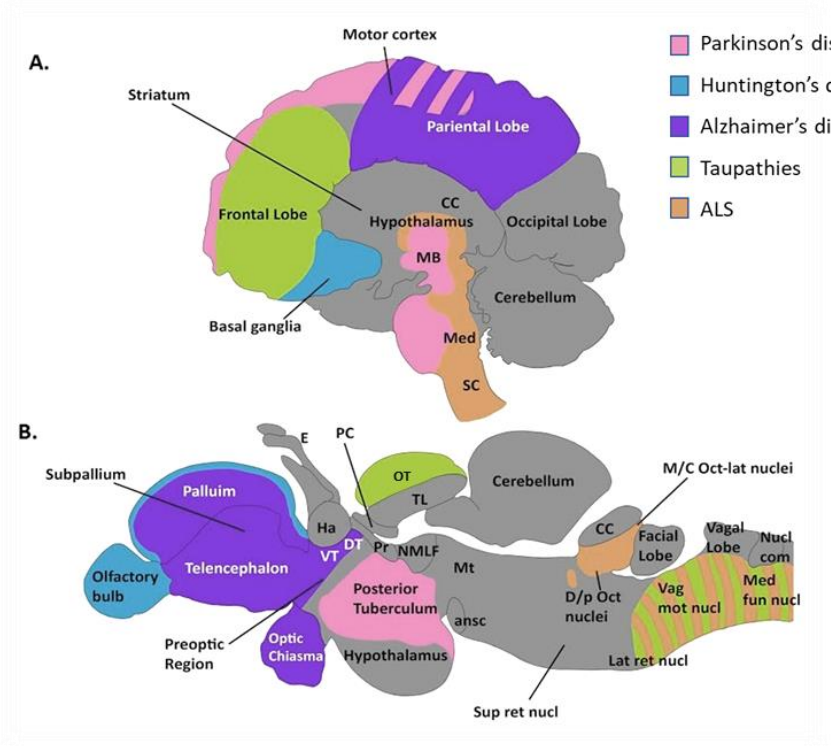

Figure 1.6 Proposed color-coded anatomical comparison scheme of regions involved with memory-loss related neurodegenerative diseases in human (A) and adult zebrafish (B), according with a data compilation *(Bandmann & Burton, 2010; Paquet et al., 2009; Xi, Noble, & Ekker, 2011). CC, crista cerebellaris; MB, midbrain; SC, spinal cord; E, epiphysis; PC, posterior commissure; Ha, habenula; VT, ventral telencephalon; DT, distal thalamus; Pr, pretectum; TeO, tectum opticum; TL, torus longitudinalis; NMLF, Nucleus of medial longitudinal fascicle; Mt, Mesencephalic tegmentum; ansc, ansulate commissure; D/p oct nuclei, descending/posterior octaval nuclei; Vag mot nucl, vagal motor nucleus; Lat ret nucl, Lateral reticular nucleus; Med fun nucl, medial funicular nucleus; Nucl com, nucleus commissaries; Sup ret nucl, superior reticular nucleus.*

Since larval stages, zebrafish can be habituated (Best et al., 2008), dishabituated or subjected to sensitization (Zhuo, 2016), and undergo classical conditioning in which a conditioned stimulus is linked with a reinforcing (unconditioned) stimulus (Kalueff et

al., 2014). These resources may be helpful to predict the behavioural outcome in the presence of an unconditioned stimulus (Roberts et al., 2013).

We know that with some exceptions, zebrafish are usually sociable animals after 3-weeks old. This socialization can be translated as the existence of a particular type of declarative memory (Hamilton et al., 2016a). Furthermore, it is possible to modify natural social behaviour. If a fish is raised in isolation, the fish won't learn how to behave around other fish later, and the only presence of near conspecifics will cause stress and anxiety responses (Dreosti, Lopes, Kampff, & Wilson, 2015).

Furthermore, a couple of decades ago, it was reported that the sudden presence of injured conspecifics produces an alarm substance called "Schreckstoff", which yields a fear response in animals that are nearby. In zebrafish, this response is characterized by tighter shoaling, erratic movements with a tendency to swim at the bottom and freeze (deCarvalho et al., 2013; Waldman, 1982). Recent studies have proven the use of this substance as a suitable method to assess associative learning in zebrafish. Brain activity areas were found mainly in the medial and lateral pallium when performing Immunohistochemical staining of the immediate early gene (IEG) *c-fos* (Ruhl, Zeymer, & von der Emde, 2017).

1.4.3 Novel Object Recognition to test memory formation in ZF

Almost three decades ago, the novel object recognition tests surged as a tool of cognition evaluation in mammals. In zebrafish (Danio Rerio), these experiments are becoming a trend in parallel with the surge of novel zebrafish models of amnesia and other neurodegenerative diseases. The basis of the novel object recognition tests consists of two main phases. The training phase, which consists in habituate the subject in an arena containing two identical objects. Then, after a given time, the animal is subjected to a testing phase, where it is introduced in the arena containing one of the familiar objects and an unknown one. The results are obtained by measuring the time the subject spends exploring each object (Moore, Deshpande, Stinnett, Seasholtz, & Murphy, 2014). More about the traditional novel object recognition (NOR) test, history and modifications will be discussed in more detail in Chapter 3.

In zebrafish, NOR is one of the most straightforward approaches to study declarative memory, and the use of this method is still recognized. For instance, Leighton et al., 2018 tested a novel zebrafish line lacking prp2, responsible for encoding the standard version of cellular prion protein (PrPc). This protein can lead to impairment conditions to the worsening of other neurodegeneration diseases (Westergard, Christensen, & Harris, 2007). They found that NOR tasks appear to be affected in just 3-years old prp2$^{-/-}$ fish, compared with the wild-types.

Eventually, other variations of this method were tested, and even though most of the basics are established, there are still some topics that remain unclear. More about this method uses, and its modifications will be discussed in more detail in Chapter 3, along with our own experimental reproduction and original proposed approach of analysis.

1.5 Calcium imaging *in vivo* for synaptic research

Calcium ions are essential in all neurons and other excitable cells. During the action potential of a synaptic cell, we can determine changes in the intracellular concentration of this ion, helping us in the measurement of other synapse properties such as the spike timing or level of synaptic activation (Reviewed by Akerboom et al., 2013). In the beginning of calcium imaging experimentation, chemical dyes administered by local injection were used for this purpose. These dyes were esterified in a way that allowed the permeability through the cell membrane and deposited accumulatively after the hydrolysis from the hydrophobic portion, leading to the earliest presentations of calcium dynamics in glia using in vivo models such as anesthetised and non-sleeping mice (Ye, Haroon, Salinas, & Paukert, 2017). Nevertheless, this technique has many disadvantages apart from the local damage given by the administration, such as the lack of specificity if the injection does not occur directly in the cell, and the fact that experiments longer than a couple of hours are not recommended due to the poor concentration upkeep over time (J. Akerboom et al., 2012b; Marvin et al., 2013; Ye et al., 2017).

One of the characteristics of calcium indicators is the increased affinity and less background noise during the imaging process, compared with GFP, allowing to perform studies *in vitro* and *in vivo* (Mittmann et al., 2011a), becoming one of the most valuable tools in neuroscience research. Thus, markers that have been valuable in neuroscience

are the genetically encoded calcium indicators (GECIs), such as the most used GCaMPs (Nakai, Ohkura, & Imoto, 2001), and the derived from the red fluorescent protein mRuby, RCaMPs (Jasper Akerboom et al., 2013).

1.5.1 Genetically encoded calcium indicators (GECIs)

As the name suggests, the Genetically encoded calcium indicators (GECIs) are calcium indicators encoded genetically into the cells of the living model into a specific sequence of DNA (Li et al., 2021). GECIs are produced by the addition of a protein or peptide sequence, usually looking for the peptide affinity to a specific type of cells or location that we are interested in imaging. This sequence must contain at least one component responsive to calcium, which changes its optical properties when calcium binding excites a light radiating protein also included within the GECI (Figure 1.7). Conventionally, GCaMPs are based on circularly permuted green fluorescent protein calmodulin (CaM) and the calcium/calmodulin-binding "M13" peptide (J. Akerboom et al., 2012b; Jasper Akerboom et al., 2013).

Even though the first generations of GECIs were less advantageous than the calcium dyes, the structure has been improving steadily. For instance, GCaMP2 was brighter and a steadier molecule than its predecessor, and two years later, GCaMP3 was even brighter and a broad dynamic range, allowing for the detection of single-cell action potentials (AP). Successively, new versions of GCaMP families were generated to improve the kinetics of this molecule (Ahrens, Orger, et al., 2013a). Nevertheless, despite the differences made between generations of these GECIs, studies have shown that the calcium dynamics of the recorded activity from both GCaMP3 or GCaMP6 are not significantly different, and the results from studies made with older generations can be used with a little caution when comparing results using novel versions such as GCaMP6 or GCaMP7 in models like the mouse and zebrafish (Ye et al., 2017).

1.5.2 Use of calcium indicators in zebrafish

Imaging calcium dynamics in this animal model has been demonstrated to be achieved for over 24 consecutive hours. Therefore, scientists are able to visualise and characterise functional pathways during long periods of time, which tends to be proven challenging in other species (Leung, Wang, & Mourrain, 2013). The fusion of synaptic markers such as the pan neuronally expressed *elav1* or the post-synaptic protein

synaptophysin with GECIs using different light wavelengths at the same time such as GCaMP and RGECO permits the study of multiple synapse interactions between different cells in the brain (Meshalkina et al., 2017; Walker, Burrone, & Meyer, 2013a) (See Fig 1.3).

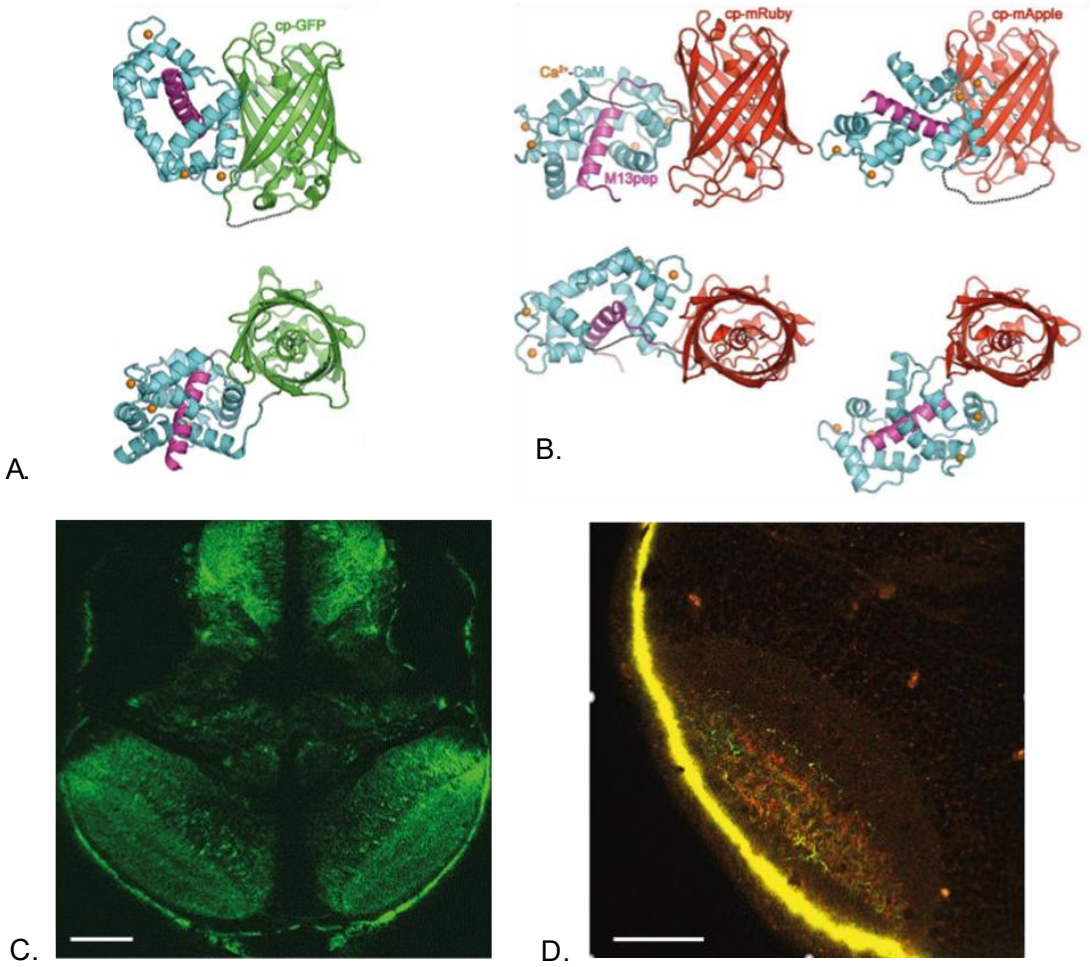

Figure 1.7 Frequently used calcium indicators in ZF. (A) *Cristal structure of GCaMP in two different views.* **(B)** *Most commonly used red calcium indicators RCaMP (left) and RGeCO (right), molecular structures shown in two different views.* **(C)** *Whole brain confocal imaging of a 14dpf ZF expressing NBT(elav):GCaMP3 using a 20X objective.* **(D)** *Two-photon imaging of a 13dpf ZF optic tectum expressing isl2b:SyRGeCO taken with a 40X objective. Scale bars: 50um. Images A-B are adapted from Akerboom et al., 2013.*

In a model like the zebrafish Dario rerio, calcium indicators add to the advantage of transparency during the first stages of life. This feature allows non-invasive synaptic activity *in vivo* recording either using confocal or two-photon microscopy (Del Bene &

Wyart, 2012). Additionally, its size allows to image in a wide options in terms of location and area size going from the whole brain to a single synapse being able to represent even >100,000 neurons at 6dpf (Li et al., 2021; Marvin et al., 2013). Some brain regions might represent a challenge in terms of imaging in other animal models such as mammals due to the deepness and overlapping of other structures. Some examples of these are the amygdala, the hippocampus and the habenula which in contrast ZF represents a more suitable and accessible model for *in vivo* research (Aoki et al., 2013; Leung et al., 2013).

1.6 Visual processing in the zebrafish

The main anatomical features related to the input of the visual system, such as the retina, are highly conserved between vertebrates (Bilotta & Saszik, 2001; Gestri, Link, & Neuhauss, 2012). As shown in figure 1.6 B-C, mammals and zebrafish share multiple similarities in the retinal cells, such as their development, purpose, morphology and configuration (Schmitt & Dowling, 1999).

General advantages of using ZF as a model have been discussed in subchapters 1.3.1 to 1.3.3, yet additional benefits associated with vision include their regeneration ability (Timothy V P Bliss et al., 2017; Nagarajan et al., 2020). When the retina becomes damaged, the Muller cells go through a series of events that stimulate its division and generation of a pluripotent retinal progenitor capable of regenerating the rest of the other retinal cell types (Wan & Goldman, 2016). Another advantage is that in ZF, the visual responsiveness and the similarity with the human retina is already present by the third-day post-fertilisation (Richardson, Tracey-White, Webster, & Moosajee, 2017). The ZF preference for daylight and the structure of their photoreceptors is very well organised in a mosaic pattern. PR also converge in a zone highly dense in cones (Schröder et al., 2021). These properties simulate the human macula and thus results in a colour vision range similar to humans (Dehmelt et al., 2019).

Other aspects differentiate the visual processing in this fish in comparison with other vertebrates. Studies have shown that the ZF retina contains photoreceptors sensible to wavelengths ranging from UV to red light. However, the distribution of the bipolar cells by functionality varies across the area and depends on individual exposition to their natural scenes (Zimmermann et al., 2018).

Perhaps the most evident disparity between fish and mammals in relation to higher visual processing is the absence of visual cortex in ZF. In fact, there is no brain cortex at all. Instead, the visual information is received after passing through the optic chiasm and tracts into the optic tectum (OT). The OT is considered the equivalent of the superior colliculi in mammals, discussed in Chapter 1.4.3. In the next section, I review some of the leading knowledge about morphology and function of the zebrafish OT.

1.6.1 Optic tectum

In ZF, the optic tectum is the closest analogue structure in charge of the higher visual processing in the brain. The tectum is known as the primary visual area in ZF and receives more than 97% of the RGC input (Robles, Laurell, & Baier, 2014b). Although the tectum also receives feedback from other somatosensory areas in the brain (Xiao & Baier, 2007), in terms of visual input, the OT is the continuation of RGCs congregating in the optic nerve towards the deeper areas of the brain. After some of these axonal fibres pass through the optic chiasm, they will converge into the neuropil, a highly organised layered area of the OT mainly formed by white matter (Gebhardt et al., 2019a). The neuropil has an uneven oval shape and changes its morphology during the ZF development, mainly larval stages. The space between the neuropil and the mid-ventricular system is an area surrounded by a crowd of rounded and monopolar cells known as pyramidal cells or periventricular neurons (PVN). (Sajovic & Levinthal, 1982). Thus, the two main areas forming the OT are the neuropil and the cell bodies also referred to as *stratum periventriculare* (SPV) (Figure 1.8).

The layers of the neuropil were established decades ago and even though there is no agreement on the exact number, it is agreed that are more than ten (Gonzalez, Morales, Villarreal, Derrick, et al., 2014; Robles, Laurell, & Baier, 2014a). The most superficial coating is the *stratum marginale* (SM), which in ZF does not contain input from the RGN, contrary to other teleost varieties (DeMarco, Xu, Baier, & Robles, 2020). However, the SM contains presynaptic projections from the *torus longitudinalis* (TL), a highly myelinated structure located in the dorsal midline that has been characterised by a strong presence of OFF-responses (Förster et al., 2020a; Northmore, 2017; Robles, Fields, & Baier, 2020). The intermediate layers receive input from diverse retinal ganglion neurons and can be divided into five main zones from external to ventral: The *stratum opticum* (SO), formed by two layers; *stratum fibrosum griseum superficiale*

(SFGS) with six layers; the *stratum griseum centrale* (SGC), which is sandwiched by non-retinorecipient thin layers on each side; the *stratum album centrale* (SAC) and the SPV mentioned before. The last two are also surrounded by cells without retinal input (Del Bene, Wyart, Robles, Tran, Looger, Scott, Isacoff, Baier, et al., 2010; Heap et al., 2018) (Fig 1.8).

It is worth mentioning that most of the RGC input in the neuropil projects to the contralateral neuropil, and it is localised mainly within the SO and SFGS (Robles, Filosa, & Baier, 2013) (Figure 1.7-A). The SGC zone has projections coming from the SM and passes through the PVN, reaching the midbrain (Robles et al., 2014a; Sajovic & Levinthal, 1982). However, there is visual communication within the same tectal hemisphere due to projections in between the OTs known as inter-thalamic neurons (ITNs) (Gebhardt et al., 2019b)(Figure 1.7-C). Moreover, this system is essential in other fish for the consolidation of binocular vision, used for instance, during prey hunting in the absence of RGCs.

It was established that in ZF, the RGCs are branching into around ten main areas called arborisation fields (AFs) before reaching the neuropil, considered itself as the last and biggest of them (AF10). Since the era of Hubel and Wiesel, it was already suspected that the organisation of the tectum is related to functional features. Years later, it was proven that indeed certain areas are more size and direction-selective (Abbas & Meyer, 2014). For instance, the OT outer layers seem to be more responsive to stimuli of a bigger size, whereas smaller size stimuli can be processed by deeper layers (Preuss, Trivedi, Vom Berg-Maurer, Ryu, & Bollmann, 2014b). Interestingly, it was discovered that this selectivity is lost in the absence of ITNs, suggesting that impairment of these cells will affect prey hunting (Del Bene, Wyart, Robles, Tran, Looger, Scott, Isacoff, & Baier, 2010).

Direction selectivity (DS) is another local feature that has been widely studied. We know that before reaching the OT, DS-neurons finish at the level of the AF5-AF6, and within the neuropil, we can find them just in the outer layer of the SFGS and can be classified in 3 different types according to their motion selection being 120 degrees apart from each other (Matsuda & Kubo, 2021).

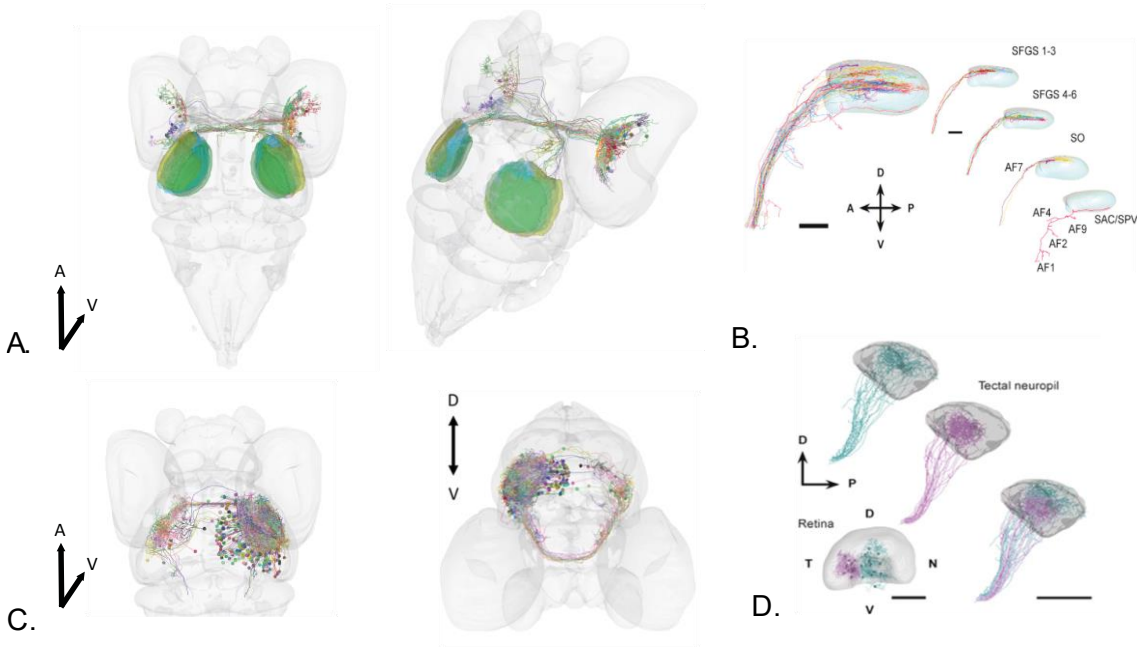

Figure 1.8 Retinotopic organisation in the optic tectum. (A) *Left: Schematic top view of a zebrafish brain showing RGC projections towards the midbrain. Right: Tilted view from the same schematic. Deepness is appreciated, and cells are randomly colour-coded for an enriched visualisation.* **(B)** *Dissected 3D view from a single OT, including the retinal input. The typical highly organised layers are shown. Scale bar represents 20µm. Adapted from Kunst et al., 2019.* **(C)** *Left: 3D top view schematic of a zebrafish telencephalon and midbrain showing randomly colour-coded PVN and ganglion cells projecting from the OT neuropil. Right: Same schematic viewed from a coronal perspective for better appreciation of the deepness.* **(D)** *Schematic of a representative example of retinotopic organisation in the OT neuropil. Ganglion cells from the temporal (pink) projecting in a more centralised manner compared to nasal ganglion cells in blue, which spread superficially in a more distributed way (Kunst et al., 2019). Scale bar represents 100µm.*

Figures A and C were generated with permission from the ZF brain atlas, available at Mapzebrain from the Max Plank webpage https://fishatlas.neuro.mpg.de/neurons

1.6.2 Plasticity of receptive fields

All somatosensory cells have receptive fields (RFs). The term was first utilised in 1906 by Sherrington to describe the area where a given stimulus, in this case, the light touch of a dog's skin surface, would elicit a response (scratch reflex) (Sherrington, 1906). However, this principle can be applied to other sensory systems. A visual receptive field was first described as the region of the retina, which must be illuminated to obtain a

response in any given "fibre" (Hartline, 1938b). In this case, "fibre" refers to the axon of a retinal neuron. The concept has been slightly modified to specify that any visual neuron, from a photoreceptor to a visual cortical neuron, has a visual RF (Hubel & Wiesel, 1962). Sometimes, this can be a point of confusion since all the sensory cells have a region of space that excites them; however, depending on the type of response, some can be contrast, direction, or orientation detectors. Some visual neurons are just responsive to specific wavelengths only.

In the research carried by Hubel & Wiesel, 1962, experience plays an essential role in the correct development of the visual function. They showed that following long-term visual deprivation in cats by covering one eye after birth, the binocular vision was affected, and later visual stimuli did not trigger any responses in the impaired eye and were no longer recoverable. This experience-dependent theory was soon reinforced by Blakemore & Cooper, 1970.

Muller glial cells, described in Chapter 1.4.1, are the protagonists in terms of regeneration properties, and it is hypothesised that in mammals, these MCs are also a robust set of pluripotent cells with retinal neurogenic abilities, which might be promising for drug target discoveries for the treatment of many visual impairment diseases (Gestri et al., 2012; Schroeder et al., 2021). Another example of the malleability of RFs is an unconventional protocol performed in frogs in which a third eye was surgically attached in their early stages of development, demonstrated that it was possible to create an artificial projection to the already placed optic tracts (Figure 1.9-A). Therefore, even though there was no pupillary reflection -thus, no innervation by the oculomotor nerve-, morphologically, the supernumerary eye appeared normal, and the retinotectal projections arborised to compete with the natural ones creating a third middle optic tract and clumping in the frog's tectal neuropil (Constantine-Paton & Law, 1978).

A. 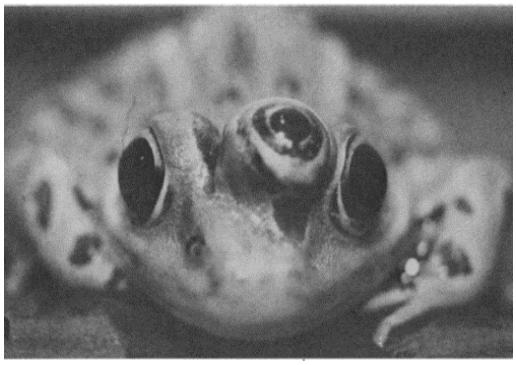

B. 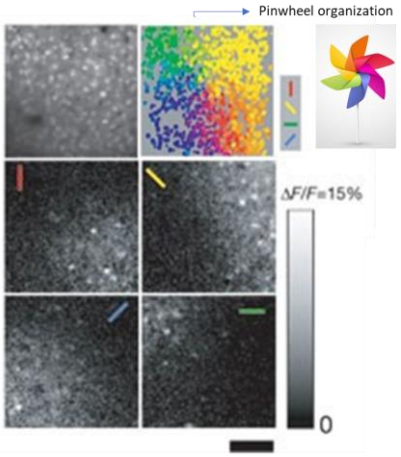

Figure 1.9 Visual plasticity and orientation pinwheel selectivity. (A) *Three-eyed frog from Constantine-Paton & Law, 1978.* **(B)** *Orientation tuning follows a pinwheel organisation, modified from (Ohki et al., 2006). Scale bar: 100µm.*

In zebrafish, the RFs have been mapped using small moving spots and flashing bars. This method has successfully been used in both young and adult ZF (Bergmann, Santoscoy, et al., 2018). Angle selectivity has been found to be organised around a centre in a pinwheel configuration (Figure 1.9-B). These pinwheels have been demonstrated using a variety of experiments such as electrophysiological recordings and two-photon calcium imaging in vivo (Y.-J. Liu, Hashemi-Nezhad, & Lyon, 2017; Ohki et al., 2006)

By nature, ZF has regenerative properties, which suggest that the plasticity of the visual RFs is highly adaptable (Mittmann et al., 2011b). For instance, following damage in the retina using photoablation, toxin injections at different levels of the visual pathways, or even physical damage up to the point of the enucleation of a whole eye, it was proven that the ability to recover any lost photoreceptors or other retinal neurons is as efficient to the point of full visual function recovery (McDowell, Dixon, Houchins, & Bilotta, 2004).

1.7 Thesis aim

Understanding how visual information is processed from the outer layers of the OT to the deeper areas of the ZF brain would provide us with helpful insight into how non-associative memory is encoded in the brain.

In this PhD project, we firstly aimed to replicate and evaluate the proficiency of some of the current behavioural paradigms used to assess learning and memory formation in zebrafish. With this basis, we chose the NOR paradigm and VLNOR to discuss and provide an unbiased approach to perform and analyse these assays through a computerised and semi-automatic system (Chapter 3).

Secondly, we aimed to define brain areas involved in producing visual memories regarding novel objects in zebrafish, using the IEG *c-fos* with a combination of traditional and fluorescent whole-mount ISH techniques using late-stage zebrafish larvae. Furthermore, in Chapter 4, I suggest modifications to optimise these protocols for the utilisation in late-stage ZF fry suitable for non-invasive *in vivo* calcium imaging (up to 22dpf).

The overall goal of this PhD was to identify the zebrafish brain areas responding to novel visual stimuli and define how plasticity is involved in the computation of these images. In other words: what changes in their brain when the fish encounters with a new visual stimulus? Thus, after the determination of the areas related to the formation of new visual memory, I focused on the tectal neuropil to propose an initial physiological characterisation of synapse plasticity during visual processing using multiphoton calcium imaging *in vivo*.

In Chapters 5, I deep dive into the concept of visual adaptation and the related elements that I found in the OT neuropil using 2-P calcium imaging. Here, I aimed to explore how certain environmental modifications such as fear, and the combination of other sensory systems change this neural activity and described possible molecular pathways interacting with this process.

One of the main aims of this PhD project was to provide an initial characterisation of the functional organisation in the tectal neuropil in relation to its tunning properties such as contrast and frequency selectivity. In chapter 6, I describe the relationship with the layered organisation in the neuropil and these tunning properties. Lastly, I propose a novel approach to define a model of the Contrast sensitivity function as of high visual processing brain areas in zebrafish, proven to be close to what has been previously reported using other measurable methods.

Chapter 2. Materials and Methods

MATERIALS AND METHODS

2.1 Zebrafish Husbandry and Handling

2.1.1 Zebrafish strains

2.1.2 Novel environments

2.2 Behavioural experiments

2.2.1 Experimental setup

2.2.2 Visual Lateralisation Novel Object Recognition (VLNOR) Test

2.2.3 Traditional Novel Object Recognition (NOR) Test

2.2.4 Data Analysis

2.3 Whole-mount in situ hybridisation

2.3.1 Synthesis of antisense RNA c-fos probe

2.3.2 Sample preparation

2.3.3 Generation of positive controls of neural activity

2.3.4 Fluorescence WISH.

2.3.5 Mounting and Imaging

2.4 Generation of model reporting synaptic strength

2.5 Multiphoton calcium imaging

2.5.1 Calcium imaging

2.5.2 Experimental setup

2.5.3 Fish preparation

2.5.4 Visual stimuli

2.5.5 Image acquisition and processing

2.6 Data analysis

2.7 Statistical analysis

2. MATERIALS AND METHODS

2.1 Zebrafish Husbandry and Handling

All zebrafish were maintained according to the UK Home Office regulations and UK Animals (Scientific Procedures) Act 1986, under the project and individual research licenses. Additionally, all the experiments were previously approved by the local ethical committee and the UK Home Office. Breeding was done through both marbling (addition of marbles overnight) and pair-mating methods depending on the individual needs of each experiment (Fig 2.1.). The following morning embryos were collected and raised in E3 medium in a 28.5°C incubator until 5.2 days post-fertilisation (dpf) (Table 2.1).

Concentration	Component
10x	5mM NaCl (2.87g), 0.17mM KCL (0.13g), 0.33mM CaCl. 2H2O (0.48 g), 0.33 Mg2SO4. 7H2O (0.82 g). Filled with deionised water (dH2O) up to 1 litre.
1x	100 mL from the 10x stock and 900 mL of dH2O.

Table 1. Contents of the E3 Medium

All fish were kept at a light/dark cycle 14/10h respectively, and at 5.2 dpf, they were moved to a Tecniplast system (Tecniplast S.P.A., Italy), and housed in groups of no more than 40 fish per tank. Feeding was done twice daily from days 5-10 post-fertilisation with dry food diet for zebrafish larvae (50-100 size particle). From days 10-15 post-fertilisation, fish were fed daily with dry food diet (100-200 size-particle) and a combination of brine shrimp (saline artemia) and saltwater rotifer two times until used in experiments.

All fish Individuals were culled and disposed of according to regulations after the experiments.

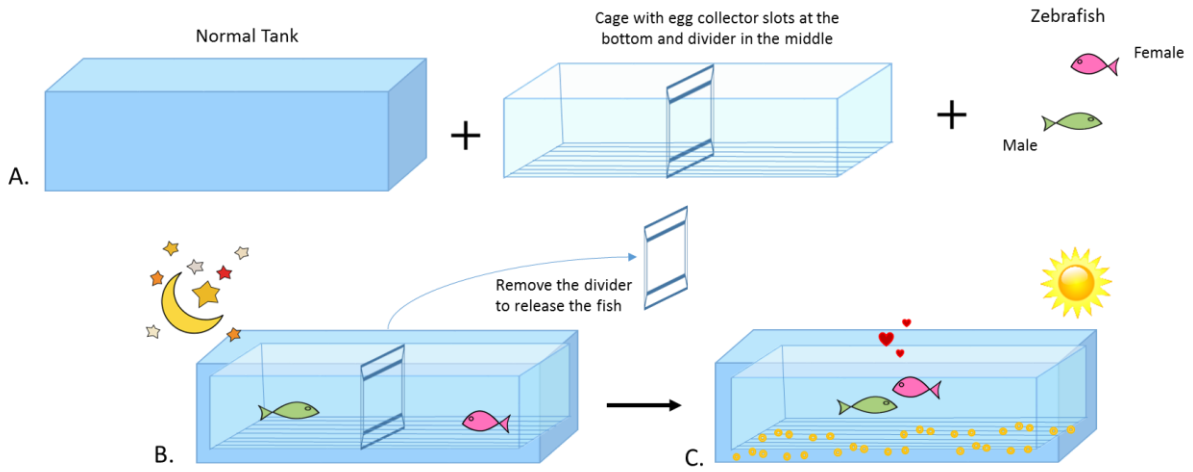

Figure 2.1. **Zebrafish pair-mating procedure and egg isolation. (A)***Elements needed for breeding the fish***. (B)** *After selecting a proper male and female couple, we placed them in the breeding tank in separated compartments during the night* **(C).** *The next day in the morning, we release the fish to let them lay eggs, which will be easily collected from the slots at the bottom of the tank after changing the fish into a new fish-tank*

2.1.1 Zebrafish strains

For the behavioural experiments, we used two strains of fish, wild-type zebrafish AB Danio rerio, and a nacre mutant which lacks the melanophores in the skin without affecting the epithelium in retina required to allow a natural vision. This strain has the xenopus neural beta-tubulin promoter expressed through the green calcium indicator GCaMP3 (NBT:GCaMP3) (J. Akerboom et al., 2012b; Lister, Robertson, Lepage, Johnson, & Raible, 1999). These were all bred by natural spawning by marbling overnight and raised in the aquarium facilities at the Bateson Centre in The University of Sheffield. The zebrafish were fed before the experiments and housed in groups of less than 25 fish per tank with age-matched siblings.

The calcium imaging experiments for chapters 5 and 6 were performed using NBT: GCaMP3 (Figure 2.2-B), a strain previously described, which was generously given by Dr Vincent Cunliffe (University of Sheffield), and for other 2-photon experiments we used a line expressing the pan-neuronal promoter *Huc* (also known as elav3) with the calcium indicator GCaMP6. This line has proven to be brighter in fluorescence than GCaMP3 in the embryonic and initiation of larvae stages. However, we found that *Huc* strain suffered an evident decrease of fluorescence after the day ten post-fertilisation.

Lastly, a strain expressing the pan-neuronal promoter isl2b (Walker et al., 2013a) in presynaptic synaptophysin-containing cells (Wiedenmann & Franke, 1985) through the red calcium indicator Sy-RGeCO (Walker et al., 2013a). This isl2b: SyRGeCO strain was kindly provided by Dr Takeshi Yoshimatsu and Dr Tom Baden (Sussex University) (Figure 2.2-C). The embryos were sorted the second-day post-fertilisation for GFP and red fluorescence using a stereoscopic fluorescent microscope (Figure 2.2-A), and subsequently raised after 5dpf in the Tecniplast system with around 25 fish per tank and fed twice a day until the day of the experiment.

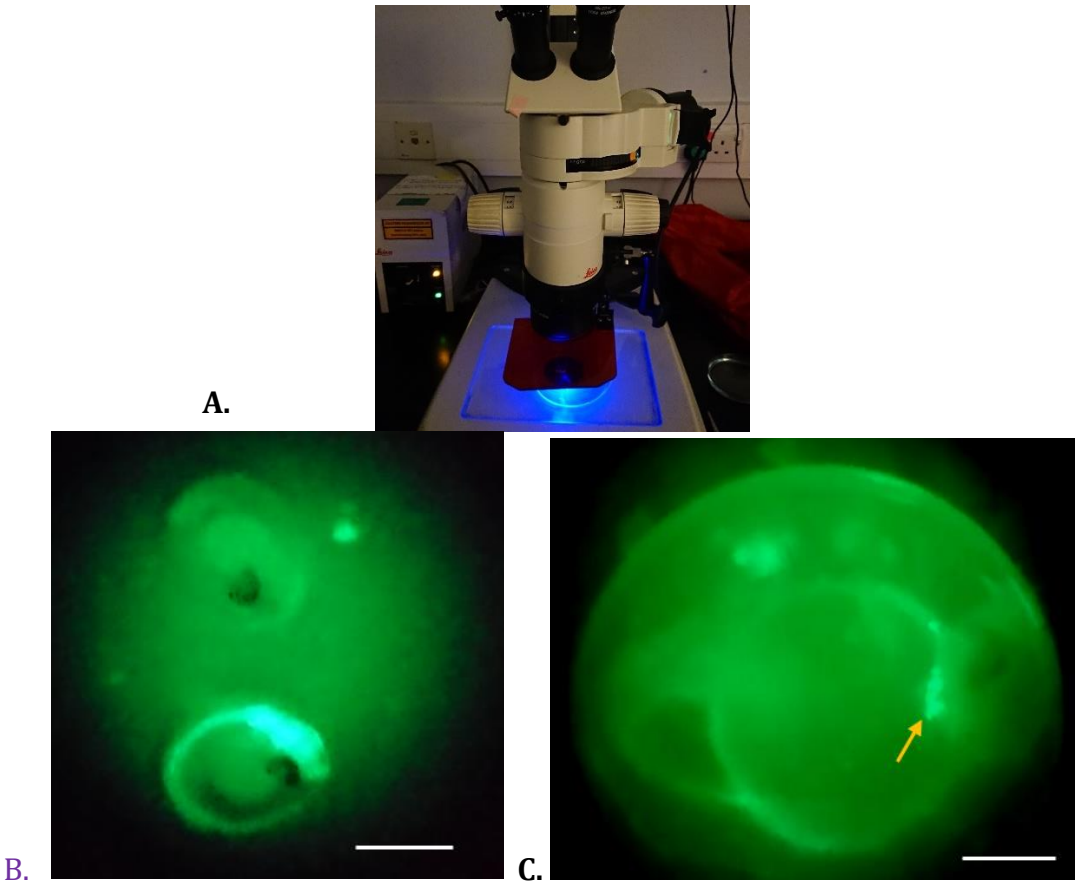

Figure 2.2 GFP+ nacre GCAMP3 zebrafish vs nacre only. (A) *Fluorescent Stereoscope used for sorting transgenic fish.* **(B)** *Stereoscopical image from two zebrafish embryos NBT:GCaMP3 36hpf. Above: nacre GFP negative and below expressing GCAMP3 under the pan-neuronal promoter elav3. Scale bar: 5mm.* ***(C)*** *Fluorescent image from a isl2b:SyRGeCO ZF embryo expressing clmx2 (cardiomyocytes specific) GFP+ (yellow arrow). Scale bar: 2mm*

2.1.2 Novel environments

Additional to the normal raised fish, some of the experiments (Chapter 6) were done using subjects raised in two different types of novel environments. A set of experiments were performed with fish which were wrapped in all walls by either a grey or striped background mimicking a 0 and 100% contrast situation (Figure 2.3). Due to these differences, we named the different groups according to these raising conditions as described in Table 2.

Figure 2.3 Novel environments. *The novel raising environments consisted of normal aquarium-approved tanks wrapped with opaque paper attempting a 50% contrast environment (left) and a medium frequency 100% contrast black and with stripes (right).*

Groups	Condition
Normal Raised (NR)	Fish raised under normal aquarium conditions in a transparent tank in the Tecniplast system as described in Section 2.1
0% Contrast Raised (0CR)	Fish raised housed in groups of no more than 20 fish in a tank surrounded by a grey background.
100% CR (100CR)	Fish raised in a tank wrapped in a background with 100% contrast static stripes. (Figure 2.3)

Table 2. Fish Groups according to their different raising conditions.

2.2 Behavioural experiments

We performed two main types of behavioural experiments, the visual lateralisation novel object recognition (VLNOR) test and the traditional simple novel object recognition (NOR). In total, we performed six different sets of experiments with the principle of VLNOR in a free-swimming environment with variations (See Table 3).

2.2.1 Experimental setup

For these experiments, we used different behavioural tanks in the search for optimum performance. First, we used modified tanks provided by the aquarium team. Then, two custom 3D printed tanks were made with opaque white walls to diffuse the light evenly into the chamber while avoiding external disturbances to the fish, and its own reflection.

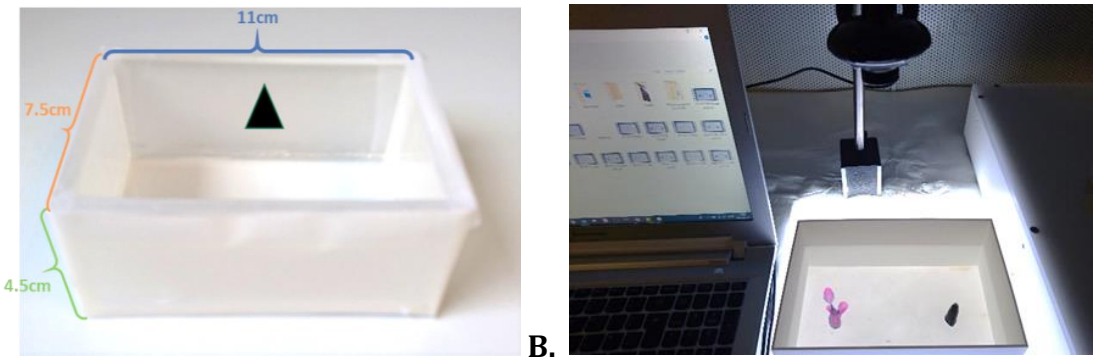

A. **B.**

Figure 2.4 Setup and measurements of the custom-made arenas used for behavioural experiments. (A) *First imaging chamber used for smaller fish with a 2D black triangle as a novel object* **(B)** *Custom-made setup of camera and light with an arena containing two different 3D objects. The size of the big tank is: 18(L) x 12(W) x 9(H).*

One of the tanks was bigger than the other and were used depending of the fish age since the size of the ZF changes significantly during their early stages of development. The outer measurements of the small behavioural tank, mostly used for the VLNOR experiments were 11cm (L) x 7.5cm (W) x 4.5cm (H) (Fig 2.4-A). The size of the big tank was 18cm(L) x 12cm(W) x 9cm(H) (Figure 2.4-B). The tanks were filled with water from the Tecniplast aquarium. In all cases, the fish were allowed at least 15 minutes of acclimation/habituation period first, and all phases were recorded using either the Viewpoint Zebrabox system or later, a custom made videocam system.

2.2.2 Visual Lateralisation Novel Object Recognition (VLNOR) Test

For the VLNOR test, we based our experiments on work previously described by (Andersson, Ek, & Olsson, 2015a). We used zebrafish larvae between 10-21dpf since it is a suitable stage in the development regarding exploration and the 3D-printed arena described above. The fish behaviour was compared in different setups where the position of the 3D object in the arena was changed to assess whether variability produced a significant difference in the outcome. (Fig 2.5-A).

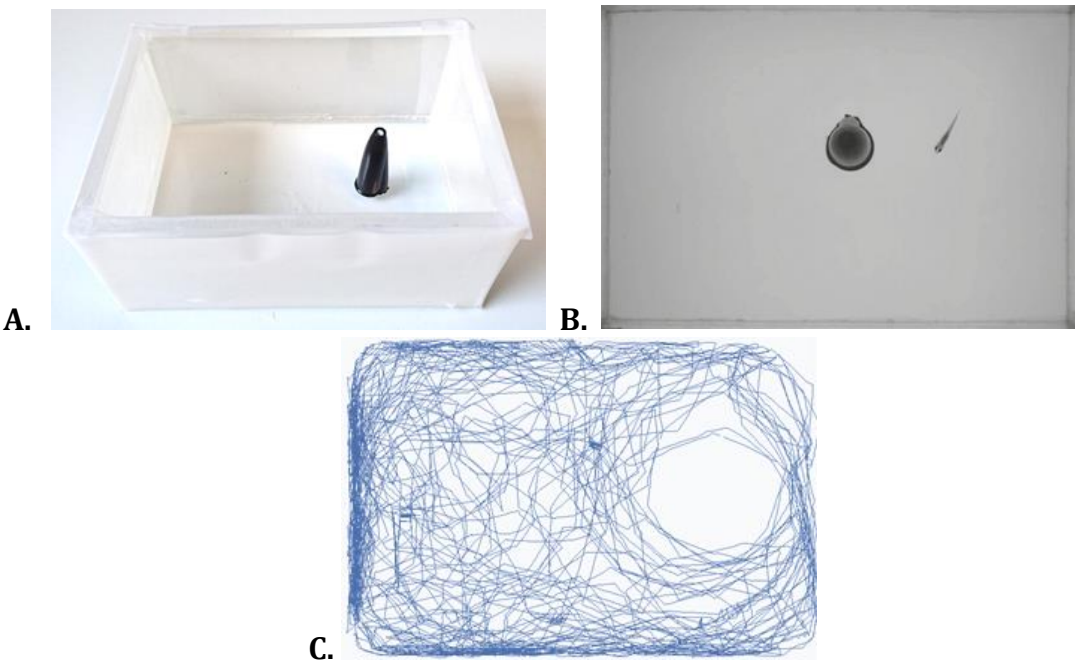

Figure 2.5. VLNOR experiment set up with a black object on one side. (A) *Basic set up of the Novel object Recognition experiment in zebrafish larvae using a 3D object placed on one side of the behavioural tank.* **(B)** *Representative outcome after 30 minutes of familiarisation recorded with the zebrafish ViewPoint software.*

Since the aim of the VLNOR test assess the exploration of novel objects in relation with the most used eye, the protocol followed consisted of 15 minutes of familiarisation period, followed by 30 minutes of familiarisation where the novel 3D object was immediately introduced on one side or in the middle of the tank (Fig 2.5-A-B), and then the behaviour was recorded from the top and plotted in lapses of 5 minutes (Fig 2.5-C)

We assessed the configuration of the path trace on 11-16dpf WT and NBT: GCaMP3 zebrafish. The rationale behind using GCaMP fish was to know if there were any significant differences in behaviour related with the genetical strains. The first set of

experiments consisted in habituation of the fish (no objects) for at least 1 hour the day prior to the familiarisation with a 2D object (black triangle) stuck from outside in between the opaque wrapping of the tank on one of the larger sides for at least 1 hour (Fig 2.4-A). Then, we decided to study whether this behaviour persisted when introducing 3D objects (See Fig 2.4-B).

Experiment	Summary of description
Set 1	Black 2D black triangle stuck to one larger side of the tank
Set 2	Black 3D pen lid same place as the novel object of set 1
Set 3	Black 3D Object placed on one half of the tank
Set 4	Black 3D object in the centre of the tank
Set 5	Violet flower as a novel object in the middle of the tank
Set 6	Green leaf as a novel object in the middle of the tank

Table 3. Different configuration sets to study VLNOR.

The first 3D object was a black pointed pen-cap placed in the same location as the novel triangle (Fig 2.4a). For the following setups, the novelty was introduced immediately after acclimation. The third and fourth setup was done to assess the patterns of exploration by introducing the same black 3D object in two different locations. One set of experiments consisted of placing the novel object on one side of the rectangular tank, whereas the other set of experiments was with the object in the middle of the tank respectively. These experiments were performed on 17-21dpf WT and GCaMP3 ZF (See Fig 2.5). Further particulars from each of the pattern exploration assessments and the reason behind the methods will be discussed in further detail on chapter 3.

Finally, the fifth and sixth sets of experiments were done using two different 3D objects placed in the middle of the tank (Table 3). One object was a violet flower and the other a green leaf, respectively. Here, 19 to 21dpf WT and GCaMP3 ZF were used (Fig 2.6). These objects were thought to assess novelty mimicking a more natural 3D object. Here we performed VLNOR analysis and then traditional NOR test.

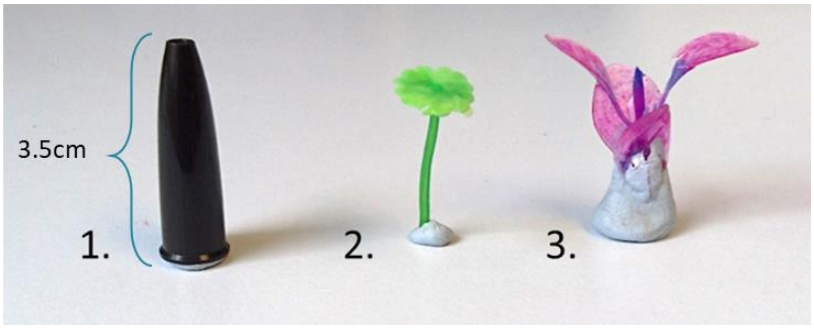

Figure 2.6 3D objects used for the traditional NOR memory experiments: *1. Black pointed object, 2. Green leaf, and 3. Violet flower, respectively. And the objects both are 3.5cm(h), the black pen lid is1.5 cm diameter whereas the flower has 3.5cm in diameter.*

As previously stated, the first set of experiments consisted of two phases, a period of habituation and then a familiarisation period using a 2D object (black equilateral triangle 1.5cm per side) and recorded the top view of the tank for analysis using the Viewpoint Zebrabox (The University of Sheffield). In this case, the habituation period (no object) given was 30 minutes, and then we left the fish 24 hours of resting period where we placed the fish back into normal aquarium conditions in individual tanks to keep control before the next phase. During the Familiarisation stage, we placed the fish in the tank now containing the black 2D triangle and recorded for at least 15 minutes (Fig 2.7).

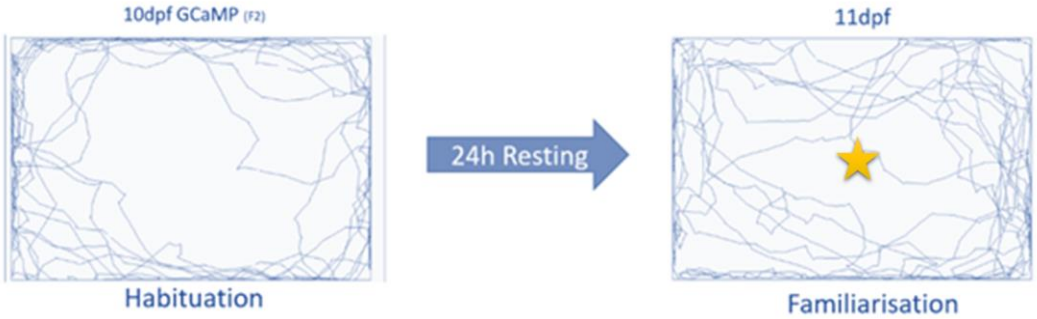

Figure 2.7. Setup of behavioural experiments with 3D Novel Object. Top view of the path trace given by an individual fish during habituation and familiarisation phases with 24 hours of resting period. The yellow star represents the location of the object.

2.2.3 Traditional Novel Object Recognition (NOR) Test

Traditionally, the novel object test requires at least 2 objects and is divided into three phases. First, the habituation is when the animal is freely allowed to explore the area in

the absence of objects (Randlett et al., 2019a). Then in the familiarisation phase, one or two identical objects are introduced and finally, the test phase when a novel object is included for the animal to explore (Antunes & Biala, 2012). The assessment of behaviour is done comparing the time-lapse occurred during the exploration of the novel object against the familiarised one. Subsequently, we used three different pairs of 3D objects of the same height but varying in colour and shape (Fig 2.6). In order to assess the reproducibility of this test, we decided to mimic the conditions as much as possible with previous reports (Leighton et al., 2018; May et al., 2016a).

In the set of experiments where we used the 3D objects, the fish was first allowed to swim freely in the arena without any objects (habituation period) for 10 minutes. Then, two similar objects randomly selected between two pink flowers, or two black pen lids or green leaves were introduced for the fish to familiarise for 10 minutes. We followed the familiarisation with a resting phase of 5 minutes without any objects to allow the fish to swim freely again before the testing phase, where we introduced a familiar along with a new one, randomly selected between the flower and the pen lid accordingly.
The experiments were recorded using a customised video recording setup (Fig 2.4-B), and then we acquired the coordinates from the top view and plotted them on Igor Pro (Fig 2.5). The preference index (PI) was calculated by the time spent in frames on one side of the arena divided by the total number of frames.

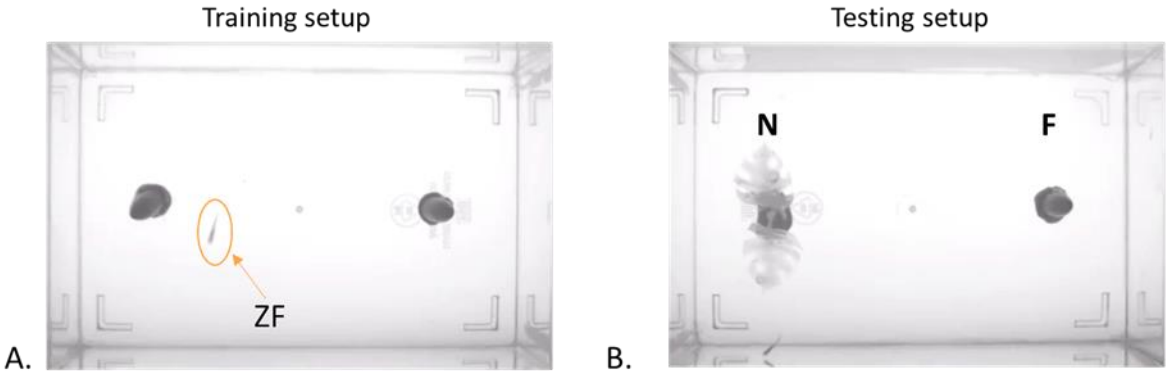

Figure 2.8 Novel object Recognition test. (A) *Training setup where two identical objects are placed.* **(B)** *Testing setup where one of the objects is changed into a novel one.*

2.2.4 Data Analysis

All videos were analysed using a custom-written code for Python (version 3.7.1, 64-bit) with Spyder (version 3.3.2) and OpenCV (version 3.4.1) to get the coordinates and the

angle position of the fish per frame (25fps) on .txt format. Additionally, some experiments were processed by a tracking-software through a temporal full licence trial to the University of Sheffield (Ethovision). Then, the data were plotted and analysed through a combination of Excel and custom-written scripts for Igor Pro (Wave Metrics). Finally, all statistical analysis was done using GraphPad Prism (version 7.04).

Some of the particulars related with the analyses of the VLNOR tests will be discussed in more detail in Chapter 3.

2.3 Whole mount in situ hybridisation

Whole-mount in situ hybridisation (WISH) was done following the protocol published by Thisse & Thisse, 2008. For protocol optimisation, we first achieved in situs on zebrafish embryos between 24hpf to 3dpf old previously treated with 20mM of the GABA antagonist pentylenetetrazole (PTZ) for 30-60 minutes and the DNA probes used were *c-fos*, *bdna* and *Stxbp1 since these were the markers of brain activity available* (Fig. 4.1 from Chapter 4).

2.3.1 Synthesis of antisense RNA c-fos probe

The c-fos DNA plasmid vector (pBK-CMV, GenBank: CF943701) was kindly given by Dr Vincent Cunliffe at a concentration of 1ug/µL (Fig 2.9).

Then, we proceeded to perform a restriction enzyme digestion using either Bam HI or SpeI restriction enzymes (Table 43).

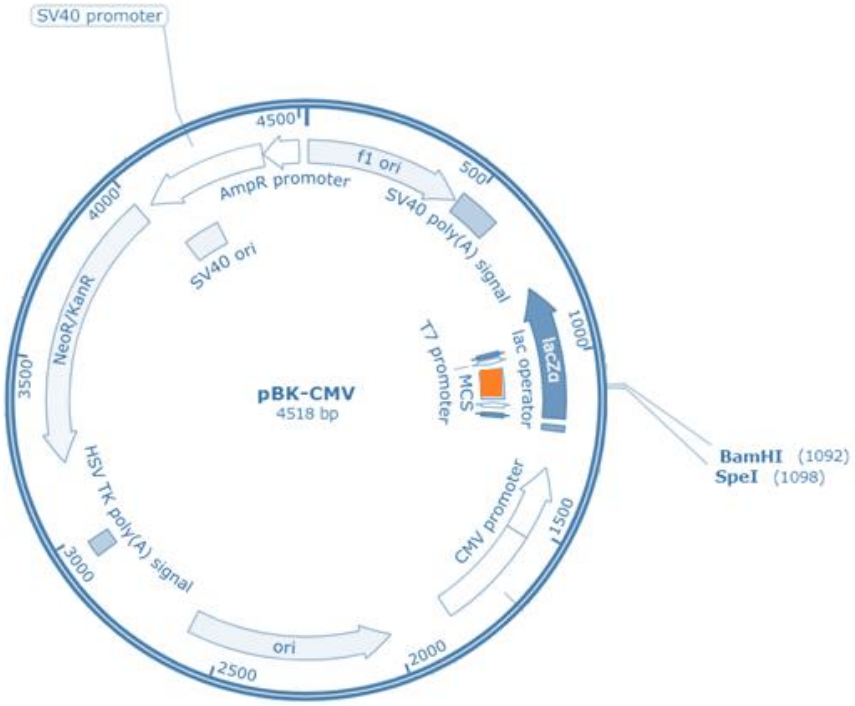

Figure 2.9. Map of the pBK-CMV plasmid. *Sequence Author: Agilent Technologies. In orange is shown the multiple cloning site (MCS), the region where cfos was inserted. Map modified from Snap gene.*

Reagent	Volume
c-fos DNA (160ng/µL)	6.25µL (1ug)
CutSmart 10X	5µL (1X)
SpeI or BamHI	1µL
Nuclease free water	37.75µL (up to 50µL)

Table 4. Reagents needed for the restriction digestion with SpeI or Bam HI. The preparation was incubated at 37°C for 15 minutes, and then the enzymes were inactivated at 80°C for 20 minutes.

After obtaining the linearised plasmid, we used a Nanodrop spectrophotometer to measure the concentration and purity of the linear DNA. For this, we previously calibrated the equipment with 1µL of nuclease-free water as blank, after which we placed 1µL of our DNA sample. Then, we proceeded to the DIG-labelling and in vitro transcription to produce c-Fos Digoxigenin-labelled RNA probes (Table 5).

Reagent	Volume
Transcription buffer	2µL
1ug of linearised DNA	X (In this case 1µL)
Dig RNA labelling mix	2µL
RNAseOut	1µL
RNA polymerase	2µL
Milli Q H2O	13µL – X (In this case 12µL)
Total volume	**20µL**

Table 5. DIG-labelling mix volumes. These reagents were mixed and then incubated at 37°C for 2 hours to allow in vitro transcription.

After the transcription reaction, we added 3µL of RNase-free DNase I and incubated at 37°C for 30 minutes (this volume depended on the quality of the DNase I; usually 1µL is enough). Then, we column precipitated using the QIAGEN Purification RNA clean-up following the protocol advised by the manufacturer.

Firstly, we adjusted the sample volume to 100µL with RNase-free water included in the kit. Then added 350µL of Buffer RLT and 250µL of Ethanol (96-100%) to the diluted RNA and mixed by pipetting. This sample (700µL) was then transferred to an RNeasy Mini spin column placed in a 2mL collection tube. Then, centrifuged for 15 seconds at > 8,000 x g and discarded the flow-through. Subsequently, we added 500µL of Buffer RPE to the RNeasy spin column, closed the lid and centrifuged for 15 seconds at >8,000 x g to wash the membrane, and discarded the flow-through. Another 500µL of Buffer RPE was added and centrifuged at the same speed to wash the membrane for two minutes, and afterwards, the column was placed in a new collection tube for final centrifugation by its own for 2 minutes to remove any excess left. Finally, the column was placed in a new sterile Eppendorf 1.5mL collection tube and added 30µL of RNase-free water, being careful to add this volume right in the middle of the membrane. To test the quality of the yielded *cfos* probe, we ran in an agarose gel at 1% (80mL TAE + 0.8g agarose + ethidium bromide) and then ran 1µL of the RNA with Loading dye and 4µL of Milli-Q water along with a 1kb ladder for 20 minutes at 120 mV.

2.3.2 Sample preparation

Zebrafish under 5dpf were dechorionated if needed and fixed using Fix Fish solution containing paraformaldehyde (Table 6) and 0.1M PO buffer (Table 7). Fish above 5dpf

was submerged in 100% tricaine solution for instantaneous culling and immediately followed submersion in fix fish. In all cases, the fixative solution was left rocking overnight at 4°C.

Reagent	Volume/Mass
0.1M PO buffer	25mL
1M $CaCl_2$	3µL
PFA powder	1g
Sucrose	1g

Table 6. Fish Fix solution. Reagents used to make 25mL of 1X concentration stock.

These were mixed by applying heat up to 65°C. This solution was stored at 4°C.

Solution	Volume
H2O	100mL
NaH2PO4	20mL
Na2H2PO4	80mL
Total	**200mL**

Table 7. 0.1 M PO buffer (Contents for a 0.1M stock)

In all cases, the paraformaldehyde solution was removed no later than 20 hours. After this time, we proceed to remove the pigment from the skin by changing the fish fix with bleaching solution (Table 8) to allow better visualisation of the probe. The bleaching solution was changed at least twice per tube depending on the fish strain and developmental stage. Usually, a nacre zebrafish required around 20 minutes of immersion to remove pigmentation thoroughly. It is possible to use wild-type zebrafish at 21 dpf but require a longer immersion time and change of the bleaching solution at least three times every 20 minutes to entirely remove the pigment. After this, we did a series of dilution washes using a solution of PBS with MeOH 50:50 two times for 20 minutes followed by two washes of MeOH only for five minutes before storing the samples at -20 °C until the hybridisation protocol.

Solutions	Volume
PBS	40mL
30% H2O2	5mL
5% KOH	5mL
Total	50mL

Table 8. Bleaching Solution (for use before hybridisation)

2.3.3 Generation of positive controls of neural activity

Pentylenetetrazole or $C_6H_{10}N_4$ (PTZ) is a chemical convulsant which acts as an antagonist of the gamma-aminobutyric acid (GABA) A receptors (J. Liu & Baraban, 2019). The seizures induced by the exposure of PTZ produce an increased expression of synaptic-activity dependent Immediate Early genes (IEG) such as *cfos* (Minatohara et al., 2016a). In these experiments, we used 20mM of PTZ to induce a pan-neuronal activation as a positive control of c-fos expression, under most protocols published (Baxendale et al., 2012a). After successfully acquiring positive and negative controls of c-fos WISH in fish under 5dpf, this technique was further tested in fish of 8, 15 and 21dpf. Since there are no protocols available regarding late-stage zebrafish, the same concentration was used, and the effect assessed by observation over time.

For instance, it was found that younger fish (>3dpf-8dpf) can last up to 2 hours before entering a tetanisation stage, whereas fish between 15-22dpf required less than 60 minutes. In all ages, we found that 40 minutes is a suitable window time for exposure to the concentration of this drug to produce the expected c-fos expression. After PTZ exposure, fish were immediately culled according to Home Office regulations and fixed in the paraformaldehyde solution mentioned before. Negative controls were culled and fixed the same way. The next day, the fixation solution was changed into methanol through a series of washes to store the samples at -20 °C.

The main steps of the in-situ hybridisation were performed in three consecutive days. To optimise the protocol according to our needs, we did slight modifications to the protocol from Thisse & Thisse, 2008:

Day 1

The first day, we did a series of washes to slowly rehydrate the embryos, changing the -20°C methanol into phosphate-buffered saline (PBS) solution with 0.1% Tween 20 (PTW) at room temperature (RT). The first wash was done with PBS/MeOH 50:50 by manual pipetting in the Eppendorf tubes and then put in a rocking platform for 5 minutes. Afterwards, we used PTW to wash four times at room temperature, also for 5 minutes each time. Then we incubated the embryos in 10ug/mL of Proteinase K in PTW at RT with different timings depending on the developmental stage of the zebrafish (Table 9).

Developmental stage	Proteinase K incubation time
24 hpf	10 min
48 hpf	20 min
3 dpf	25 min
4 dpf	30 min
5-21 dpf	40 min

Table 9. Proteinase K incubation times.

Proteinase K allows the probe to enter the cells at the cost of softening the tissue. Therefore, after the incubation, we immediately re-fixed the samples with the Fix fish solution (Table 6) at room temperature for 20 minutes, and then washed five times with PTW for five minutes each time. Then, we rinsed each Eppendorf tube containing the samples with 400uL of hybridisation solution lacking tRNA and heparin (Table 10), and pre-hybridised with other 400uL of hybridisation solution for three hours at 65 °C. Finally, we hybridise overnight with the solution containing heparin and tRNA (Table 10) and adding the DIG-labelled cfos probe in a 1:200 dilution at 65 °C previously heated for 10 minutes to avoid temperature shock.

Reagent	Volume
Formamide	25ml
20X SSC	12.5ml
dH2O	10ml
tRNA (25mg/ml) *	1ml
Tween 20 (10% IN H2O)	0.5ml
1M citric acid	0.46ml
Heparin (50mg/ml) *	50ul
Total volume	**50mL**

Table 10. Contents of the hybridisation solution. Heparin and tRNA (starred) were used in the incubation overnight only.

Day 2

The second day we first changed the hybridisation solution slowly into 0.2% saline-sodium citrate (SSC) buffer with a series of dilutions that were previously heated at 65 °C. The first dilution was done with 50:50 Hybridisation solution with 2X SSC and incubated at 65 °C for 20 minutes. Then, the solutions were changed 20 minutes with 2X SSC followed by two dilutions of 0.2X SSC left for 60 minutes each at 65 °C. The next

washes were done at room temperature to slowly change the solution into the blocking solution (PBT) (Table 11). The blocking solution needs to be fresh every time.

Reagent	Quantity
PBS	48.5mL
Sheep Serum	1mL
10% Tween-20	0.5mL
BSA	100mg

Table 11. Blocking solution (PBT). PTW with 2% sheep or goat serum and 0.2% BSA.

The first was with a 50:50 dilution of PBT with 0.2 SSC for 10 minutes, then PBT only for 10 minutes and then left blocking with more PBT for 1-3 hours at RT. Finally, the samples were incubated overnight in a gentle shaking at 4 °C in 1mL of PBT containing anti-DIG at a concentration of 1:2000.

Day 3

The last day we slowly exchanged the blocking solution (PBT) into PTW at room temperature through a series of six washes of 20 minutes each and then proceeded with the staining step. For this, the embryos were transferred into 6-12 well plates (depending on the number of samples) labelling each well accordingly and adding 1-2mL of staining buffer (Table 12). The staining solution was made fresh for every in situ and carefully changed four times every 10 minutes and equilibrated in a rocking platform.

Reagent	Volume
dH2O	40.75ml
1M Tris pH 9.5	5ml
1M MgCl2	2.5ml
5M NaCl	1ml
Tween 20 (10%)	0.5ml
Total	**50mL**

Table 12. Staining buffer.

Subsequently, we added 4.5ul/ml of nitro-blue tetrazolium (NBT) and 3.5ul/ml of 5-Bromo-4-chloro-3-indolyl phosphate (BCIP) and let the well-plate to stain in the dark until developed, checking after the first 30 minutes and then every 10 minutes if needed under the microscope to avoid any possible background staining. The staining development usually took around 45 minutes after which we stopped the staining by adding PTW and washed at least three times for at least 5 minutes each time. Finally, we

fixed the embryos with fish fix solution (Table 5) overnight at 4 °C. We stored the embryos in the fish fix until mounting and imaging.

2.3.4 Fluorescence WISH.

The research regarding the development of protocols to produce high-quality whole-mount in situ hybridisation in late-stage zebrafish larvae has been under-reported since it is considered to be challenging to achieve (Wu et al., 2018). Therefore, it is not surprising that the fluorescent version (FWISH) is not used in this developmental stage and even for some, the thought alone might produce scepticism (Chatterjee, Tran, Shams, & Gerlai, 2015). Therefore, there is no clear literature available, and we decided to optimise the protocols available according to our needs.

In general, the steps to follow were very similar to the traditional WISH with NBT/BCIP. The main differences rely upon the use of the Fluorescein-labelling NTP mix (Roche cat# 11685619910) instead of Digoxygenin to label the probe when doing the in vitro transcription (Table 13), and the secondary antibody should be Anti-Fluorescein peroxidase conjugate (POD) (Invitrogen cat# A-21253) for detection of the fluorescein-labelled probe during the second day of the protocol.

Reagent	Volume
Transcription buffer	2uL (10X)
1ug of linearised DNA	1-2uL
Fluor NTP labelling mix	2uL
RNAseOut	1uL
T7 RNA polymerase	2uL
Milli Q H2O	13uL – X (In this case 12uL)
Total volume	**20uL**

Table 13. Reagents needed to produce Fluorescein labelled probe. These reagents were mixed and then incubated at 37°C for 2 hours to allow in vitro transcription.

Similarly, to traditional WISH, after the transcription, we stopped the reaction by adding 2uL of DNase I followed by 15 minutes of incubation at 37 °C. Then, we column precipitated using the QIAGEN Purification RNA clean-up following the protocol advised by the manufacturer (Chapter 2.3.1). The Fluorescent labelled probe was then suspended in nuclease-free water with 1uL of RNase inhibitor at -20 °C until use. The collection and preparation of the samples were performed, as described in chapter 2.3.2. We used fish fix solution (Table 6) to fix embryos overnight at 4 °C and the

following day did a series of methanol dilutions to store the samples in 100% methanol at -20 °C until the first day of in situ.

Day 1

The rehydration of the embryos used for the FWISH was done through a series of dilutions of methanol with PTW (75%, 50%, 25% methanol, with PTW) washing five minutes each time. We followed with four more washes of five minutes each with PTW only and then proceeded to the treatment with proteinase K 1ug/mL /PTW to increase the cell permeability allowing the probe to enter. The timings followed were the same as cited in Table 9. After this, the proteinase K was removed by washing twice in PTW, for five minutes. Then, we re-fixated the embryos in fish fix (Table 6) for 20 minutes and washed again with PTW five times (five minutes each time) to remove any leftover from the proteinase K and fixative solution. All these washes were done at RT over a rocking platform.

After rehydrating and permeabilising the samples, we replaced the PTW with the pre-hybridisation solution (Table 10) and incubated at 68°C in a heat block for 3-4 hours. Then, we replaced the pre-hybridisation solution with fresh pre-hybridisation solution previously heated at 68 °C, just enough to cover the embryos (200uL usually) and added no more than 200ng of the Fluorescein-labelled probe to each sample. Finally, we hybridised overnight at 68 °C.

Day 2

The probes were removed, labelled, and stored at -20 °C for reuse up to three times. We then washed the samples with a series of solutions containing SSC, formamide and Tween-20 in different proportions 5X, 2X and 0.2X (See table 14), previously heated at 68 °C.

Reagent	5X Volume	2X Volume	0.2 Volume
Formamide	100mL	-	-
20X SSC	50mL	40mL	4mL
20% Tween-20	2.5mL	5mL	5mL
dH2O	47.5mL	355	391mL
Total	200mL	400mL	400mL

Table 14. Contents of the post-hybridisation solutions for FWISH. All these solutions were prepared as stock. 5X solution was stored at 4 °C and the others at room temperature.

These washes were done for five minutes over a rocking platform previously heating the solutions at 68 °C. The first wash was done with 5X and the next three with dilutions of 5X:2X as follows: 3:1, 1:1, and 1:3. Then one more wash of 2X only for five minutes, followed by three washes of 0.2X SSC, 20 minutes each at 68 °C. The next two washes were done at room temperature with PTW for 10 minutes each, and then we replaced the solutions with 2%H2O2 in PTW and agitated for an hour at RT. Afterwards, we rinsed four times with a TNT solution containing 0.1 M Tris adjusted to pH 7.5 with hydrochloric acid, 0.15 M NaCl, and 0.5% Tween20 (Table 15), five minutes each time.

Reagent	Volume
Tris pH 7.5	100mL
5M NaCl	30mL
20% Tween-20	25mL
dH2O	845mL
Total	**1L**

Table 15. TNT Stock solution for FWISH. This solution was stored at room temperature.

Then we proceeded to block the embryos in a solution containing TNT with 0.5% Perkin-Elmer Blocking powder (TBSTB) (See table 16) for 3-4 hours at room temperature over a rocking platform (usually 400uL per tube). Then we replaced this solution with fresh pre-absorbed 1:5000 anti-Fluorescein-POD in TBSTB solution and shaken overnight at 4 °C.

Reagent	Quantity
TNT (See table 13)	50mL
Perkin Elmer Blocking Powder	0.25g
Total	**50mL**

Table 16 TBSTB Stock solution for FWISH. In order to get a full dissolution of the powder is necessary to mix and heat at 68 C for one hour. This solution was aliquoted and stored at -20 °C.

Day 3

During the last day of FWISH, we washed eight times over 2 hours in TNT at RT. Then, we washed in 50uL of Perkin Elmer Amplification diluent for five minutes. Afterwards, we replaced the amplification diluent with 50uL of 1:50 Tyr-Fluorescein and shake the tubes upright in the dark (wrapped in aluminium foil) for up to an hour. This time must not exceed to avoid background staining. Keeping the samples in the dark, we washed twice with TNT for 5 minutes each time and then shake for an hour in 2% H2O2 in TNT (this step was found to improve the signal to noise ratio. Finally, the embryos were washed four times in TNT for five minutes each before being stored in fish fix (Table 6) solution at 4 °C until imaging, since staining lasts several months under these conditions.

2.3.5 Mounting and Imaging

The process of mounting the embryos consisted of first removing the fixation solution where we stored the samples at 4°C. Additionally, we dissected the upper dorsal half of the fish, removing the chorion to facilitate mounting carefully exposing the brain. The dissection was done as fast as possible under dry conditions over the lid of a petri-dish to improve handling avoiding dehydration. The tools we used were fine surgical forceps (No. 5) and a surgical non-sterilised scalpel (No. 15) after a second rinse with PBS under the microscope. After dissecting, we proceeded to carefully rest each sample in a series of droplets containing different dilutions of glycerol in PBS, five minutes per dilution (25, 50, 75 and 100%). After the last dilution of Glycerol, we carefully took the sample with a point metal stick and placed in the microscope slide under microscopy visualization to orientate and place in the desired position prior to carefully cover with a coverslip. Finally, we imaged the samples in a Nikon stereoscopic microscope.

2.4 Multiphoton calcium imaging

The zebrafish strains used for the two-photon microscopy experiments were NBT: GCaMP3 (5-21 dpf), Huc: GCaMP6 (3-10 dpf) and isl2b: SyRGeCO larvae zebrafish (8-14dpf). The following experimental setup served as a basis for experiments performed for Chapters 5 and 6.

2.4.1 Calcium imaging

Initially on this PhD project, I used an Olympus confocal microscope (FV1000, Tokyo, Japan) available at The University of Sheffield Wolfson Imaging facility as part of the preliminary experiments for chapter 5 and 6. All of these experiments were done using NBT: GCaMP fish (12-21dpf) using a 40X LUMPlan/Water objective (NA 0.8). Most of these experiments were then replicated using multiphoton microscopy described next (Figure 2.11).

The two-photon *in vivo* recordings were acquired using a custom-built Bergamo II System laser-scanning microscope at Walter Marcotti's lab, from Thorlabs Inc. (Newton, NJ, USA). (Figure 2.11-A). Here I used all the zebrafish strains expressing calcium indicators mentioned in Section 2.1.1 of this chapter. The laser was used at a 925nm with a pulsation repetition rate of 80-MHz regulated with a Mai Tai HP/Deep See system from Spectra-Physics (Malpitas, CA, USA). The photomultiplier was a GaAsp-Hamamatsu (Hamamatsu City, Japan), coupled with a bandpass filter of 525/40 type FF02-525/40-25, from Semrock (Rochester, NY, USA). (Ceriani, Pozzan, & Mammano, n.d.).

Depending on the age of the fish and the desired planes for each experiment the objectives used were either LUMFLN 25XW, 40XW or 60XW (NA 1.1) from Olympus (Tokyo, Japan). The sampling rate for strains expressing GCaMP3 and GCaMP6 signals were 15 frames per second (fps), and the resolution was 512 x 512 pixels per plane, using the green calcium channel. For fish expressing red calcium signalling (SyRGeCO), we used the red calcium channel, and the resolution was decreased to 256 x 256 pixels in-plane and the sampling rate was increased to 117fps to compensate for the noise created by the notch-filter to block for any possible red-light waves from the environment projecting into the screen. All these imaging specifications will be stated in the correspondent sections of this thesis.

2.4.2 Experimental setup

The projector used for the experiments in Chapters 5 and 6 (Figure 2.11-B) was an Optoma DLP Pico Projector PK320 (Watford, UK), and the refresh-rate used to present the stimuli was 60Hz. The distance between the projector and the imaging chamber was

maintained at 19cm to ensure full coverage of the screen and the resolution was adjusted accordingly.

For the projection of visual stimuli to the fish expressing GCaMP, a notch filter HQ620/60x (Fig 2.11-C) was placed on the projector lens which targets the screen of the imaging chamber to avoid any green light waves to interfere with the 2-photon recording, thus creating a red background. To avoid red-light to scatter into the recording of the ZF expressing RGeCO, a notch filter NF488-15 from Thorlabs Inc. (Newton, NJ, USA) was placed instead, thus generating a blue background in these experiments.

A. 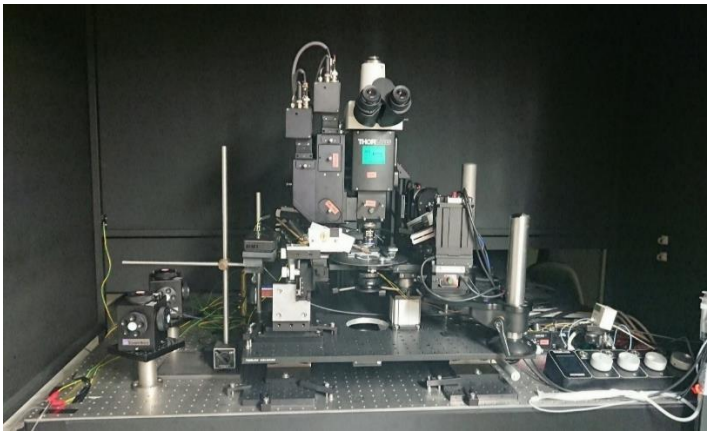 B. 

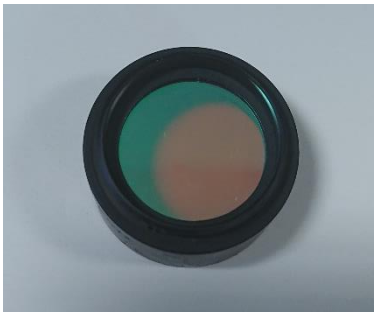

C. 

D. 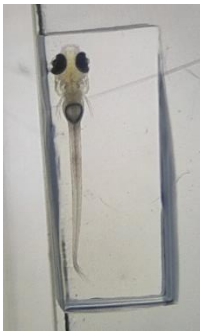

E.

Figure 2.11 Two-photon general experimental setup. (A) *Custom-built two-photon microscope (Thorlabs). Note the microscope at the left side of the setup* **(B)** *Projector used for the application of the visual stimuli* **(C)** *Notch band-pass filter* **(D)** *Imaging chamber used to mount the fish with glass slide attached by magnets and a squared plastic coverslip.* **(E)** *Top view of ZF larvae mounted in agarose.*

For the imaging setup we used a customised rectangular imaging chamber with a screen on one of the long sides. The chamber fabrication was done by the University of

Sheffield CBE workshop (from Perspex) and had the following measurements: 90mm (L) x 70mm (W) x 15mm (H) and a wall thickness of 3mm (See figure 2.11-D). Overall, the experimental setup was done based on Bergmann et al., 2018 with appropriate modifications to be used in late-stage zebrafish fry (up to 21dpf). The screen located in one of the sides was manually fitted using a diffusive filter paper by Rosco EMEA, Cinegel #3026 (London UK); the remaining walls were covered in black insulation tape to prevent from any reflection or any other visual stimulus. A black cardboard was added to fit in between the chamber and the objective to enhance the attention on the screen area only.

2.4.3 Fish preparation

Fish preparation was done according to their age. Fry between 3-10 dpf were mounted using 2.5% low-melting point (LMP) agarose from BioGene, (Huntingdon, UK), whereas ZF between 11-21dpf the LMP agarose concentration was of 3.5% to avoid any possible movements from the awake fish (Figure 2.11-E). Additionally, in these fish the imaging solution was prepared to increase the saturation of oxygen surrounding the fish during the experiment. The imaging solution consisted of aquarium water previously filtered using a Whatman filter paper Grade 1 from GE Healthcare UK Limited (Little Chalfont, UK). For fish above 11dpf, the oxygen saturation of the imaging solution was increased through the addition of $NaH2PO2$ (1.2mM), and $NaHCO3$ (23mM) and posteriorly aerated for at least 30 minutes with a mix of $O2$ (95%) and $CO2$ (5%). This was done to improve the natural transdermal oxygen absorption. Additionally, to increase the oxygen supply the agarose was removed from the gills of fish above 18 dpf on one of the sides as done by Bergmann et al., 2018.

In all cases the larvae were mounted in a dorsal position, so that the view from the objective was from the top, and for most experiments the fish was facing the screen with one eye only. This mounting was done over a plastic coverslip from Agar Scientific Ltd, (Stansted, UK), which was then attached to a glass slide using Bostik blue tack (Stafford, UK). The level of the eyes was measured to be placed at the middle of the screen width and the distance between the fish and the screen was fixed to 3.5 cm using magnets.

2.4.3.1 Focal plane

In all cases, the imaging point of view was done from the top. To always image the same region as accurate as possible, we took in consideration the width of the whole OT measuring from the top region where the first cell bodies start appearing. Then, the bottom was considered where the optic nerve is clearly visible after the optic chiasm. From these cues, we chose the first third top-to-bottom area. The second anatomical reference was the shape of the tectum. In this sense, we seek for the most even oval-shaped region where some blood vessels were visible. (Figure 2.12)

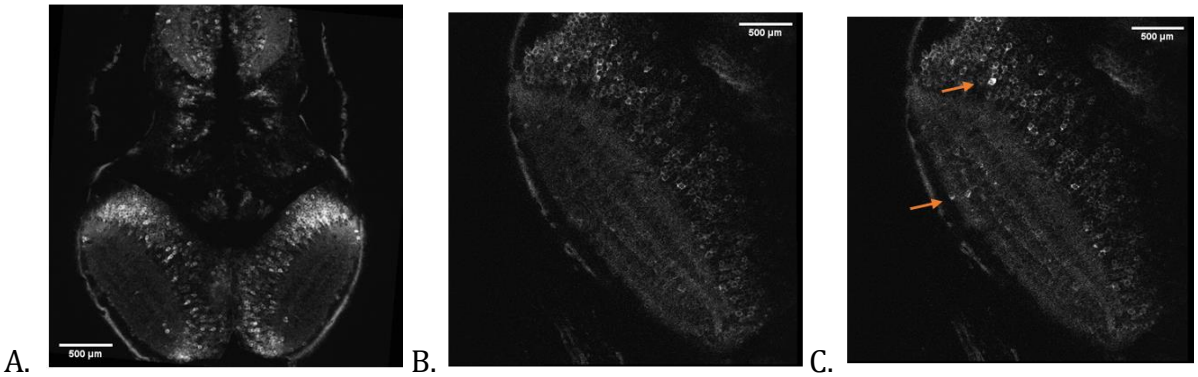

Figure 2.12 Focal plane of multiphoton microscopy. (A) Top view of a 14dpf NBT: GCaMP3 ZF whole brain using a 25x objective. **(B)** View of the tectal neuropil without stimulation and **(C)** during stimulation. Note the responding neuropil and responding PVN (orange arrows) This view was achieved with a 40X objective.

Is worth mentioning that in all cases we tried to expose the fish to 5 minutes of the laser to get the fish acclimatized to the environment and temper the agarose. We found that doing this process improved considerable the quality of the imaging and prevent the focal plane from changing in the z-axis or any other plane drastically.

2.4.3.2 Experiments in sleepy fish

To assess whether the adaptation process is not just a response to a light change and if a level of consciousness is required, we performed a set of experiments in fish that were induced to a light anaesthesia with Tricaine. In order to do this, we followed previous guidelines and set the minimal required tricaine dose needed to induce stage III by assessing the level of responsiveness (swimming activity stopped, loss of equilibrium, decreased muscle tone, decreased respiration and response only to strong tactile stimuli) (Zahl, Samuelsen, & Kiessling, 2012).

The same mounting methods were done and a sedative maintenance dose of tricaine was added to the imaging chamber. After the experiments fish was freed in aquarium water and were checked for full recovery from the anaesthesia.

2.4.3.3 GABA inhibited protocol

In Chapter 5 we explored the role of GABA in adaptation. For this we subjected the fish to the GABA inhibitor PTZ, used for WISH and FWISH protocols described in sections 2.3.3 of this chapter. Since we learnt that the effect of the PTZ is immediate and it does cross the blood-brain barrier, and the PTZ molecule is small enough to cross the porosity of the LMP agarose, it was decided to keep the same mounting concentration of 3.5% agarose and to add PTZ to the imaging chamber during the recording using a micropipette. After looking at different concentrations and measuring the time from the application of PTZ and the initiation of the increment in spontaneous activity *in vivo*, we decided that the most representative outcome was successfully achieved through the addition of 12.5mM of PTZ from a 1M stock and then recorded immediately without visual stimuli for 10 minutes. This time allowed for the agarose to set and to start identifying the rise in synaptic activity characteristic from the PTZ. Therefore, these experiments were recorded after around 12 minutes from the application of the GABA inhibitor.

2.4.3.4 Auditory Stimuli

To assess how adaptation works when pairing with an auditory stimulus, we used a fluid jet to generate a quick soundwave under the imaging water at enough pressure to produce a mechanosensory auditory response from the fish without generating any damage to the fish or movements on the setup. For pragmatism, we called the stimulus "puff" and was performed using a borosilicate glass micro needle pulled with a horizontal puller from Sutter Instruments Co., (Novato, CA, USA). These needles were then filled with imaging water and attached to a piezoelectric system which generated a pressure of around 3psi which was adjusted manually before the experiments according to the diameter of the glass micropipette aperture which diameter was kept between 2 - 4 um to ensure a steady and even pump. The needle was then placed guided by microscope at ~3mm from the ZF posterior auditory canal in an angular position between 35-60 degrees in relation with the length of the ZF.

2.4.4 Fate of the fish

All the adjustments described above allowed to image 14-21 dpf fish for up to 3 hours without further oxygenation required during the experiment. All fish were liberated, assessed for good motor reflexes, and culled immediately after the experiments according to the UK Home Office regulations under the Animals (Scientific Procedures) Act 1986 and approved by The University of Sheffield Ethical Review Committee.

2.5 Visual stimuli

All the visual stimuli were created using a customised code in MATLAB, The MathWorks, Inc (Natick, MA), using the open-source toolbox Psychophysics. To synchronise the beginning of the imaging with the onset of each stimulus, the initiation command was given through a Lab Jack via TTL pulse (Labjack, Co., Lakewood, CO). The distance between the projector lens and the opaque wall in which the stimuli were delivered was of 19cm, and the distance between the screen and the fish was 3.5cm (Figure 2.13-A). Two main types of visual stimuli were projected.

The sets of experiments used for Chapter 5 were done by projecting a black moving circle passing consecutively through the screen four times in a rostro-caudal direction, followed by a resting phase of 30 seconds after which the circle passed again four consecutive times. This pattern was repeated ten times and recorded in 9,250 frames, giving a total duration of 615 seconds long (Fig 2.13-B). We referred to this stimulus as "Moving ball".

For Chapter 6 we performed a series of stimuli consisting in sinusoidal moving gratings which were varying in spatial frequency and contrast levels (See figure 2.13-C and D). Contrast was defined as the relative brightness difference from the background, and can be described by the Michelson equation as follows:

$$\frac{(L_{max} - L_{min})}{(L_{max} + L_{min})}$$

Where L_{max} is maximum stimulus luminance, and L_{min} the luminance minimum (Rizzo, 2013). The frequency was previously determined using the custom-written script for MATLAB under the following frequency parameters on Table 17.

Frequencies	Lowest	---------->					Highest
Size of full cycle b/w (mm)	98.118	60.879	47.793	30.646	16.250	6.380	3.148
Size of 1 grating (mm)	49.059	30.439	23.896	15.323	8.125	3.190	1.190
Visual angle 1 cycle (degrees)	**55.988**	**36.430**	**28.970**	**18.812**	**10.040**	**3.950**	**1.950**
1/2 cycle - 1 grating (degrees)	27.994	18.215	14.485	9.406	5.020	1.975	0.975
Visual acuity / cpd - whole	**0.018**	**0.027**	**0.035**	**0.053**	**0.1**	**0.253**	**0.513**

Table 17. Parameters used for different Frequency stimulation.

The frequencies were measured according to the visual angle (VA) and then converted to cycles per degree (cpd).

All presentations started with 30 seconds of 50% contrast background to let the fish stabilize their neural response to baseline levels and ended with 10 seconds of black screen were left before stopping the recording. Preliminarily, the stimulus was applied in a hierarchical manner and consisted of just 5 sets of sinusoidal gratings with different frequencies. This type of presentation was named Show Gratings (SG) 1. In the same fashion, the stimuli consisting of gratings with variations were designated a number depending on the variation. For instance, moving gratings varying in contrasts were assigned even numbers, whereas frequency-related were keep with odd ID numbers.

A description of all the stimuli used for Chapter 6 can be summarised in Table 18.

Stim ID	No. of Sets	Duration per set	Total duration	Description
SG1	5	30 s	5:32mins	Hierarchised frequencies
SG2	5	30 s	5:32 mins	Hierarchised contrasts
SG3	7	30 s	7:42mins	Alternated frequencies
SG4	7	30 s	7:42 mins	Alternated contrasts
SG6	49	10 s	18:50mins	Frequencies vs contrasts
SG7	49	10 s	18:50mins	Alternated frequencies vs angles
SG8	49	10 s	18:50mins	Alternated contrasts vs angles

Table 18. Sinusoidal moving gratings variations. Note there is no stimulus for SG5 to keep a coherence with pair numbers related to contrasts and unpaired related with frequencies.

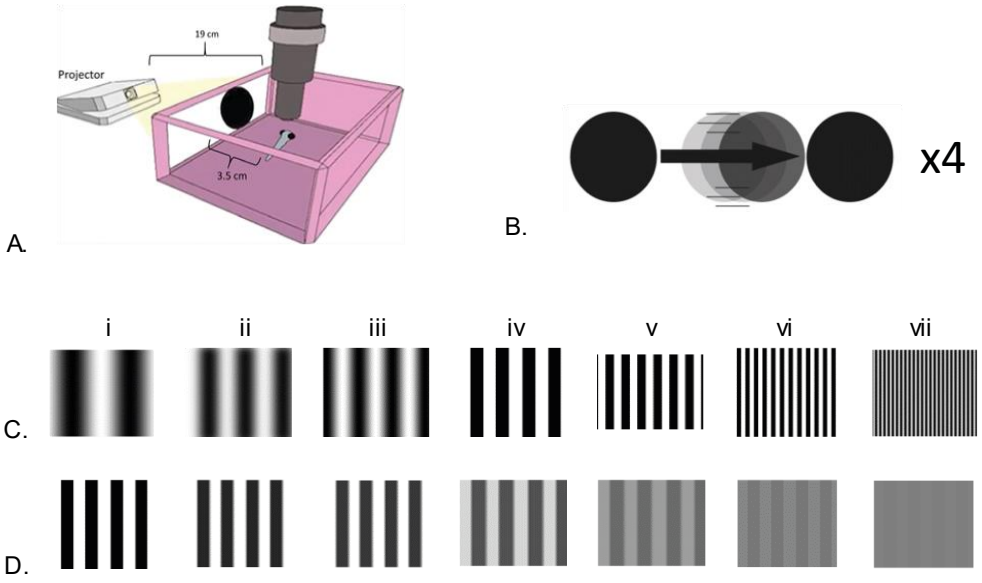

Figure 2.13. General multiphoton imaging setup and visual stimuli. (A) Imaging setup. The projector was placed at 19cm from the imaging chamber. The fish was mounted in 3.5% LMP agarose previously aerated and placed 3.5cm from the screen. The imaging chamber was filled with imaging solution. (B) Representation of the moving ball stimuli. This stimulus consisted in a ball covering the full width of the screen moving in a rostro-caudal direction to the fish (C) Representation of moving gratings varying in frequency. The visual angles used were the following: i) 55.88º, ii) 36.43º, iii) 28.97º, iv) 18.18º, v) 10.04º, vi) 3.95º vii) 1.95º (D) Representation of moving gratings varying in contrast as follows: i) 100%, ii) 75%, iii) 50%, iv) 20%, v) 10%, vi) 5%, vii) 1%.

The rationale behind applying alternated instead of randomised stimuli was that in these cases the analysis was planned to be done manually and learning where the different contrasts were given, facilitated the recognition of the typical response patterns and where the different variations occurred so that the classification occurred in a straight-forward manner and minimise any possible errors from visual sorting.

To get a close idea of the contrast tunning sensitivity curve in the ZF tectum, we did SG6. Here, we basically alternated both sinusoidal gratings at the seven different frequencies and mixed with the seven different contrasts in an alternated pattern making a total of 49 different sets. Each set lasted 10 s, followed by a 30 s rest in which a 0% contrast screen was presented. All stimuli ended with a black screen before the end of the recording.

Finally, we assessed angle and direction selectivity by mixing the sinusoidal gratings at 100% contrast level with different spatial frequencies against 7 different angles in SG7; and in SG8 the seven different contrasts were presented with the second lowest spatial frequency (18.18° VA) mixed with seven different angles, giving 49 different sets per stimulus. The order of the angles was changed every 7 sets and was as follows: 90°, 135°, 180°, 225°, 270°, 315° and 360°.

2.5.1 Image acquisition and processing

All images were processed first using FIJI (Image J software). First the videos were averaged between every five frames and then registered using the TurboReg rigid body algorithm available open source (TurboReg) for Image J (Thevenaz, Ruttimann, & Unser, 1998). This process allowed for correction of any minimal movements in 'x' and 'y' axis when needed. Finally, the neuropil was manually selected and positioned in a horizontal manner to facilitate the voxel analysis described next.

2.5.2 Data analysis

The data was analysed first using a custom-written script for Igor Pro 6.3 from WaveMetrics (Lake Oswego, OR) and SARFIA. Fluorescence dynamics of individual voxels within the neuropil were analysed using the voxel-wise method previously described (Bergmann, Meza Santoscoy, et al., 2018). The fluorescence was determined as $\Delta F/F0$, were F0 was the mean intensity of the responding voxel during the first 4 seconds, recorded in the absence of visual stimulus (10 frames) (Fig 2.14-A). The chosen responding voxels were defined by a skewness > 0.8. Since Skewness measures symmetry, non-responding traces will present a value of 0 skewness.

Additionally, we were able to determine the depth in which the responding voxels are in the neuropil (Figure 2.14-B). This was done by fitting the images using a customed script to define the positions based on an ellipse which was selected manually according to the shape of each neuropil.

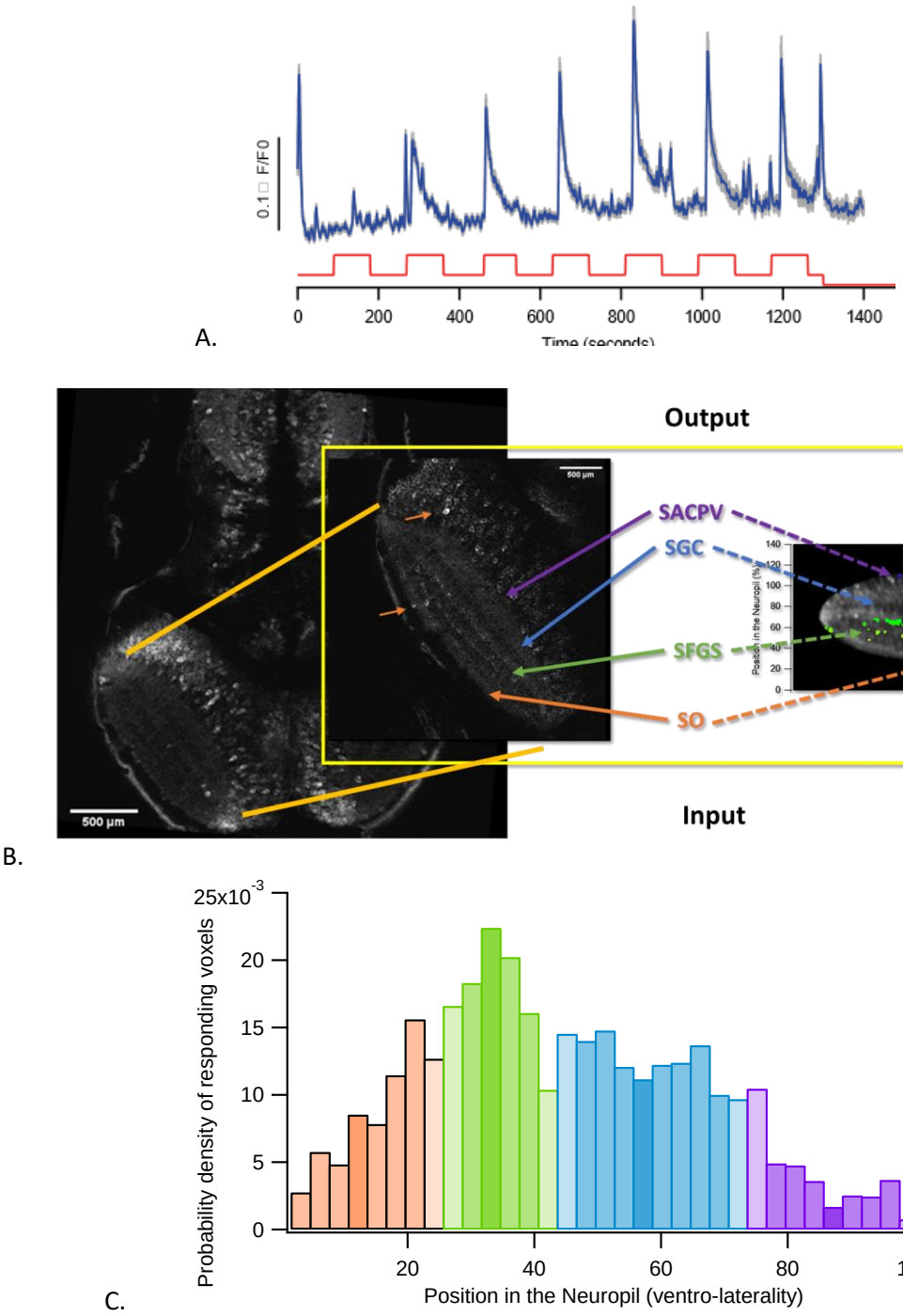

Figure 2.14 General analysis of multiphoton calcium imaging. (A) *Representative trace from a modified SG1 stimulus (moving gratings varying in frequencies) from a 12dpf Huc:GCaMP6 ZF*. **(B)** *Voxel-wise analysis selection and processing in image J and Igor Pro. After normalisation, the ROIs are labelled automatically after a distribution was tested for kurtosis. The position of the neuropil from 0 to 100 represents the ventrality from the external areas to the most ventral.* **(C)** *Number of responding voxels in the neuropil arranged by ventrality and color-coded as in B.*

Finally, the positions of the responding traces were plotted in a histogram using Igor Pro, by converting into percentual values, therefore giving the probability of responding traces with respect of the ventrality in the tectum. Thus, in this case the cell bodies were near the 100% (Figure 2.14-C).

2.5.3 Statistical analysis

The statistical analysis was done using a combination of GraphPad Prism. Ink (version 9.2) and custom-made scripts for Igor Pro 6.3 (Wavemetrics). Data are displayed as mean ± SEM. Statistical comparisons were done either by student's two-tailed t-test or analysis of variance (one or two-way ANOVA followed by the relevant post-test accordingly). Significance was considered as $p < 0.05$.

Chapter 3. Behavioural and molecular approaches to learning

3.1 Introduction

There is a broad history of independent studies in which a variety of human memory loss-related neurodegenerative disorders have been partially compared functionally and anatomically with zebrafish (Fig 2, Chapter 1). However, although sets of neurons have been identified using a variety of tools such as neurotransmitter regulation areas (dopamine, serotonin, histamine, etc.), the precise roles and interactions within other systems, are still far from being well understood and behavioural research offers an alternative scope in this subject (Panula et al., 2010; Schröder, Oesterle, Berens, & Yoshimatsu, 2021).

A large number of behavioural phenotypes had been already described in zebrafish. From larval stages, zebrafish can be habituated (Best et al., 2008), dishabituated or subjected to sensitisation and undergo classical conditioning in which a conditioned stimulus is linked with a reinforcing (unconditioned) stimulus (Kalueff et al., 2014). This may result in the ability of the fish to predict an unconditioned stimulus (Roberts et al., 2013). For instance, some behavioural studies with zebrafish modify the perception of given stimuli such as light in different wavelengths, by combining other sensory inputs such as pain or sounds (Aoki et al., 2013).

The main experiments in this chapter, can be divided in two. First, the memory-related behavioural paradigms with the analysis of exploratory behaviour from the data generated by video recordings. In addition, the modelling of methods to solve the problem of human bias and improve the protocols to get more accurate measurements and analysis that might be suitable for the study of short and long-term synaptic plasticity in ZF. In total, we performed 6 different sets of experiments (Table 3) using the principle of Novel Object Recognition on a free-swimming environment. Further details about the experimental setup are detailed in the Materials and methods section (Chapter 2.2.1).

3.2 Visual fields and its relationship with Novel objects

Is worthy to note the difference between the terms of visual fields (VF), and receptive fields already discussed in Chapter 1.5.2. In comparison, VF is a humbler subject to grasp. While receptive fields are the range in which a stimulus received by a neuron produces a response, the visual field is simply the range of light that enters such input (eyes) (Yin, Li, & Du, 2019b).

Typically, the visual field is divided into four quadrants in binocular species: Up, down, nasal and temporal. In normal conditions, the optic nerve will receive all the information from the four visual fields (Arcaro, Mcmains, Singer, & Kastner, 2009; Benson et al., 2012). Then, assuming healthy conditions, the receptive fields in the mammalian visual cortex or in the OT when referring to ZF, will contain the information of all four visual fields (Chapter 1.4.3 to 1.5.2).

Even though it is possible to experimentally modify how the visual fields are computed in V1, the brain will activate adaptative mechanisms to overcome the abnormalities. For instance, in 1988 Schall et al., artificially induced an abnormal ipsilateral visual field representation in the geniculocortical pathway of normally pigmented cats by sectioning one of their optic tracts at neonatal stage. In these experiments they found out that RGC projections stabilized in a pattern that allowed to compensate the visual field of up to 20 degrees of the ipsilateral side (Schall, Ault, Vitek, & Leventhal, 1988).

Ranging from prey capture to escape behaviours, ZF is a very virtuous model capable of executing a variety of visual evoked behaviours (Dehmelt et al., 2019). In general, most species of fish have a lateralised point of view and specifically in ZF, their visual field encompasses around 160 degrees in each eye, giving a binocular vision of 33 degrees and just a blind spot of about 21 degrees at their back side (Pita, Moore, Tyrrell, & Fernández-Juricic, 2015). It is important to consider these measurements when performing behavioural experiments involving any kind of visual input, especially when locating a visual stimulus within the visual field for the study of behaviour with novel object tests.

Despite the amount of evidence, it seems that an agreement is difficult in regard of the reproducibility of the results reported in behavioural experiments involving novel

objects in ZF at different developmental stages. In this chapter I will discuss some examples.

3.2.1 Assessing ZF exploratory behaviour using a bidimensional stimulus.

To perform a preliminary evaluation of exploratory behaviour in the ZF larvae, we assessed the configuration of the path traces on 11-16dpf WT and GCaMP3 zebrafish when habituating with an empty arena. As mentioned in Chapter 2, the reason behind using GCaMP3 fish was that we were testing whether there is a significant difference in the behaviour related with this strain. In table 19 the general concepts used for these experiments are outlined for future convenient reference.

Concept	Definition
Habituation/acclimation	First time on empty arena
Familiarisation	Presentation with the object(s) for the first time.
Resting	Removal of the objects and empty arena after familiarisation
Reintroduction (ReI)/Testing	Addition of objects after the resting period

Table 19. General concepts in behavioural analysis.

The preliminary tests included 1 hour of acclimation to the empty behavioural tank. The following day a static 2D black equilateral triangle (1cm), was placed from outside the tank on one of the larger sides for at least 1 hour. Thus, the resting period was of 24 hours (Chapter 2.2.1).

Here, we found out that the fry presented exploratory behaviour when approaching the novel triangle. Compared with the habituation recordings, the ZF kept an average distance of around 2.5cm from the object. It is arguable to think that the distance kept was due to fear-like behaviour to the black shadow. However, further analysis of the distance revealed that the fish allowed a visual angle of around 20 degrees from its position ($2 \times \arctan(1.7 / 5.2)$). Thus, is likely that the fish retrocedes in order to get a full view of the novel triangle (Figure 3.4).

3.2.2 Preliminary tests using a 3D object.

The next step was to study whether the interaction seen with the novel triangle persisted if the stimulus was a three-dimensional object. The initial aim was to

determine whether the fish swims more to the left (counterclockwise) or to the right (clockwise) on an arena without objects (habituation) and compare these results with the data obtained after the introduction of a novel object (familiarisation) (Figure 3.1)

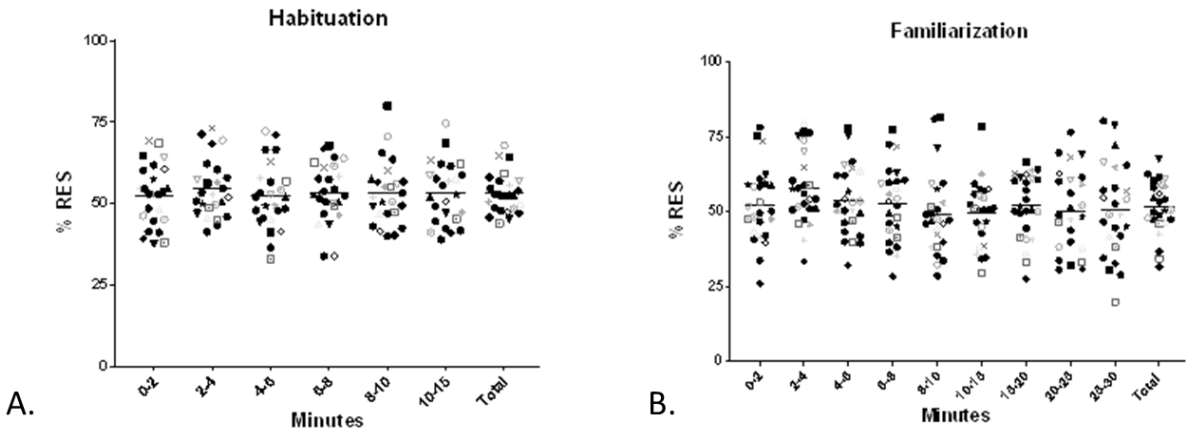

Figure 3.1 Clockwise swimming preference over time. *Results obtained from the analysis of the percentage of right eye system (RES) preference over time among individuals. There is no statistically significant difference on the swimming direction preference between the* **(A)** *Individual values with group means were plotted over time during Habituation and* **(B)** *Familiarisation period (p > 0.05) (n=25 represented by each symbol). Lines represent the mean.*

To get a closer idea of the differences between the 2D triangle and a three-dimensional object, we chose a black conical pen-cap placed in the same location as the novel triangle as the first 3D object (Fig 3.2). For the following setups, the novel object was introduced immediately after acclimation.

Similar with the results obtained with the novel 2D triangle, we found out that the distance kept between the 3D object and the fish was between 2 - 3 cm, allowing a visual angle of around 40°. Therefore, we hypothesized that this length was in relation with the visual receptive field distance needed to visualise the entire object.

A.

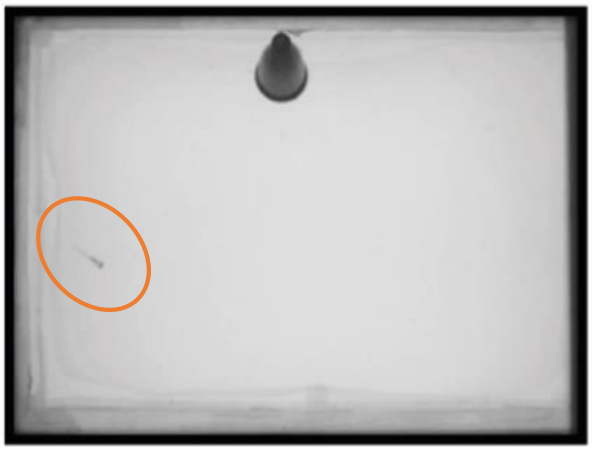

B.

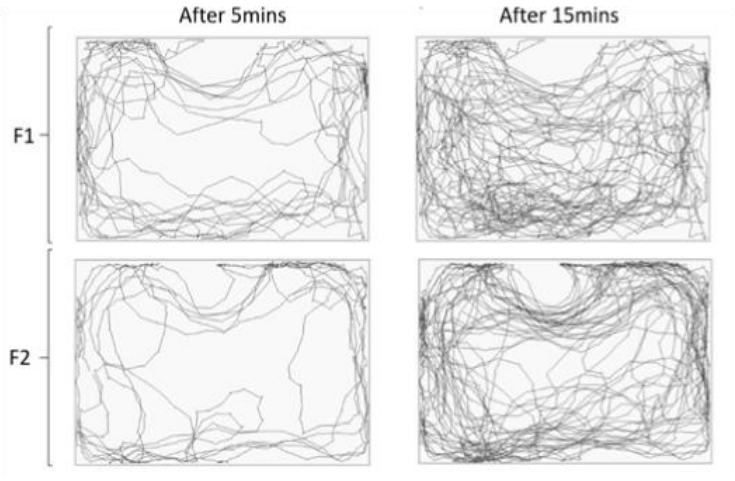

Figure 3.2 Behavioural Experiments with 3D Novel Objects (A) *Top view of the small behavioural tank with the black 3D object used to assess novelty in the same location as the 2D triangle. In this frame, the 16dpf WT fish (circled in orange) looks at the black 3D object with the left eye.* **(B)** *Representative results of the tracking path of two WT zebrafish F1 (top) and F2 (bottom) 16dpf old during the familiarization period (presence of the object), at the top after 5- and 15-minutes intervals.*

To test this hypothesis, the next variations consisted of introducing the same object in different areas. First, we examined the behaviour and the distance that the ZF kept from the object when the location or the characteristics of the object were changed. Then, we tested if the shape and colour played a relevant role in this behaviour.

3.2.3 Distance from new visual cues is not context-dependent

Previous reports have shown that adult ZF is able to retain memories related with a location dependency (Messina et al., 2020). For instance, it was shown that if fish was habituated to an object in a particular quadrant, then when fish is presented with the same object in a different context such as quadrant or colour of the walls, they spent more time in the novel quadrant. Thus, it can be assumed that ZF exhibit episodic-like memory. In other words, they seem to remember in the context of *what*, *where* and *how* a new situation was presented (Hamilton et al., 2016b).

To assess if the distance kept from the novel object had a fear-like relationship or was dependent on the location of the object, we examined the behaviour of the ZF by placing the black 3D-object on different locations. For instance, we placed the black cone on one side of the tank and centrally on the y axis. (Figure 3.3)

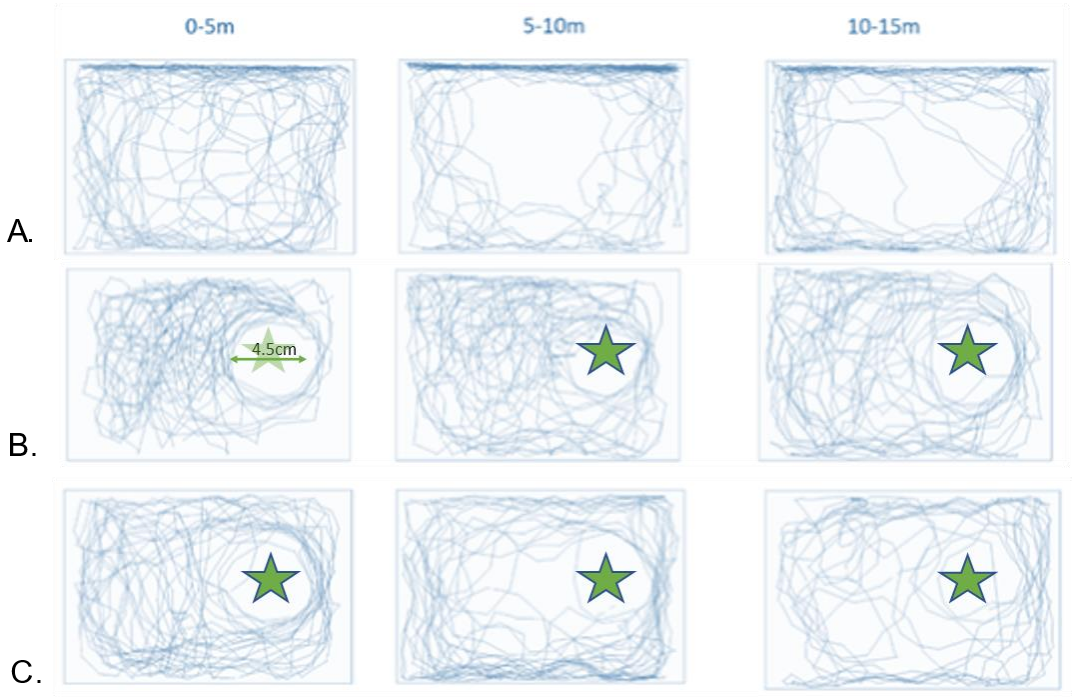

Figure 3.3 Exploration pattern in relation with object location. *Representative results of the path traced by a 19dpf old WT zebrafish through 5 minutes intervals up to 15 minutes per stage.* **(A)** *In this case, we allowed the fish to habituate per 15 minutes (Hab).* **(B)** *Then, we immediately placed the object to let the fish familiarize per 15 minutes (Familiarisation).* **(C)** *Finally, we reintroduced the object for another 15 minutes after a 30-minute rest (ReI). Distance to the object is kept regardless of location*. The star represents the object location.

We then look at the pattern of movement during the habituation period (no object) for 15 minutes and then compared with the familiarisation (presentation of the object) for 15 minutes by placing the object on one side. Finally, we measured the distance kept at different time-points (Figure 3.4-B). Furthermore, we added a Reintroduction period which happened after 30 minutes of resting without any objects on the arena, this reintroduction was done in exactly the same place as in the Familiarisation period. On both occasions, the distance kept was around 2 – 3 cm, with an average of 4.5cm in diameter (Figure 3.3-B). These tests were performed on 17-21dpf WT and GCaMP3 ZF.

Since there was no difference between the Familiarisation and re-introduction period, we decided to increase the time spent with the novel object during the first presentation to identify if there was any change in the exploratory behaviour over time. One hypothesis was that the time spent near the novel object, measured by distance would decrease due to an habituation behaviour. Therefore, the next sets of experiments were done by placing the novel object in the middle of the arena and analyse the behaviour for 30 minutes after 15 minutes of habituation (no object). We analysed the difference between the pattern of the distance that the fish kept from the middle of the tank before and after placing the object (Figure 3.4) This was calculated using the coordinates of the fish in relation to the object.

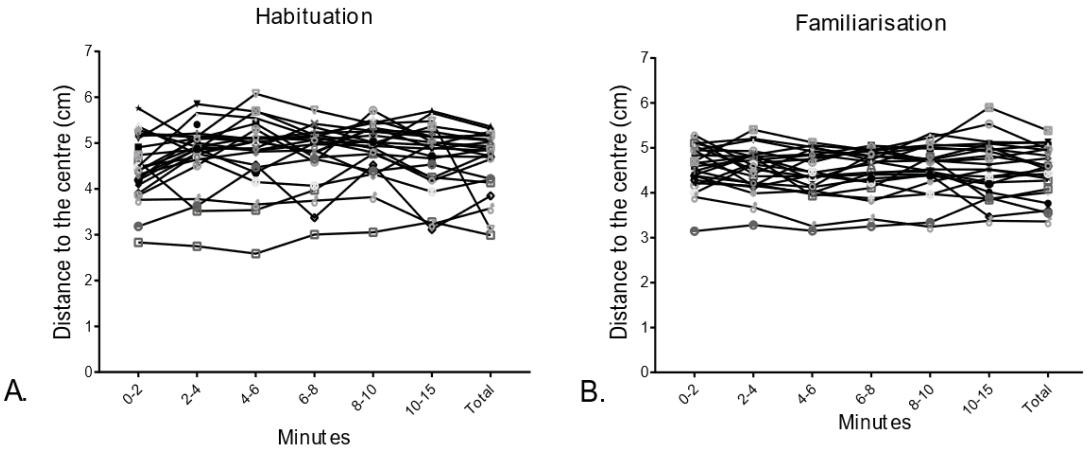

Figure 3.4 Distance to midpoint analysis. Results obtained from the analysis of the distance that each fish kept from the centre of the tank over time-intervals. **(A)** Average distance per fish over time was plotted with connecting lines for a clear visualisation of the pattern followed by each ZF during Habituation and **(B)** Familiarisation periods.

Interestingly, we found that the exploration pattern towards the centre of the tank was peculiar. During the time when the arena was empty (Habituation), the distance to the centre was disperse over time with a few exceptions (Fig 3.4-A). During the introduction of the novel object the fish kept a steady distance from the centre oscillating between 4 to 6 cm, after which the pattern was dispersed from minute ten (Fig 3.4-B).

All fish tested were culled and disposed of according to regulations after the experiments. Some of these were used to test in situ hybridisation assays which will be discussed in following sections.

3.2.4 Dynamics of exploration

After understanding that the location context was no different, we asked ourselves if the shape and colour of the object were relevant for this behaviour. Therefore, in the last 2 sets of experiments we decided to assess novelty mimicking a more natural 3D object. This was done by placing in the centre of the tank an artificial violet flower or a green leaf (See Figure 2. From Materials and methods). The fish used in this case was between 19 to 21dpf WT and NBT: GCaMP3 since we will use these fish for future multiphoton imaging.

The rationale behind using the nacre NBT:GCaMP3 was to assess whether the GECI expression had any consequences in exploratory behaviour of the fish compared to wild-type (Figure 3.5-A). We find out that there were no differences between WT and ZF expressing GCaMP (Figure 3.5-B).

In general, we found that a typical behaviour during the habituation period (no objects), present two robust characteristics: First, the affinity towards the walls. Most fish tend to swim in circles following the walls closely. Secondly, the swimming pattern, either clockwise or anti-clockwise in general follows an eight-like (8) shape, changing its direction constantly, at a rate which depend on the individual speed and size of each subject, approximately every 3-8 seconds in 12-22 dpf fry.

Despite the comparatively similar pattern already described, it is worth notice some peculiar patterns that were interesting, some more frequent than others. For instance, while most of the fish showed certain affinity towards the wall and occasionally

swimming randomly free over the arena, there were some fish that had a preference towards the centre during both habituation and familiarisation periods (Figure 3.5-C). On the other hand, despite the opacity of the tank and no reflecting areas, some fish had more affinity towards the walls even after being presented with an object (Figure 3.5-D)

Other behaviours worthy to show are when fish swam either under or over the object, further demonstrating that the distance kept is not prompted by fear but an exploratory behaviour (Figures 3.5-E, F). Finally, more examples of exploratory patterns from individual fish are displayed in Figures 3.6 and 3.7.

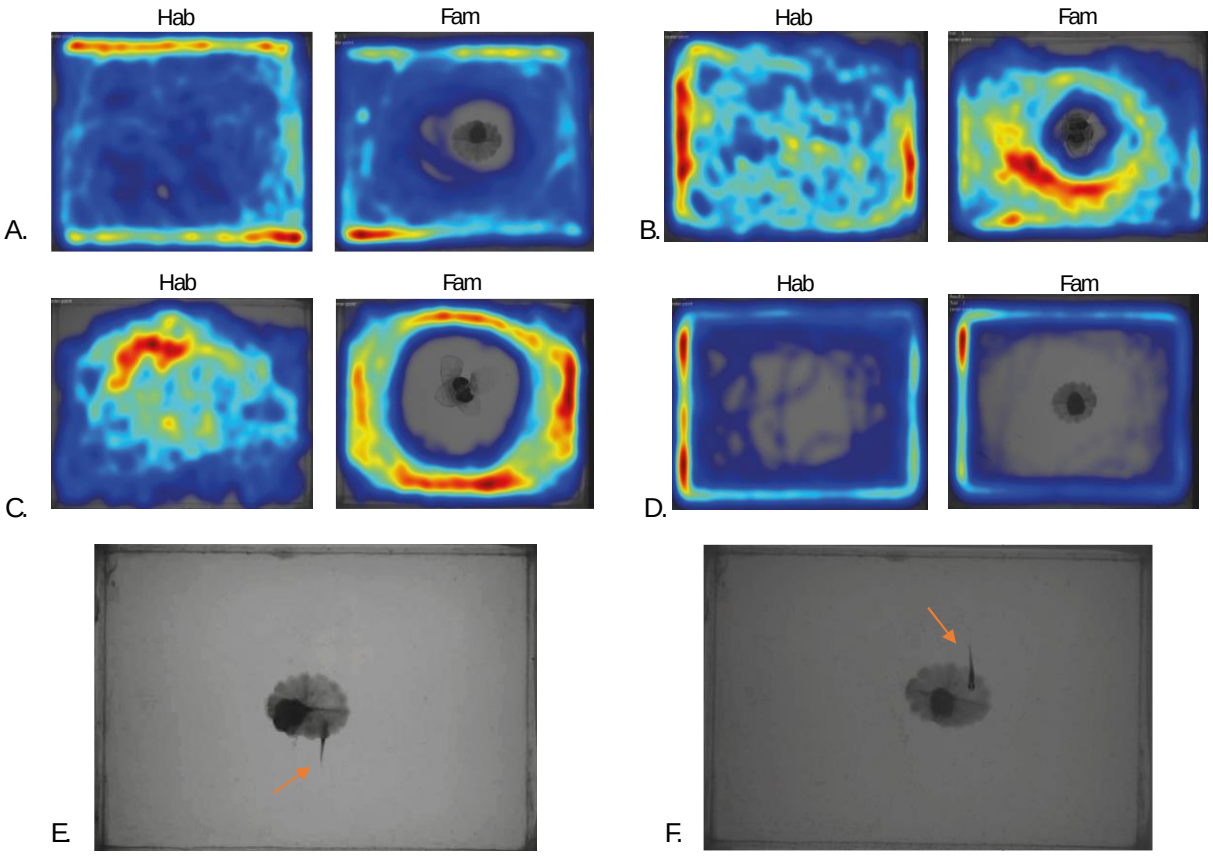

Figure 3.5 Heatmaps of different exploratory behaviours. (A) *Habituation and familiarisation of a 19dpf WT fish with a green leaf. In this case, the fish presents higher affinity towards the walls of the tank than the novel object.* **(B)** *21dpf NBT: GCaMP3 fish during habituation and familiarization with an artificial violet (Figure 2.6-3). In this case the fish shows a closer distance from the novel object during exploration.* **(C)** *Typical exploratory behaviour from a 20dpf WT during habituation (15mins) and familiarisation (30mins) with a violet flower. (**D**) Heatmap from a 19dpf WT during habituation and familiarisation with a green leaf. There is no exploratory behaviour towards the leaf here.* (A-D heatmap representing zones of activity; warm high, blue; low) **(E)** *Frame*

took from the familiarisation period of a 21dpf WT (25',50"). Here the fish swam under the object. **(F)** *Frame took after 1 min, 02 s of familiarisation. In this case the fish is swimming above the green leaf.*

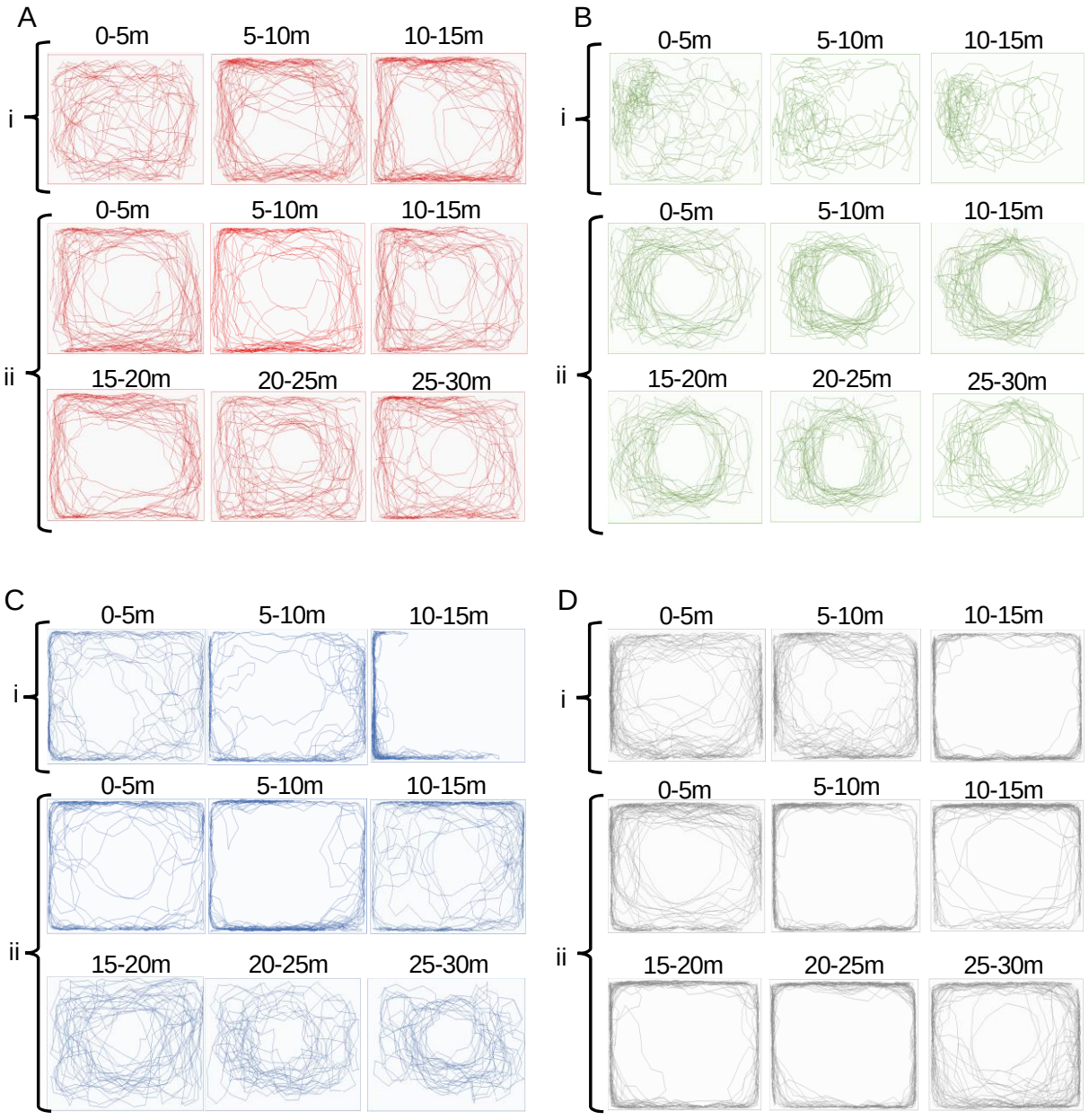

Figure 3.6 Diversity of exploring patterns (Black 3D object in the centre). *Representative examples of 4 different fish during (i) Habituation (No objects) for 15 minutes, and (ii) Familiarisation (30 minutes) in 5-minute intervals.* **(A)** *23dpf WT fish presenting an exploration pattern typical of most of the fish*. **(B)** *23dpf WT ZF showing an exploration pattern without wall-affinity.* **(C)** *20dpf WT ZF presenting a time-dependent mix-pattern of wall-affinity.* **(D)** *21dpf WT zebrafish with high affinity towards the wall.*

Note that there is a higher explorative behaviour during the first 0-5m interval and the last 25-30m, with a low exploration pattern during the 10m interval.

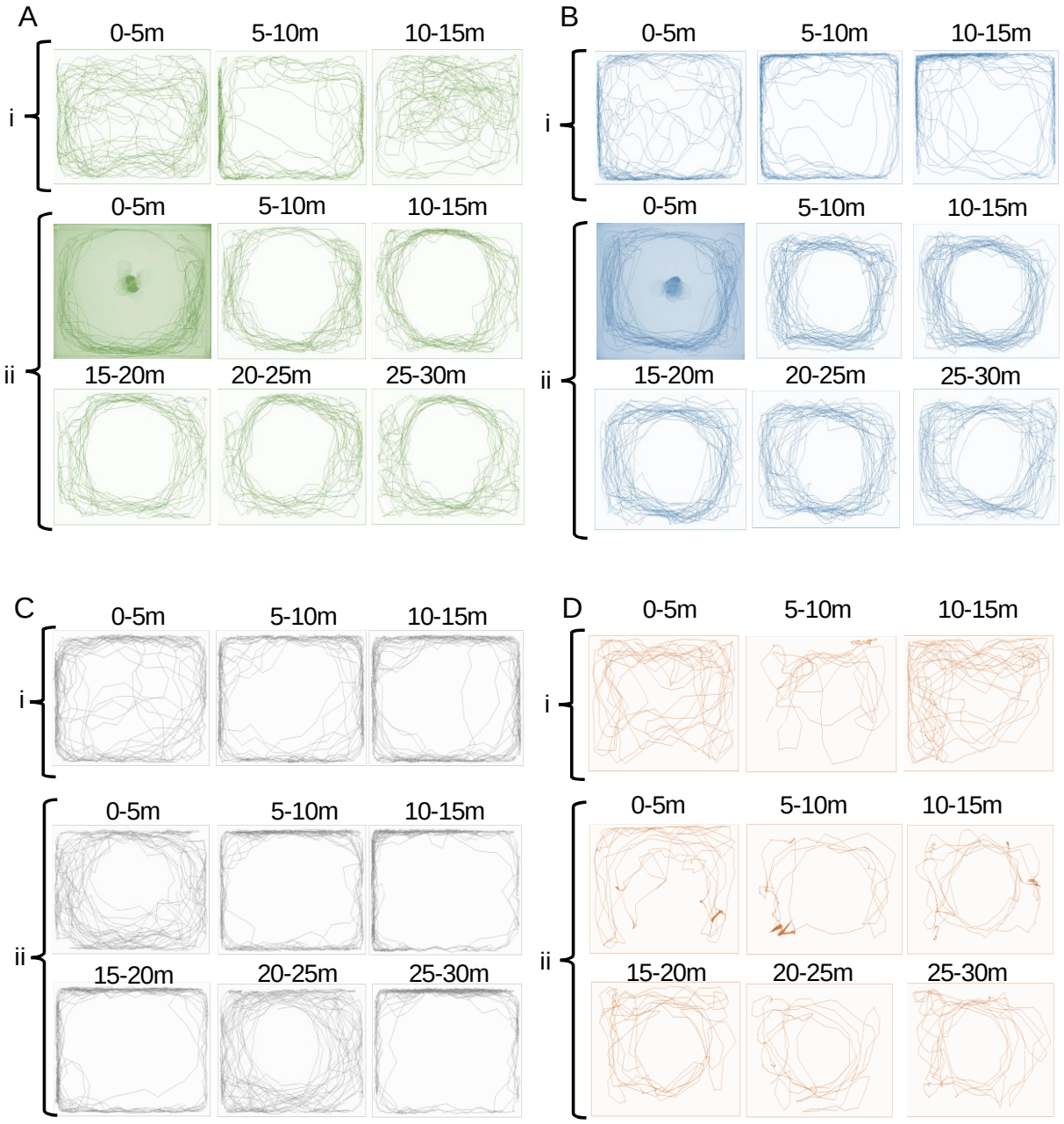

Figure 3.7 Diversity of exploring patterns (Artificial Violet in the centre). *Representative examples of 4 different fish during (i) Habituation (No objects) for 15 minutes, and (ii) Familiarisation (30 minutes) in 5-minute intervals.* **(A)** *20dpf WT ZF presenting typical exploration pattern.* **(B)** *23dpf NBT:GCaMP3 nacre fish with a typical exploration pattern.* **(C)** *20dpf WT fish showing general wall-affinity.* **(D)** *Atypical exploratory behaviour from a 23dpf NBT:GCaMP3 fry. In this case the general motion was very low.*

3.3 Visual lateralisation Novel Object Recognition (VLNOR)

Brain laterality has been observed in many vertebrates and even invertebrates, and these brain function asymmetries have some homology between species (Halpern, 2005). For instance, facial recognition is mainly a right-hemisphere function in humans (Broad, Mimmack, & Kendrick, 2000).

The concept of visual-lateralisation in NOR, refers to the preference of using an eye over the other to examine unknown stimuli (Andersson, Ek & Olsson, 2015). Specifically for ZF, this phenomenon has been reported relatively recently (1998) for adult specimens (Miklósi, Andrew, & Savage, 1997). Similar behaviours have been published for other fish, including several of the teleost group. These reports had claimed that ZF and other vertebrates exhibit a strong preference for the left eye system over the right eye when exploring a novel environment. This includes the recognition of other fish and its reflection on a mirror (Andersson, Ek & Olsson, 2015).

3.3.1 Evaluation of VLNOR reproducibility

Previous reports suggest that in ZF, the reaction to a novel object can be validated by VLNOR, testing whether the fish approaches the object with the left or the right eye and this information can be retained at least for 2 hours. (Andersson, Ek, & Olsson, 2015b). These studies claim that when viewing an object for the first time, the fish consider this object as a novelty during the first 2 minutes, and they become familiarised with it 4 minutes after the exposition. However, when the object is introduced again after 3 hours, the fish respond as if it was novel again (May et al., 2016b). Thus, the use of VLNOR in ZF has become a popular method for experiments related with learning, giving a valuable tool for memory research.

In these studies, the behaviour was recorded by video from above the test tank. Then, the methods consisted in calculate the angle between the fish length and the novel object every chosen frame at fixed intervals of 2 seconds to determine the changes in position of the fish through the experiment (Sovrano & Andrew, 2006). The cut-off values were then set to establish if the reference was on the left or right visual field of the fish. The number of right-facing frames was then compared to the left-facing ones to find out the index of preference.

Similar experimental setups investigated the zone preference within a tank. For this, they used high time-resolution analysis through software such as Ethovision, allowing to acquire data from every frame of each experiment's recording (May et al., 2016c). We acknowledged these methods are more in line with video-based automatic track analyses, so we later implemented this approach to further investigate ZF VLNOR.

First, we used the methods described in the mentioned publications. We manually counted the number of turns that the fish did every couple of fixed seconds from the recordings. Then by naked eye measured the angle given by the length of the fish in relation with the object and the direction in which the fish was facing to. This process was done independently by four different scientists; however, the results did not agree between each other (data not shown).

We hypothesize that among the reasons behind this disagreement were firstly, the difficulty that represents following the fish for a long period of time in the case of counting the "left-right" turns, and secondly, the frames chosen for the angle measurement method were different in many cases. Furthermore, the fact that a fish can change its direction even three times per second added to this discrepancy. Therefore, we decided to optimise the analysis by automation. The general retrieval of the position of the fish in each frame is described in Chapter 2 (Section 2.2.4 of materials and methods).

3.3.2 Optimisation of VLNOR analysis by automation

Given the advantage that fish only in exceptional circumstances swim backwards, we based this analysis mainly on the position of the fish per each frame in relation with the next. Subsequently, we set these measurements on conditionals of what might happen in terms of the use of left eye system (LES) or right (RES), when the fish swims in a direction from a known location.

In total, four different methods of analysis were designed for the VLNOR test, aiming to reduce any fundamental errors. For the first two methods, we divided the tank into quadrants and for the third method in zones (Fig 3.8-A,B). The fourth method was done by converting the x and y-axis into polar coordinates and comparing angle changes per frame. Similarly, we determined the direction of the fish by assessing the movements in

relation to the next frame. Finally, we obtained the average of all four methods used per time interval per fish, as these conditionals could be mistaken in extraordinary positions and since the outcomes were very close between each other (Fig 3.8-C).

A.

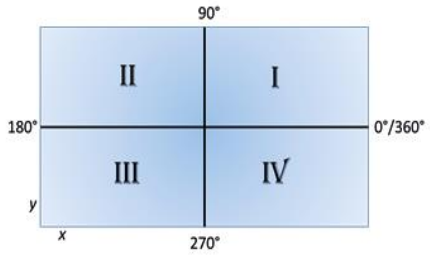

B.

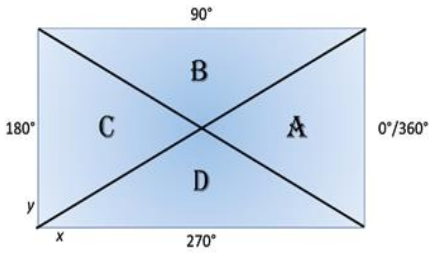

C.

	Horizontal		Vertical		Polar coordinates		Zone		AVERAGE	
	LES	RES	LES	RES	LES	RES	LES	RES	LES	RES
Total %	49.4%	50.6%	50.3%	49.7%	51.1%	48.9%	47.0%	53.0%	50.2%	49.8%
Total time	7.21	7.3973	7.3426	7.2667	7.45	7.15	6.8793	7.762	7.34	7.27
0-2 mins	49.9%	50.1%	52.9%	47.1%	52.6%	47.4%	48.7%	51.3%	51.8%	48.2%
2-4mins	50.6%	49.4%	56.0%	44.0%	57.0%	43.0%	47.1%	52.9%	54.5%	45.5%
4-6mins	52.5%	47.5%	55.2%	44.8%	56.8%	43.2%	47.9%	52.1%	54.8%	45.2%
6-8mins	58.1%	41.9%	52.5%	47.5%	58.6%	41.4%	47.5%	52.5%	56.4%	43.6%
8-10mins	51.4%	48.6%	52.9%	47.1%	54.7%	45.3%	46.3%	53.7%	53.0%	47.0%
10-15mins	43.0%	57.0%	42.9%	57.1%	41.1%	58.9%	46.0%	54.0%	42.3%	57.7%

Figure 3.8 VLNOR analysis protocol. *Methods used for video analysis of behaviour.* **(A)** *Schematic view of the quadrants (Romanic numbers) and angles in which the tank was divided for analysis. For the horizontal method, we determined that if the position of the fish changed negatively on the x-axis in quadrants I and II, and positively on quadrants III and IV, then the fish swims counterclockwise. For the vertical method, we considered that the fish swam clockwise if its position changed negatively in the y-axis on quadrants I and IV, and positively on II and III quadrants.* **(B)** *Scheme representation of the zones used for the 3rd method of analysis.* **(C)** *Representative results acquired after the analysis of a 14dpf WT fish over time during the habituation period, using the four-calculation methods and obtained average.*

This average was considered for statistical analysis to determine the difference in %RES preference towards the centre before and after the introduction of the novel object in the middle of the tank per intervals of 2-minutes and in an overall performance between habituation and familiarisation periods (Figure 3.9-A)

Then, we compared both % RES preference and distance patterns, to evaluate the existence of a novelty behaviour. Unexpectedly, we did not find any statistical differences between habituation and familiarisation regarding % RES over time.

However, we found more consistent and statistically significant changes of pattern regarding the distance kept from the object than %RES (Fig. 3.9-B).

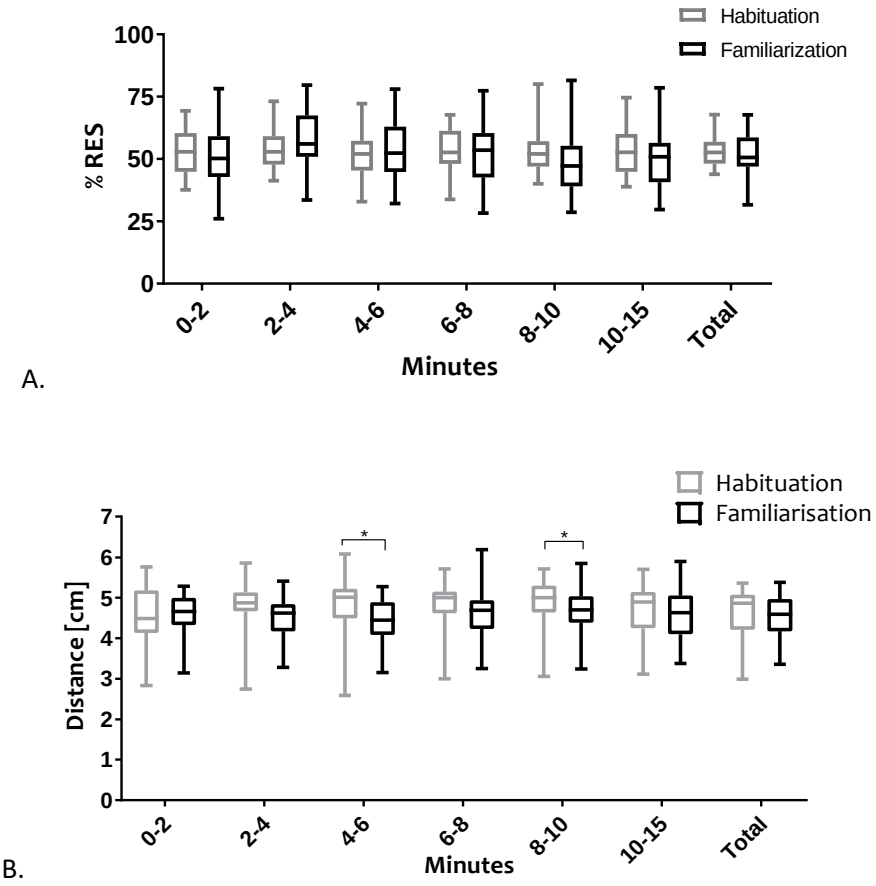

Figure 3.9 Comparison between Habituation and Familiarisation overall results. **(A)** *% RES preference over time. When comparing both data sets, there is no statistical difference between groups neither time points. Group means with SEM are shown, n = 25.* **(B)** *Comparison of data sets obtained before and after introduction of the novel object regarding distance to the midpoint. The distance kept from the centre of the tank during the full duration of the experiments is not statistically different between habituation and familiarisation. In contrast, when assessing shorter intervals there is a statistical difference between the average kept at 4-6 minutes (t=2.044, p=0.0002) and 8-10 minutes (p=0.0186) breaks. Group means with SEM are shown, and statistical significance is indicated (n=25).*

3.4 Novel Object Recognition paradigm as a method to assess synaptic plasticity.

In VLNOR, we used a single novel object. In the traditional novel object recognition (NOR) without assessing lateralisation, it is essential the introduction of two objects. The first published assays of a NOR paradigm along with novel location recognition assays were performed in rodents almost half a century ago (Ennaceur & Delacour, 1988). Subsequently, this behavioural test has been widely used in a replicate manner mostly in mammals and later other models have been used (Bickle, 2009). Usually the test consists of the exposition of the subject to a given visual object aiming to be "habituated". After a certain period, a new object is presented along with the known/familiar object. A normal response in rodents is considered to be the increase of time used to explore the novel object, compared with the time spent near the familiar one (Antunes & Biala, 2012). Differing from most behavioural methods that evaluate cognitive functions, the NOR test is a relatively straightforward assessment which avoids the confusion of external stress, motivation rewards or punishment outcomes (deCarvalho et al., 2013)

3.4.1 Traditional NOR

The traditional novel object recognition tests (NOR) rely on the preference for an object or situation (new or familiar) versus the other. This is given from calculating the index of preference which is the time spend near an object or close to a situation over the total time of the testing phase (Antunes & Biala, 2012). Several studies in mice and other mammals including humans, report novelties as the predominant choice versus the familiar ones when measuring the time spent near them and that such behaviour could be due to their innate curiosity (Moore et al., 2014). However, despite the vast number of reports regarding novel object recognition tests in zebrafish, it seems that there is no agreement on the object preference in zebrafish. There are a variety of publications reporting that like other vertebrates, zebrafish spends more time exploring the novel object, while other studies had reported fear performance towards new objects in fish as opposed to the classic behaviour in rodents and subsequently, having a preference towards the familiar object (Hamilton et al., 2016a; Leighton et al., 2018; May et al., 2016a).. This preference seems to be decreased after around 5 minutes.

3.4.2 Results from traditional NOR test

As described in Chapter 2, we decided to mimic the conditions of previous reports as much as possible (Leighton et al., 2018; May et al., 2016a). In this case, we performed the novel object recognition (NOR) tests on AB wild type and nacre NBT: GCaMP3 zebrafish on three groups with a different age range between 15dpf to 2 months old.

The first group consisted of fish between 19-22 days post-fertilisation since it is known that fish already presents a more robust exploratory behaviour compared with younger stages (Okimura, Tanaka, Maeda, Kato, & Mimura, 2015). Additionally, the optimisation of a WISH protocol for these ZF stages was being developed in parallel (Chapter 4).

These experiments took place over two days. On day one, after 15 minutes of acclimation the fish swam freely in an experimental tank containing two identical objects (black pen lids or artificial flowers) placed an equal distance from the centre (Figure 3.10-A). On day two, one of the original objects was replaced with a novel object (flower or pen lid accordingly) (Figure 3.10-B). All objects were attached to the bottom of the tank and covered by aquarium water. On both days, the duration of the experiments was 30 minutes.

For this range of age, the zebrafish movement was recorded throughout both phases of the experiment using Viewpoint system, and then fish was tracked through a custom-written code for Python. Subsequently, the coordinates of the fish per frame were acquired and plotted using Igor Pro 6.3 (Figure 3.10-C, D).

Overall, these experiments showed that the fish spent most of the time on the left side of the tank during the whole experiment. When assessing the time spent near the novel object against the familiar during the recognition phase, we found a statistically significant preference towards the novelty (P=0.0096) (Fig 3.11-A).

To assess the preference index (PI), we used the following equation:

$$PI = \frac{Time\ in\ (L) - Time\ in\ (R)}{Total\ time}$$

Here, the time spent on the left area (frames) was divided by the total number of frames. When two identical objects were explored, there was a preference index of 0.58, and after the introduction of the novel object, the PI increased to 0.62. The PI difference in the familiarisation versus the testing phase showed no significance (n = 24) (Fig 3.11-B).

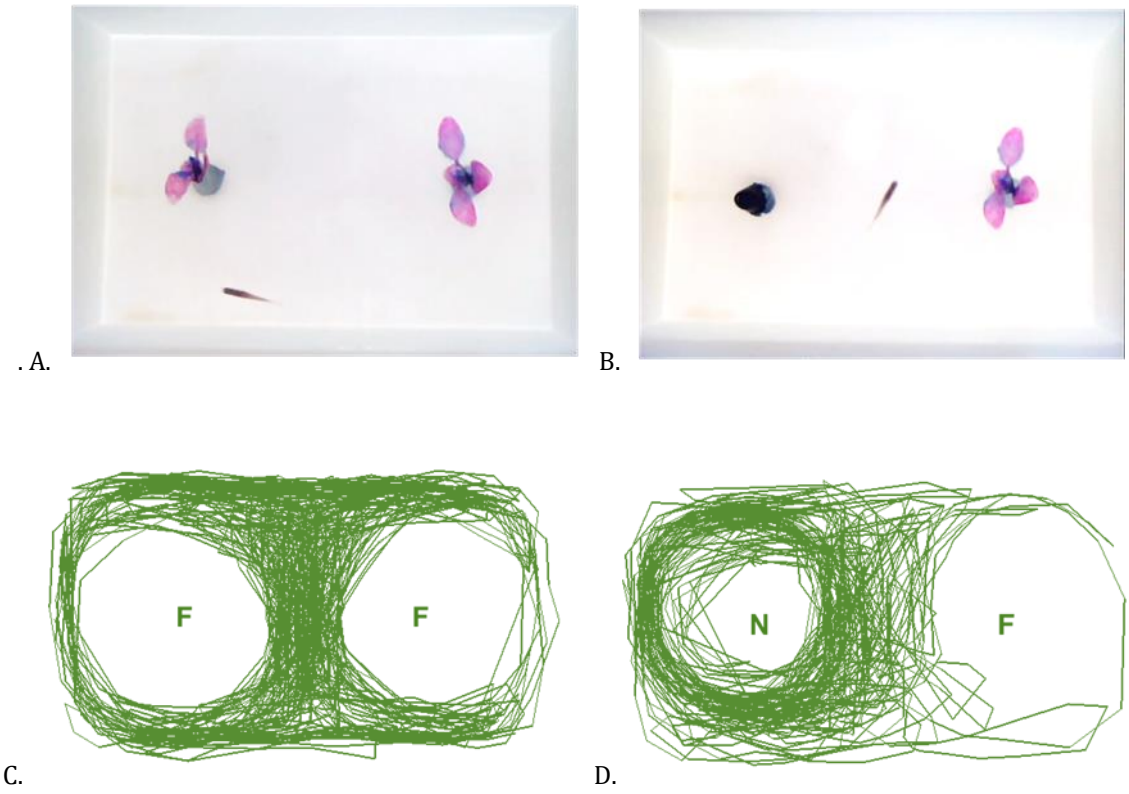

Figure 3.10 Novel object recognition test. Example of behavioural arena used for the Novel Object Recognition tests with a 38dpf WT ZF for the **(A)** familiarisation and **(B)** testing phase (right). **(C)** Plot of the path from a representative individual fish overtime during familiarisation and **(D)** testing phase. F stands for the familiar object, and the N shows the novel object located on the left side of the arena. In this case, the fish showed a clear preference towards the novel object during the test.

Surprisingly, when comparing the time spent near the identical objects during the familiarisation stage, we also found a significant preference for the left object despite being identical (*P*=0.0038) (Fig 3.11-A).

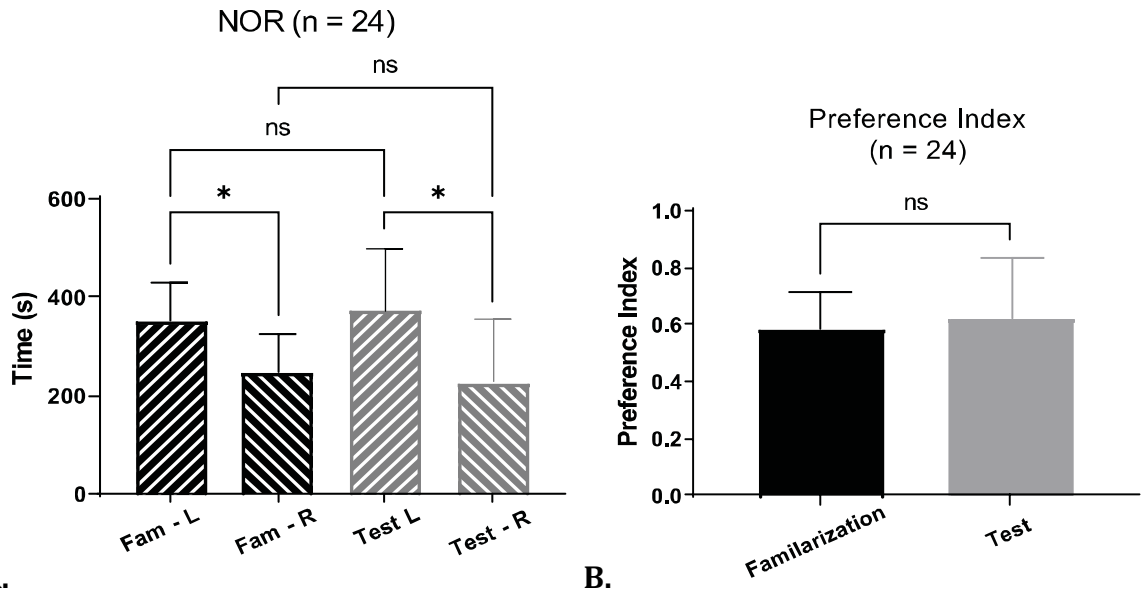

Figure 3.11 NOR Preference Index (PI) (**A**) *Time spent on the left (L) and right (R) side during familiarisation and testing phase. During familiarisation the fish spent significantly more time (p = 0.05) near the left object (Fam – L) than then right one (Fam – R) despite being identical. A similar result was observed during the Testing setup, where the left familiar object was replaced by novel object (Test – L), while the right one remained the same (Test – R). Conversely, there were no statistical differences between the time spent near the right nor the left object during both sessions (p = 0.05).* **(B)** *Preference index.*

However, for this set of experiments, the novel object was always placed on the left side of the tank to facilitate the analysis.

To identify whether the fish prefer to explore the familiar or the novel object, the data from the largest group of subjects within the same developmental stage were analysed individually and in a concatenated manner (Figure 3.12-A, B).

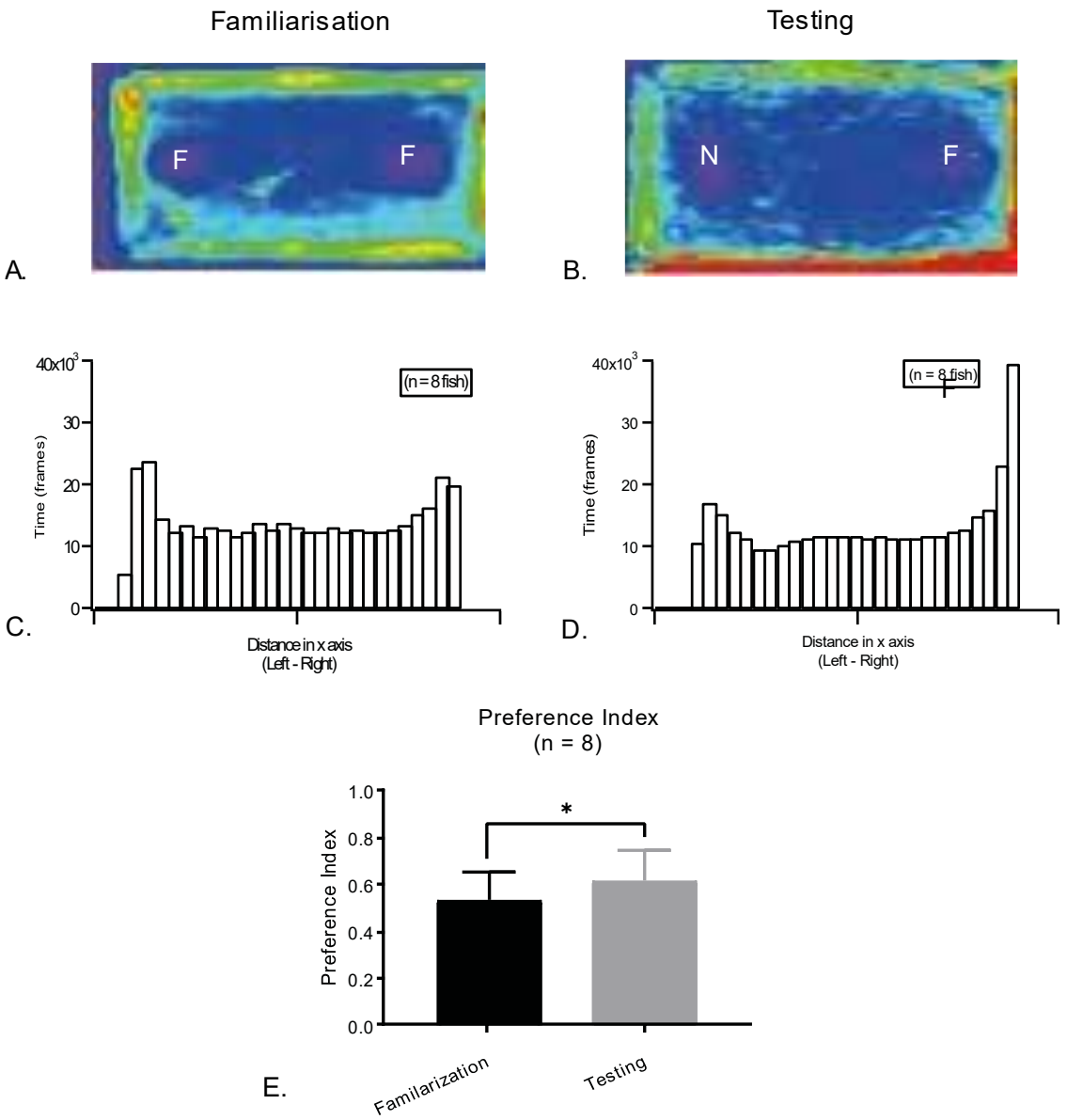

Figure 3.12 Concatenated results from NOR. *Heatmaps from the concatenation of the traces of the group between 19-22dpf fry during* **(A)** *familiarisation and* **(B)** *testing phases. (n = 8)* **(C)** *Histogram of the distribution of the fish location within the x-coordinates from the training phase in the first group of fish. There is a similar preference to the left and right zones.* **(D)** *Distribution of x-coordinates in the testing phase. An increase of preference for the familiar object is evident. (n = 8).* **(E)** *Preference index from the same fish ($p < 0.05$).*

For the analysis, the coordinates of the position of the fish acquired were adjusted so that the novel object was always placed to the left. Then, distribution of the x-coordinates of the fish per frame in each experimental phase was used to analyse how much time the fish spent in each zone along the length of the tank. (Figure 3.12-C, D)

3.5 WISH and FWISH in late-stage ZF larvae after novel object exposure

The use of in situ hybridisation in its whole mount version (WISH) has been developed in many organisms and is in constant optimisation depending on the needs of each research. The principle is the same as the traditional ISH and consist of the addition of a labelling probe for a specific target RNA to complement the sequence existing in the desired tissue to measure the gene expression occurring within the treated sample (He, Mo, Chen, & Luo, 2020).

Despite its many advantages, in ZF some of the obstacles that of the use of WISH is the poor penetration of some labelled probes in tissues from whole samples beyond the 2dpf (Thisse & Thisse, 2008b). For this reason, in this chapter I explore this technique by first replicating the traditional steps to be followed for early stage-larvae and then tried different empirical variations to achieve a good quality staining in tissues beyond 5dpf.

The aim of this part of my research was to look for the expression of IEG to identify areas of synaptic strength immediately after a novel visual exploration in ZF larvae that were at a developmental stage far enough to reach the age limits of what we find suitable for *in vivo* 2-photon calcium imaging (21dpf). Since the details of the protocol were already outlined in Chapter 2 (Materials and Methods), here I will mainly highlight some of the relevant modifications and show some of the results obtained.

3.6 Whole-Mount In situ Hybridisation (WISH) for detection of IEG

Nowadays, along with some of the most common IEG used to map synaptic activity are *c-fos, stxbp1, arc, homer1a*, *egr1* and *bdnf*. These genes are characterised to encode transcription factors which adjust the synaptic homeostasis to regulate the expression

of what we called late-response genes (Gallo et al., 2018b). Due to availability and recommendations, the preliminary experiments were done using *bdnf* (Figure 3.13-A), *stxbp1* (Fig 3.13-B) and *c-fos* (Fig 3.13-C, D) in early-stage ZF larvae up to 3dpf.

To generate positive controls we decided to treat the samples using the GABA-inhibitor Penta tetrazole (PTZ), as it is known to induce seizures at a pan-neuronal level, thus activating the whole CNS which likely release these IEG. As negative controls, the fish was just treated with E3 media only (See materials and methods).

The Brain-derived neurotrophic factor (*Bdnf*) is a protein found in the CNS responsible for promoting the growth, maturation, and appropriate homeostasis of the brain cells to ensure its survival. This protein is transcribed from the *bdnf* gene, and it is known to play a key role in learning and memory (Bathina & Das, 2015; Miranda, Morici, Zanoni, & Bekinschtein, 2019).

On the other hand, Stxbp1 transcribes the Syntaxin-binding protein 1, which among their main duties is to facilitate the release of neurotransmitter (López-Rivera et al., 2020). *C-fos* is known to interact with other encoding genes related with synaptic plasticity and it has been reported to have a robust expression in neural activation following behavioural tasks, which makes it an ideal synaptic marker for these experiments (Cruz, Javier Rubio, & Hope, 2015b; Minatohara, Akiyoshi, & Okuno, 2016b).

A strong and generalised c-fos expression is evident in positive controls particularly in areas related with high-level visual processing such as the OT, pretectum and telencephalon (Fig 3.13.1-C, D). For this reason, we chose *c-fos* as our IEG of choice for further WISH protocols.

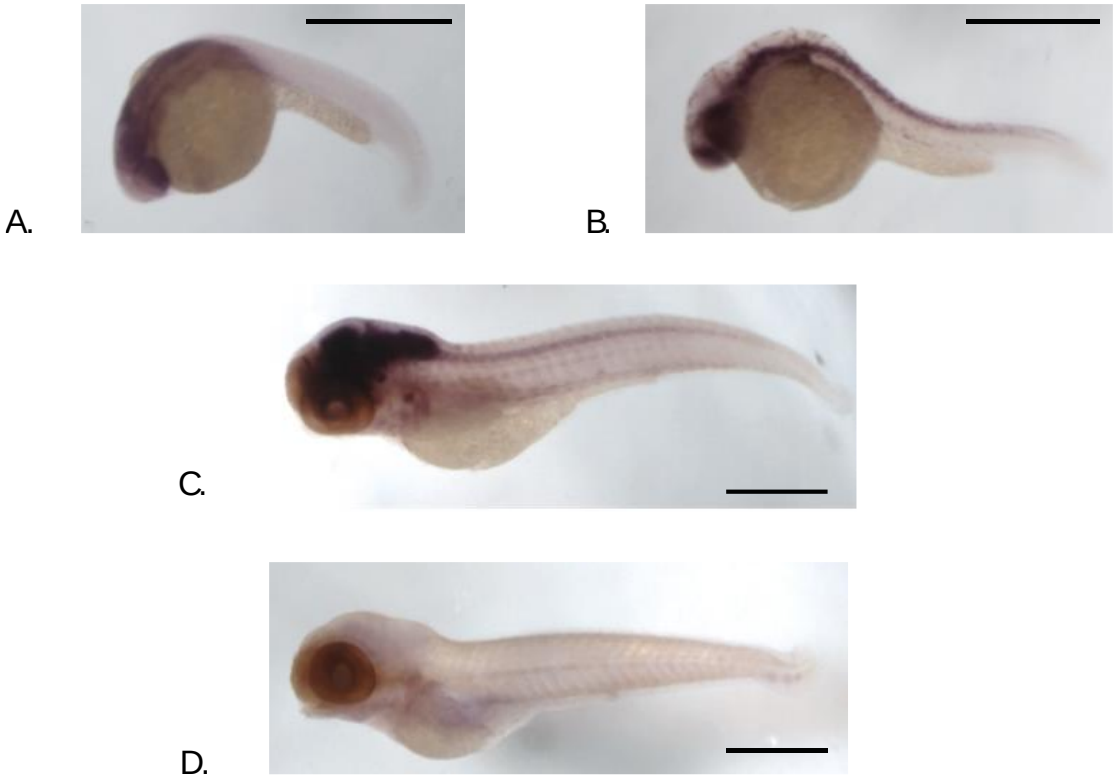

Figure 3.13 Representative results of WISH. (A) *Representative example of the result of a whole mount in situ hybridisation (WISH) performed on 24hpf ZF labelled with Bdnf gene, previously treated with PTZ as a positive control.* **(B)** *Expression of Stxbp1 gene after WISH, achieved on 30hpf ZF previously submitted to PTZ during 60 minutes before fixation.* **(C)** *C-fos gene expression obtained from a 3dpf old WT zebrafish treated with 60-90 minutes treatment of PTZ before immediate fixation.* **(D)** *Result of WISH performed on a 3dpf WT fish submitted with E3 media only (negative control or non-PTZ treated). Scale bars: 1mm.*

3.6.1 Traditional WISH and optimization to study late-stage ZF

After successfully developed positive and negative controls of *c-fos* WISH in fish under 5dpf, this technique was further tested in fish of 8, 15 and 22dpf. Based on previous protocols, here I used 20mM of PTZ to induce pan-neuronal activation as a positive control of *c-fos* expression (Baxendale et al., 2012b).

In general, there were slight changes in the protocols during the generation of controls and the WISH procedure itself. For instance, it was found that younger fish (>3dpf-8dpf) last up to 2 hours before entering a tetanisation stage, whereas fish between 15-22dpf

required less than 60 minutes. In all ages, we found that 40 minutes is a suitable window time of exposure to this drug concentration, to produce a good *c-fos* expression.

After PTZ exposure, fish were immediately sacrificed according to Home Office regulations, and fixed with a paraformaldehyde solution. Negative controls (no PTZ-treated) were culled and fixed in the same way. The following day, the fixation solution was washed and changed to methanol to store the samples until the WISH protocol was performed.

Another main modification in the protocol was the exposure of the proteinase K after the series of washes to transition to the hybridisation solution in day 1 (See Chapter 2.3.3). We found that regardless of the developmental stage, beyond 5dpf the best time window for Proteinase K exposure was between 35 and 40 minutes as showed in Table 8 from the materials and methods section. Any less than that would compromise an optimal incubation to allow the probe to penetrate the tissue to an optimal saturation concentration. Likewise, any more than that would soften the tissue to a point of near degradation.

For the compilation of good quality images via stereoscopic microscope, we decided to dissect the ventral area of the fish to improve exposure of the brain in a flat-mounted arrangement using glycerol after a series of washes as described in Chapter 2. These changes resulted in the obtention of good quality results in c-fos expression through WISH in fish up to 22dpf (Figure 3.14).

A.

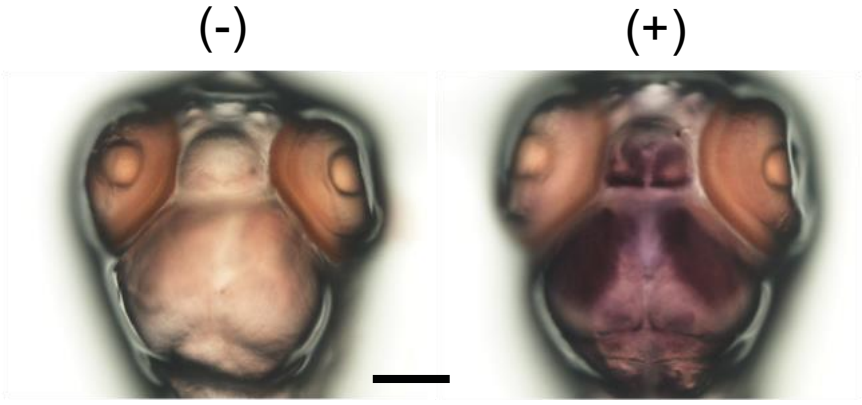

B.

Figure 3.14. Traditional WISH in late-stage zebrafish. (A) *Representative results of positive and negative controls of c-fos expression using WISH in 8, 15 and 22 dpf. A strong and generalised c-fos expression is evident in positive controls (fish exposed to 20mMPTZ compared with fish exposed to aquarium water only. Scale bar: 1cm* **(B)** *Zoomed view from the 15 dpf ZF fish larvae outlined by the green box in (A). Scale bar: 500µm.*

3.6.2 *c-fos* visualisation through post-WISH histological sectioning

Next, we wanted to identify if there was any *c-fos* labelling immediately after the exploration of a novel object. However, the expression obtained by WISH in the object exposed (OE) fish, was not clear enough and would possible be mistaken with noise

(image not shown). We hypothesised that the reason of this was that the location of this expression could be stronger in deeper areas where a stereoscopical visualisation is not sufficient (Sundquist, Nisenbaum, & Sarah J. Sundquist, 2005). To test this, the next step was to process the samples for histological sectioning using a cryostat as described in chapter 2 (Figure 3.15).

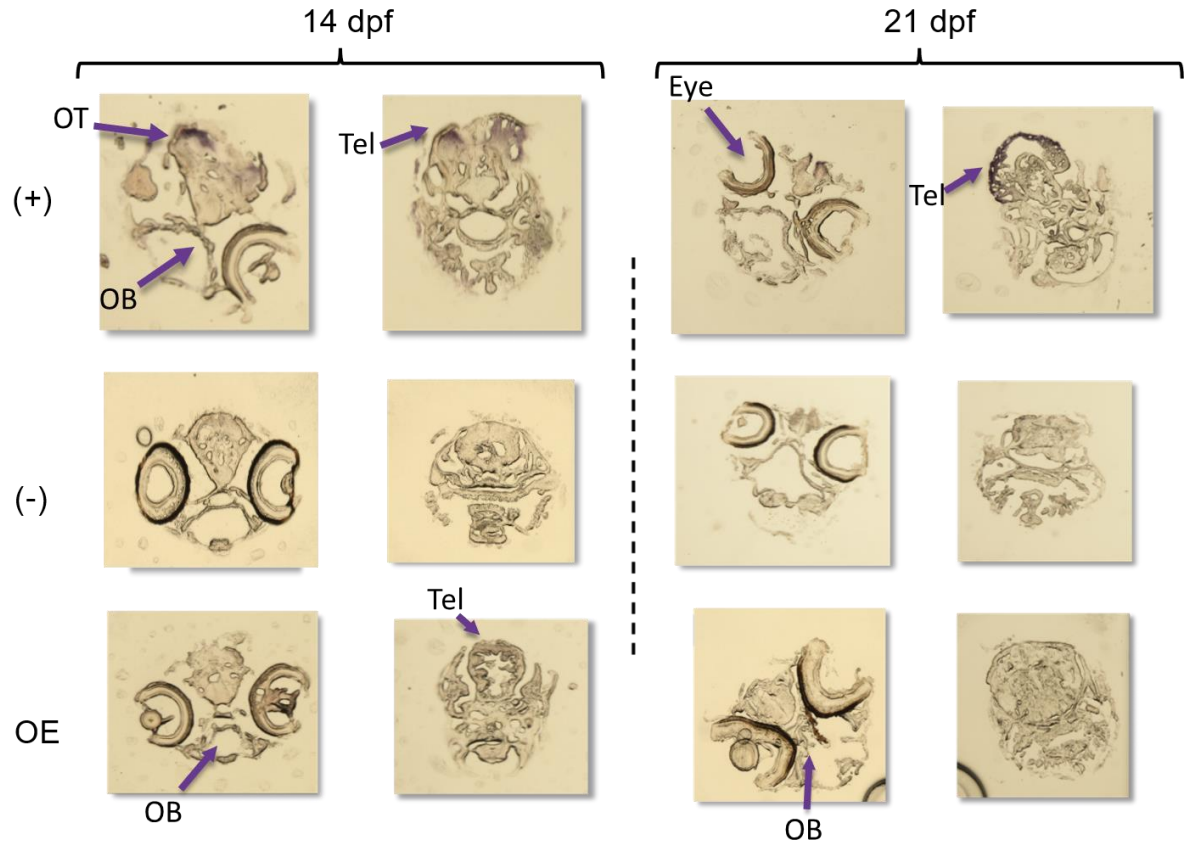

Figure 3.15. Brain slices from Late-stage ZF after WISH. *Left: 14dpf. Right: 21 dpf. Top: (+) Positive controls generated by induction with PTZ. Purple arrows show clear expression in the tectum, olfactory bulb, retina, and spinal motor areas respectively. Middle: (-) Negative controls from ZF. Bottom: OE - Fish exposed to a novel object for 10 minutes before being culled and fixed immediately before WISH. Purple arrows show strong expression in OB, and spinal cord. There is poor expression in motor areas in 21dpf fish compared with the positive control.*

It is possible to visualise some level of *c-fos* expression in OE-fish through cryosectioning in deep brain areas such as the tectum and the olfactory bulbs. However, we found that this method might not be ideal due to the high level of skills and time costs required to acquire good quality results. Therefore, we hypothesized that a better

method to achieve a more accurate visualisation might be through the addition of fluorescent labelled probes, which will be discussed in the next section.

3.7 FWISH

Fluorescent in situ hybridisation (FWISH), was developed as a more sensitive method to identify the expression of RNA probes. The variation of this method includes the use of Digoxigenin and fluorescein, the conjugation with alkaline phosphatase (AP) and the detection by tyramide signal amplification (TSA), which have shown to yield a cleaner signal labelling compared with other methods (Vigouroux et al., 2021). Compared to the traditional WISH, some reports claim that the signal amplification sensitivity can be increased to a single-cell level resolution, achievable with confocal or multiphoton imaging (He et al., 2020).

Here we used FWISH with some modifications to make it suitable for the identification of any expression of *c-fos* in late-stage ZF immediate after free exploration of a novel object (chapter 3.4). Among the adjustments made, we increased the proteinase K incubation period like in the traditional WISH protocol, as indicated in table 8 from the Materials and methods section (Chapter 2.3.3).

Finally due to accessibility, we decided to use two-photon microscopy to scan the fish previously processed for FWISH and mounted in 2% agarose to acquire a suitable position for imaging (Figure 3.16).

3.7.1 Use of multiphoton imaging in FWISH

Here, we explored the use of fluorescent dyes to identify neural activity through the expression of *c-fos* in WISH and adapted the protocols available for the use of FWISH in late-stage ZF after immediate exploration. Then we used 2-photon microscopy to identify the regions of interest with possible labelling of the probe (Figure 3.16).

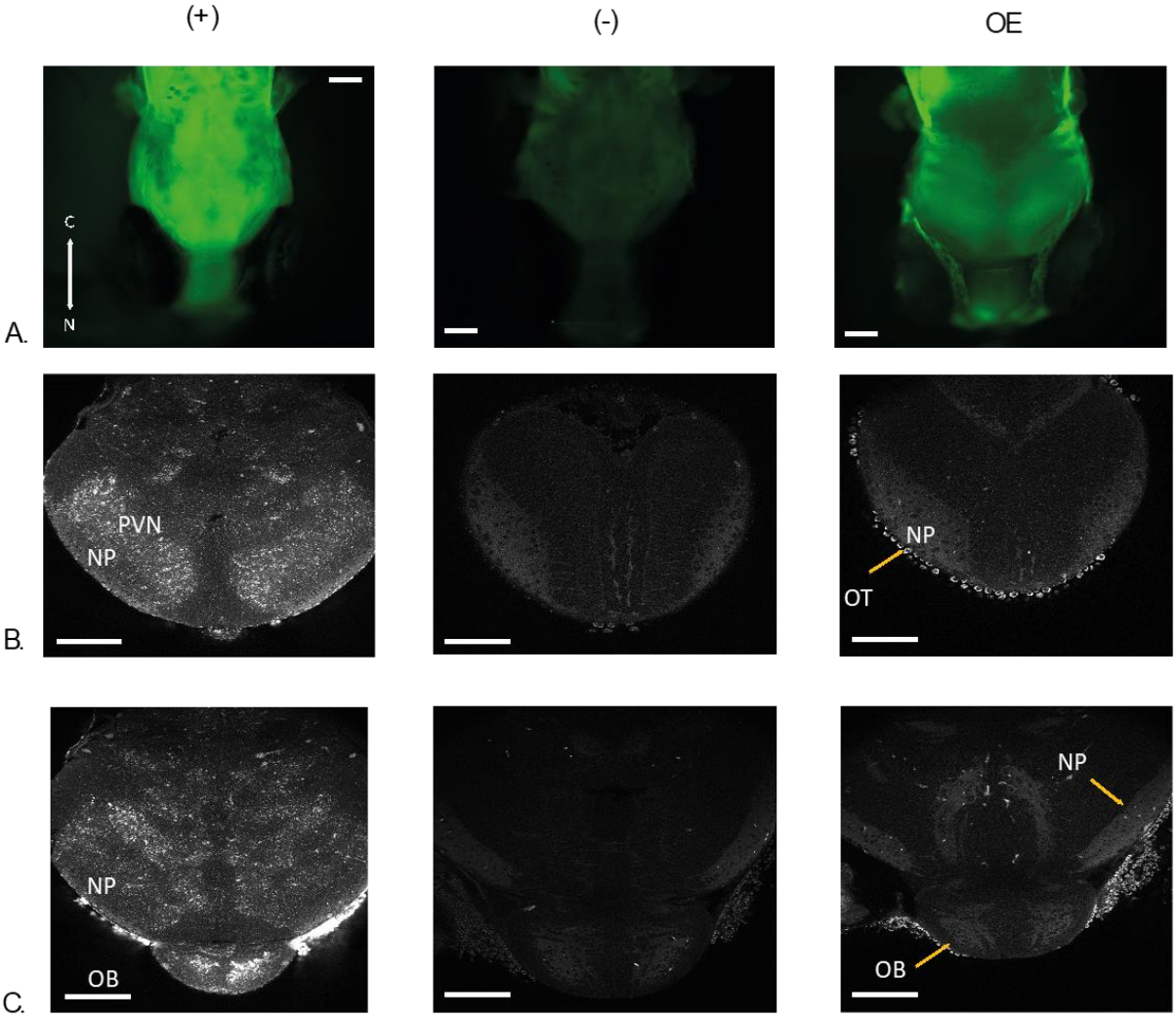

Figure 3.16. FWISH in late-stage ZF exposed to a novel object with *c-fos*. *Left: Positive control expressing c-fos induced by PTZ. Middle: Negative control, fish culled and fixed immediately. Right: Object exposed fish.* **(A)** *Top view of fluorescent microscopy of 15 dpf ZF larvae using GFP filter*. **(B)** *Two-photon imaging of a transverse view from the same ZF at the level of the superior third of the tectum.* **(C)** *Transverse view of the inferior third of the OT showing part of the olfactory bulb. Scale bars: 500µm. C: caudal, N: nasal, OB: olfactory bulb, OT: optic tectum, NP: neuropil, PVN: periventricular neurons.*

3.8 Conclusions

When assessing the exploratory behaviour of a fish in a novel environment before and after the introduction of a novel object, the change in exploratory performance is visually evident. Here, the sample size used in every experiment setup was bigger than in published reports and the analysis methods used were designed to avoid any subjective bias. Unfortunately, in these experiments, VLNOR was not supported as a method to assess memory behaviour as in our results the use of left vs right eye during exploration was not significantly different. Therefore, we decided to move on with the traditional novel object recognition (NOR) tests with two objects.

Additionally, we found that the results are not affected by age, sex, or context such as position of the object, change of size and colour. The result of the analysis of the object preference supports previous reports (May et al., 2016a); while, in the training phase, the preference for both identical objects are alike (Figure 3.14-C), there is a notable increase of preference for the familiar object in the testing phase after 24 hours (Figure 3.14-D). As a result, there is a statistically significant difference yielded in the Preference index (Fig 3.14-E).

WISH and FWISH are promising tools to identify areas of synaptic strength after short-term memory paradigms through the expression of IEG such as c-fos. Many protocols have been established for the use of these methods in zebrafish, mainly being visualised after micro-slicing of the tissue. PTZ is a suitable drug to generate positive controls of IEG expression in ZF over 5dpf. We found that the exposure of 40 minutes is enough to generate a good activation. The incubation time of proteinase K is important to achieve a good penetration of the probe without damaging the tissue structure. Between 35 to 40 minutes is the best window for this process for both WISH and FWISH.

FWISH coupled with multiphoton imaging shows to be a good combination to identify deep areas of synaptic activation at a fine-detailed level (single cell). For instance, after exposure of a novel context. Novel visual exploration seems to generate synaptic activation in deep areas of the OT, pre-tectum, and olfactory bulbs. Mainly in the superficial layers of the OT neuropil, such as SO and SFGS, as well as some scattered PVN.

Chapter 4. Visual Neuroplasticity in the ZF larvae. "The moving ball paradigm"

4.1 Introduction

Fundamental concepts depicted within the neuronal plasticity mechanisms include adaptation, facilitation, depression, habituation, sensitization, desensitization, dishabituation, potentiation (See Chapter 1.2). These will be frequently used to explain our findings in this chapter. The use of these learning components had been done arbitrarily in the past (Dong, Gao, Lv, & Bao, 2016b; Pellegrino, Sinding, de Wijk, & Hummel, 2017); even though the definitions and mechanisms are different, they are often confused, sometimes falling into unintentional incongruities (Poon & Song, 2007). These concepts are not fully exempt from being correlated with one another; therefore, it is worth starting this chapter by clarifying them.

4.1.1 Involuntary sensory mechanisms of learning

Adaptation, the protagonist in this chapter, is a fundamental property of any sensory system which originates at the early stages of sensory development, modifying the sensitivity continuously to stimuli to fit the environmental variations accordingly. The classic literature establishes that sensory adaptation is caused by either a fall in the receptor activity or a limitation of the effector response. Common examples of this learning property are the saturation of receptors in the taste buds or olfactory cells after being encountered with an overpowering flavour or smell, respectively. In other words, it is a physiological neural process that cannot be voluntarily reversed (C. S. Harris, 1963).

Short-term plasticity (STP), which will be described in further detail in the next section, includes other involuntary learning components. For instance, the increment of presynaptic calcium is caused by the decline of inhibitory feedback from the retinal amacrine cells to bipolar cells (Nikolaev et al., 2013a). When adaptation occurs by depletion of neurotransmitters, thus involuntarily decreasing the response to a repeated stimulus, we refer to this phenomenon as Short-Term-Depression (STD) (Chung, Li, & Nelson, 2002). On the other hand, Short-Term Facilitation (STF) happens when a stimulus produces an increase in the number of released neurotransmitters, thus increasing the synaptic response (Deperrois & Graupner, 2020; Castellucci & Kandel, 1976).

4.1.2 Voluntary non-associative learning

When there is a decrease in response to the exposure of a repeated stimulus without the contribution of physiological sensory exhaustion (adaptation), then we are describing habituation (Rankin et al., 2010; Siniaia, Young, & Poon, 2000). Habituation involves a behavioural component with the sensory response, like the voluntary ability to filter the background noise when it is raining or the voluntary visual filtering of people passing by your sight or conversing while working at a coffee shop. The sensing subject can consciously avoid paying attention to a specific feature of the sensory information from the repeated given stimulus. In this way, habituation is reversible; it is possible to bring back an increased response to the stimulus voluntarily, a mechanism called dishabituation (Bernhard & Van Der Kooy, 2000; Messina et al., 2020; R. F. Thompson & Spencer, 1966).

The opposite of habituation is sensitization. In a similar way to facilitation, here, there is an increased response to a repetitive stimulus. However, this response is voluntary, and it has no direct relation with sensory fatigue or depletion of neurotransmitters. A typical example would be the response to a pleasant gustatory stimulus where the subject consciously decides to increase the attention, thus the response to a specific feature (Çevik, 2014; Poon & Song, 2007). Moreover, sensitization can also be reversed (desensitization) (Pellegrino et al., 2017).

Additional to this terminology, other authors have included other terms to describe further other complexities that might be added to this net, although occasionally, some of these neologisms are not easy to grasp or fall in redundancies. An example is the case of the "secondary habituation", which is parallel to desensitization; "habituation to dishabituation" when a dishabituation is followed by habituation again (secondary habituation); or the "primary and secondary" types of sensitizations which stand for a similar idea. Primary sensitization is the first time a behavioural response increases, whereas secondary sensitization happens after a desensitization mechanism (Poon & Song, 2007; Siniaia et al., 2000).

To summarize the relevant terminology in this regard, I proposed a scheme of concepts and correlations of the terms according to what most publications agreed to follow (Figure 4.1).

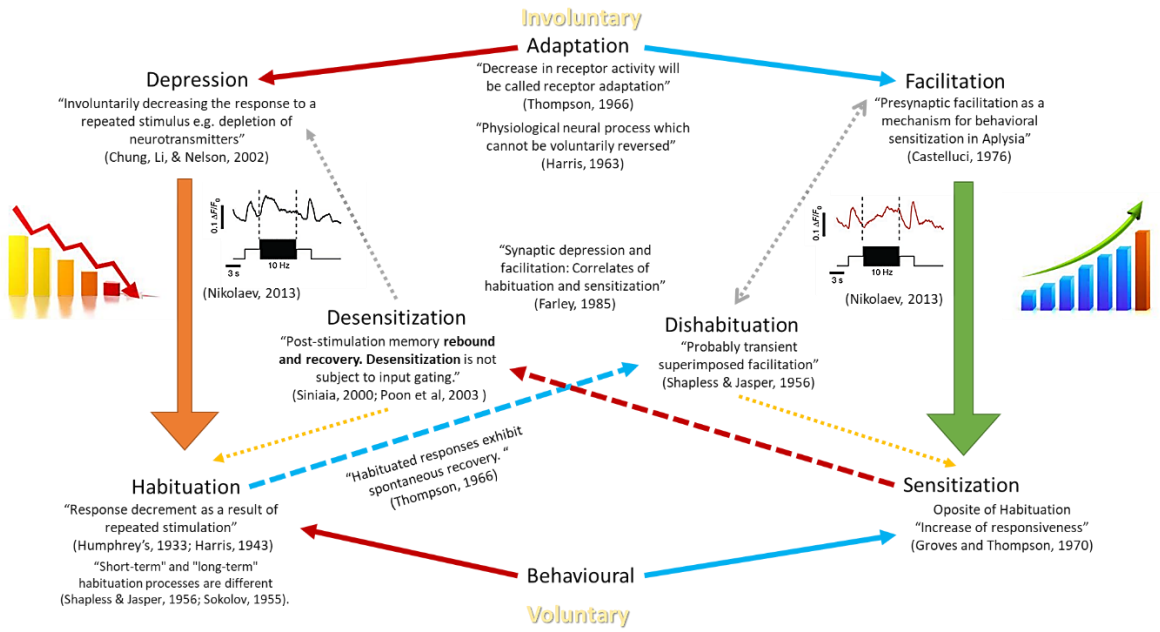

Figure 4.1 General concepts in learning. *Proposed diagram of the differentiation and correlation of the lexicon used to describe learning mechanisms according to the classic and modern literature.* (Castellucci & Kandel, 1976; Chung, Li, & Nelson, 2002; Groves & Thompson, 1970; C. S. Harris, 1963; J. D. Harris, 1943; Humphrey, 1933; Nikolaev, Leung, Odermatt, & Lagnado, 2013a; Poon & Song, 2007; Siniaia et al., 2000; Sokolov, E N, VIinogradova, 1955; R. F. Thompson & Spencer, 1966; Turatto, Bonetti, & Pascucci, 2018)

4.1.3 Short-Term Synaptic Plasticity

The general description of LTP and LTD, which shape the mechanisms of long-term plasticity, were covered in Chapter 1. However, this chapter will benefit from the addition of concepts related to short-term synaptic plasticity (STP). While LTP and LTD are involved in synaptic changes which last hours or longer and are primarily correlated with a specific firing frequency of pre-, and post-synaptic action potentials (AP) such as spike-timing dependent plasticity(STDP) (See Chapter 1.1.2), STP occurs over milliseconds to minutes (Deperrois & Graupner, 2020; Regehr & Abbott, 2004).

As mentioned in section 4.1.1, upon presynaptic stimulation, a synapse can undergo a rise in response to a stimulus (STF) or a decrement (STD). Thus, STP is displayed in a variation of synapses which can be either facilitating, depressing, sustained, and even have a mixture of both (Nikolaev, Leung, Odermatt, & Lagnado, 2013b). In general,

depression is accredited to the diminution of a pool of presynaptic vesicles, whereas facilitation is associated with the calcium dynamics in the post-synaptic terminal (Deperrois & Graupner, 2020; Fioravante & Regehr, 2011).

4.2 Mechanisms of visual adaptation in the ZF

With more frequency, a variety of publications have advocated that even though individual neurons adapt in a different manner, it is crucial to study adaptation at the level of population of neurons (Gutierrez & Denève, 2019; Solomon & Kohn, 2014). In line with this, in the visual system, the populations of bipolar and ganglion cells are an illustration of this importance. It has been demonstrated that the sign and dynamics of adaptation in these cells exhibit an enormous diversity: while some cells depress upon an increase in stimulus intensity, others sensitize (Baden et al., 2014; McMains & Kastner, 2011; Nikolaev et al., 2013a). Furthermore, depression has been reported to have a synaptic origin, while facilitation can be secondary to depression in the inhibitory feedback to bipolar cells (Nikolaev et al., 2013a).

It is proposed that the diversity of adaptation dynamics within the same population of neurons aims to improve the coding of visual input changes efficiently (e.g. increment or decrement of temporal contrast and mean luminance) (Ghodrati, Zavitz, Rosa, & Price, 2019; McMains & Kastner, 2011; Odermatt, Nikolaev, & Lagnado, 2012). Main adaptation dynamics in the ZF retina have been characterized in the past (Graydon et al., 2018); however, since different modes and dynamics of adaptation may contribute to the population coding of visual information, it is essential to understand whether the plasticity dynamics observed in the early sensory neurons exist in the downstream areas of the brain.

For instance, adaptation in the V1 cortex and in the optic tectum has been shown to differently change the sensitivity in different individual cells suggesting that other modes of adaptation demonstrated in the retina may indeed be preserved downstream. (Ahrens, Li, Orger, Robson, & Alexander, 2013; Zariwala et al., 2011). Even though recent publications have tackled the analysis of functional cell diversity at a higher function level in vertebrates (Bergmann, Santoscoy, et al., 2018; Förster et al., 2020a; Kunst et al., 2019), adaptation dynamics in the visual system are still far from being well understood, and a systematic, reproducible analysis had not been proposed yet.

During development, the plasticity changes that endure the neural sensory circuits, such as the visual system, depend in great part on environmental (a sensory experience), and genetic factors (Marachlian, Avitan, Goodhill, & Sumbre, 2018a; Walker, Burrone, & Meyer, 2013b). However, it is not clear whether different modes of adaptation are morphology dependent. For instance, are these neuroplasticity properties stratified in different organized layers, like in a filter manner? Or is the overall visual input coded across the tectum within the same brain area? Also, is it possible to modify these computations in an artificial manner? And how do different variations of the same paradigm affect the outcome of the tectal visual processing? Here I aimed to target these questions using 2-photon *in vivo* imaging in late-state ZF larvae while presenting a simple visual stimulus.

4.3 Simple experiment to assess neuroplasticity properties: The moving ball experiments

As stated in the Materials and Methods section, in this chapter, the visual stimuli consisted in a straightforward one. The "moving ball", a black circle passing through the screen in a rostral-to-caudal caudal direction with respect to the position of the fish, with a visual angle (VA) of 13.125° and a speed of 38 degrees per second (Figure 4.2-A) four consecutive times is considered as a set. The complete stimulus consists in ten sets, thirty seconds long, followed by thirty second rest.

Genetically encoded calcium indicators (GECIs) along with two-photon calcium imaging were used in zebrafish larvae ranging from 4 dpf to 21 dpf. The fish was mounted parallel to the screen (124 x 35 degrees size), allowing full monocular vision in 3.5% low-melting-point agarose previously oxygenated as described in the materials and methods section (Chapter 2.5.3) (Figure 4.2-B). Depending on the developmental stage and thus the size of the fish, two microscope objectives were used, 25X usually enough to image both OTs and part of the motor brain areas (Figure 4.2-C) to 60X to achieve a single cell resolution image from the contralateral tectum (Figure 4.2-D).

The proposed "moving ball" paradigm is a simple stimulus that can be categorized as a non-associative learning model; we analyse the changes in neural responses to the repetition of a single type of stimuli (Bernhard & Van Der Kooy, 2000). In this case, the inter-stimuli interval (ISI) was also fixed to 30 seconds to keep a streamlined approach.

The aim was to primarily assess the properties of adaptation to this repetitive stimulus across the neural population of the OT neuropil circuit.

We hypothesized that the layered organization of the OT neuropil might present different adaptation dynamics to improve the efficiency of the output signal downstream the ZF brain. Additionally, we expected to find variations of visual plasticity dynamics according to the developmental stage of the fish and genetic strain. Finally, we used this paradigm to answer further interrogations such as the impact of size, GABA inhibition, and the combination of other sensory systems in adaptation dynamics.

4.4 Properties of visual plasticity in the OT

It is known that zebrafish display a well-established optokinetic response (OKR) -eye reflex in response to visual movement- at three dpf, and by 5dpf, prey hunting behaviour is exhibited (Bögli, Afthinos, Bertolini, Straumann, & Huang, 2016). Additionally, the ZF OT is considered morphologically and functionally mature at eight dpf (Niell & Smith, 2005). For the basis of our experiment analysis, we used aquarium raised NBT: GCaMP3 nacre ZF between 14 and 15 dpf. The Huc: GCaMP6 strain was available; however, despite presenting a higher calcium fluorescence signal during the early days post-hatching, we found that the brightness significantly decreases overtime after a week, making it problematic to image above 10 dpf with a few exceptional cases.

After the presentation of the moving ball with the primary conditions mentioned above, the average distribution of the responding neurons across the OT, measured by the probability of responding voxels in the neuropil, has three evident high-density population zones: Input formed mainly by the SO (i); the medial which we divided in the voxels corresponding to the SFGS (ii) and SGC (iii) zones; and the output, formed by the SAC and SPV (iv) (Figure 4.2-E). We observed that using a custom-written code for Igor Pro 6.3 (Wavemetrics) after applying a filter that selects by skewness ≥ 0.8, the average number of responding traces detected per fish in each neuropil stands approximately between 800 to 4,000, from which in total 16 421 traces were selected as responsive from 13 fish (Figure 4.2-F).

All the detected responses were averaged to determine the fluorescent dynamics in the tectal neuropil as a synaptic population. In all fish-by-fish scenarios, we found steady

characteristics that stand from the responses averaged in the full neuropil, which will be described next.

1. The response to the very first visual presentation (of the black circle passing through the screen) will always trigger the most significant response.
2. A subsequent second, third and fourth continuous presentation of the same stimulus will generate a continuously smaller response as the stimulus is not novel anymore.
3. After an inter-stimulus interval (ISI) of 30 seconds, the initial response of a subsequent set usually generates a first peak that is higher than the non-first peaks from the previous set.

It is possible that the third statement happens because a physiological recovery period took place, and there is still a response coming from the retina, which has not been adapted.

Subsequently, we sorted the responses by layer on an individual basis (fish-by-fish) according to the normalized histogram generated for the detection of population density of responding voxels which varied due to the slight difference in the focal plane imaged in each fish (Figure 4.2-G). After layer sorting, we noticed additional plasticity properties happening across the tectal neuropil (Figure 4.2-H). To describe these findings, we used different mathematical approaches.

4.4.1 Adaptation

As previously mentioned, adaptation relates to the physiological ability of neurons to respond to a stimulus independently of their habituation (will). Thus, the dynamics of adaptation were measured, taking into account each set of the stimulus. To determine the general adaptation properties, we used the adaptation index (AI) calculated as the ratio between the first and the fourth peak-response amplitudes (P_1/P_4) in each set (Figure 4.3-A). Furthermore, we decided to average the AI from the first three sets per fish. The reason behind choosing this average was that this was usually the time point where the response dynamics were kept similar onwards. Thus, it is more likely to achieve a closer value in each fish. A value of ≤ 0.74.9 was considered depressing, ≥ 0.75 to 0.99 steady-state, and above one facilitating.

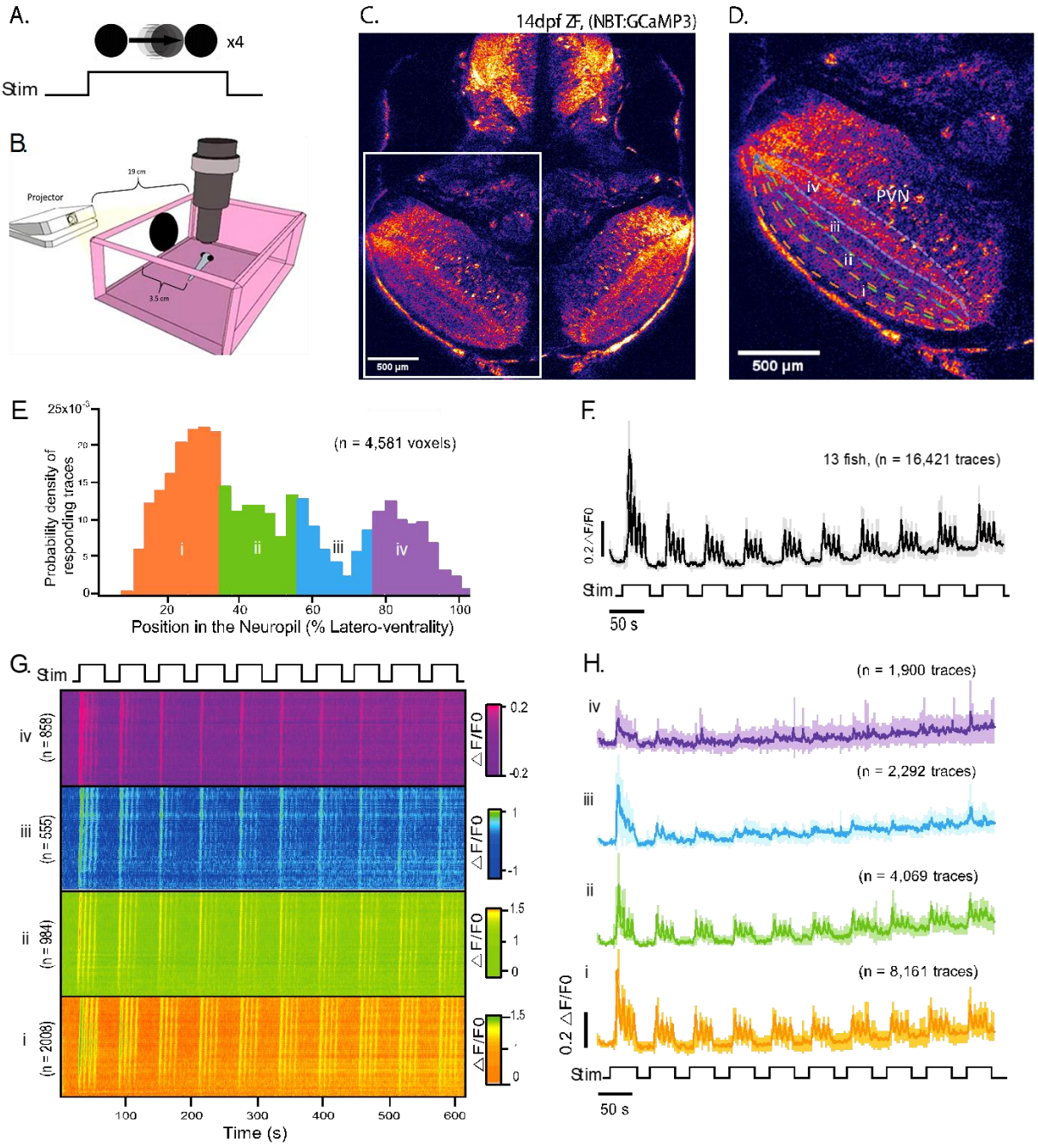

Figure 4.2. Optic tectum neuropil responses to the moving ball paradigm. **(A)** *The stimuli consist of a black circle passing four consecutive times in a lapse of 30 seconds with 30 seconds of ISI.* **(B)** *General imaging setup. A late-stage ZF larva is embedded in 3.5% LMP agarose (previously aerated) inside a custom-made chamber with a screen on one side. The ZF is facing towards the screen with one eye only, to which the stimulus is projected* **(C)** *Multiphoton imaging of a 14dpf NBT: GCaMP3 ZF-brain using a 25Xw objective.* **(D)** *Zoomed view from*

the highlighted area in B. OT neuropil with manually drawn dashed lines indicated four main layered zones. i) SO, ii) SFGS, iii) SGC and iv) SACPV. **(E)** *Representative histogram of the normalized responding voxels from one fish colour-coded according to the zones of the neuropil zones in D.* **(F)** *Average response from 13 NBT: GCaMP zebrafish OT neuropils (14-15dpf). Shaded area delimits the S.E.M.* **(G)** *Heat maps of the responses from the same single fish in E. divided by neuropil layers, the number of responding traces is shown.* **(H)** *Average layered responses from 13 NBT: GCaMP3 fish. Shading represents S.E.M.*

4.4.2 Habituation

In most cases, it was detected that the tectal response behaviour across the fish tested in standard conditions was kept similar from the 4th set onwards as a neural population. We hypothesized that this might be driven by a habituation mechanism. Thus, it was considered as Habituation Index (HI), the ratio between the area under the curve (AUC) from the first and fourth sets, which we named as $\theta 1$ and $\theta 4$ (Figure 4.3-A) since habituation does not relate with the response fatigue of a synapse. In this case, a value below one is considered habituation; ≤ 0.74.9 to 0.99 was considered non-habituated, while ≥ 1 was considered sensitization.

We found that for our experiment, in normal conditions, the average adaptation dynamics across the whole neuropil population is carried out by short-term depression, and this behaviour remains constant when analysing the responses across all the NP layers (Figure 4.3-B). However, whereas the average of the whole-population dynamics in the NP and the input zone (SO) leans towards habituation, there is a disparity in the behaviour in the output layers: while some fish habituate, others seem to sensitize (Figure 4.3-C).

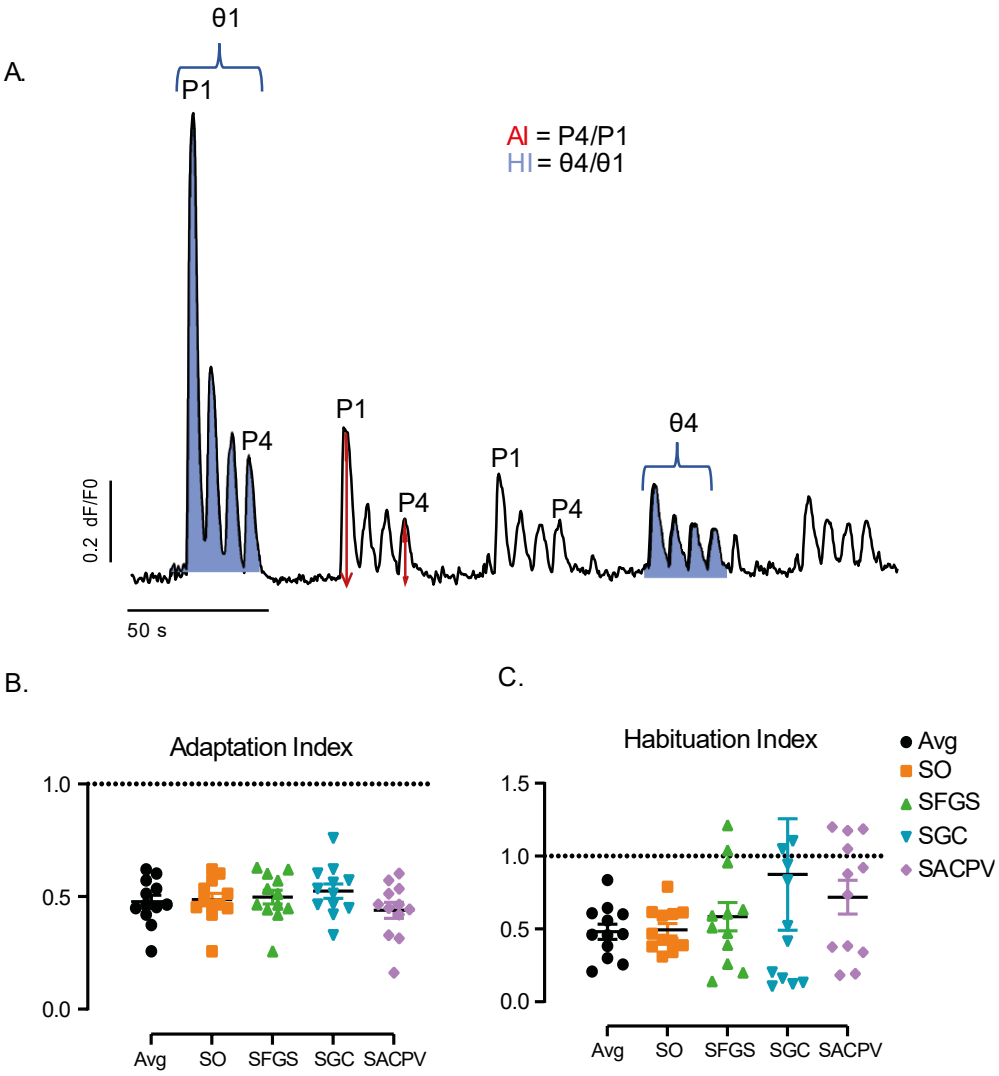

Figure 4.3 Adaptation and Habituation Index. **(A)** *Calculation of adaptation index (AI), where "P1,4" represents the amplitude of the first and fourth peak responses respectively (red arrows); and Habituation index (HI), where θ stands for the area under the curve of the selected sets (blue shade).* **(B)** *Results obtained from the AI of NBT: GCaMP3 zebrafish larvae between 14 - 15dpf (n = 12)* **(C)** *HI results from the same fish from B. Note despite being a broad diversity in the output layers (SGC, SAC, and SPV), the overall response habituates in all subjects.*

4.4.3 Additional neuroplasticity properties

When describing plasticity events, it becomes apparent that both adaptation and habituation dynamics comprise other behaviours that suggest other neuroplasticity sub-properties. Among these properties are the speed of habituation, the speed of adaptation and dishabituation and desensitization components.

4.4.3.1 Habituation speed

As mentioned earlier, even though we determined that the 4th set presentation onwards does not generate a massive change in the overall response in normal conditions, we observed that different cells and layers reached this plateau state at different time points. Therefore, the speed of habituation was determined by normalizing the area under the curve relative to the first set (Figure 4.4-A) through the following equation:

$$y = (y0 - Plateau)\, e^{-\frac{1}{\tau} * Set\#} + Plateau$$

In which y is the speed of habituation measured through the relative change in fluorescent intensity ($\Delta F/F_0$) where ΔF is calculated by subtracting the baseline given by the average fluorescence of the first 15 frames of the calcium signalling generated during the beginning of the experiment (no stimulus), to the fluorescence at a given time determined by the frames recorded when the stimulus starts, y_0 is the reference value of the response; in other words, the average baseline value (activity without stimuli), τ is the time constant multiplied by the number of set repetition (1, 2, 3…). In normal conditions, the behaviour of the average neuropil population and within layers can be fit in different exponential fit equations according to the extra sum of squares *f*-test, $p < 0.05$ (Figure 4.4-B).For the data presented, n= 16,421 traces, from 13 fish, the common model still describes every curve adequately (R^2: 0.91, 0.89, 0.87, 0.55, 0.8; respectively for the average NP, SO, SFGS, SGC and SACPV) by the following equation:

$$Speed\ of\ Habituation = (309.43)\, e^{-\frac{1}{0.64} * Set\#} + 34.87$$

In this case, the time constant (τ) oscillates around 0.64, with a range of 0.3490 to 0.9515 for 95% confidence interval (CI). Thus, a value above 0.95 will be considered fast habituated and < 0.34, slow habituation.

4.4.3.2 Dishabituation and sensitization mechanisms

The simplicity of this experiment shows that most of the times when a stimulus is repeated multiple times, the subject tested "gets bored", hence it decides to voluntary pay less attention over time; in other words, it habituates. We found out that this

mechanism is voluntary because it can be reversed at the subjects will, and the response to the stimuli can be increased again, or dishabituate. In the same manner, we found a small number of cells which did not undergo habituation and from the start show an increment in the first peak response over time, hence, sensitization.

Here I aimed to find the presence of dishabituation or sensitization components through a mathematical model. For this, we decided to measure the relative first peak area (Figure 4.4-C). In this case, the average NP response and most layers excluding the most ventral areas (SAC and SPV areas) can be fitted to an exponential decay curve (Figure 4.4-D) which can be described with the same exponential decay model used for the habituation speed. In this case, y is the function representing the area percentage of the first peak from each set in arbitrary units of fluorescent intensity ($\Delta F/F_0$), relative to the first peak of the very first set from the whole experiment.

$$Relative\ 1st\ Peak\ Area\% = (175.69)\ e^{-1.437 * Repeat\ Number} + 58.81$$

In these conditions, the tau reached up to 1.687 repetitions (95% CI:). When the relative first peak area percentage cannot be described adequately by this function, we can safely assume that there is a phenomenon of dishabituation or even sensitization which should be further analysed using a linear regression model.

4.4.3.3 Speed of Adaptation

To determine the speed of adaptation, we measured the slope (m) generated between the first and the 4th response peak in each set (Figure 4.4-E). This value was calculated initially with a linear regression fit per set. The rationale behind using the slope instead of the tau is that adaptation not always will be depressing, and an exponential decay model will not be a suitable model that fits all, however, a simple linear regression will be. A value equal to or less than -1.0e-03 would be considered fast adapting, whereas near to 0 will be slow adapting, and > 0 non-adapting (facilitating).

4.4.3.4 Habituation to visual adaptation

Previous literature had reported the dynamics of adaptation over time in other sensory systems (Pellegrino et al., 2017). This mechanism could be interpreted as habituation to adaptation (Dong et al., 2016b). As its name suggests this concept refers as to how a cell will undergo a voluntary adaptation behaviour. Even though most of the times what we

see is a constant depression dynamic, it is important to remember that is possible to have both depressing and facilitating dynamics and as they are voluntary, a sudden change is also possible.

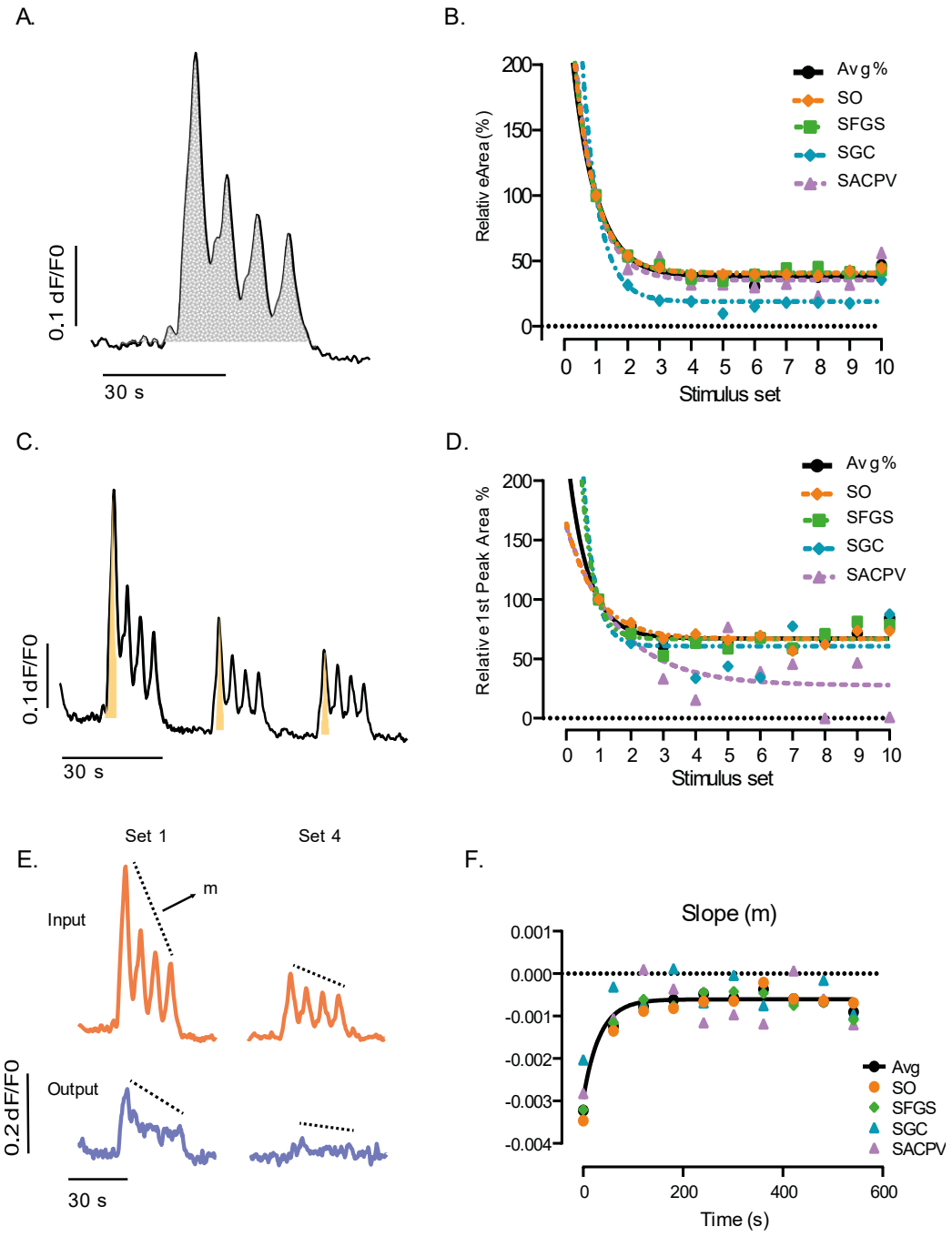

Figure 4.4. Plasticity dynamics in standard conditions follow exponential curve trends. *To simplify the description of the dynamic neuroplasticity components using the moving ball paradigm, we calculated the following statistics:* **(A)** *The amplitude of each set was calculated by the AUC per set. This*

value was later used to calculate the HI. **(B)** *The relative AUC give information about the level of habituation dynamics to the stimuli repeats over time. This is measured considering the AUC of the first set as 100%.* **(C)** *Average response to the first three sets of the experiment (n = 12 fish). The amplitude of the response to the first presentation per set is shown in yellow.* **(D)** *The AUC of the first peak corresponding to the very first presentation of the moving circle was considered as 100%. Thus, the relative 1st peak area contributes to the definition of adaptation and habituation dynamics.* **(E)** *Comparison of responses from the input (orange) vs output (purple) areas of the OT during the presentation of the 1st (left) and 4th (right) sets. The dashed line shows the slope (m).* **(F)** *The slope measured in E. determines the speed of adaptation dynamics. This was later plotted over time and per layer in the neuropil. Note an exponential decay pattern that is possible to fit within the same non-linear fit in average and across layers (described in the text). (p < 0.05).*

In this case, we considered the average pendent (m) in the experiment per set using an exponential decay curve fitting (Figure 4.4-F). In normal conditions, the slope as a function of the number of stimuli repetitions can be defined as:

$$m = (-0.0035592)\, e^{-\frac{1}{\tau} * Set\#} + 0.0006062$$

Where tau ranges between 15.74 to 49.70 (extra-sum-of-squares F-test, $p < 0.05$).

4.5 Size-dependent plasticity properties

How visual responses filtered by the size of a stimulus have been studied in the past, mainly being described by how the information is processed through the retinal ganglion circuits (Förster et al., 2020b; Preuss et al., 2014a; Yin et al., 2019b). For instance, it has been reported that most of the superficial interneurons (SINs), which branch to the SO and SFGS layers of the OT neuropil, appear to be receiving already size-filtered inputs, although it is hypothesized that there is a non-RGC-component which sharpens this size-tunning property (Del Bene, Wyart, Robles, Tran, Looger, Scott, Isacoff, Baier, et al., 2010).

Here, I aimed to investigate whether the adaptation dynamics are object-size dependent or if size plays an independent role regarding visual adaptation. In other words, we

wondered whether the size of the stimuli might modify the response that reaches the visual system downstream. For this, we decided to perform the moving spot experiment changing the size to a smaller and into a bigger moving circle than the previously tested (**13.125**° of VA). The small spot had a VA diameter of **3.274**° and the big circle **24.74**°.

Qualitatively, there is no significant difference between the responses obtained from the small spot and the medium-sized circle overall. However, it appears that some of the central to ventral layers comprising the SGC zone remain with similar adaptation dynamics per set over time (Figure 4.5-A). Additionally, the responses obtained from the big size circle show a bigger first peak amplitude in each set compared with the small and medium size, suggesting a different adaptation and habituation dynamic component (Figure 4.5-B).

To test these results, we measured the habituation behaviour through the mathematical models previously described. We found the AI to be 0.464 and 0.415 for the small and big ball, respectively ($p < 0.05$); the HI of 0.445 for the small spot and 0.494 for the big circle ($p < 0.05$).. These results show a similar general adaptation and habituation compared with the medium ball. Another similarity relied upon the distribution of the responding traces across the neuropil in three main zones: outer, medial, and ventral. However, we found a higher number of responses in the most outer or ventral layers, namely SACPV for the big and small spots, compared with the medium-sized (Figure 5.6-A).

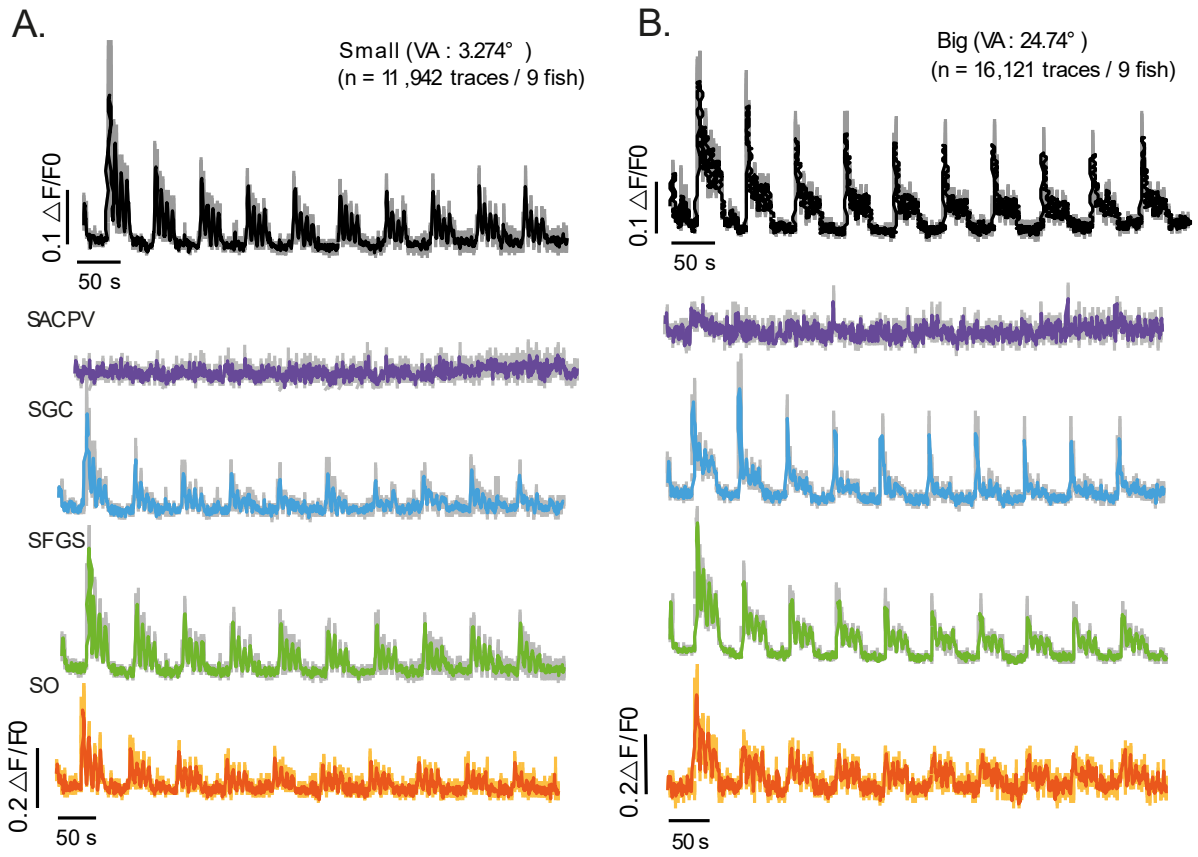

Figure 4.5 Responses to different sizes of the moving ball paradigm. *There is a qualitative difference in the overall averaged neuropil responses between the smaller and larger sizes of the moving ball paradigm—Black (above): Averaged NP.* **(A)** *Responses to the small moving spot. Note there is no apparent response in the most ventral layer (SACPV).* **(B)** *The responses to the big circle appear to present a higher first peak amplitude over time across layers and per set.*

Overall, we found that the behaviour of the neuropil response averages was reasonably well described by applying non-linear regression to a one-phase-decay fit as previously done (R^2 values were 0.4558, 0.7924, and 0.661 for small, big, and medium-sized ball, respectively). Comparing them using an extra sum of squares F-test showed that there is no single mathematical model that adequately describes the behaviour in all these presentations, $p < 0.05$ (Figure 4.6-B). In this case, the best model that describes the average of the overall NP response to the small spot is the following:

$$1st\ PA\% = (622.37)\ e^{-3.64*x} + 83.63$$

Where x is the set number, and the tau is 0.274 which is faster than the medium-sized stimulus response. Whereas the values for the averaged NP responses to the big stimulus can be substituted as follows:

$$1st\ PA\% = (-36.02)\ e^{-0.4661*Set\#} + 125.4$$

Where the time constant is faster than the smaller and normal-sized stimuli, being 2.145 repeats, $p < 0.05$ (Figure 4.6-B).

Finally, I decided to further test these plasticity properties in a layer-by-layer basis comparing the response to the different sizes of stimuli. In the case of the response dynamics to the small ball, we did not find any statistically significant difference compared with the medium-sized stimulus. Interestingly, when running this same procedure (non-linear fit and extra sum of squares F-test) for the SO layer, we observed that the three data sets of different sizes can be modelled after the same phenomenon ($p < 0.05$). Said model is as follows:

$$1st\ PA\ \% = (97.67)\ e^{-1.473*Set\#} + 77.83$$

In this most outer layer, the τ was of 0.6791 repeats, using an extra sum of squares F-test, ($p < 0.05$, asymmetric 95% CI). A similar situation happens in the most ventral areas (SACPV), where the equation including the substitute values is described as:

$$1st\ PA\% = (37.43)\ e^{-0.41*x} + 93.67$$

The time constant in this case was 2.425 repeats. This could be explained by the fact that this layer usually displays fewer calcium fluorescence response, and the change over time is minimal.

In the intermediate layers, SFGS and SGC, we found that whereas there is no difference in the habituation dynamics between the small and the medium sized stimulus, and both contexts can share the same model, it was not possible to fit the relative area responses from the big moving ball to a one-phase decay model, hence showing a component of dishabituation (Figure 4.6-C).

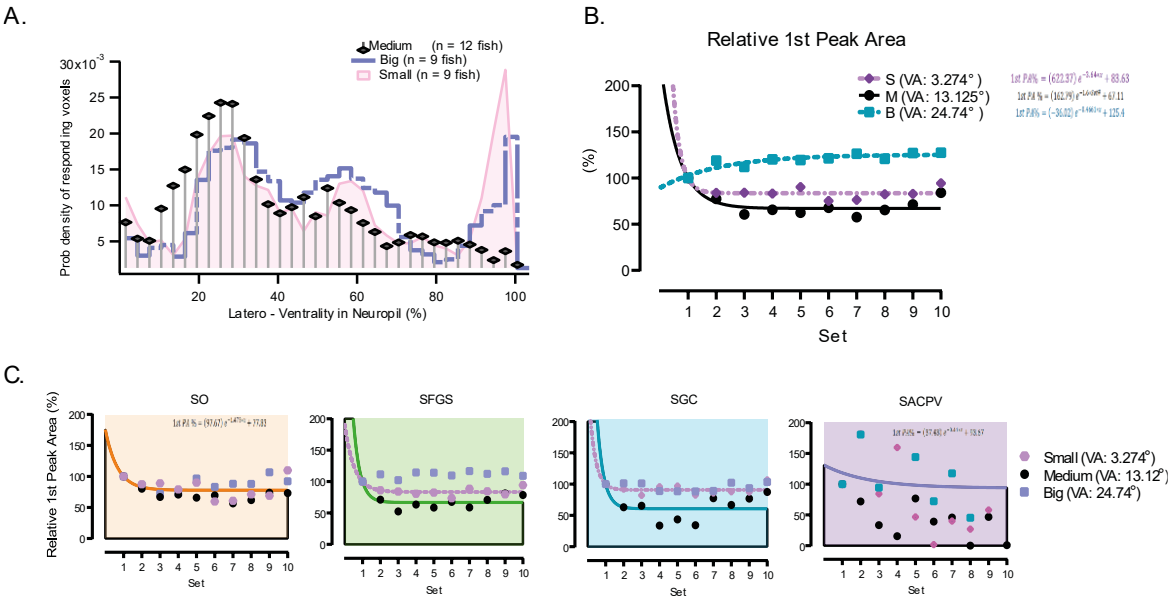

Figure 4.6 Adaptation dynamics according to size of stimuli. (A) *The layered distribution of responding voxels is analogous across the neuropil. However, there is an increase in the number of responding voxels in the output area when the big and small moving spots are applied.* **(B)** *The dynamics of the relative AUC of the first spot-presentation in each set changes overtime. Whereas for a medium and small sized spot there is an exponential decay decrease in the response of the first presentation in the first sets relative to the next, this property shows an opposite model when the big stimulus is applied.* **(C)** *The response to the stimuli is dependent on the size of the stimuli in the intermediate layers of the neuropil. Small ball (n = 11, 942 traces from 9 fish), Big ball (n = 16, 121 traces from 9 fish). SEM is shown in grey.*

Interestingly, when comparing the AIs between the four main zones, there is a direct correlation between the size of the stimulus and the adaptation dynamics in the layers near the periventricular cell bodies (SACPV). Whereas there is no response, thus no adaptation when presenting the small stimulus; the biggest circle triggers a higher first peak response, and therefore, higher AI, hence, facilitation (See table 20).

	NR		SMALL		BIG	
	AI	SEM	AI	SEM	AI	SEM
AVG	0.445877	±0.06538	0.464068	±0.04500	0.41579	±0.036603
SO	0.484221	±0.07654	0.565869	±0.06058	0.553573	±0.172741
SFGS	0.465071	±0.13008	0.443616	±0.07766	0.481249	±0.027803
SGC	0.708623	±0.28482	0.336795	±0.11510	0.298029	±0.092888
SACPV	0.164866	±0.21840	0.503948	±0.11984	0.656573	±0.187624

Table 20. Comparison of the AI in different size of stimulus. *Warm colour coding represents values close to non-adapting or steady state, whereas cold represents highly adapted index towards depression.*

A viable explanation for these response dynamics might be the context in which the size of a stimulus plays a role in the decision to down-stream the visual information into deeper areas. A big stimulus may represent a possible hazard such as a predator approaching, thus habituation mechanisms are less likely to occur due to constant awareness to danger. On the other hand, a small sized might represent an unreachable prey taking in account the movement restriction in which the ZF is situated. However, this hypothesis needs additional investigation. For this reason, we decided to keep the medium moving ball as the standard size in further experiments we kept.

4.6 Post-synaptic ganglion-specific adaptation (SyRGeCO)

To look at the neuropil responses that corresponded only to the retinal ganglion cells component, we used ZF expressing red calcium indicator coupled with synaptophysin in the isl2b promoter, which is expressed in RGC. isl2b: SyRGeCO ZF (Walker et al., 2013a). In this case, we used a blue filter suitable for imaging in the red channel preventing any interference as much as possible and then, a secondary filtering was performed using image analysis to eliminate scattering (See Chapter 2).

In these experiments, we obtained responses to every passing ball in each set. Surprisingly, we found that even though the responses within the first presentation sets were higher, the adaptation index was 0.622 ± 0.065, which is higher compared with the overall responses in the neuropil found in NBT: GCaMP3 or Huc: GCaMP6 ZF. This suggests that the presynaptic RGC-component might adapt less to a repeat-stimuli (Figure 4.7-A). It is worth noticing the presence of occasional scattered responses across the neuropil reaching up to the PVN (Figure 4.7-B).

Finally, the HI was 0.704; thus, it correlates with a habituated behaviour even though it is on the higher side. The best non-linear fit given by the relative first peak area in this case is:

$$1st\ P\ A = (129.1)\ e^{-\frac{1}{1.302}*\ Set\#} + 41.2$$

These values are within the normal habituation range (extra-sum of squares f-test, $p < 0.05$).

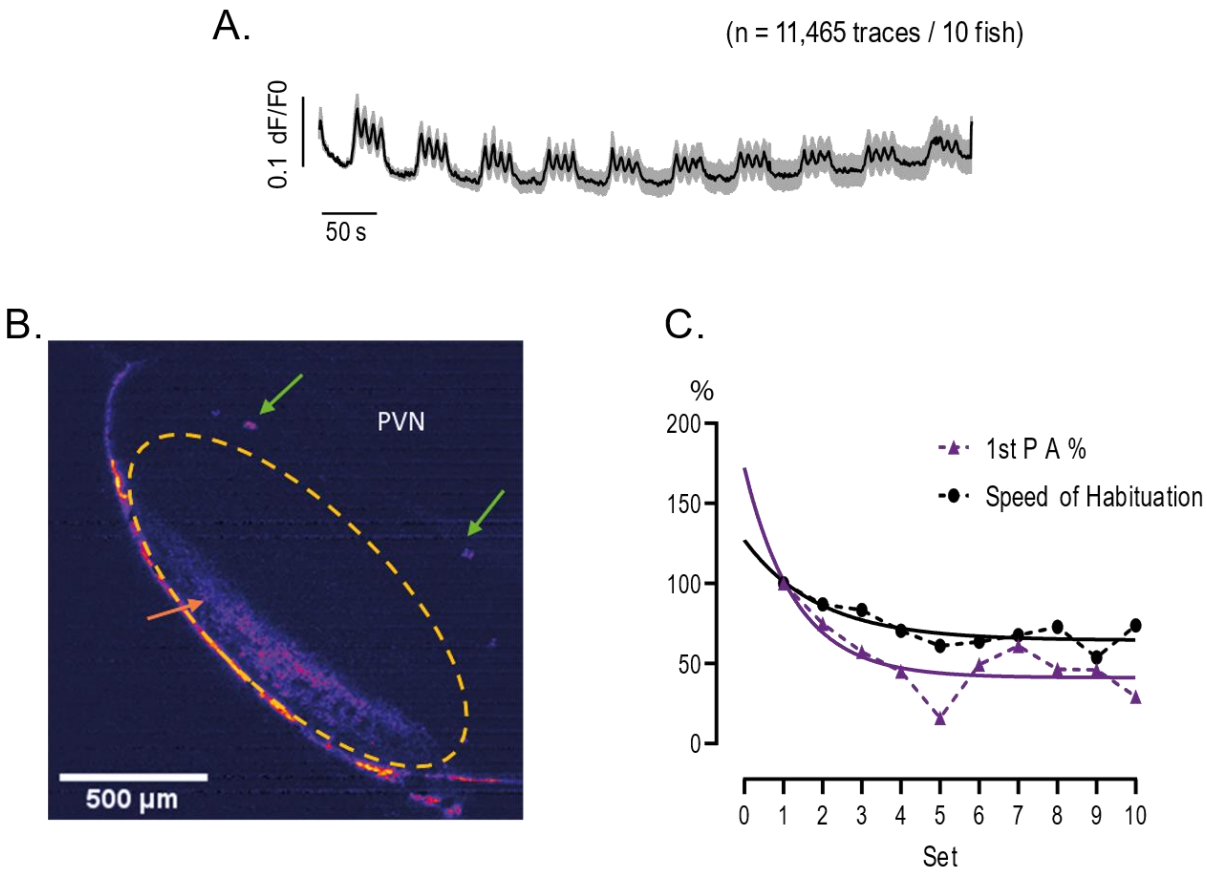

Figure 4.7 Post-synaptic plasticity dynamics in the OT with RGC origin. (A) *Averaged responding traces from 10 isl2b: SyRGeCO ZF between 11 and 14dpf. SEM is shown in grey.* **(B)** *Two-photon image from a representative 14dpf isl2b: SyRGeCO tectum. The neuropil was manually highlighted in dashed yellow lines to assist the identification. The orange arrow (bottom) shows the main area where the RGC responses occur, whereas the green arrows (top) show scattered responding cells projecting to the PVN.* **(C)** *Dynamics of Habituation in RGC. The speed of habituation is measured by the relative AUC with respect to the first. The relative first peak area aids to evaluate other aspects such as habituation to adaptation.*

In terms of the habituation speed, the relative area can be fitted using the following model:

$$Speed\ of\ Habituation = (62.64)\ e^{-\frac{1}{1.884}*\ Set\#} + 64.46$$

In this case, the time constant (τ) oscillates between 0.586 to 11.34 repetitions (extra-sum of squares f-test, 95% CI). Therefore, these values are on the normal to fast-habituated side (Figure 4.7-C).

A summary of all the proposed mathematical models can be seen in Figure 4.8.

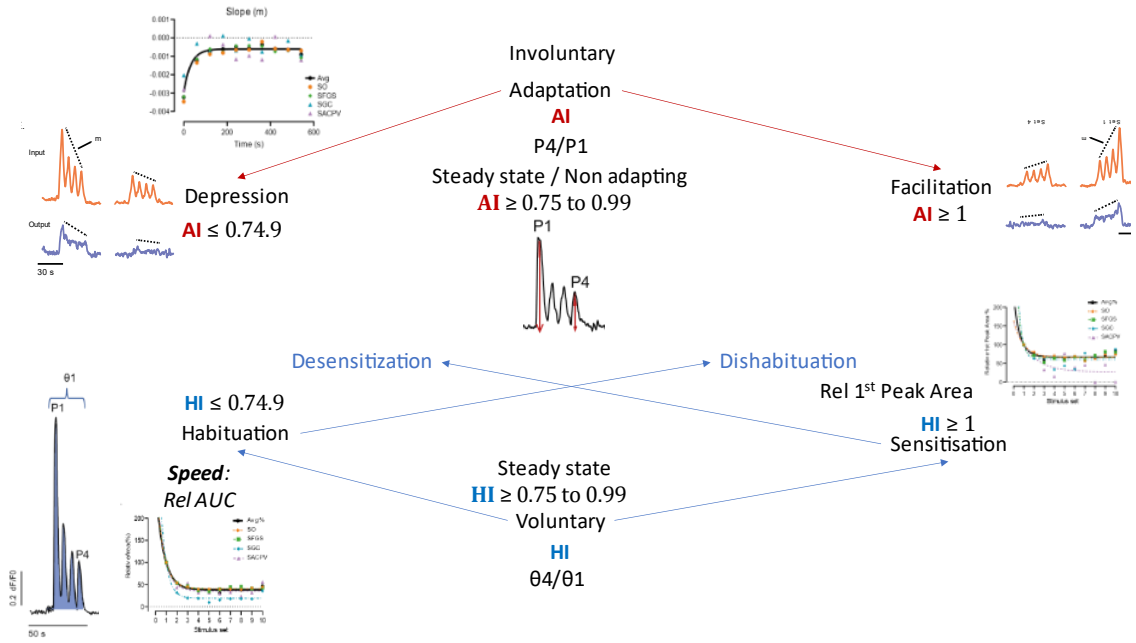

Figure 4.8 Proposed models to define plasticity mechanisms. *Summary of the proposed mathematical definitions of plasticity mechanisms.*

4.7 Neuroplasticity mechanisms in alternative contexts

How can be sure that the decrease in response is a consequence of depression? or is the decreased response in the neuropil output layers (SAC, SPV) a consequence of voluntary habituation? To investigate this, we decided to assess the responses to the moving ball paradigm while the fish was asleep and then by blocking GABA receptors using PTZ.

4.7.1 Adaptation and Habituation during sleep/unconsciousness

It was previously shown that the recovery from inactivation of sodium channels induces facilitation. Furthermore, it has been suggested that a rise in presynaptic calcium could lead to facilitation (Jackman & Regehr, 2017). Thus, we hypothesized that the increase of extracellular sodium might induce a decreased habituation mechanism secondary to facilitation.

Tricaine or MS-222 is a sodium channel blocker, a derivative of benzocaine and is commonly used for anaesthesia and sedation in fish. We found out that the optimal method to induce light sedation in late-stage ZF larvae between 8 to 16 dpf was by immersion of the subject in 1.1mM of tricaine (0.5mL of a 1M stock into 45mL of aquarium water) in a monitored petri dish for less than 1 minute until signs of stage 3 sedation are evident and confirmed by exploration as described in Chapter 2.5.3.2. Then, after mounting, a maintenance concentration of tricaine was added to the imaging chamber (0.8 mM) for imaging.

During these experiments (Figure 4.9), a gradual rise in the presynaptic calcium was apparent, which might be confused with facilitation. However, we found that there was no significant change in the adaptation or habituation dynamics after normalising and analysing the data compared with controls. This suggests a mechanism of non-voluntary decrease in response, without any depletion of a response, hence, depression.

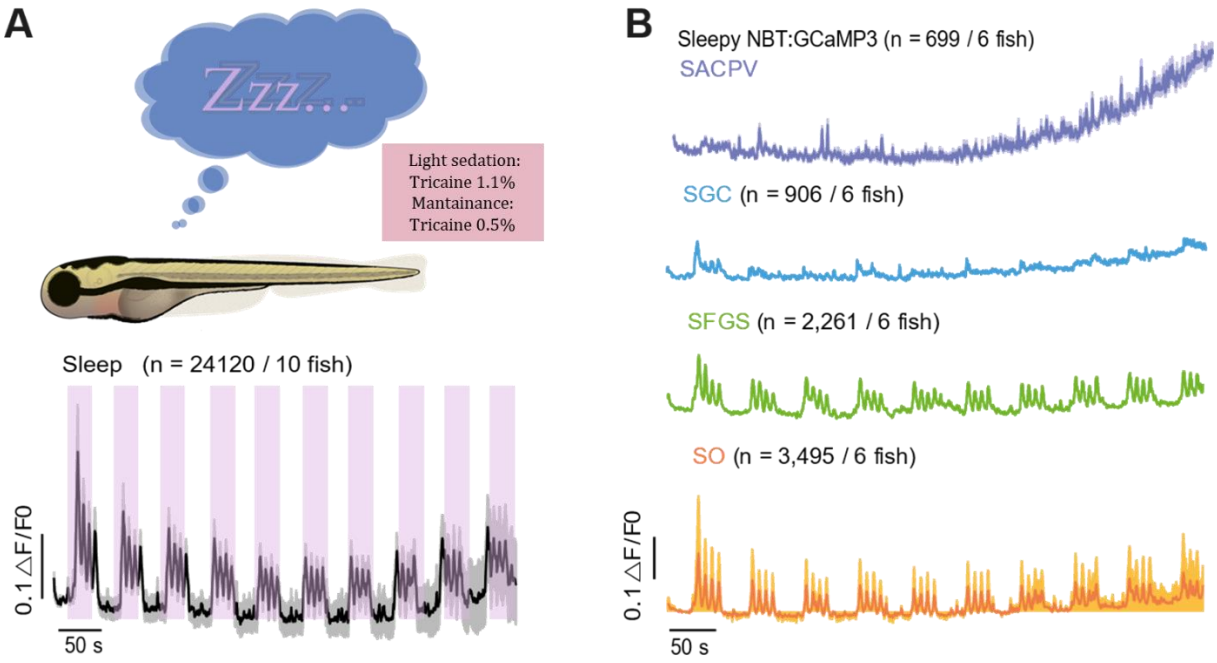

Figure 4.9 Responses in the OT during light sedation. (A) *Average ⧋F/F0 response from the OT neuropil to the moving ball paradigm of ten ZF between 8 to 17 dpf that were induced into light sedation before and during the experiment, n = 8 NBT: GaMP3, and 2 Huc: GCaMP6. SEM is shown in grey*. **(B)** *Average responses of the NP layers in the tectum from 6 NBT: GcaMP3 ranging between 14 to 17dpf under light sedation while being presented the moving ball. The first peak response from each set of stimuli is the highest compared with the rest.*

4.**7.2** Role of GABA-inhibition in plasticity using PTZ

In Chapter 1, we discussed how the major inhibitory neurotransmitter in the CNS, the γ-aminobutyric acid (GABA), play an essential role in the visual system being present in a wide range of cells in the retina and other downstream brain areas (Sadamitsu et al., 2021), and how blocking these receptors, specifically $GABA_A$, has been shown to modify the regulatory feedback in the retinal bipolar cells (Nikolaev et al., 2013b). However, how this inhibition affects higher visual functions are still poorly understood.

Here I used Pentylenetetrazole (PTZ) (See Chapters 2 and 3) to test these plasticity dynamics during the inhibition of $GABA_A$ receptors in awake late-stage ZF larvae. This molecule has been used in multiple studies to mimic and research the effect of epileptic seizures during memory paradigms and in the search for treatments (Kundap, Kumari, Othman, & Shaikh, 2017).

It has been reported that for 48hpf to 4dpf fish, 20mM of PTZ generated a robust response suitable for ISH assays (Baxendale et al., 2012b). First, I performed an endurance test under the two-photon microscope prior to these experiments assessing for clinical signs of health (heart rate, motor response) and found that for ZF between 6 to 21dpf from the strains Huc: GCaMP6 and NBT: GCaMP3, 12.5mM of PTZ was enough to induce involuntary seizure responses without compromising other vital functions (Section 2.5.3.2). Thus, we used this concentration for these tests.

Since the effect of this convulsive agent is almost immediate, the fish was first imaged before and after the PTZ induction without any stimulus and then with the moving ball paradigm (Figure 4.10-A, B). A generalised increment of responses across the neuropil was evident, as well as apparent dynamic changes, which were analysed on a case-by-case basis. Then, we decided to eliminate the pre-exposition to the stimulation. Thus, further experiments were done by adding PTZ immediately before the first moving ball presentation after 5 minutes, in which spontaneous response was imaged to evaluate the change in the synaptic dynamics (Data not shown).

During the experiments, and after the normalisation and analysis of the response from the PTZ-tx fish, we observed that the averaged neuropil traces (Figure 4.10-E) and the responses by layer (Figure 4.10-F) lacked the common signs of the standard habituation and adaptation dynamics found in the normal and other previous conditions. In this case, we found an AI = 0.767 ± 0.099 for the averaged NP ($p < 0.05$). Therefore, the adaptation dynamics after $GABA_A$ inhibition, rather than depressing, trigger a steady-state or non-adapting type of response.

The HI was 0.928. This non-habituating value was further described by the first peak area and relative AUC as a function of time which was not defined by a non-linear exponential decay fit, but a simple linear regression was a better model to describe this plasticity dynamics (Figure 4.10-C). This graphical representation suggests that not only there is no habituation over time, but GABA inhibition might trigger dishabituation or sensitisation mechanisms (Figure 4.10-G).

Additionally, we assessed the sub-properties of adaptation. We found that over time the non-adaptative responses persisted, and it was not possible to follow the usual exponential curve when measuring the slope, but rather a simple linear regression fit (Figure 4.10-D). In the averaged NP, the model that best described the PTZ-induced adaptation overtime was as follows:

$$PTZ\ m\ = -2.047\ e^{-006*\ Set\#} - 0.0003$$

Finally, we measured the relative slope and found that neither the averaged NP nor the SO layer correlated with the non-linear exponential decay model, indicating no habituation to adaptation in GABA inhibition (Figure 4.10-H). The linear regression fit from these data had an associative tendency (upwards) suggesting that it might be

possible to find a facilitation component over time. However, more extended experiments are needed to test this hypothesis further.

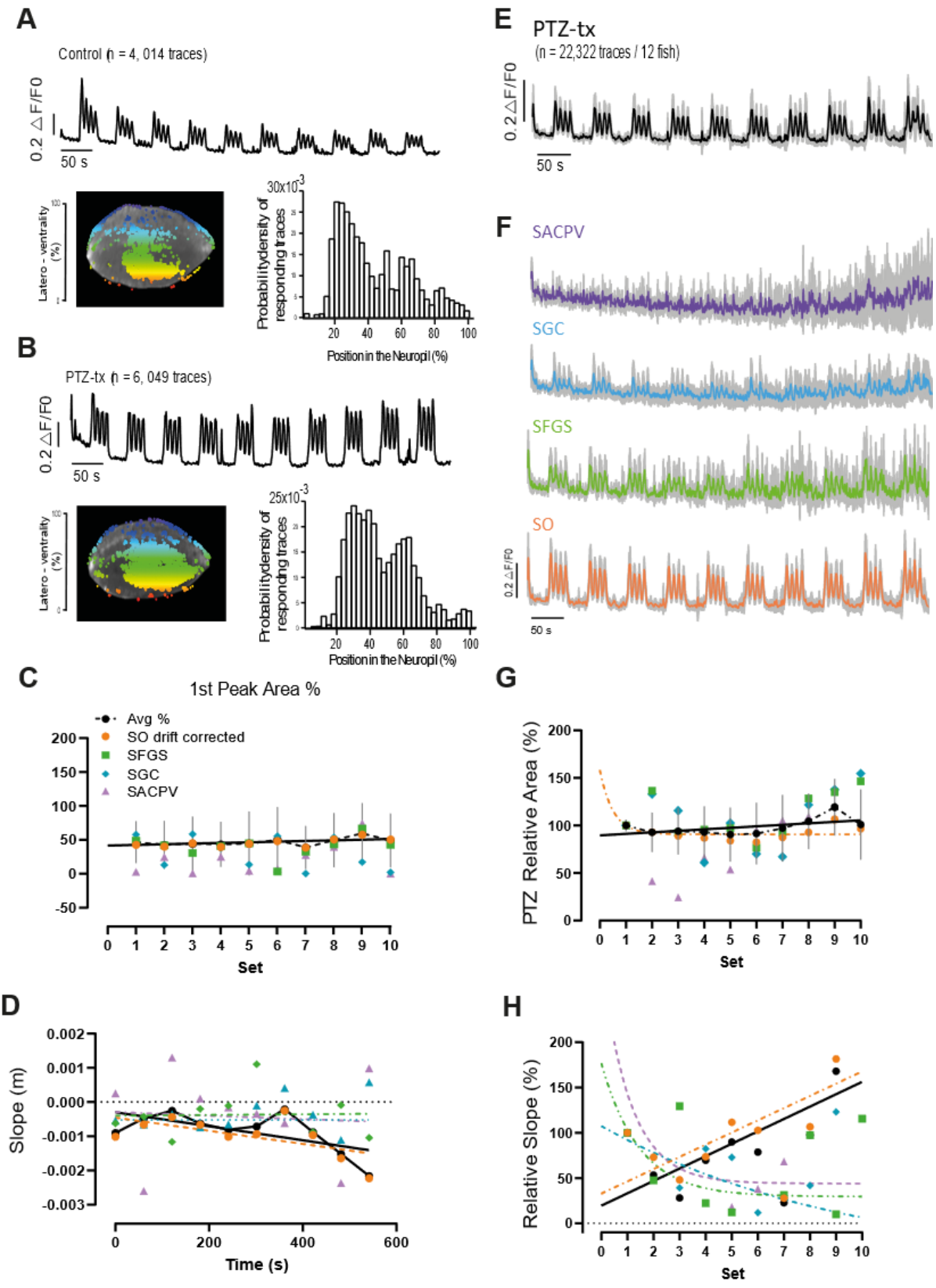

Figure 4.10 Effect of GABA inhibition on adaptation and habituation. (A) *Representative example of the neuropil response from a 6dpf HucGCaMP6 ZF larvae before and* **(B)** *after the treatment with PTZ. (A-B) Top: Average traces from the Neuropil. Left: Position of the responding traces on the neuropil. Right Layered distribution of responding traces (latero-ventrality)* **(C)** *Habituation is measured as the relative first peak area percentage per set. Over time, it was not possible to fit this property in an exponential decay curve but rather a linear fit that described the dynamics as an average NP response and in each layer. This suggests that there is no habituation* **(D)** *Adaptation dynamics over time cannot be described with an exponential growth function. The average adaptation response overtime for the averaged neuropil and the SO layer, resulted in a linear regression model.* **(E)** *Average responses from 12 PTZ-tx fish between 13 to 15dpf NBT: GCaMP3 ZF fry in the averaged tectum NP* **(F)** *Responses of the PTZ-tx fish displayed by NP layers form the same fish used in E.* **(G)** *Habituation dynamics measured with the relative AUC percentage.* **(H)** *The relative slope percentage was used to visualise the dynamics of adaptation over time (See text). (C, D, G, H) (n =22, 322 traces from 12 fish). SEM is shown in grey.*

4.8 Visual plasticity and relation with other sensory systems

There is a close relation across different sensory inputs in terms of communication. For instance, sight, olfaction, and hearing are needed to work together at the same time in order to evoke an escape response. Here we wanted to know if it was possible to induce a change in the neuroplasticity dynamics by coupling other sensory systems without the use of neurochemicals. To do this, we decided to modify the experiment from a non-associative into a form of associative sensory modality by combining auditory sensory stimulus along with the “moving ball” paradigm.

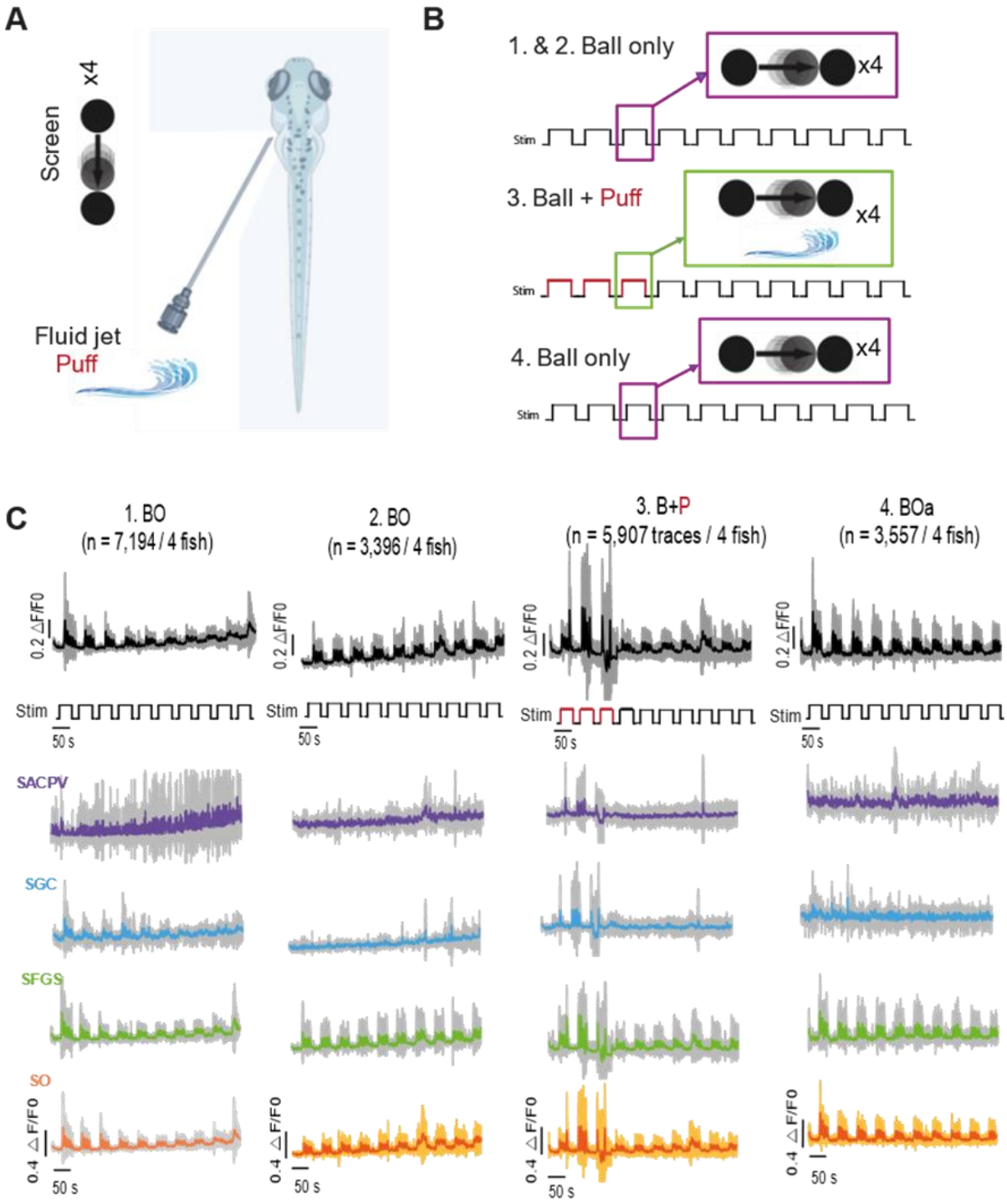

Figure 4.11 Visual plasticity coupled with sudden auditory-paired stimulation. (A) *Experimental setup. A fluid jet water stream, namely "puff", is applied near the ZF acoustic meatus.* **(B)** *Auditory-paired protocol with its four experimental steps explained. The puff is applied only during the third step (B+P)* **(C)** *Averaged responses from four ZF subjected to the auditory-paired protocol.*

4.8.1 Auditory-induced visual plasticity properties

For these experiments, we used a fluid jet stream of aquarium water as described in section 2.5.3.3 of the Materials and Methods chapter, which I will refer to as "puff" for simplification purposes (Figure 4.11-A). In this case, the fish were 15 and 19 dpf NBT: GCaMP3 ZF. The protocol consisted of four steps (Figure 4.11-B). First, the presentation of the usual ten-minute stimuli consisting of 10 sets of 4-times passing black circle, followed by an immediate second step of the exact same 10-minute stimuli. With this approach, we aimed to reach a maximum level of adaptation and habituation to the visual stimuli.

The third step consisted of coupling the same moving ball experiment in which during the first three sets, each of the four moving circles was paired with a 1 second puff at the level of the medial VF of the fish (Figure 4.11-A). Finally, the fourth step consisted of simply repeat the experiment without any auditory stimulation to test whether there was a significant change in adaptation dynamics (Figure 4.11-C).

In this case, the AI for the first step (Ball only) was 0.361 ± 0.056, and the HI was 0.438 (n = 7194 traces, 4 fish). Interestingly, using the same analysis method on the same fish for the fourth and last step, consisting of the repetition of the moving ball after the exposition to sudden auditory-paired stimulation, we found that the responding voxels decreased (n = 3,557 traces). However, the values for both adaptation and habituation index increased. The AI n was 0.567 ± 0.074, whereas the HI increased to 0.599 ($p < 0.05$).

4.9 Conclusion

Habituation happens as a consequence of adaptation (R. Thompson, 2001) in the same way as facilitation occurs as a consequence of sensitization (Castellucci & Kandel, 1976). In normal conditions, despite the age of the fish (3 to 21dpf), the overall neuropil response to the moving ball paradigm will tend towards the decrement in response over time. However, one of the most evident observations in this chapter was that the dynamics of adaptation and habituation happen differently across the tectum neuropil.

Whereas the outer input layers (SO and SFGS) adapt relatively fast in normal conditions, the output areas (SGC, SAC and SPV) adapt and habituate even faster.

It is important to measure the sub-properties of both adaptation and habituation to best describe the dynamics of visual plasticity. For instance, we found that even though the size of the stimulus does not determine the AI and HI, the habituation to visual adaptation is significantly less for the biggest sized tested compared with the medium and small circles (t-test, $p \leq 0.05$). Additionally, we found that post-synaptic RGC-derived zones in the neuropil display faster habituation and adaptation over time, which might require more investigation into why this is the case

Light sedation induced with tricaine does not change the plasticity dynamics. Interestingly, the response towards the stimuli is still present overtime despite the fish being in an unconscious state. However, when blocking the $GABA_A$ receptor through PTZ, we found the most significant changes in plasticity (Figure 4.10). As expected, there was an increment in the volume of voxels responding or presenting a high activity level. Surprisingly, this activity was not random but responded in relation with the stimuli despite the additional activity coming involuntary from other neurosensory systems. Here, there is no adaptation, nor habituation and these responses are kept analogous across layers.

Finally, sudden auditory-paired stimulation changed the adaptation and habituation dynamics over time. While in a normal context, the repeat of a stimulus causes a decreased response overtime (fish getting "used to" and/or "bored of" the stimuli), the sudden pairing with an uncomfortable stimulus (mechanosensory auditory stimuli) will produce an increase in the voluntary awareness to the same stimuli. Thus, decreasing the "habituation to adaptation" potentially secondary to the fear of receiving another "puff". This data suggests that it is possible to modify the adaptation in response of pairing a stimulus with fear and possibly with reward. However, this last assumption requires further study.

Chapter 5. Visual tuning sensitivity properties in the OT of the late-stage ZF larvae.

5.1 Introduction

The optic tectum (OT) is the primary visual processing area in lower vertebrates (Sanes & Zipursky, 2010b). The zebrafish (ZF) OT performs analogous functions to the mammalian visual cortex and is considered the anatomic equivalent to the superior colliculi (Sanes & Zipursky, 2010a), which is primarily in charge of the visual reflex in mammals (Helmbrecht et al., 2018; Jaepel et al., 2017; McMains & Kastner, 2011). The analogous mammalian visual cortex has been related to visual-motor coordination and thus has been linked to different forms of stimulus responses, similar to what happens with fish OT (Ahrens, Orger, Robson, Li, & Keller, 2013b; Zariwala et al., 2011).

Visual tuning properties like direction selectivity, contrast, size, orientation and speed motion recognition are among the main features processed by the tectal neurons; the first one described in 7-9 days post fertilization (dpf) larvae on previous research (Bergmann, Meza Santoscoy, et al., 2018). Contrast and motion detection are key functions of the visual system for survival (Del Bene, Wyart, Robles, Tran, Looger, Scott, Isacoff, Baier, et al., 2010; Nakai et al., 2017). Former research has suggested that the cells in the OT are organized according to these specialization features (Bartel et al., 2021; Gebhardt, Baier, & Del Bene, 2013; Xiao & Baier, 2007).

Earlier methods utilizing invasive approaches such as injecting dyes in the tectal area have been used to prove the tectal functional organization (Heap et al., 2018; Randlett et al., 2019b). Some of the most used methods to determine any vision-related sensitivity in ZF are the optomotor response (OMR), which consists of the measurement of the tail reflexes over time (Wang, Hinz, Haikala, Reiff, & Arrenberg, 2019; Xie, Jusuf, Bui, & Goodbourn, 2019); or the optokinetic response (OKR) consisting in the same way of reflex measurements, in this case specifically eye movement or oculomotor responses, both possibly triggered as a consequence of a determined visual stimulation (Dehmelt et al., 2019; Matsuda & Kubo, 2021; Risner, Lemerise, Vukmanic, & Moore, 2006).

These valuable techniques have served us to establish a close measurement for contrast and frequency sensitivity properties (Rinner, Rick, & Neuhauss, 2005). Thus, allowing to determine a visual acuity range that generates an OKR (Bilotta, 2000). In 5dpf zebrafish larvae, the visual acuity values had been estimated to be around 1.6 to 0.24 cycles per

degree (cpd) or 3.1° to 2.09° of minimum separable angle respectively (Rinner et al., 2005), and estimated 0.871cpd, equivalent to 0.57 degrees in adult ZF when including theoretical measurements adding in consideration the distance between the lens and photoreceptors, (Haug, Biehlmaier, Mueller, & Neuhauss, 2010; Pita et al., 2015; Sajovic & Levinthal, 1982). However, subspecialized features such as spatial frequencies and contrast sensitivity have not been determined yet in higher visual areas of the late-stage ZF brain (Odermatt et al., 2012; Rinner et al., 2005). Calcium imaging in vivo has allowed us to test these visual elements using a non-invasive approach (Marachlian, Avitan, Goodhill, & Sumbre, 2018b).

Here, I aimed to investigate how visual features such as contrast and frequencies occur within the optic tectum of the late-stage NBT: GCaMP3 zebrafish (12-21dpf). Since this mutation acts on an individual cell level, the resolution of the images that can potentially be obtained is only limited by the experiment's setup (Ai et al., 2015). Here, we performed two-photon imaging *in vivo* recordings over an extended period (between 7 to 19 minutes) in late-stage ZF up to 21 dpf. The microscopy focal plane was adjusted to encompass the OT neuropil in its entirety to study the visual tuned responses as a whole-population (Fig 5.1 A-C).

5.1.1 Visual stimulation

Contrast in general was defined as the relative brightness difference from the background and can be described by the Michelson equation as follows:

$$\frac{(L_{max} - L_{min})}{(L_{max} + L_{min})}$$

Where L_{max} is maximum stimulus luminance, and L_{min} is the luminance minimum (Rizzo, 2013). The frequency was previously determined using the custom-written script for MATLAB under the frequency parameters shown in Table 21.

Frequency	**Low**			---------->			**High**
Stim ID	*Stim 2*	*Stim 4*	*Stim 6*	*Stim7*	*Stim 5*	*Stim 3*	*Stim 1*
VA- 1 cycle (°)	**55.98**	**36.43**	**28.97**	**18.81**	**10.04**	**3.95**	**1.95**
VA - Half cycle (°)	27.994	18.215	14.485	9.406	5.020	1.975	0.975
Frequency (cpd)	**0.018**	**0.027**	**0.035**	**0.053**	**0.1**	**0.253**	**0.513**
Contrast	**Low**			---------->			**High**
Stim ID	*Stim 2*	*Stim 4*	*Stim 6*	*Stim7*	*Stim 5*	*Stim 3*	*Stim 1*
Contrast (%)	1	5	10	25	50	75	100
Angle (°)	**90**	**135**	**180**	**225**	**270**	**315**	**360**

Table 21. Variations used in stimuli of moving sinusoidal gratings. VA: visual angle.

The frequencies were measured according to the visual angle (VA) and then converted to cycles per degree (cpd).

All presentations started with 30 seconds of 50% contrast background projection, previously calibrated with a photometer, to let the fish stabilize their neural response to baseline levels and ended with 10 seconds of the black screen were left before stopping the recording.

5.2 Frequency tuning in the OT neuropil

The preliminary experiments were done using a stimulus consisting of five different sets of sinusoidal moving gratings varying in a hierarchized order from high to low-frequency oscillations to get an initial characterization of the frequency-tuned properties of the ZF OT (Figure 5.1-D). In this case, the stimulus duration was 30 seconds per set and 30 seconds of ISI. We found a correlation between the calcium dynamics and the frequencies applied, displaying a higher response towards the lower frequencies (0.018 to 0.53 cpd). These responses were fitted into a single exponential curve as a function of frequency as follows:

$$y(f) = y_0 + \omega \, exp\left(\frac{f - f_0}{\tau}\right)$$

In which y is the measured change in fluorescent intensity $\Delta F/F_0$ of the calcium signalling, y_0 is the starting value of the response, ω is a constant of the amplitude, f_0 is the initial cpd value of the stimulus, f is the variable value of the stimulus in cpd, and τ is the time constant for the curve.

For the data presented (n= 23,154 traces, 23 fish), the results are described by the following equation:

$$y = y_0 + 0.4353\, e^{\left(\frac{f - f_0}{58.417}\right)}$$

The distribution of the responding cells in the NP was normalized and fitted to an ellipsoidal area for analysis (Figure 5.1-C). Then, the probability of responding traces was plotted in a histogram from 0 to 100% according to its latero-ventral position, respectively (Figure 5.1-E). We found that in most fish, there was a robust layered distribution of responses to all the stimuli in mainly three areas: an outer zone -labelled in orange- comprising the *stratum opticum* (SO); a medial zone containing the *stratum fibrosum griseum superficiale* (SFGS) -green- and part of the *stratum griseum centrale* (SGC) -blue-and a ventral area consisting in the rest of the sublayers from the *stratum griseum centrale* (SGC) and the *stratum album centrale and periventriculare* (SACPV) -purple- (Figure 5.1-F).

The preliminary tests determined that fish can easily detect frequencies of up to 10.04 degrees of visual angle (VA) or 0.1 cycles per degree (cpd). For this reason, we decided to increase the parameters of the frequencies by adding two sets with higher frequencies up to 0.513 cpd or 1.95° VA. When designing these experiments, habituation and adaptation mechanisms were taken into account (Ahrens, Li, et al., 2013). However, to discard any doubts about the responses being a product of sensitization (Nikolaev et al., 2013a), we tested this seven set experiment in a semi-randomized aleatory order of presentation. The reason behind using an alternated rather than proper randomization was to facilitate the analysis to determine the diversity of the responding traces on a manual basis.

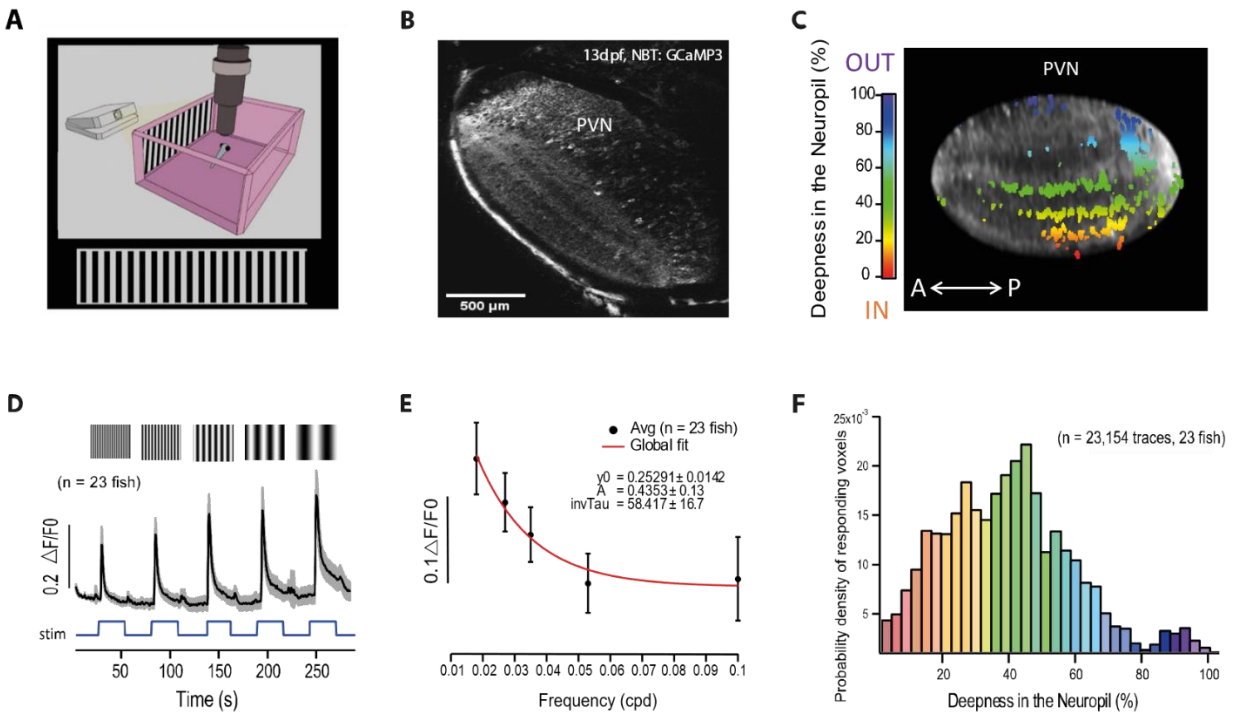

Figure 5.1. Frequency-dependent evoked responses. (A) *Schematic of the two-photon imaging setup. The living zebrafish is embedded chamber facing the left eye 35mm away from the screen where the stimuli are presented.* **(B)** *Two-photon microscopy of an OT neuropil from a 13 dpf NBT: GCaMP3 larval ZF. PVN: Peri-ventricular neurons. Scale bar is shown.* **(C)** *Representative neuropil from vignette B with color-coded ROIs selected by voxel-wise analysis. The position of the neuropil from 0 to 100 represents the ventrality from the external areas to the most ventral. IN: input; OUT: output; A: anterior; P: posterior. (Fish ID: B1116F2SG3).* **(D)** *Averaged responses across the contralateral neuropil to the presentation of 5 sets of sinusoidal moving gratings at different frequencies (n= 23,154 traces, 23 fish). SEM is shown in grey.* **(E)** *Different frequencies display different amplitude of responses. The average was fitted globally by a simple exponential curve (shown in red).* **(F)** *The position of the responding voxels to gratings at different frequencies is distributed by layers across the neuropil. Color-coding correlates with that in C.*

We found that the response dynamics in this longer assay behaved as in the hierarchical order despite the change in sequence (Figure 5.2-A), being the lowest frequency 0.01 cpd (55.88° VA) the presentation in which the amplitude was the highest and then this amplitude adjusted relative to the frequency. On average, we found a contrast-suppressed component at the end of each set of stimuli up to 10.04° of VA (Figure 6.2-Biv). The anatomical focal plane chosen for imaging was the most medial horizontal cut in the OT, where the neuropil shape was usually ellipsoidal. At the beginning of each set presentation, the contralateral tectum receiving the stimuli displayed synaptic activity from its most anterior region and in a latero-ventral direction towards the periventricular neurons (Figure 5.2-C).

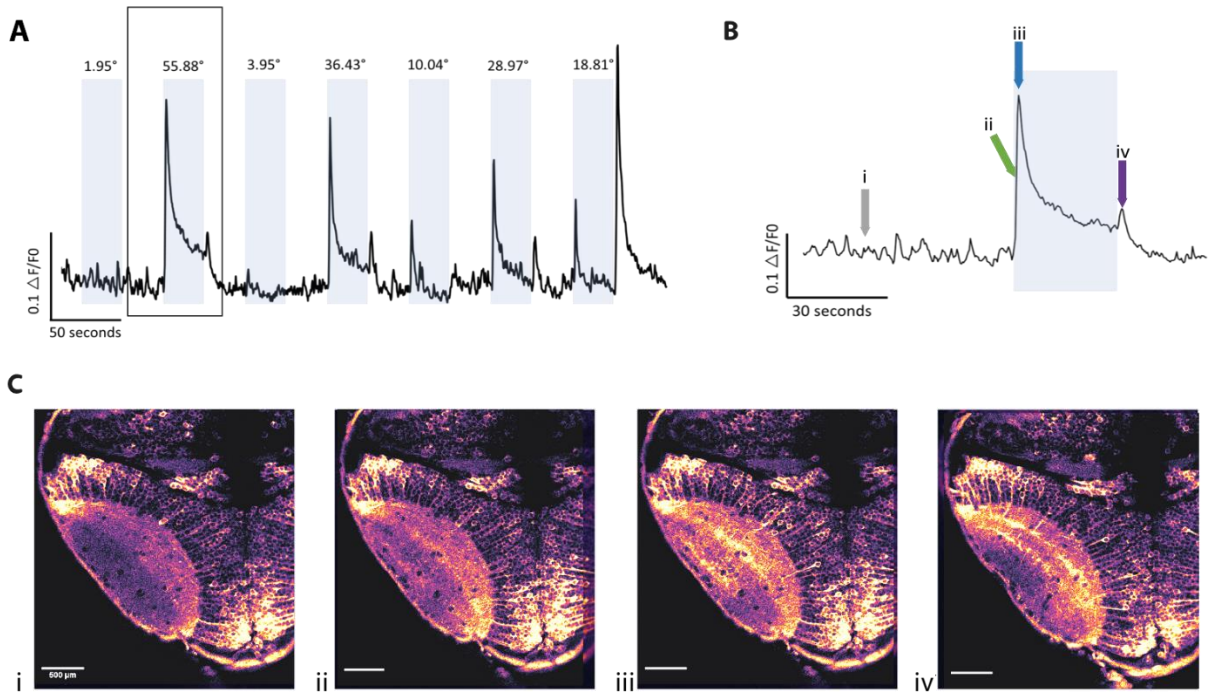

Figure 5.2. Tectal response dynamics to sinusoidal moving gratings. (A) *Average responses from the neuropil of a 5-9 dpf Huc: GCaMP6 zebrafish during alternated frequency stimulation (blue shadow) (n = 18 fish).* **(B)** *Detail from the highlighted area in A, showing the response dynamics. i) steady-state, ii) response at the beginning of the stimulus, iii) Maximum peak response, iv) Response after the end of the stimulus.* **(C)** *Two-photon microscopy imaging series from the same tectal plane of a 5dpf Huc: GCaMP6 ZF displaying the dynamic phases shown in B. (Fish ID: D0314F4SG3).*

5.2.1 Frequency tuned classes and topography

The average population response in the neuropil showed a positive correlation with the frequencies displayed (Figure 5.3-A). However, we found a generally more robust response in the outer layers (IN) of the neuropil comprising the SO and external layers of the SFGS, compared with the periventricular areas (Figure 5.3-A, B). Despite the amplitude disparity across layers, we found that from the most outer layers, SO and SFGS, the same exponential function as the average can be used to describe the responses (Fig 5.3-B). With this set of experiments, the equation can be described as follows:

$$y(f) = y_0 + 0.074988 \pm 0.0131\, exp\left(\frac{f - f_0}{34.824 \pm 5.69}\right)$$

In which y is the measured change in fluorescent intensity $\Delta F/F_0$, and y_0 is the starting value of the response, f_0 is the initial cpd value of the stimulus, f is the variable value of the stimulus in cpd, and τ is the time constant for the curve ($p < 0.05$).

The voxel-wise analysis allowed us to sort all the responding traces with skewness of ≤ 0.8. We obtained an average of ~3,000 responding voxels per experiment from which we manually sorted for three main classes: high-pass, (HP) those responding to high frequencies, low-pass (LP) when responding to low frequencies, and bandpass (BP), those by which the response did not vary despite the difference in frequency and which sensitivity was higher for the medium frequencies (Figure 5.3-C). Occasionally, we found that the band-pass cells could not be easily determined, thus having a subgroup of complex cells not shown (George, Lyons-Warren, Ma, & Carlson, 2011). When there was no direct correlation with the frequency, we considered these as non-sigmoidal (NS). After manual sorting, we found that the location of the responding cells across the neuropil was mainly covered by low-pass class cells, with a higher distribution towards the middle and outer areas, SO, SFGC and SGC (Figure 5.3-D). By overlapping the normalized probability density of responding traces in a comparative histogram (Figure 5.3-E), we found that there was no difference in the LP-HP ratio of latero-ventrality distribution location-wise. However, there was a more organized layered distribution in the voxels responding to higher frequencies (n = 13, 684 voxels, five fish).

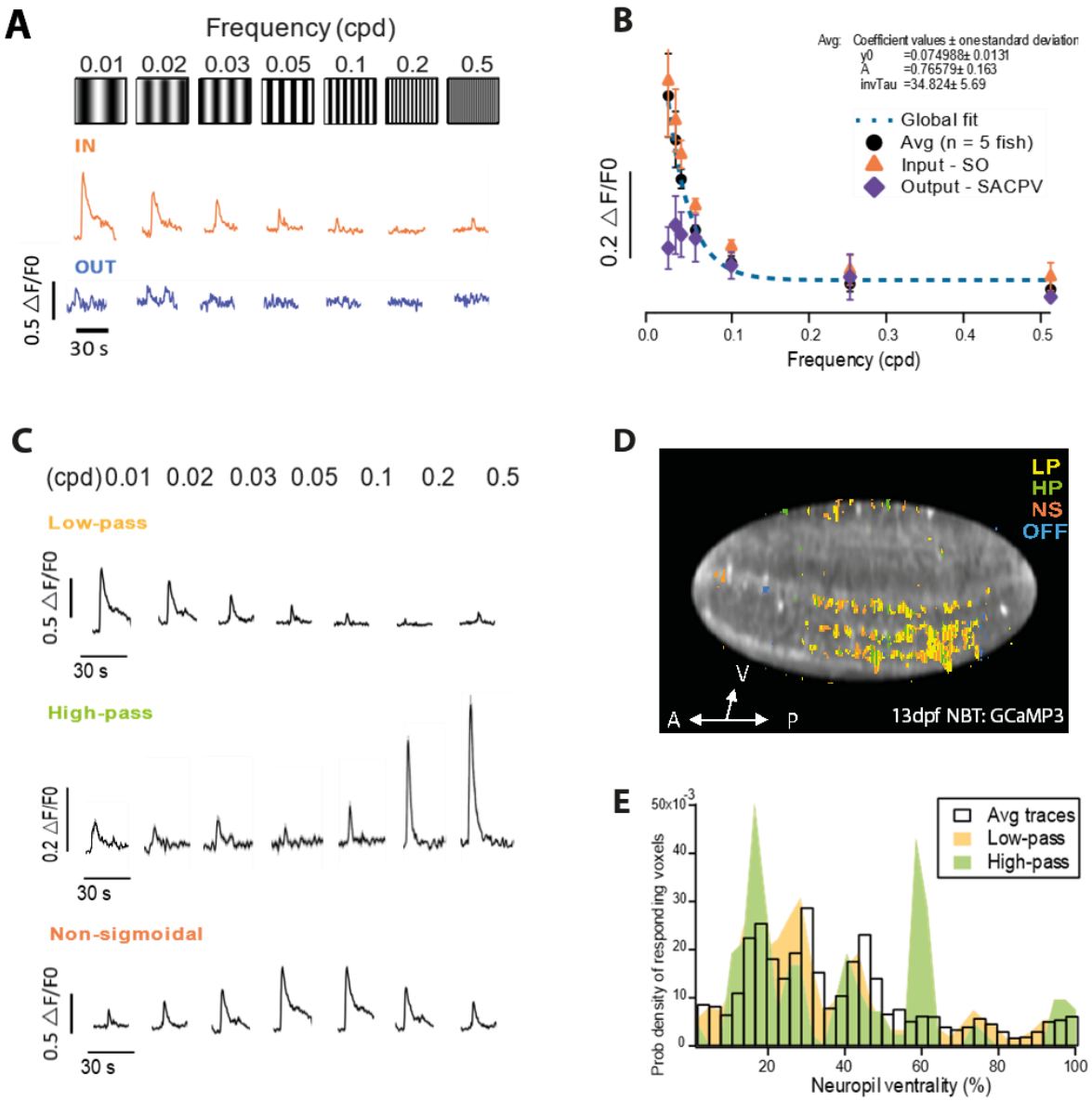

Figure 5.3. Diversity of frequency-tuned responses across the neuropil. **(A)** *The stimuli consisted of sinusoidal moving gratings varying in frequencies shown in cycles per degree (Top). Comparison of the averaged responses input (orange) vs output (purple) of the whole neuropil from 13-14dpf zebrafish raised in standard aquarium conditions (n=5 fish). IN: input; OUT: output.* **(B)** *The peak of calcium response as a function of frequency. Exponential fit of averaged responses in the Neuropil to the stimulus on frequency-varying moving gratings. Error bars represent SEM. (n = 5 fish)* **(C)** *Top: Representative traces of a low-pass responding cell; Middle: Example of High-pass response; Bottom: Trace example from a non-sigmoidal responding voxel.* **(D)** *A representative cluster from a 13dpf NBT: GCaMP3 zebrafish shows different cell classes according to their frequency*

preference in the neuropil. LP: Low-pass; HP: High-pass; NS; Non-sigmoidal; OFF: Off-responses; A: anterior; P: posterior; V: ventral. **(E)** *Distribution of different frequency-tunning classes of responding voxels in the optic tectum neuropil.*

5.3 Contrast tuning

The properties of at least 20 classes of RGCs have been studied in different manners to determine frequency and contrast sensitivity (Zhou et al., 2020). Conventionally, the cells which become stimulated by an increase of contrast are classified as ON, whereas if the response occurs to low contrast, for instance, in the presence of sudden darkness, we defined them as OFF. A group of cells display a high peak amplitude when both increment or negative contrast happens independently; these are called ON-OFF cells. (Jacoby & Schwartz, 2018). There is a fourth classification that includes neurons that display a negative response as a consequence of contrast change. In other words, the baseline activity of the steady-state luminance is decreased; these are what we call suppressed by contrast (SbC), and it is considered that these cells could be further classified in the same form as the impressed by contrast-cells (Tien, Pearson, Heller, Demas, & Kerschensteiner, 2015).

We investigated whether the dynamics of contrast computations had an analogous correlation as in the experiments with frequencies. For this, we performed a similar experimental approach. We imaged the OT of 13-14 dpf old NBT: GCaMP3 zebrafish while being presented with seven different sets of sinusoidal moving gratings, with a fixed frequency of 0.02 cpd for 30 seconds, after which we let a 30-second rest interval where a grey (0% contrast) screen was placed in between (Figure 5.4-A). During the previous experiments used to determine the frequency selectivity in the tectum, the presence of OFF cells was clear, displaying a high peak amplitude at the end of each set. These OFF-cells presented a higher activation after the second-highest contrast (75%) (Figure 5.4-A), although this selectivity was varied per fish and individual voxels.

Additional ON-OFF cells were found in these experiments where the ON-response was slightly delayed compared with the average neuropil response. For instance, Figure 3-B shows an example from a 14 dpf Huc: GCaMP6 with 122 ON-responding traces tuned to 75% contrast which have an onset at second 216.45 with a complete stimulus duration response of 30 s ranging from 0.378 to 0.0677 ±SEM 0.017 to 0.01 $\Delta F/F_0$ calcium

signalling (n = 122). The OFF traces, on the other hand, have a 3-second delayed onset with a total response range from 219.45 to 246.75 seconds and a response amplitude ranging from 0.329 to 0.626 ±SEM 0.047 to 0.073 ΔF/F0 (n = 14) (Figure 5.4-B).

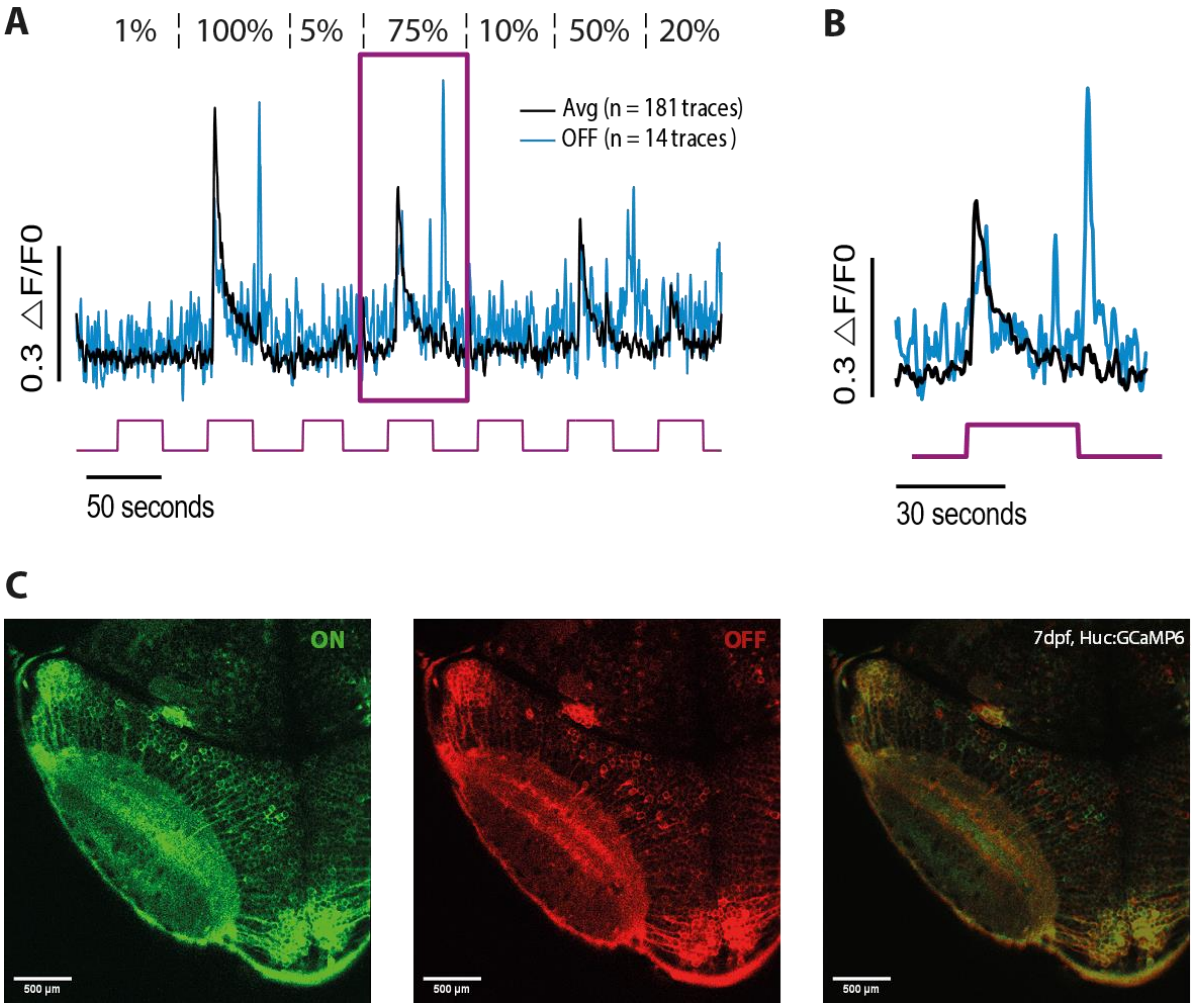

Figure 5.4. ON and OFF responding cells display an intertwined alternated organization. **(A).** *Representative average traces from a 14dpf NBT: GCaMP3 zebrafish neuropil (black) overlapped with manually sorted OFF-responding traces (blue).* (B) *Expanded view from the highlighted response in A. The maximal peak response in the ON-OFF cells presents a delay of 3s compared with the average response.* **(C)** *ON and OFF cells in the OT neuropil. Multiphoton imaging from the top of an OT neuropil of a 7dpf Huc: GCaMP6 zebrafish showing responses to light increase (left green), dark (middle red), and merged ON and OFF responding areas (right). The intertwined configuration of fibres within the layers corresponding to SCG, SAC, and SPV areas is evident. (Exp ID: D0312F5SG3)*

When looking at the functional in vivo two-photon imaging, we found a layered distribution of ON, OFF, ON-OFF cells, previously described by Robles et al., 2013. We found that even though the number of the cells comprising these types were different between subjects, the relative proportion of ON, OFF and ON-OFF cells was approximately 60%, 25% and 15%, respectively. Decades ago, it was thought that tectal cells did not have separate ON and OFF areas (Sajovic & Levinthal, 1982). In Figure 5.4-C, we overlapped the frames from two different responses within the same OT to show how these contrast dependent cells ON (green) and OFF (red), are highly organized in an intertwined configuration, mainly in the medial to outer layers of the neuropil (SCG, SAC and SPV) further elucidating findings previously thought otherwise and in agreement with more updated literature (Förster et al., 2020a; Robles et al., 2020, 2013).

5.3.1 Main types of contrast-sensitive tunned cells and location.

Similar to other experiments shown in this chapter and chapter 5, the highest fluorescence $\Delta F/F_0$ responses obtained across the tectal NP were those corresponding to the most external layers (SO and SFGS). The SAC and SPV areas displayed the weakest response compared with the averaged NP responses (Figure 5.5-A). We found a positive exponential correlation of the gain responses as a function of the contrast level (Figure 5.5-B). In this case, the contrast response can be predicted with the following equation:

$$Contrast = 0.0211 + (0.355) * (1 - e^{-0.034 * Contrast\ \%})$$

The three primary classes of contrast sensitive cells can be divided into low-contrast sensitive (LCS), high contrast sensitive (HCS) and OFF -cells, previously described. Not to be confused with the ON, OFF, ON-OFF types (See page 152). The main classes were manually sorted by localizing the regions of interest (ROIs) from the responding voxels using an automatized script in Igor (See methods). We found that despite being different voxels, the responses from the LCS and HCS cells are scattered very closely to one another (Figure 5.5-C). This distribution was further seen when plotting the normalized histogram to assess for latero-ventrality (Figure 5.5-D).

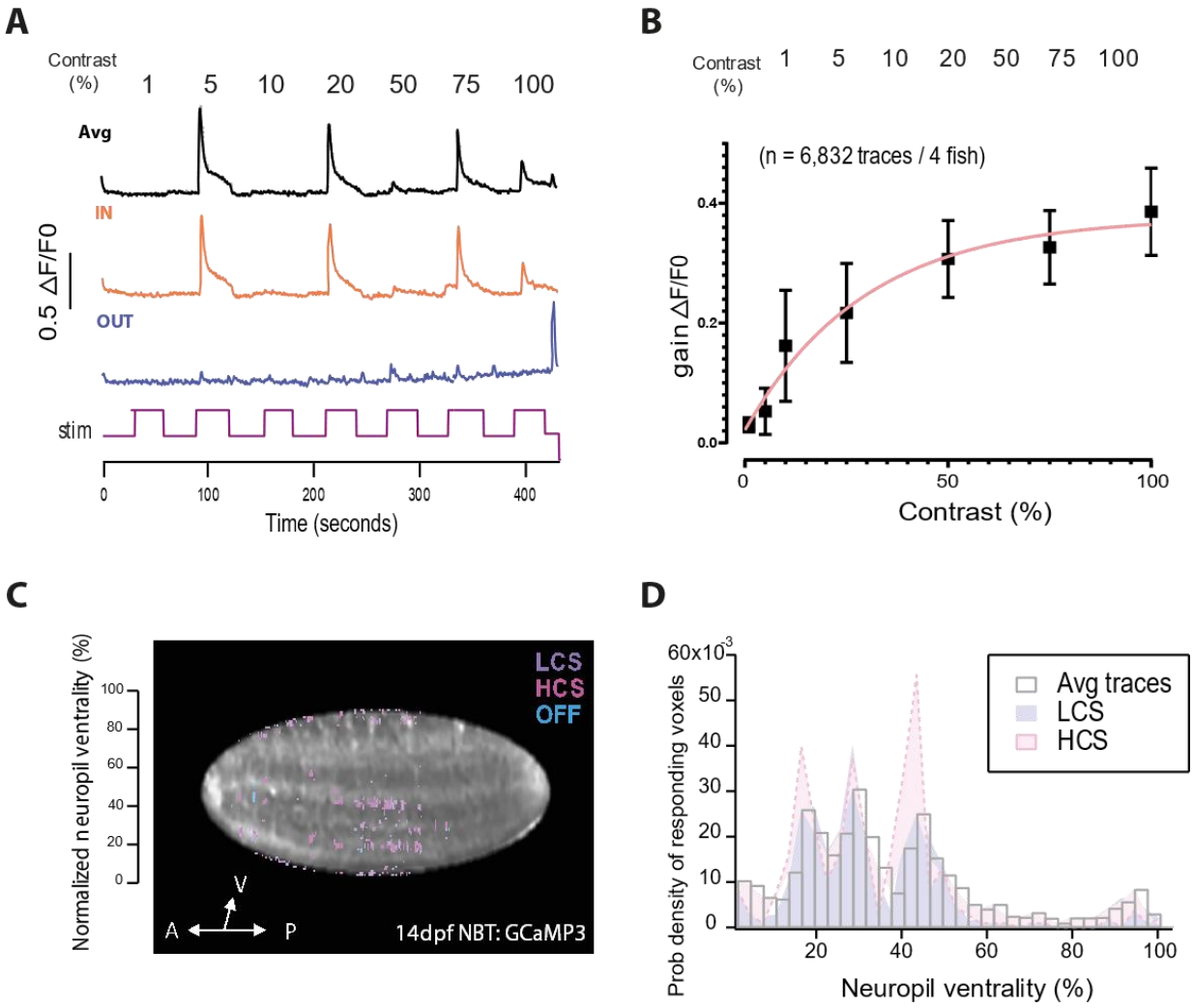

Figure 5.5. Neuropil responses to sinusoidal semi-randomized contrast-varying moving gratings. (A) *Responding traces from an in vivo experiment showing the averaged NP responses (top black), input (orange), and output (deep purple) areas to moving gratings varying in contrasts (n=6832 traces, four fish. S.E.M. is shown).* **(B)** *Fluorescence gain ΔF/F₀ response as a function of contrast level.* **(C)** *Colour-coded ROIs in a masked OT neuropil from a 14dpf ZF displaying the scattered responses corresponding to LCS, HCS and OFF responses across the NP layers.* **(D)** *Distribution of responding voxels to different contrast-tunning sensitivity in the optic tectum neuropil.*

5.3.2 Contrast-sensitivity subclasses

During the manual sorting of dozens of thousands of traces, we realized that the primary classification of LCS, HCS and OFF cells was insufficient to describe the wide range of diverse tunning types. Therefore, a further sub-classification was added to the catalogue (Figure 5.6-A).

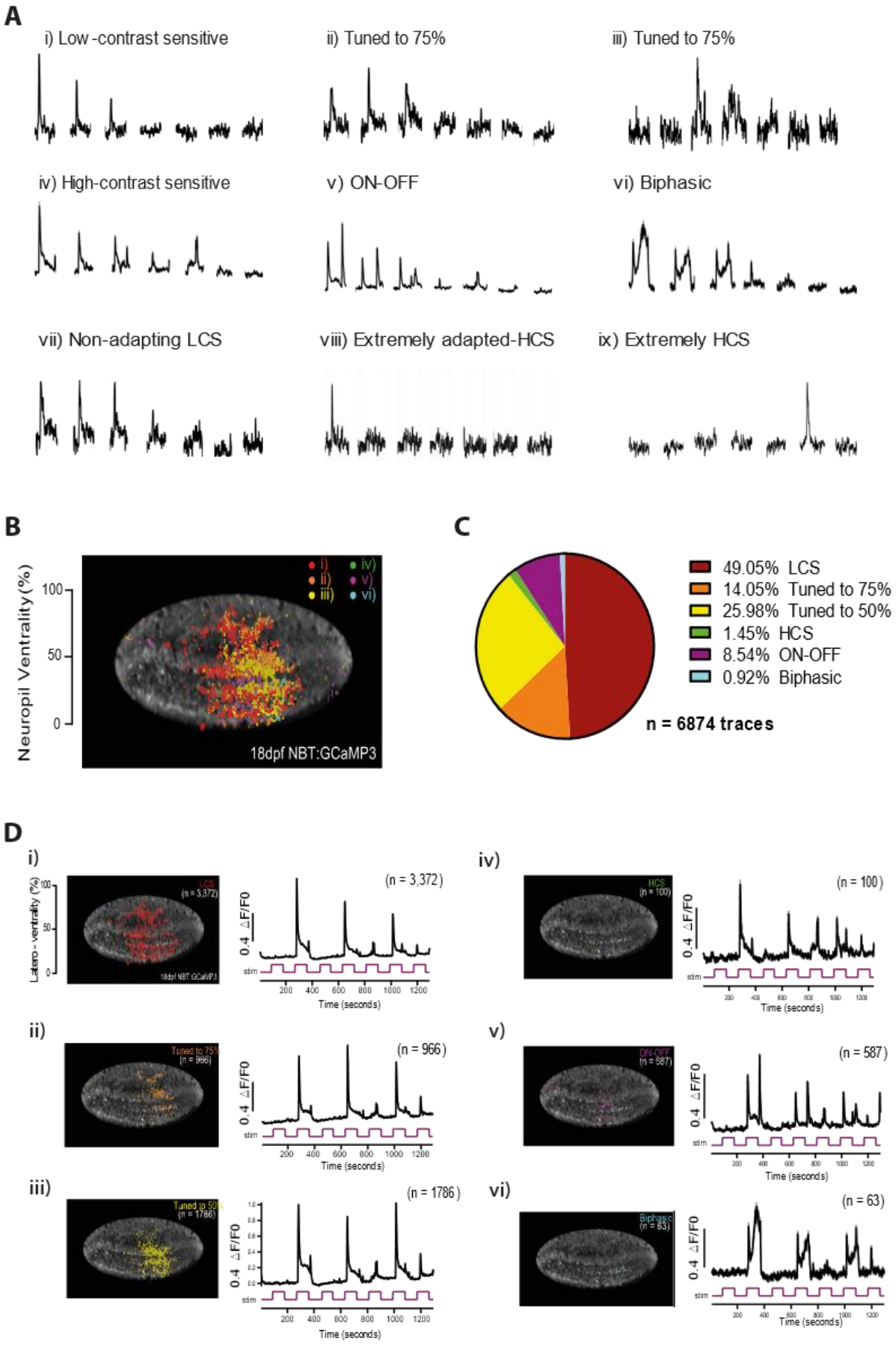
A
i) Low -contrast sensitive
ii) Tuned to 75%
iii) Tuned to 75%
iv) High-contrast sensitive
v) ON-OFF
vi) Biphasic
vii) Non-adapting LCS
viii) Extremely adapted-HCS
ix) Extremely HCS
B
Neuropil Ventrality (%)
100
50
0
18dpf NBT:GCaMP3
C
49.05% LCS
14.05% Tuned to 75%
25.98% Tuned to 50%
1.45% HCS
8.54% ON-OFF
0.92% Biphasic
n = 6874 traces
D
i)
(n = 3,372)
ii)
(n = 966)
iii)
(n = 1786)
iv)
(n = 100)
v)
(n = 587)
vi)
(n = 63)
0.4 ΔF/F0
stim
Time (seconds)

Figure 5.6 Representative examples of different types of contrast-tunned subclasses. (A) *Representative traces of different contrast-sensitivity responses; Seven responses per class arranged in contrast level presentations as follows: 100%, 75%, 50%, 25%, 10%, 5%, 1%.* **(B)** *The colour-coded cluster of ROIs according to the different subclasses shown in A.* **(C)** *Pie-chart distribution of the different classes of cells encountered in B.* **(D)** *Individual clusters and traces for better appreciation of the cataloguing. Here the contrast levels of the stimuli were presented in an alternate form as follows: 1%, 100%, 5%, 75%, 10%, 50%, 25%.*

It is worth mentioning that not all the contrast-tunned subclasses were found in all the fish. When clustering the subclasses in the tectal NP, we found that these cells coexist harmoniously across the NP layers (Figure 5.6-B,D). However, the proportional ratio was consistent in most fish (Figure 5.6-C). The LCS cells were the most common type, representing almost half of the responding voxels, whereas the HCS and other interesting subclasses, such as the biphasic responding, represented less than 2% of the total.

5.4 Theoretical model of contrast sensitivity function (CSF) based on higher brain areas.

To model a theoretical contrast sensitivity function (CSF), we combined different contrasts and frequencies as described in Chapter 2. We presented a total of 49 different gratings. The time in which each set was presented was reduced to 10 seconds, giving a total of around 19 minutes of uninterrupted recording time at a sampling rate of 15.1 fps. We imaged 23 Huc: GCaMP3 ZF larva at 6-7dpf, from which 13 were suitable for analysis due to movement in the focal plane during the experiment.

It was previously established that there is a close response-parallelism with the surrounding pixels for most voxel responses. Therefore, we decided to analyze this data by manually choosing ROIs rather than using the voxel-wise method. Another reason that influenced this decision was the high memory size of the experiment and analysis efficiency. For this, we picked at least 2 ROIs from each main neuropil area (outer, medial, ventral) depending on the size of the neuropil.

In total, we selected 136 ROIs from which 38 corresponded to the outer layers (SO, SFGS1-2), 61 to the medial (SFGS3-6, SGC), and 36 to the ventral (SAC, SPV) areas.

After the responses were normalized, we analyzed each set of the 49 presentations. We considered a response: a peak of more than 0.03 F/F_0 of arbitrary units within the presentation interval (Figure 5.7-A). The responses were then averaged for statistical analysis. Then, I reordered the frequencies and contrasts and plotted the responding traces and the averaged NP responses on a fish-by-fish basis in each set containing a different frequency with contrast variations (Figure 5.7-B). A 20-percentile was chosen as the response limit in each group using a simple conditional selection per contrast condition. This value was averaged across the sample size, thus determined the average limit threshold.

Finally, the responses corresponding to the closest 20-percentile limit were chosen in each experiment, and with this data, we proceeded to plot the CSF in a non-linear Gaussian distribution as follows:

$$CSF = A * exp^{-0.5\left(\frac{x-x_0}{w}\right)^2}$$

Here, the CSF is the result of the Amplitude (A) 82.22, x_0 = mean (0.4234). In this case, w is the measure of the width of the distribution in cycles per degree (Figure 5.7-C). The area under the Gaussian distribution equals the Amplitude*w/0.3989. That constant equals the reciprocal of $(2\pi)^2$.

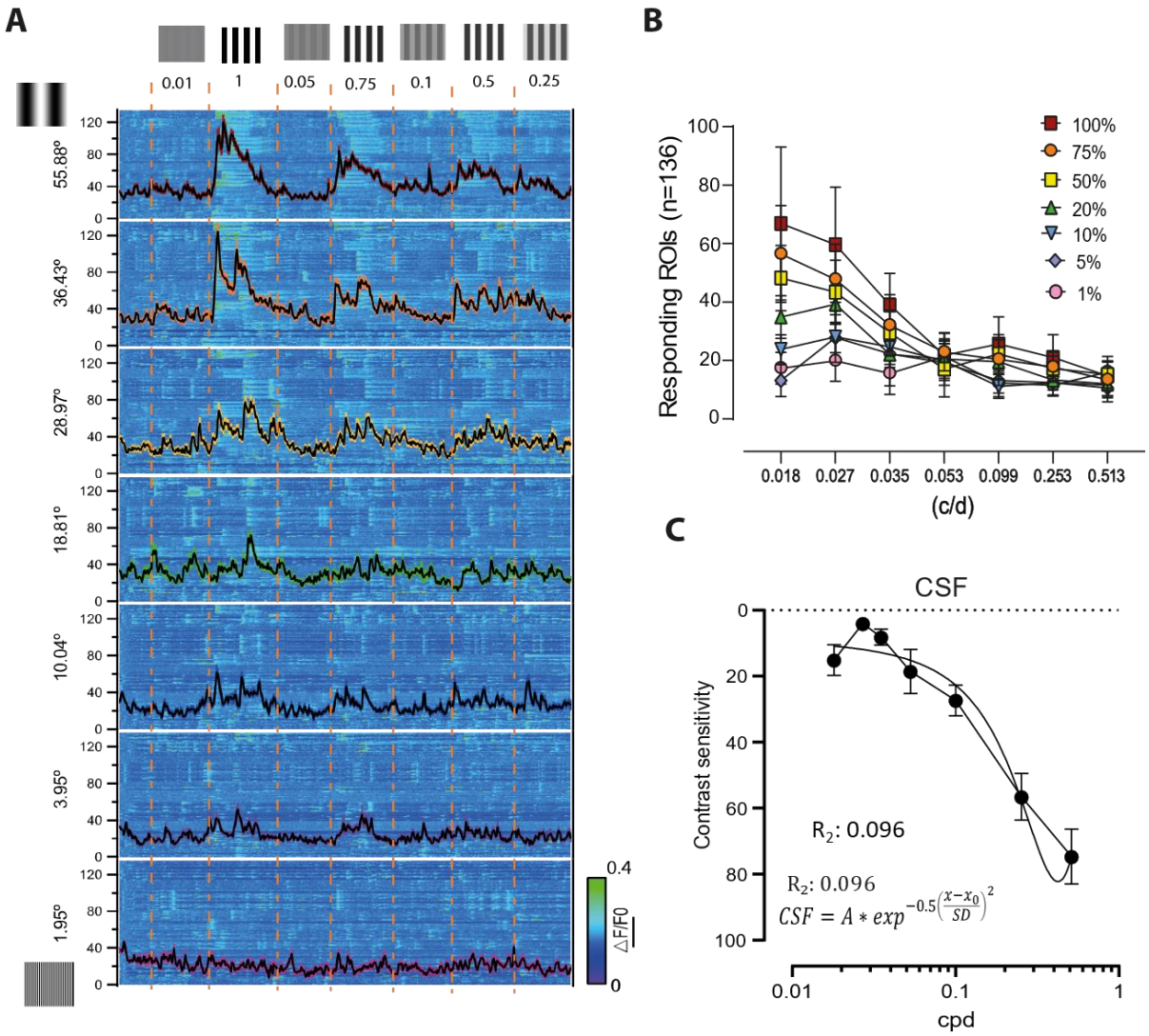

Figure 5.7. Theoretical contrast sensitivity function in higher visual areas. **(A)** *Responses to sinusoidal moving gratings varying in contrast and frequency during a single experiment (n = 136 ROIs, 13 fish). The manually selected ROIs were compiled in a heatmap in which the average trace was overlapped for better visualisation.* **(B)** *Number of responding ROIs according to their frequency and contrast tunning, SEM is shown.* **(C)** *Proposed contrast sensitivity function derived from the tectal responses to the combined contrast and frequency-varying moving gratings (See text).*

In order to compare this theoretical CSF, we plotted our values against those published (Figure 5.8), where the OKR was used to determine this function (Santon et al., 2019; Tappeiner et al., 2012). We found that it was not possible to describe the tendencies from all the data sets using a single model (extra-sum of squares f-test, $p < 0.05$).

The Amplitude of the Gaussian distribution for the OT theoretical model was 34.13, whereas the compared amplitudes were 0.744, 0.972, and 1.254 for the OKR responses generated at 25°/s, 10°/s, and in adults, respectively. These values suggest that the contrast limit is reduced at higher frequencies to produce an OKR, whereas for the OT, the contrast limit is significantly higher (Figure 5.8).

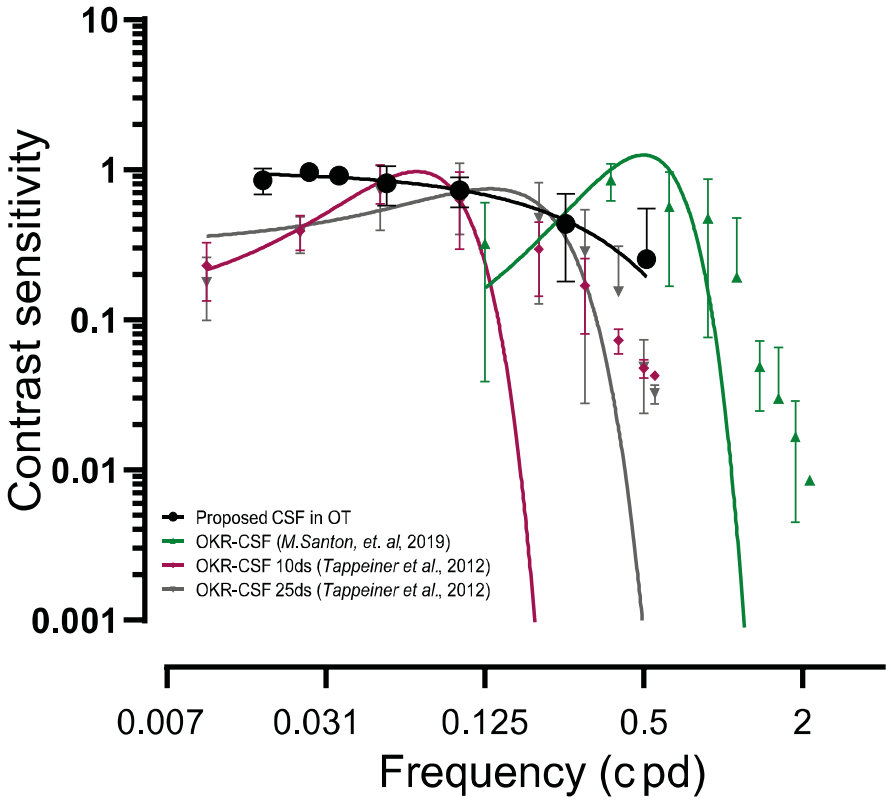

Figure 5.8. Graphical comparison of theoretical CSF via OT response with OKR tests. *The contrast sensitivity function (CSF) obtained from different methods assessing optokinetic responses, was compared with the proposed model obtained by evaluating the neuronal activity of higher function brain areas (OT). In this case, it is clear that the curve amplitude of our proposed method is wider than those published using OKR. Thus, suggesting the possibility that the zebrafish OT in the late-larvae stages might be able to detect beyond the contrasts and frequencies needed to generate an optokinetic or OMR.*

5.5 Visual contrast tunning and novel raising environments

In the early 1970s, experiments with kittens demonstrated that the visual RFs were experience-dependent (Groves & Thompson, 1970). For instance, kittens raised in an unnatural environment surrounded only by black and white lines were impaired to detect stripes in the transverse direction from those raised in a standard background (Blakemore & Cooper, 1970). Can different raising conditions modify the filtering mechanisms to contrast variations computed across the optic tectum neuropil in late-stage larvae zebrafish?

To test this question, we raised NBT: GCaMP3 ZF larvae in two novel environments. One consisting of a black and white striped tank at 100% contrast (100%CR), and another group in a grey background (0%CR) tank (Figure 5.9-A) and compared these responses with the normal raised (NR) fish.

The datasets from the protocol used in Figures 6.7 and 6.8 were further tested through non-linear regression to find a model that could best describe these observations. In general, for all datasets, an exponential decay model was found to fit best. Subsequently, we used the extra sum-of-squares F test to determine if all the datasets can be explained by a single best mathematical model. The datasets were found indeed to be best fitted into a single curve rather than individual curves for each one ($p < 0.05$), The equation was found to be:

$$A(f) = (0.4987 - 0.04325)e^{-0.06358f}$$

Where A(f) is the Amplitude of the measured response as a function of frequency, *f*. The correlation coefficient for this model was 0.06399, likely given the high amount of noise on the data (Figure 5.9-B).

The data was further separated into groups according to the location of the responding traces: one encompassing the whole optic tectum (ALL), one for the input layer of the system (IN), and one for the output layer (OUT) (Figure 5.9, C-D). Analysis through 2-way ANOVA (with Tukey multiple comparisons test) showed no significant differences between any of the raising schemes for none of the tested frequencies ($p < 0.05$).

Instead, we found that in each group, a single global fit curve was able to describe all the conditions between the raising conditions and the neuropil layers (Figure 5.9, E-F).

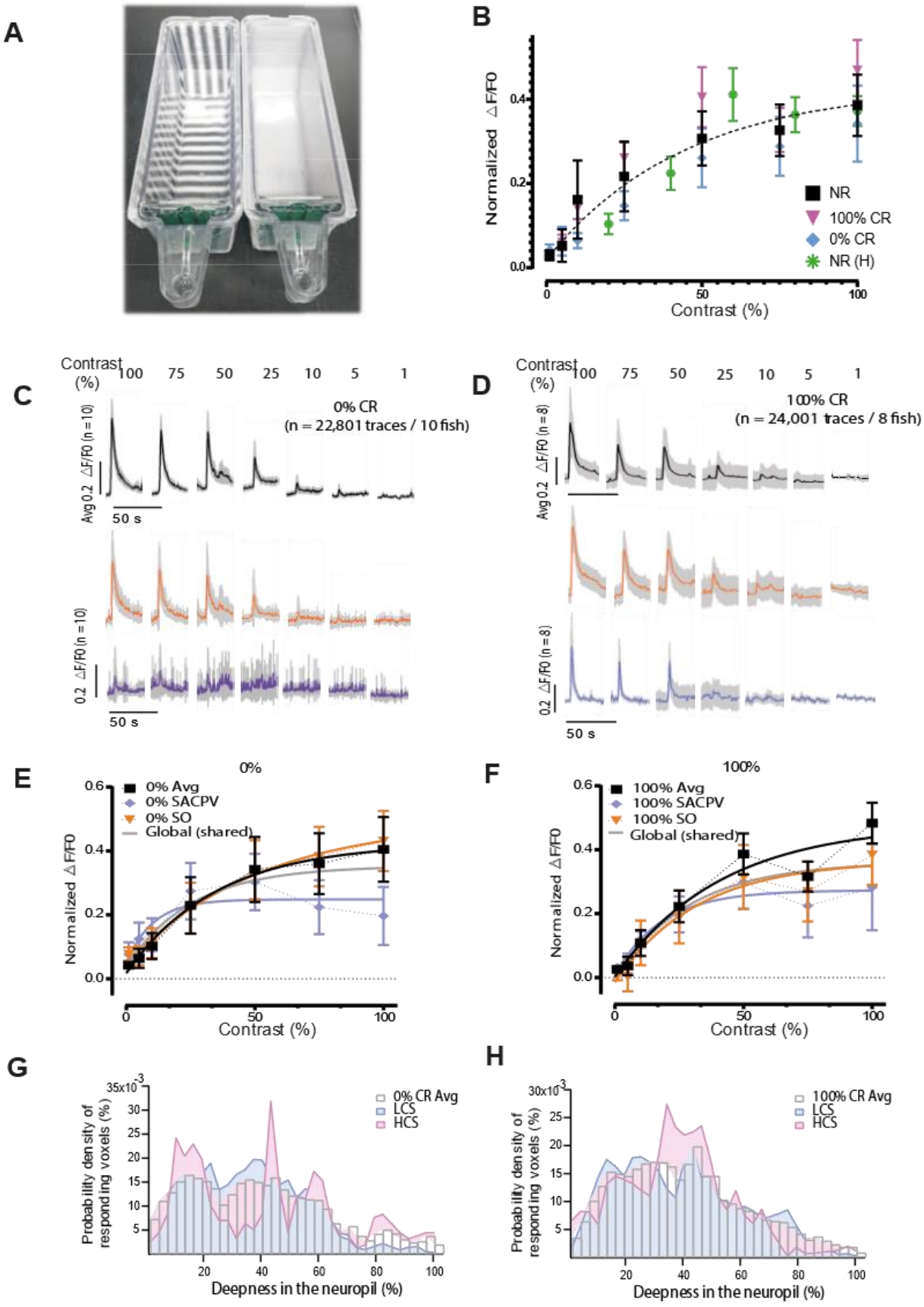

Figure 5.9 Visual contrast tunning in novel environments. (A) *The novel raising environments consisted of two tanks: One with black and white stripes with 100% contrast (left) and a 0% contrast-surrounded tank (right).* **(B)** *A single exponential curve fit described all the averaged NP responses from the four groups. NR: Normal raised, 100%CR: 100% contrast-raised, 0%CR: 0% contrast-raised, H: hierarchical (in order).* **(C)** *Averaged NP responses (top black), in the input (orange), and output (deep purple) from 0% CR fish presented with alternated moving gratings varying in contrasts.* **(D)** *Responses from a 100% CR fish.* **(E-F)** *Values from C and D were fitted in a globally shared exponential curve.* **(G)** *Distribution of tunned voxels to low-contrast and high contrast compared with the whole NP response in the 0% CR fish group.* **(H)** *Distribution of the responding voxels tunned to LCS, HCS and averaged NP from the fish raised in 100% gratings environment.*

Finally, we manually selected the responding voxels corresponding to the two main tunning classes: LCS and HCS and compared them with the average response distribution (Figure 5.9 G-H). It was found that the NR and 100% CR fish show a broad distribution comprising two main zones towards the lateral areas on average and tuned HCS and LCS cells. However, there is a slight change in the tunning distribution from the 0% CR fish responses, displaying three main layers rather than two for the HCS cells.

5.6 Conclusion

When measuring the input-output responses in the OT neuropil, it is evident that the filtering computations happening across all the layers before reaching the motor brain areas are complex. Whereas the input layers (SO and SFGS) usually display the highest responses (Figure 5.3-B and 5.5-A), we often find small clusters of subspecialized cells tuned for higher frequencies and low contrasts in the most profound areas (SGC, SAC and SPV) (Figure 5.3-D and 6.5).

Previous research has found that the ON, OFF and ON-OFF cells might present a parallel encoding system to filter the diming information according to other multiple visual

features, spatial and temporal frequency, shape, angle and size (Oliveira, Silveira, Chacon, & Luchiari, 2015). Here we found evidence that agreed with this statement. At the end of each stimulus, the cells triggered by a contrast shift were always present (Figure 5.4).

Functional characterization in the torus longitudinalis and periventricular cells have suggested a further classification of these classes according to their sensitivity response, such as high, low and broad contrast sensitive (Robles et al., 2020). In these *in vivo* calcium imaging experiments, we show that this is also the case for the frequency and contrast tuning properties in the ZF tectal neuropil, being most of the layers tunned to higher contrasts and lower frequencies. Based on these results, we produced a hypothetical CSF and proposed a model to predict this behaviour at a higher visual system level (Figure 5.8), which was never done before. When comparing this model with the published findings using OKR, our data shows a wider amplitude suggesting that maybe there is input reaching deeper areas of the tectum which will not generate an OKR. However, this hypothesis will need further investigation.

6. Final thoughts

6.1 Discussion

Even though visual organs are usually what comes to mind when referring to visual systems, in truth, the experience of vision happens within the brain. As pointed out in the literature, individual light-sensing cells are "blind", and only their collective processed information can be called vision (Webster, 1996). One of the clearest examples of this can be found in patients with cortical blindness, where the retinas keep receiving and relaying visual information, but the visual cortex is incapable of interpreting it: the result being a functionally blind patient who is not aware that is blind (Nicolas et al., 2016). It is during this processing that all the information encompassed as vision becomes interpreted by the brain, such as colour, spatial position, contrast, or motion.

At a receptor level, plasticity can be manifested in several ways, including increased or decreased activity, inhibiting signals, disabling of the receptors, or even endocytosis of receptors from the cell's membrane; resulting in a reduced outgoing signal from that sensory cell to the rest of the system (Langley, Simmons, & Welchman, 2003; Wark, Lundstrom, & Fairhall, 2007). This behaviour can be detected as changes in the synaptic activity of neural pathways in live-imaging studies (Wark et al., 2007; C. Zhang, Kolodkin, Wong, & James, 2017b).

Among other main roles, the sensory systems are needed to filter out repeated stimuli that do not provide new information (and therefore no further benefit) for the organism's function or survival (Wark et al., 2007); with this process, benefiting the attention to processing information that do provide a relevant use for life. One of the post-sensory mechanisms that arise to help streamline the flow of information from sensory systems is adaptation (Nikolaev et al., 2013b; Wark et al., 2007).

The fact that there are still many unanswered questions after all this time reveals that comprehending the mechanisms of visual memory formation is not an easy task, and even though several different approaches have been made in terms of models and techniques, there are still many more to come. However, remarkable advances in this field, such as the understanding of LTP and LTD or the emergence of novel visualization techniques -to mention a few- may help us to keep finding more hints in the investigation of these numerous remaining questions.

Among the questions that my project has left open are for instance, how can we determine with hundred percent certainty when the filtration of information happens in a voluntary or involuntary manner? How does the switch from adaptation (either facilitation or depression) undergoes habituation or sensitisation and why? Are our brains capable of detect a broader range of wavelengths, frequencies, and contrasts without us being conscious about it? In other words, can the signal of photons or even smaller components of them capable of reaching deeper structures of the brain which are not big enough to produce a conscious or even an unconscious response?

Previous optomotor and OKR studies have suggested that fish can detect features with frequencies as high as 1.18 ± 0.3 cpd (Santon et al., 2019). Visual acuity of the ZF was first hypothesized to have a physical limit of about 0.24 cpd by histological measurements of the larval ZF retina (Haug et al., 2010). The same study reported that the 5 dpf ZF showed visual acuity of 0.16 cpd. In other studies, it was determined that the ZF visual acuity was about 1.12 cpd in each eye, increasing to 1.7 cpd in binocular vision during the larval stages up to 6 dpf (Bögli et al., 2016). Similarly, these methods have been helpful to have an idea of the general contrast sensitivity of the ZF. However, the higher brain processing of these subspecialized properties had not been yet fully characterized.

6.1.1 Challenges

The use of zebrafish conveys many challenges when studying brain systems. For instance, the blood-brain barrier development is something that we must be aware of when performing experiments with drugs. Before nine days post-fertilization, this system is highly permeable, leading to leakage of hydrophilic substances and even polar vesicles which have been demonstrated through real-time analysis of fluorescent leakage (Jeong et al., 2008). Another issue is that even though we have already the entire genome-sequencing of ZF since 2001 and broad information regarding genome data (Howe et al., 2013), the number of discovered polymorphisms up to date is vast and increasing. This problem, makes difficult the use of genome editing tools such as CRISPR or morpholino oligonucleotide-inhibitors since it is common to find many non-specific off-target effects (Bedell, Westcot, & Ekker, 2011; Eisen & Smith, 2008).

In the experiments performed for this thesis, we used NBT: GCaMP3 and Huc: GCaMP6. The problem with *Huc* is the inconsistency in signal intensity. We have encountered the Huc: GCaMP6 strain in our lab; despite being brighter during early development, the calcium signal intensity decreases considerably, making it very difficult to image above 9dpf without using high laser power, thus making it possible to damage the fish. For this reason, the 2-photon experiments performed with this strain were done up to 9dpf only.

Finally, it is worth notice that there are some concerns to take into consideration when studying memory. Firstly, the information available regarding the mechanisms of memory formation is not always applicable to all models or all brain areas. How the environment act as a significant modifier of memories and how these circuits alter the motor behaviour are just some of the specifics that remain unclear until these days.

6.2 Conclusions

In this PhD, zebrafish was chosen as a model for the many advantages regarding vision.. For instance, affordability, fast development, and transparency. The aims were initially to describe how novel visual information is processed in zebrafish, firstly by identifying behavioural methods to test memory formation and then using molecular labelling tools to find where the visual information is first processed in the brain of the late-stage ZF fry.

The optic tectum (OT), the analogue of the superior colliculi in mammals, is the primary visual processing area in the zebrafish (ZF) brain. The OT neuropil is an organized, layered structure mainly formed by myelinated cells in charge of transmitting the retina's visual information to the downstream central nervous system (CNS).

In Chapters 5 and 6, I used multiphoton *in vivo* imaging to understand how visual information is first computed in the ZF brain. With this approach, we described an initial characterization of the plasticity mechanisms *in vivo* while presenting a simple repetitive non-associative stimulus. Finally, we presented stimuli consisting of moving sinusoidal moving gratings to give an idea of the ZF tectal capabilities in terms of visual contrast and frequency tunning properties. Some of the highlights of this thesis can be summarize in the following subtitles and justified below.

6.2.1 Behavioural studies should be considered carefully.

Visual-motor behaviour analysis is a complex multifactorial task. Computerized image analysis methods - namely video and image processing - are valuable tools to avoid systematic errors. One such instance is subjective bias as a result of visual counting and recognition by humans reported on past research (Head et al., 2015; Marsh & Hanlon, 2007). In this part of the project, we aimed to find a pattern that can be used to determine a general "novelty behaviour" in a large population, such as the findings from VLNOR tests, previously reported numerous times (Andersson et al., 2015a; Sovrano & Andrew, 2006).

Here, we performed visual lateralization studies with tracking imaging. When examining the data generated per fish, the results seemed to be promising. There was an evident qualitative difference between the behaviour of each ZF before and after the introduction of the novel object. The use of the left eye system over the right has been previously reported numerous times (Andersson et al., 2015a; Sovrano & Andrew, 2006). Unfortunately, this was not the case in our attempts to reproduce these experiments and adding an approach that eliminates any kind of human bias. In contrast with previous reports that considered the angle in which the fish happened to be in relation to the novelty on each established time (2-5secs), we assessed the relation of the ZF regarding the angle and distance within the object per frame (25 fps). This method gave us a more accurate set of data to analyse since fish can change its position several times in one second.

These data revealed that it is likely that the relation of the distance kept between the location of the novel object before and after the introduction of it could be considered a more consistent feature in novel exploratory behaviour among most of the fish tested, above the preference between left or right visual system. These findings suggest that further behavioural analysis should be done before making any conclusions regarding using VLNOR as a method to assess memory formation.

6.2.2 Use of WISH might be helpful in late-stage ZF larvae for synaptic research.

In Chapter 3, we optimized WISH and FWISH to be used in late-stage ZF successfully. After improving the skills on the traditional techniques and learnt the proper methods to perform FWISH we found that fish immediately exposed to a novel object displayed

activation in the lateral areas of the OT and the OB when labelled with *c-fos*, compared with controls.

6.2.3 Plasticity in the OT

The processing of any kind of sensory information requires a level of plasticity which is originated from the early stages of development. Reviewing the literature, we found that the main components of plasticity are, without doubt, adaptation, and habituation. The input of adaptation in the visual system is the retina. Previous studies (Nikolaev et al., 2013b; Nikolaou et al., 2012; Yin et al., 2019b) have demonstrated a large variety of adaptation dynamics among populations of retinal bipolar and ganglion cells such as depression and facilitation.

The standardization of the terminology regarding learning was not an easy task, as some of the words might be used subjectively in publications. The proposed scheme in Chapter 5 (Figure 5.1) is an attempt to round up and summarize the most relevant and often used concepts in the literature in a practical manner that is within reach of non-experts in the matter to avoid any confusion. It would not be fair to assume that this scheme is complete or that it agrees entirely with the literature out there. As implied before, there are publications within each branch of sensory systems (auditory, visual, somatosensory, etc.) with exceptional methods and results that give us incredibly useful information about the mechanisms underlying certain aspects of non-associative learning. However, it is not uncommon to find terms used in an interchangeable way, often mistakenly, thus complicating the message of the research along the way.

In this thesis, I reported that similarly to retinal cells, neurons in the optic tectum display different plasticity dynamics. Using two-photon imaging along with synaptic calcium reporters, we showed how adaptation diversity is organized across the neuropil layers, usually exhibiting faster adaptation in the input layers and getting slower to the output (periventricular neurons) accordingly. Some regions within the input (*SO, SFGS*) display a less profound adaptation compared to output layers (*SAC* and PVN), suggesting the existence of an additional component of this property.

Additionally, we found that these innate adaptation dynamics are generally maintained in presynaptic ganglion cells and when different changes to the stimulus presented are made. However, it is possible to modify some adaptation dynamics by altering

conditions such as inhibition of GABA-receptors or the addition of a paired-auditory and at the same time possibly scary stimulus.

6.2.4 Contrast and Frequency tunning in the OT NP

In chapter 5, I used 2-photon *in vivo* recordings of the tectal neuropil on late-stage ZF fry while encountering visual stimuli consisting of sinusoidal moving gratings varying in spatial frequencies (SF), and contrasts. The optical input is coded and filtered across the tectum in a tunned organization depending on visual properties like contrast, spatial frequency, and angle selectivity.

There are three main classes of neurons related to SF selectivity: low-pass, high-pass and bandpass; and three main classes according to contrast sensitivity: highly contrast-sensitive (HCS), low contrast sensitive (LCS), and contrast-suppressed cells. For the first time, in this thesis I presented examples of these classes and additional subclasses encountered with its topography in the neuropil which have not being published before. The presence of cells displaying super-specialized properties in the tectum, which location is not the same between individuals, suggests that despite functional synaptic variations, the filtering computations within the neuropil are likely to occur in a clustered-population manner rather than in a single-synapse level.

Furthermore, in our recordings, we found that at a fixed contrast and speed, the maximum response peak was reached at the lowest frequency tested in this case, 0.01 cpd (55.88°). Therefore, we proposed a contrast sensitivity function (CSF) model that did not fully correlate with previous reports using OKR. In this case, the amplitude of the frequencies and contrasts detected by the tectal cells in our experiments is wider than those published considering the OKR. This data suggests that the higher visual processing areas of the brain (namely OT), might be capable of detecting a broader range of stimuli which is not enough to generate a motor response. However, this should be further assessed by increasing the range of the frequencies and contrasts in further stimuli.

Finally, it was determined that the modification of environmental raising conditions have minimal impact on the tunning-filtering pathway in ZF up to 18 days post-fertilization (dpf). However, the reasons as to why require further investigation.

6.3 Future directions

In the search for answers to forever ongoing mysteries, it is always challenging to find an end. Further questions emerged as a result of this thesis. For instance, are the OMR and OKR-derived VA measurements and responses the only ones reaching higher visual processing areas? Or does the larval ZF brain in fact captures more than what is needed to generate an OKR or OMR? We know that ZF can detect light wavelengths that are impossible for humans (Bartel et al., 2021; Oliveira et al., 2015; Risner et al., 2006; Zhou et al., 2020). However, as humans, there are still visual detection features picked up at a higher brain level that are difficult to understand, such as phosphenes, the luminous floating star-like particles, which might appear in certain conditions often after applying pressure to the eyes, but also when closing the eyes and being overly conscious of the vision, and also being described by blind people(Mathis et al., 2017; Sannita, Narici, & Picozza, 2006).

It might not be entirely fair to consider the optic tectum as the fish equivalent of the superior colliculi, judging by all the functions and processing that it manages. For instance, the adaptation dynamics found in the neuropil mimic in a way some of the ones found in the cortex of some mammals (Gutierrez-Castellanos et al., 2017b; Jin, Lindsey, & Glickfeld, 2020). At the same time, the intermediate layers of the OT present a generally slower adaptation, and the most ventral layers (SAC and SPV) adapt faster and recover slowly, similarly to cortical intracellular firing in contrast with the thalamic responses (Chung et al., 2002).

Maybe some not-so-well understood white-matter structures related to visual processing, such as the stria of Gennari (Chapter 1.3.3) is a remanent of neuropil layers that once were evaluatively crucial for survival (Ide et al., 2012; Trampel et al., 2011). The fact is that many other hypotheses which will require more research will benefit from the constant generation of data and the persistent development and optimization of imaging techniques such as the FUGIMA method, which is a precision optogenetic tool kit which allows to trace neurons correlated with a specific stimulus or known behaviour (Kramer, Wu, Baier, & Kubo, 2019).

Chapter 7. References

Abbas, F., & Meyer, M. P. (2014). Fish Vision: Size selectivity in the zebrafish retinotectal pathway. *Current Biology*, *24*(21), R1048–R1050. https://doi.org/10.1016/j.cub.2014.09.043

Ahrens, M. B., Li, J. M., Orger, M. B., Robson, D. N., & Alexander, F. (2013). Brain-wide neuronal dynamics during motor adaptation in zebrafish. *Nature*, *485*(7399), 471–477. https://doi.org/10.1038/nature11057.Brain-wide

Ahrens, M. B., Orger, M. B., Robson, D. N., Li, J. M., & Keller, P. J. (2013a). Whole-brain functional imaging at cellular resolution using light-sheet microscopy. *Nature Methods*, *10*(5), 413–420. https://doi.org/10.1038/nmeth.2434

Ahrens, M. B., Orger, M. B., Robson, D. N., Li, J. M., & Keller, P. J. (2013b). Whole-brain functional imaging at cellular resolution using light-sheet microscopy. *Nature Methods*, *10*(5), 413–420. https://doi.org/10.1038/nmeth.2434

Ai, M., Mills, H., Kanai, M., Lai, J., Deng, J., Schreiter, E., … Suh, G. (2015). Green-to-red photoconversion of GCaMP. *PLoS ONE*, *10*(9), 1–11. https://doi.org/10.1371/journal.pone.0138127

Akerboom, J., Chen, T.-W., Wardill, T. J., Tian, L., Marvin, J. S., Mutlu, S., … Looger, L. L. (2012a). Optimization of a GCaMP Calcium Indicator for Neural Activity Imaging. *Journal of Neuroscience*, *32*(40), 13819–13840. https://doi.org/10.1523/JNEUROSCI.2601-12.2012

Akerboom, J., Chen, T.-W., Wardill, T. J., Tian, L., Marvin, J. S., Mutlu, S., … Looger, L. L. (2012b). Optimization of a GCaMP Calcium Indicator for Neural Activity Imaging. *Journal of Neuroscience*, *32*(40), 13819–13840. https://doi.org/10.1523/JNEUROSCI.2601-12.2012

Akerboom, Jasper, Carreras Calderón, N., Tian, L., Wabnig, S., Prigge, M., Tolö, J., … Looger, L. L. (2013). Genetically encoded calcium indicators for multi-color neural activity imaging and combination with optogenetics. *Frontiers in Molecular Neuroscience*, *6*. https://doi.org/10.3389/fnmol.2013.00002

Andersson, Ek, F., & Olsson, R. (2015). Using visual lateralization to model learning and memory in zebrafish larvae. *Scientific Reports*, *5*, 1–7. https://doi.org/10.1038/srep08667

Andersson, M. Å., Ek, F., & Olsson, R. (2015a). Using visual lateralization to model learning and memory in zebrafish larvae. *Scientific Reports*, *5*, 1–7. https://doi.org/10.1038/srep08667

Andersson, M. Å., Ek, F., & Olsson, R. (2015b). Using visual lateralization to model learning and memory in zebrafish larvae. *Scientific Reports*, *5*. https://doi.org/10.1038/srep08667

Antunes, M., & Biala, G. (2012). The novel object recognition memory: Neurobiology, test procedure, and its modifications. *Cognitive Processing*, *13*(2), 93–110. https://doi.org/10.1007/s10339-011-0430-z

Aoki, T., Kinoshita, M., Aoki, R., Agetsuma, M., Aizawa, H., Yamazaki, M., … Okamoto, H. (2013). Imaging of neural ensemble for the retrieval of a learned behavioral program. *Neuron*, *78*(5), 881–894. https://doi.org/10.1016/j.neuron.2013.04.009

Arcaro, M. J., Mcmains, S. A., Singer, B. D., & Kastner, S. (2009). Retinotopic Organization of Human Ventral Visual Cortex. *Behavioral/Systems/Cognitive*. https://doi.org/10.1523/JNEUROSCI.2807-09.2009

Ashby, M. C., Rue, S. A. D. La, Ralph, G. S., Uney, J., & Graham, L. (2012). Removal of AMPA Receptors (AMPARs) from Synapses Is Preceded by Transient Endocytosis of Extrasynaptic AMPARs, *24*(22), 5172–5176. https://doi.org/10.1523/JNEUROSCI.1042-04.2004.Removal

Baden, T., Euler, T., & Berens, P. (2020a). Understanding the retinal basis of vision across species. *Nature Reviews Neuroscience*. Springer US. https://doi.org/10.1038/s41583-019-0242-1

Baden, T., Euler, T., & Berens, P. (2020b). Understanding the retinal basis of vision across species. *Nature Reviews Neuroscience*, *21*(1), 5–20. https://doi.org/10.1038/s41583-019-0242-1

Baden, T., Nikolaev, A., Esposti, F., Dreosti, E., Odermatt, B., & Lagnado, L. (2014). A Synaptic Mechanism for Temporal Filtering of Visual Signals. *PLoS Biology*, *12*(10). https://doi.org/10.1371/journal.pbio.1001972

Bailey, C. H., & Chen, M. (1988). Morphological basis of short-term habituation in Aplysia. *The Journal of Neuroscience*, *8*(7), 2452 LP – 2459. Retrieved from http://www.jneurosci.org/content/8/7/2452.abstract

Bandmann, O., & Burton, E. A. (2010). Genetic zebrafish models of neurodegenerative diseases. *Neurobiology of Disease*, *40*(1), 58–65. https://doi.org/10.1016/j.nbd.2010.05.017

Bartel, P., Janiak, F. K., Osorio, D., & Baden, T. (2021, March 8). Colourfulness as a possible measure of object proximity in the larval zebrafish brain. *Current Biology*. Cell Press. https://doi.org/10.1016/j.cub.2021.01.030

Bathina, S., & Das, U. N. (2015). Brain-derived neurotrophic factor and its clinical Implications. *Archives of Medical Science*, *11*(6), 1164–1178. https://doi.org/10.5114/aoms.2015.56342

Baxendale, S., Holdsworth, C. J., Meza Santoscoy, P. L., Harrison, M. R. M., Fox, J., Parkin, C. A., … Cunliffe, V. T. (2012a). Identification of compounds with anti-convulsant properties in a zebrafish model of epileptic seizures. *Disease Models & Mechanisms*, *5*(6), 773–784. https://doi.org/10.1242/dmm.010090

Baxendale, S., Holdsworth, C. J., Meza Santoscoy, P. L., Harrison, M. R. M., Fox, J., Parkin, C. A., … Cunliffe, V. T. (2012b). Identification of compounds with anti-convulsant properties in a zebrafish model of epileptic seizures. *Disease Models & Mechanisms*, *5*(6), 773–784. https://doi.org/10.1242/dmm.010090

Bear, M. F., Connors, B. W., & Paradiso, M. A. (2015). *Neuroscience: Exploring the Brain*. Wolters Kluwer.

Bedell, V. M., Westcot, S. E., & Ekker, S. C. (2011). Lessons from morpholino-based

screening in zebrafish. *Briefings in Functional Genomics*, *10*(4), 181–188. https://doi.org/10.1093/bfgp/elr021

Beique, J.-C., Lin, D.-T., Kang, M.-G., Aizawa, H., Takamiya, K., & Huganir, R. L. (2006). Synapse-specific regulation of AMPA receptor function by PSD-95. *Proceedings of the National Academy of Sciences*, *103*(51), 19535–19540. https://doi.org/10.1073/pnas.0608492103

Benson, N. C., Butt, O. H., Datta, R., Radoeva, P. D., Brainard, D. H., & Aguirre, G. K. (2012). The retinotopic organization of striate cortex is well predicted by surface topology. *Current Biology*, *22*(21), 2081–2085. https://doi.org/10.1016/j.cub.2012.09.014

Bentivoglio, M., Cotrufo, T., Ferrari, S., Tesoriero, C., Mariotto, S., Bertini, G., … Mazzarello, P. (2019). The Original Histological Slides of Camillo Golgi and His Discoveries on Neuronal Structure. *Frontiers in Neuroanatomy*, *13*. https://doi.org/10.3389/fnana.2019.00003

Bergmann, K., Meza Santoscoy, P., Lygdas, K., Nikolaeva, Y., MacDonald, R., Cunliffe, V., & Nikolaev, A. (2018). Imaging Neuronal Activity in the Optic Tectum of Late Stage Larval Zebrafish. *Journal of Developmental Biology*, *6*(1), 6. https://doi.org/10.3390/jdb6010006

Bergmann, K., Santoscoy, P. M., Lygdas, K., Nikolaeva, Y., Macdonald, R. B., Cunliffe, V. T., & Nikolaev, A. (2018). Imaging Neuronal Activity in the Optic Tectum of Late Stage Larval Zebrafish. *Journal of Developmental Biology*. https://doi.org/10.3390/jdb6010006

Bernhard, N., & Van Der Kooy, D. (2000). A behavioral and genetic dissection of two forms of olfactory plasticity in Caenorhabditis elegans: Adaptation and habituation. *Learning and Memory*, *7*(4), 199–212. https://doi.org/10.1101/lm.7.4.199

Best, J. D., Berghmans, S., Hunt, J. J. F. G., Clarke, S. C., Fleming, A., Goldsmith, P., & Roach, A. G. (2008). Non-associative learning in larval zebrafish. *Neuropsychopharmacology*, *33*(5), 1206–1215. https://doi.org/10.1038/sj.npp.1301489

Bickle, J. (2009). *The Oxford Handbook of Philosophy and Neuroscience*. (J. Bickle, Ed.) (Vol. 1). Oxford University Press. https://doi.org/10.1093/oxfordhb/9780195304787.001.0001

Bilotta, J. (2000). Effects of abnormal lighting on the development of zebrafish visual behavior. *Behavioural Brain Research*, *116*(1), 81–87. https://doi.org/10.1016/S0166-4328(00)00264-3

Bilotta, J., & Saszik, S. (2001). The zebrafish as a model visual system. *International Journal of Developmental Neuroscience*, *19*(7), 621–629. https://doi.org/10.1016/S0736-5748(01)00050-8

Blakemore, C., & Cooper, G. F. (1970). Development of the Brain depends on the Visual Environment. *Nature*, *228*(5270), 477–478. https://doi.org/10.1038/228477a0

Bliss, T V P, & Gardner-Medwin, A. R. (1973a). Long-lasting potentiation of synaptic transmission in the dentate area of the unanaesthetized rabbit following stimulation of the perforant path. *The Journal of Physiology*, *232*(2), 357–374.

Retrieved from http://www.ncbi.nlm.nih.gov/pmc/articles/PMC1350459/

Bliss, T V P, & Gardner-Medwin, A. R. (1973b). Long-lasting potentiation of synaptic transmission in the dentate area of the unanaesthetized rabbit following stimulation of the perforant path. *The Journal of Physiology*, *232*(2), 357–374. Retrieved from http://www.ncbi.nlm.nih.gov/pmc/articles/PMC1350459/

Bliss, Timothy V P, & Cooke, S. F. (2011). Long-term potentiation and long-term depression: a clinical perspective. *Clinics (Sao Paulo, Brazil)*, *66 Suppl 1*, 3–17. Retrieved from http://www.ncbi.nlm.nih.gov/pubmed/21779718

Bliss, Timothy V P, Gardner-Medwin, A. R., Heap, L. A., Vanwalleghem, G. C., Thompson, A. W., Favre-Bulle, I., … Du, J. L. (2017). Low-frequency stimulation induces long-term depression and slow onset long-term potentiation at perforant path-dentate gyrus synapses in vivo. *Science*, *9*(1), 1259–1273. https://doi.org/10.1152/jn.00941.2012

Bögli, S. Y., Afthinos, M., Bertolini, G., Straumann, D., & Huang, M. Y. Y. (2016). Unravelling stimulus direction dependency of visual acuity in larval zebrafish by consistent eye displacements upon optokinetic stimulation. *Investigative Ophthalmology and Visual Science*, *57*(4), 1721–1727. https://doi.org/10.1167/iovs.15-18072

Bollmann, J. H. (2019). The Zebrafish Visual System: From Circuits to Behavior. *Annual Review of Vision Science*, *5*, 269–293. https://doi.org/10.1146/annurev-vision-091718-014723

Broad, K. D., Mimmack, M. L., & Kendrick, K. M. (2000). Is right hemisphere specialization for face discrimination specific to humans? *European Journal of Neuroscience*, *12*(2), 731–741. https://doi.org/10.1046/j.1460-9568.2000.00934.x

Buckner, R. L., & Krienen, F. M. (2013). The evolution of distributed association networks in the human brain. *Trends in Cognitive Sciences*, *17*(12), 648–665. https://doi.org/10.1016/j.tics.2013.09.017

Buonomano, D. V., & Merzenich, M. M. (2002). CORTICAL PLASTICITY: From Synapses to Maps. *Annual Review of Neuroscience*, *21*(1), 149–186. https://doi.org/10.1146/annurev.neuro.21.1.149

Cajal, S. R. Y. (1894a). The Croonian Lecture: La Fine Structure des Centres Nerveux. *Proceedings of the Royal Society of London*, *55*(331–335), 444–468. https://doi.org/10.1098/rspl.1894.0063

Cajal, S. R. Y. (1894b). The Croonian Lecture: La Fine Structure des Centres Nerveux. *Proceedings of the Royal Society of London*, *55*(331–335), 444–468. https://doi.org/10.1098/rspl.1894.0063

Castellucci, V., & Kandel, E. R. (1976). Presynaptic facilitation as a mechanism for behavioral sensitization in Aplysia. *Science*, *194*(4270), 1176–1178. https://doi.org/10.1126/science.11560

Ceriani, F., Pozzan, T., & Mammano, F. (n.d.). Critical role of ATP-induced ATP release for Ca 2+ signaling in nonsensory cell networks of the developing cochlea. https://doi.org/10.1073/pnas.1616061113

Çevik, M. Ö. (2014). Habituation, sensitization, and Pavlovian conditioning. *Frontiers in Integrative Neuroscience*, *8*(FEB), 1–6. https://doi.org/10.3389/fnint.2014.00013

Chatterjee, D., Tran, S., Shams, S., & Gerlai, R. (2015). A Simple Method for Immunohistochemical Staining of Zebrafish Brain Sections for c-fos Protein Expression. *Zebrafish*, *12*(6), zeb.2015.1147. https://doi.org/10.1089/zeb.2015.1147

Chung, S., Li, X., & Nelson, S. B. (2002). Short-term depression at thalamocortical synapses contributes to rapid adaptation of cortical sensory responses in vivo. *Neuron*, *34*(3), 437–446. https://doi.org/10.1016/S0896-6273(02)00659-1

Citri, A., & Malenka, R. C. (2008a). Synaptic plasticity: Multiple forms, functions, and mechanisms. *Neuropsychopharmacology*, *33*(1), 18–41. https://doi.org/10.1038/sj.npp.1301559

Citri, A., & Malenka, R. C. (2008b, January). Synaptic plasticity: Multiple forms, functions, and mechanisms. *Neuropsychopharmacology*. https://doi.org/10.1038/sj.npp.1301559

Connor, S. A., & Wang, Y. T. (2016, August 1). A Place at the Table: LTD as a Mediator of Memory Genesis. *Neuroscientist*. SAGE Publications Inc. https://doi.org/10.1177/1073858415588498

Constantine-Paton, M., & Law, M. I. (1978). Eye-specific termination bands in tecta of three-eyed frogs. *Science*, *202*(4368), 639–641. https://doi.org/10.1126/science.309179

Cruz, F. C., Javier Rubio, F., & Hope, B. T. (2015a). Using c-fos to study neuronal ensembles in corticostriatal circuitry of addiction. *Brain Research*, *1628*, 157–173. https://doi.org/10.1016/j.brainres.2014.11.005

Cruz, F. C., Javier Rubio, F., & Hope, B. T. (2015b). Using c-fos to study neuronal ensembles in corticostriatal circuitry of addiction. *Brain Research*, *1628*, 157–173. https://doi.org/10.1016/j.brainres.2014.11.005

Dan & Poo. (2006). Spike Timing-Dependent Plasticity: From Synapse to Perception. *Physiological Reviews*, *86*(3), 1033–1048. https://doi.org/10.1152/physrev.00030.2005

deCarvalho, T. N., Akitake, C. M., Thisse, C., Thisse, B., & Halpern, M. E. (2013). Aversive cues fail to activate fos expression in the asymmetric olfactory-habenula pathway of zebrafish. *Frontiers in Neural Circuits*, *7*(May). https://doi.org/10.3389/fncir.2013.00098

Dehmelt, F., Meier, R., Hinz, J., Yoshimatsu, T., Simacek, C., Wang, K., … Arrenberg, A. (2019). Gaze stabilisation behaviour is anisotropic across visual field locations in zebrafish, 1–45. https://doi.org/10.1101/754408

Del Bene, F., & Wyart, C. (2012). Optogenetics: A new enlightenment age for zebrafish neurobiology. *Developmental Neurobiology*, *72*(3), 404–414. https://doi.org/10.1002/dneu.20914

Del Bene, F., Wyart, C., Robles, E., Tran, A., Looger, L., Scott, E. K., … Baier, H. (2010). Filtering of visual information in the tectum by an identified neural circuit. *Science*,

330(6004), 669–673. https://doi.org/10.1126/science.1192949

Del Bene, F., Wyart, C., Robles, E., Tran, A., Looger, L., Scott, E. K., … Baraban, S. C. (2010). Filtering of visual information in the tectum by an identified neural circuit. *ENeuro*, *330*(1), 669–673. https://doi.org/10.1038/s41467-019-13484-9

DeMarco, E., Xu, N., Baier, H., & Robles, E. (2020). Neuron types in the zebrafish optic tectum labeled by an id2b transgene. *Journal of Comparative Neurology*, *528*(7), 1173–1188. https://doi.org/10.1002/cne.24815

Deperrois, N., & Graupner, M. (2020). Short-term depression and long-term plasticity together tune sensitive range of synaptic plasticity. *PLoS Computational Biology*, *16*(9), 1–25. https://doi.org/10.1371/journal.pcbi.1008265

Dong, X., Gao, Y., Lv, L., & Bao, M. (2016a). Habituation of visual adaptation. *Scientific Reports*, *6*, 1–14. https://doi.org/10.1038/srep19152

Dong, X., Gao, Y., Lv, L., & Bao, M. (2016b). Habituation of visual adaptation. *Scientific Reports*, *6*, 1–14. https://doi.org/10.1038/srep19152

Drapeau, P., Saint-Amant, L., Buss, R. R., Chong, M., McDearmid, J. R., & Brustein, E. (2002). Development of the locomotor network in zebrafish. *Progress in Neurobiology*, *68*(2), 85–111. https://doi.org/10.1016/S0301-0082(02)00075-8

Dreosti, E., Lopes, G., Kampff, A. R., & Wilson, S. W. (2015). Development of social behavior in young zebrafish. *Frontiers in Neural Circuits*, *9*(August), 1–9. https://doi.org/10.3389/fncir.2015.00039

Eisen, J. S., & Smith, J. C. (2008). Controlling morpholino experiments: don't stop making antisense. *Development*, *135*(10), 1735–1743. https://doi.org/10.1242/dev.001115

Ennaceur, A., & Delacour, J. (1988). A new one-trial test for neurobiological studies of memory in rats. 1: Behavioral data. *Behavioural Brain Research*, *31*(1), 47–59. https://doi.org/10.1016/0166-4328(88)90157-X

Feldman, D. E. (2012). The spike timing dependence of plasticity. *Neuron*, *75*(4), 556–571. https://doi.org/10.1016/j.neuron.2012.08.001.The

Fioravante, D., & Regehr, W. G. (2011). Short-term forms of presynaptic plasticity. *Current Opinion in Neurobiology*, *21*(2), 269–274. https://doi.org/10.1016/j.conb.2011.02.003

Förster, D., Helmbrecht, T. O., Mearns, D. S., Jordan, L., Mokayes, N., & Baier, H. (2020a). Retinotectal circuitry of larval zebrafish is adapted to detection and pursuit of prey. *ELife*, *9*, 1–26. https://doi.org/10.7554/eLife.58596

Förster, D., Helmbrecht, T. O., Mearns, D. S., Jordan, L., Mokayes, N., & Baier, H. (2020b). Retinotectal circuitry of larval zebrafish is adapted to detection and pursuit of prey. *ELife*, *9*, 1–26. https://doi.org/10.7554/eLife.58596

Gallo, F. T., Katche, C., Morici, J. F., Medina, J. H., Weisstaub, N. V, Gallitano, A., … De Bartolomeis, A. (2018a). Immediate Early Genes, Memory and Psychiatric Disorders: Focus on c-Fos, Egr1 and Arc. https://doi.org/10.3389/fnbeh.2018.00079

Gallo, F. T., Katche, C., Morici, J. F., Medina, J. H., Weisstaub, N. V, Gallitano, A., … De Bartolomeis, A. (2018b). Immediate Early Genes, Memory and Psychiatric Disorders: Focus on c-Fos, Egr1 and Arc. *Frontiers in Behavioral Neuroscience*, *12*(79). https://doi.org/10.3389/fnbeh.2018.00079

Gebhardt, C., Auer, T. O., Henriques, P. M., Rajan, G., Duroure, K., Bianco, I. H., & Del Bene, F. (2019a). An interhemispheric neural circuit allowing binocular integration in the optic tectum. *Nature Communications*, *10*(1), 1–12. https://doi.org/10.1038/s41467-019-13484-9

Gebhardt, C., Auer, T. O., Henriques, P. M., Rajan, G., Duroure, K., Bianco, I. H., & Del Bene, F. (2019b). An interhemispheric neural circuit allowing binocular integration in the optic tectum. *Nature Communications*, *10*(1), 5471. https://doi.org/10.1038/s41467-019-13484-9

Gebhardt, C., Baier, H., & Del Bene, F. (2013). Direction selectivity in the visual system of the zebrafish larva. *Frontiers in Neural Circuits*, *7*(MAY), 1–6. https://doi.org/10.3389/fncir.2013.00111

George, A. A., Lyons-Warren, A. M., Ma, X., & Carlson, B. A. (2011). A diversity of synaptic filters are created by temporal summation of excitation and inhibition. *Journal of Neuroscience*, *31*(41), 14721–14734. https://doi.org/10.1523/JNEUROSCI.1424-11.2011

Gestri, G., Link, B. A., & Neuhauss, S. C. F. (2012). The visual system of zebrafish and its use to model human ocular Diseases. *Developmental Neurobiology*, *72*(3), 302–327. https://doi.org/10.1002/dneu.20919

Ghodrati, M., Zavitz, E., Rosa, M. G. P., & Price, N. S. C. (2019). Contrast and luminance adaptation alter neuronal coding and perception of stimulus orientation. *Nature Communications*, *10*(1). https://doi.org/10.1038/s41467-019-08894-8

Gonzalez, J., Morales, I. S. S., Villarreal, D. M. M., Derrick, B. E. E., Bliss, T. V. P., Gardner-Medwin, A. R., … Du, J. L. (2014). Low-frequency stimulation induces long-term depression and slow onset long-term potentiation at perforant path-dentate gyrus synapses in vivo. *Journal of Neurophysiology*, *111*(6), 1259–1273. https://doi.org/10.1152/jn.00941.2012

Gonzalez, J., Morales, I. S., Villarreal, D. M., & Derrick, B. E. (2014). Low-frequency stimulation induces long-term depression and slow onset long-term potentiation at perforant path-dentate gyrus synapses in vivo. *Journal of Neurophysiology*, *111*(6), 1259–1273. https://doi.org/10.1152/jn.00941.2012

Graydon, C. W., Lieberman, E. E., Rho, N., Briggman, K. L., Singer, J. H., & Diamond, J. S. (2018). Synaptic Transfer between Rod and Cone Pathways Mediated by AII Amacrine Cells in the Mouse Retina. *Current Biology*, *28*(17), 2739-2751.e3. https://doi.org/10.1016/j.cub.2018.06.063

Grossberg, S. (2015). From brain synapses to systems for learning and memory: Object recognition, spatial navigation, timed conditioning, and movement control. *Brain Research*, *1621*, 270–293. https://doi.org/10.1016/j.brainres.2014.11.018

Grover, L. M., Kim, E., Cooke, J. D., & Holmes, W. R. (2009). LTP in hippocampal area CA1 is induced by burst stimulation over a broad frequency range centered around

delta. *Learning & Memory*, *16*(1), 69–81. https://doi.org/10.1101/lm.1179109

Groves, P. M., & Thompson, R. F. (1970). Habituation: A dual-process theory. *Psychological Review*, *77*(5), 419–450. https://doi.org/10.1037/h0029810

Gutierrez-Castellanos, N., Da Silva-Matos, C. M., Zhou, K., Canto, C. B., Renner, M. C., Koene, L. M. C., … De Zeeuw, C. I. (2017a). Motor Learning Requires Purkinje Cell Synaptic Potentiation through Activation of AMPA-Receptor Subunit GluA3. *Neuron*, *93*(2), 409–424. https://doi.org/10.1016/j.neuron.2016.11.046

Gutierrez-Castellanos, N., Da Silva-Matos, C. M., Zhou, K., Canto, C. B., Renner, M. C., Koene, L. M. C., … De Zeeuw, C. I. (2017b). Motor Learning Requires Purkinje Cell Synaptic Potentiation through Activation of AMPA-Receptor Subunit GluA3. *Neuron*, *93*(2), 409–424. https://doi.org/10.1016/j.neuron.2016.11.046

Gutierrez, G. J., & Denève, S. (2019). Population adaptation in efficient balanced networks. *ELife*, *8*. https://doi.org/10.7554/eLife.46926

Halpern, M. E. (2005). Lateralization of the Vertebrate Brain: Taking the Side of Model Systems. *Journal of Neuroscience*, *25*(45), 10351–10357. https://doi.org/10.1523/jneurosci.3439-05.2005

Hamilton, T. J., Myggland, A., Duperreault, E., May, Z., Gallup, J., Powell, R. A., … Digweed, S. M. (2016a). Episodic-like memory in zebrafish. *Animal Cognition*, *19*(6), 1071–1079. https://doi.org/10.1007/s10071-016-1014-1

Hamilton, T. J., Myggland, A., Duperreault, E., May, Z., Gallup, J., Powell, R. A., … Digweed, S. M. (2016b). Episodic-like memory in zebrafish. *Animal Cognition*, *19*(6), 1071–1079. https://doi.org/10.1007/s10071-016-1014-1

Harris, C. S. (1963). Adaptation to Displaced Vision: Visual, Motor, or Proprioceptive Change? *Science*, *140*(3568), 812–813. https://doi.org/10.1126/science.140.3568.812

Harris, J. D. (1943). Habituatory response decrement in the intact organism. *Psychological Bulletin*, *40*(6), 385–422. https://doi.org/10.1037/h0053918

Hartline, H. K. (1938a). THE RESPONSE OF SINGLE OPTIC NERVE FIBERS OF THE VERTEBRATE EYE TO ILLUMINATION OF THE RETINA. *American Journal of Physiology-Legacy Content*, *121*(2), 400–415. https://doi.org/10.1152/ajplegacy.1938.121.2.400

Hartline, H. K. (1938b). THE RESPONSE OF SINGLE OPTIC NERVE FIBERS OF THE VERTEBRATE EYE TO ILLUMINATION OF THE RETINA. *American Journal of Physiology-Legacy Content*, *121*(2), 400–415. https://doi.org/10.1152/ajplegacy.1938.121.2.400

Haug, M. F., Biehlmaier, O., Mueller, K. P., & Neuhauss, S. C. F. (2010). Visual acuity in larval zebrafish: Behavior and histology. *Frontiers in Zoology*, *7*(March). https://doi.org/10.1186/1742-9994-7-8

He, J., Mo, D., Chen, J., & Luo, L. (2020). Combined whole-mount fluorescence in situ hybridization and antibody staining in zebrafish embryos and larvae. *Nature Protocols*, *15*(10), 3361–3379. https://doi.org/10.1038/s41596-020-0376-7

Head, M. L., Jennions, M. D., Holman, L., Head, M. L., Lanfear, R., & Jennions, M. D. (2015). Evidence of Experimental Bias in the Life Sciences : Why We Need Blind Data Recording . Evidence of Experimental Bias in the Life Sciences : Why We Need Blind Data Recording, (JULY), 1–12. https://doi.org/10.5281/zenodo.13147

Heap, L. A., Vanwalleghem, G. C., Thompson, A. W., Favre-Bulle, I., Rubinsztein-Dunlop, H., & Scott, E. K. (2018). Hypothalamic projections to the optic tectum in larval zebrafish. *Frontiers in Neuroanatomy*, *11*(January), 1–12. https://doi.org/10.3389/fnana.2017.00135

Helmbrecht, T. O., dal Maschio, M., Donovan, J. C., Koutsouli, S., & Baier, H. (2018). Topography of a Visuomotor Transformation. *Neuron*, *100*(6), 1429-1445.e4. https://doi.org/10.1016/j.neuron.2018.10.021

Ho, V. M., Lee, J., & Martin, K. C. (2011). The cell biology of synaptic plasticity. *Science*, *334*(6056), 623–628. https://doi.org/10.1126/science.1209236.The

Howe, K., Clark, M. D., Torroja, C. F., Torrance, J., Berthelot, C., Muffato, M., … Stemple, D. L. (2013). The zebrafish reference genome sequence and its relationship to the human genome. *Nature*, *496*(7446), 498–503. https://doi.org/10.1038/nature12111

Howland, J. G., & Wang, Y. T. (2008, January). Chapter 8 Synaptic plasticity in learning and memory: Stress effects in the hippocampus. *Progress in Brain Research*. Elsevier. https://doi.org/10.1016/S0079-6123(07)00008-8

Hubel, D. H., & Wiesel, T. N. (1962). Receptive fields, binocular interaction and functional architecture in the cat's visual cortex. *The Journal of Physiology*, *160*(1), 106–154. https://doi.org/10.1113/jphysiol.1962.sp006837

Humphrey, J. (1933). The Nature of Learning. By George Humphrey. *Philosophy*, *8*(32), 493–494. https://doi.org/10.1017/S0031819100045769

Ide, S., Kakeda, S., Korogi, Y., Yoneda, T., Nishimura, J., Sato, T., … Matsuyama, A. (2012). Delineation of Optic Radiation and Stria of Gennari on High-resolution Phase Difference Enhanced Imaging. *Academic Radiology*, *19*(10), 1283–1289. https://doi.org/10.1016/j.acra.2012.05.018

Jackman, S. L., & Regehr, W. G. (2017). The Mechanisms and Functions of Synaptic Facilitation. *Neuron*, *94*(3), 447–464. https://doi.org/10.1016/j.neuron.2017.02.047

Jacoby, J., & Schwartz, G. W. (2018). Typology and circuitry of suppressed-by-contrast retinal Ganglion cells. *Frontiers in Cellular Neuroscience*, *12*(August), 1–7. https://doi.org/10.3389/fncel.2018.00269

Jaepel, J., Hübener, M., Bonhoeffer, T., & Rose, T. (2017). Lateral geniculate neurons projecting to primary visual cortex show ocular dominance plasticity in adult mice. *Nature Neuroscience*, *20*(12), 1708–1714. https://doi.org/10.1038/s41593-017-0021-0

Jaiswal, M., Sandoval, H., Zhang, K., Bayat, V., Bellen, H., & Duncan, D. (2012). Probing Mechanisms That Underlie Human Neurodegenerative Diseases in Drosophila. *Annu. Rev. Genet*, *46*, 371–396. https://doi.org/10.1146/annurev-genet-110711-

155456

Jeong, J. Y., Kwon, H. B., Ahn, J. C., Kang, D., Kwon, S. H., Park, J. A., & Kim, K. W. (2008). Functional and developmental analysis of the blood-brain barrier in zebrafish. *Brain Research Bulletin*, *75*(5), 619–628. https://doi.org/10.1016/j.brainresbull.2007.10.043

Jia, Z., & Collingridge, G. L. (2017). Learning about Synaptic GluA3. *Neuron*, *93*(2), 254–256. https://doi.org/10.1016/j.neuron.2017.01.004

Jin, M., Lindsey, X., & Glickfeld, L. (2020). Modulation of Dynamic Neural Networks: From Sensory Inputs to Motor Outputs Magnitude, time course, and specificity of rapid adaptation across mouse visual areas. *J Neurophysiol*, *124*, 245–258. https://doi.org/10.1152/jn.00758.2019.-Adaptation

Kalueff, A. V, Stewart, A. M., Gerlai, R., & Court, P. (2014). Zebrafish as an emerging model for studying complex brain disorders. *Trends in Pharmacological Sciences*, *35*(2), 63–75. https://doi.org/10.1016/j.tips.2013.12.002.Zebrafish

Kandel, E. R., Dudai, Y., & Mayford, M. R. (2014, March 27). The molecular and systems biology of memory. *Cell*. Cell Press. https://doi.org/10.1016/j.cell.2014.03.001

Karnieli, A., Rivera, N., Arie, A., & Kaminer, I. (2021). The coherence of light is fundamentally tied to the quantum coherence of the emitting particle. *Science Advances*, *7*(18), 1–8. https://doi.org/10.1126/sciadv.abf8096

Kaschula, R., & Salecker, I. (2016a). Neuronal Computations Made Visible with Subcellular Resolution. *Cell*, *166*(1), 18–20. https://doi.org/10.1016/j.cell.2016.06.022

Kaschula, R., & Salecker, I. (2016b). Neuronal Computations Made Visible with Subcellular Resolution. *Cell*. Cell Press. https://doi.org/10.1016/j.cell.2016.06.022

Keatinge, M., Bui, H., Menke, A., Chen, Y. C., Sokol, A. M., Bai, Q., … Bandmann, O. (2015). Glucocerebrosidase 1 deficient Danio rerio mirror key pathological aspects of human Gaucher disease and provide evidence of early microglial activation preceding alpha-synuclein-independent neuronal cell death. *Human Molecular Genetics*, *24*(23), 6640–6652. https://doi.org/10.1093/hmg/ddv369

Keck, T., Hübener, M., & Bonhoeffer, T. (2017, April 1). Interactions between synaptic homeostatic mechanisms: an attempt to reconcile BCM theory, synaptic scaling, and changing excitation/inhibition balance. *Current Opinion in Neurobiology*. Elsevier Ltd. https://doi.org/10.1016/j.conb.2017.02.003

Khatib, T. Z., & Martin, K. R. (2017). Protecting retinal ganglion cells. *Eye (Basingstoke)*, *31*(2), 218–224. https://doi.org/10.1038/eye.2016.299

Kitamura, T., Ogawa, S. K., Roy, D. S., Okuyama, T., Morrissey, M. D., Smith, L. M., … Tonegawa, S. (n.d.). *Engrams and circuits crucial for systems consolidation of a memory*. Retrieved from http://science.sciencemag.org/

Kitamura, T., Ogawa, S. K., Roy, D. S., Okuyama, T., Morrissey, M. D., Smith, L. M., … Tonegawa, S. (2017). Engrams and circuits crucial for systems consolidation of a memory. *Science*, *356*(6333), 73–78. https://doi.org/10.1126/science.aam6808

Kolb, H. (1995). *Simple Anatomy of the Retina*. *Webvision: The Organization of the Retina and Visual System*. Retrieved from http://www.ncbi.nlm.nih.gov/pubmed/21413391

Kolb, H. (2005). *Simple Anatomy of the Retina*. *Webvision: The Organization of the Retina and Visual System*.

Kramer, A., Wu, Y., Baier, H., & Kubo, F. (2019). Neuronal Architecture of a Visual Center that Processes Optic Flow. *Neuron*, *103*(1), 118-132.e7. https://doi.org/10.1016/j.neuron.2019.04.018

Krubitzer, L. (2009). In Search of a Unifying Theory of Complex Brain Evolution. *Annals of the New York Academy of Sciences*, *1156*(1), 44–67. https://doi.org/10.1111/j.1749-6632.2009.04421.x

Kundap, U. P., Kumari, Y., Othman, I., & Shaikh, M. F. (2017). Zebrafish as a model for epilepsy-induced cognitive dysfunction: A pharmacological, biochemical and behavioral approach. *Frontiers in Pharmacology*, *8*(AUG), 1–13. https://doi.org/10.3389/fphar.2017.00515

Kunst, M., Laurell, E., Mokayes, N., Kramer, A., Kubo, F., Fernandes, A. M., … Baier, H. (2019). A Cellular-Resolution Atlas of the Larval Zebrafish Brain. *Neuron*, *103*(1), 21-38.e5. https://doi.org/10.1016/j.neuron.2019.04.034

Landhuis, E. (2017). Neuroscience: Big brain, big data. *Nature*, *541*(7638), 559–561. https://doi.org/10.1038/541559a

Langer, K. B., Ohlemacher, S. K., Phillips, M. J., Fligor, C. M., Jiang, P., Gamm, D. M., & Meyer, J. S. (2018). Retinal Ganglion Cell Diversity and Subtype Specification from Human Pluripotent Stem Cells. *Stem Cell Reports*, *10*(4), 1282–1293. https://doi.org/10.1016/j.stemcr.2018.02.010

Langley, K., Simmons, D., & Welchman, A. (2003). Visual adaptation. *Spatial Vision*, *16*(1), 1–3. https://doi.org/10.1163/15685680260433869

Leighton, P. L. A., Nadolski, N. J., Morrill, A., Hamilton, T. J., & Allison, W. T. (2018). An ancient conserved role for prion protein in learning and memory. *Biology Open*, *7*(1), bio025734. https://doi.org/10.1242/bio.025734

Leung, L. C., Wang, G. X., & Mourrain, P. (2013). Imaging zebrafish neural circuitry from whole brain to synapse. *Frontiers in Neural Circuits*, *7*. https://doi.org/10.3389/fncir.2013.00076

Li, E. S., Saha, M. S., & Alaimo, A. (2021). Optimizing Calcium Detection Methods in Animal Systems: A Sandbox for Synthetic Biology Optimizing Calcium Detection Methods in Animal Systems: A Sandbox for Synthetic Biology. *Biomolecules*, 34. https://doi.org/10.3390/biom11030343

Lister, J. A., Robertson, C. P., Lepage, T., Johnson, S. L., & Raible, D. W. (1999). Nacre encodes a zebrafish microphthalmia-related protein that regulates neural-crest-derived pigment cell fate. *Development (Cambridge, England)*, *126*(17), 3757–3767.

Liu, J., & Baraban, S. C. (2019). Network properties revealed during multi-scale calcium imaging of seizure activity in Zebrafish. *ENeuro*, *6*(1). https://doi.org/10.1523/ENEURO.0041-19.2019

Liu, Y.-J., Hashemi-Nezhad, M., & Lyon, D. C. (2017). Differences in orientation tuning between pinwheel and domain neurons in primary visual cortex depend on contrast and size. *Neurophotonics*, *4*(3), 031209. https://doi.org/10.1117/1.nph.4.3.031209

López-Rivera, J. A., Pérez-Palma, E., Symonds, J., Lindy, A. S., McKnight, D. A., Leu, C., … Lal, D. (2020). A catalogue of new incidence estimates of monogenic neurodevelopmental disorders caused by de novo variants. *Brain*, *143*(3), 1099–1105. https://doi.org/10.1093/brain/awaa051

Luo-Li, G., Mazade, R., Zaidi, Q., Alonso, J. M., & Freeman, A. W. (2018). Motion changes response balance between ON and OFF visual pathways. *Communications Biology*, *1*(1). https://doi.org/10.1038/s42003-018-0066-y

Malenka, R. C., & Bear, M. F. (2004). LTP and LTD: An embarrassment of riches. *Neuron*, *44*(1), 5–21. https://doi.org/10.1016/j.neuron.2004.09.012

Marachlian, E., Avitan, L., Goodhill, G. J., & Sumbre, G. (2018a). Principles of functional circuit connectivity: Insights from spontaneous activity in the zebrafish optic tectum. *Frontiers in Neural Circuits*, *12*(June), 1–8. https://doi.org/10.3389/fncir.2018.00046

Marachlian, E., Avitan, L., Goodhill, G. J., & Sumbre, G. (2018b). Principles of functional circuit connectivity: Insights from spontaneous activity in the zebrafish optic tectum. *Frontiers in Neural Circuits*, *12*(June), 1–8. https://doi.org/10.3389/fncir.2018.00046

Markram, H., Lübke, J., Frotscher, M., & Sakmann, B. (1997). Regulation of Synaptic Efficacy by Coincidence of Postsynapticv APs and EPSPs. *Science*, *275*(5297), 213–215. https://doi.org/10.1126/science.275.5297.213

Marsh, D. M., & Hanlon, T. J. (2007). Seeing what we want to see: Confirmation bias in animal behavior research. *Ethology*, *113*(11), 1089–1098. https://doi.org/10.1111/j.1439-0310.2007.01406.x

Martin, S. J., Grimwood, P. D., & Morris, R. G. M. (2000). Synaptic Plasticity and Memory: An Evaluation of the Hypothesis. *Annual Review of Neuroscience*, *23*(1), 649–711. https://doi.org/10.1146/annurev.neuro.23.1.649

Marvin, J. S., Borghuis, B. G., Tian, L., Cichon, J., Harnett, M. T., Akerboom, J., … Looger, L. L. (2013). An optimized fluorescent probe for visualizing glutamate neurotransmission. *Nature Methods*, *10*(2), 162–170. https://doi.org/10.1038/nmeth.2333

Masland, R. H. (2012a). The Neuronal Organization of the Retina. *Neuron*. https://doi.org/10.1016/j.neuron.2012.10.002

Masland, R. H. (2012b). The Neuronal Organization of the Retina. *Neuron*, *76*(2), 266–280. https://doi.org/10.1016/j.neuron.2012.10.002

Mathis, T., Vignot, S., Leal, C., Caujolle, J. P., Maschi, C., Mauget-Faÿsse, M., … Thariat, J. (2017). Mechanisms of phosphenes in irradiated patients. *Oncotarget*, *8*(38), 64579–64590. https://doi.org/10.18632/oncotarget.18719

Matsuda, K., & Kubo, F. (2021). Circuit organization underlying optic flow processing in

zebrafish, *15*(July), 1–8. https://doi.org/10.3389/fncir.2021.709048

May, Z., Morrill, A., Holcombe, A., Johnston, T., Gallup, J., Fouad, K., … Hamilton, T. J. (2016a). Object recognition memory in zebrafish. *Behavioural Brain Research*, *296*, 199–210. https://doi.org/10.1016/j.bbr.2015.09.016

May, Z., Morrill, A., Holcombe, A., Johnston, T., Gallup, J., Fouad, K., … Hamilton, T. J. (2016b). Object recognition memory in zebrafish. *Behavioural Brain Research*, *296*, 199–210. https://doi.org/10.1016/j.bbr.2015.09.016

May, Z., Morrill, A., Holcombe, A., Johnston, T., Gallup, J., Fouad, K., … Hamilton, T. J. (2016c). Object recognition memory in zebrafish. *Behavioural Brain Research*, *296*, 199–210. https://doi.org/10.1016/j.bbr.2015.09.016

Mayford, M., Siegelbaum, S. A., Kandel, E. R., Long-term, N. R., Lüscher, C., Malenka, R. C., … Südhof, C. (2012). Synapses and Memory Storage. *Cold Spring Harbor Perspectives in Biology*, *4*, a005751. https://doi.org/10.1101/cshperspect.a005751

McDowell, A. L., Dixon, L. J., Houchins, J. D., & Bilotta, J. (2004). Visual processing of the zebrafish optic tectum before and after optic nerve damage. *Visual Neuroscience*, *21*(2), 97–106. https://doi.org/10.1017/S0952523804043019

McMains, S., & Kastner, S. (2011). Interactions of top-down and bottom-up mechanisms in human visual cortex. *Journal of Neuroscience*, *31*(2), 587–597. https://doi.org/10.1523/JNEUROSCI.3766-10.2011

Medina, J. H. (2018a). Neural, Cellular and Molecular Mechanisms of Active Forgetting. *Frontiers in Systems Neuroscience*, *12*. https://doi.org/10.3389/fnsys.2018.00003

Medina, J. H. (2018b). Neural, Cellular and Molecular Mechanisms of Active Forgetting. *Frontiers in Systems Neuroscience*, *12*. https://doi.org/10.3389/fnsys.2018.00003

Medina, J. H., Bargas, J., Mishra, V., Bhimrao, B., University, A., & Meneses, I. A. (2018). Neural, Cellular and Molecular Mechanisms of Active Forgetting. https://doi.org/10.3389/fnsys.2018.00003

Meshalkina, D. A., Kizlyk, M. N., Kysil, E. V., Collier, A. D., Echevarria, D. J., Abreu, M. S., … Kalueff, A. V. (2017). Understanding zebrafish cognition. *Behavioural Processes*. https://doi.org/10.1016/j.beproc.2016.11.020

Messina, A., Potrich, D., Schiona, I., Sovrano, V. A., Fraser, S. E., Brennan, C. H., & Vallortigara, G. (2020). Response to change in the number of visual stimuli in zebrafish:A behavioural and molecular study. *Scientific Reports*, *10*(1), 1–11. https://doi.org/10.1038/s41598-020-62608-5

Migues, P. V., Liu, L., Archbold, G. E. B., Einarsson, E. O., Wong, J., Bonasia, K., … Hardt, O. (2016). Blocking Synaptic Removal of GluA2-Containing AMPA Receptors Prevents the Natural Forgetting of Long-Term Memories. *Journal of Neuroscience*, *36*(12), 3481–3494. https://doi.org/10.1523/JNEUROSCI.3333-15.2016

Miklósi, A., Andrew, R. J., & Savage, H. (1997). Behavioural lateralisation of the tetrapod type in the zebrafish (Brachydanio rerio). *Physiology and Behavior*, *63*(1), 127–135. https://doi.org/10.1016/S0031-9384(97)00418-6

Minatohara, K., Akiyoshi, M., & Okuno, H. (2016a). Role of Immediate-Early Genes in

Synaptic Plasticity and Neuronal Ensembles Underlying the Memory Trace. *Frontiers in Molecular Neuroscience*, *8*. https://doi.org/10.3389/fnmol.2015.00078

Minatohara, K., Akiyoshi, M., & Okuno, H. (2016b). Role of Immediate-Early Genes in Synaptic Plasticity and Neuronal Ensembles Underlying the Memory Trace. *Frontiers in Molecular Neuroscience*, *8*(January), 1–11. https://doi.org/10.3389/fnmol.2015.00078

Miranda, M., Morici, J. F., Zanoni, M. B., & Bekinschtein, P. (2019). Brain-Derived Neurotrophic Factor: A Key Molecule for Memory in the Healthy and the Pathological Brain. *Frontiers in Cellular Neuroscience*, *13*(August), 1–25. https://doi.org/10.3389/fncel.2019.00363

Mittmann, W., Wallace, D. J., Czubayko, U., Herb, J. T., Schaefer, A. T., Looger, L. L., … Kerr, J. N. D. (2011a). Two-photon calcium imaging of evoked activity from L5 somatosensory neurons in vivo. *Nature Neuroscience*, *14*(8), 1089–1093. https://doi.org/10.1038/nn.2879

Mittmann, W., Wallace, D. J., Czubayko, U., Herb, J. T., Schaefer, A. T., Looger, L. L., … Kerr, J. N. D. (2011b). Two-photon calcium imaging of evoked activity from L5 somatosensory neurons in vivo. *Nature Neuroscience*, *14*(8), 1089–1093. https://doi.org/10.1038/nn.2879

Montague, P. R., & Sejnowski, T. J. (1982). *Regulation of Synaptic Efficacy by Coincidence of Postsynaptic APs and EPSPs The increase in Downloaded from*. *J. Neurosci. Methods* (Vol. 298). Retrieved from http://science.sciencemag.org/

Moore, S. J., Deshpande, K., Stinnett, G. S., Seasholtz, A. F., & Murphy, G. G. (2014). Object Recognition Paradigm, 174–185. https://doi.org/10.1016/j.nlm.2013.06.014.Conversion

Morris, R. G. M. (1999). D.O. Hebb: The Organization of Behavior, Wiley: New York; 1949. *Brain Research Bulletin*, *50*(5), 437. https://doi.org/https://doi.org/10.1016/S0361-9230(99)00182-3

Nagarajan, B., Harder, A., Japp, A., Häberlein, F., Mingardo, E., Kleinert, H., … Odermatt, B. (2020). CNS myelin protein 36K regulates oligodendrocyte differentiation through Notch. *Glia*, *68*(3), 509–527. https://doi.org/10.1002/glia.23732

Nakai, J., Ohkura, M., & Imoto, K. (2001). A high signal-to-noise ca2+ probe composed of a single green fluorescent protein. *Nature Biotechnology*, *19*(2), 137–141. https://doi.org/10.1038/84397

Nakai, J., Ohkura, M., Imoto, K., Chatterjee, D., Tran, S., Shams, S., … Mourrain, P. (2017). Simulation of the capacity and precision of working memory in the hypodopaminergic state: RELEVANCE to schizophrenia. *Neuron*, *7*(1), 1–12. https://doi.org/10.1038/s41467-019-13484-9

Nelson, E. E., & Guyer, A. E. (2013). Spatial behavior and seizure-induced changes in c-fos mRNA expression in young and old rats. *NIH Public Access*, *1*(3), 233–245. https://doi.org/10.1016/j.dcn.2011.01.002.The

Nicolas, R., Meike, R., Junpeng, L., Françoise, C., Lisa, S., François-Xavier, B., … Roberto, C. (2016). Residual perception of biological motion in cortical blindness.

Neuropsychologia, *93*(November), 301–311. https://doi.org/10.1016/j.neuropsychologia.2016.11.009

Nicoll, R. A. (2017, January 18). A Brief History of Long-Term Potentiation. *Neuron*. Cell Press. https://doi.org/10.1016/j.neuron.2016.12.015

Niell, C. M., & Smith, S. J. (2005). Functional Imaging Reveals Rapid Development of Visual Response Properties in the Zebrafish Tectum. *Neuron*, *45*(6), 941–951. https://doi.org/10.1016/j.neuron.2005.01.047

Nikolaev, A., Leung, K. M., Odermatt, B., & Lagnado, L. (2013a). Synaptic mechanisms of adaptation and sensitization in the retina. *Nature Neuroscience*, *16*(7), 934–941. https://doi.org/10.1038/nn.3408

Nikolaev, A., Leung, K. M., Odermatt, B., & Lagnado, L. (2013b). Synaptic mechanisms of adaptation and sensitization in the retina. *Nature Neuroscience*, *16*(7), 934–941. https://doi.org/10.1038/nn.3408

Nikolaou, N., Lowe, A. S., Walker, A. S., Abbas, F., Hunter, P. R., Thompson, I. D., & Meyer, M. P. (2012). Parametric Functional Maps of Visual Inputs to the Tectum. *Neuron*, *76*(2), 317–324. https://doi.org/10.1016/j.neuron.2012.08.040

Niswender, C. M., & Conn, P. J. (2010). Metabotropic Glutamate Receptors: Physiology, Pharmacology, and Disease. *Annual Review of Pharmacology and Toxicology*, *50*(1), 295–322. https://doi.org/10.1146/annurev.pharmtox.011008.145533

Northmore, D. P. M. (2017). Holding visual attention for 400 million years: A model of tectum and torus longitudinalis in teleost fishes. *Vision Research*, *131*, 44–56. https://doi.org/10.1016/j.visres.2016.12.001

Odermatt, B., Nikolaev, A., & Lagnado, L. (2012). Encoding of Luminance and Contrast by Linear and Nonlinear Synapses in the Retina. *Neuron*, *73*(4), 758–773. https://doi.org/10.1016/j.neuron.2011.12.023

Ohki, K., Chung, S., Kara, P., Hübener, M., Bonhoeffer, T., & Reid, R. C. (2006). Highly ordered arrangement of single neurons in orientation pinwheels. *Nature*, *442*(7105), 925–928. https://doi.org/10.1038/nature05019

Okimura, T., Tanaka, S., Maeda, T., Kato, M., & Mimura, M. (2015). Simulation of the capacity and precision of working memory in the hypodopaminergic state: RELEVANCE to schizophrenia. *Neuroscience*, *295*, 80–89. https://doi.org/10.1016/j.neuroscience.2015.03.039

Oliveira, J., Silveira, M., Chacon, D., & Luchiari, A. (2015). The zebrafish world of colors and shapes: Preference and discrimination. *Zebrafish*, *12*(2). https://doi.org/10.1089/zeb.2014.1019

Panula, P., Chen, Y. C., Priyadarshini, M., Kudo, H., Semenova, S., Sundvik, M., & Sallinen, V. (2010, October). The comparative neuroanatomy and neurochemistry of zebrafish CNS systems of relevance to human neuropsychiatric diseases. *Neurobiology of Disease*. https://doi.org/10.1016/j.nbd.2010.05.010

Paoletti, I. (1963). DISCOVERY, ON THE STRUCTURE OF THE CEREBRAL CORTEX, OF FRANCESCO GENNARI (1752-1797), PARMA ANATOMIST: THE STRIAE OF GENNARI. *Minerva Medica*, *54*, 1574–1580. Retrieved from

http://www.ncbi.nlm.nih.gov/pubmed/14129879

Paquet, D., Bhat, R., Sydow, A., Mandelkow, E., Berg, S., Hellberg, S., … Haass, C. (2009). Technical advance A zebrafish model of tauopathy allows in vivo imaging of neuronal cell death and drug evaluation. *The Journal of Clinical Investigation*, *119*(5), 1382–1395. https://doi.org/10.1172/JCI37537DS1

Pellegrino, R., Sinding, C., de Wijk, R. A., & Hummel, T. (2017). Habituation and adaptation to odors in humans. *Physiology and Behavior*, *177*(August 2016), 13–19. https://doi.org/10.1016/j.physbeh.2017.04.006

Pita, D., Moore, B. A., Tyrrell, L. P., & Fernández-Juricic, E. (2015). Vision in two cyprinid fish: Implications for collective behavior. *PeerJ*, *2015*(8). https://doi.org/10.7717/peerj.1113

Poon, C. S., & Song, G. (2007). Habituation, desensitization and sensitization of the Hering-Breuer reflex in normal and Mecp2-/y knockout mice [1]. *Journal of Physiology*. https://doi.org/10.1113/jphysiol.2007.142711

Portugues, R., Severi, K. E., Wyart, C., & Ahrens, M. B. (2013, February). Optogenetics in a transparent animal: Circuit function in the larval zebrafish. *Current Opinion in Neurobiology*. https://doi.org/10.1016/j.conb.2012.11.001

Preuss, S. J., Trivedi, C. A., Vom Berg-Maurer, C. M., Ryu, S., & Bollmann, J. H. (2014a). Classification of object size in retinotectal microcircuits. *Current Biology*, *24*(20), 2376–2385. https://doi.org/10.1016/j.cub.2014.09.012

Preuss, S. J., Trivedi, C. A., Vom Berg-Maurer, C. M., Ryu, S., & Bollmann, J. H. (2014b). Classification of object size in retinotectal microcircuits. *Current Biology*, *24*(20), 2376–2385. https://doi.org/10.1016/j.cub.2014.09.012

Rab, A. S., Polino, E., Man, Z. X., Ba An, N., Xia, Y. J., Spagnolo, N., … Sciarrino, F. (2017). Entanglement of photons in their dual wave-particle nature. *Nature Communications*, *8*(1), 4–10. https://doi.org/10.1038/s41467-017-01058-6

Ramirez, S., Liu, X., Lin, P. A., Suh, J., Pignatelli, M., Redondo, R. L., … Tonegawa, S. (2013). Creating a false memory in the hippocampus. *Science*, *341*(6144), 387–391. https://doi.org/10.1126/science.1239073

Randlett, O., Haesemeyer, M., Forkin, G., Shoenhard, H., Schier, A. F., Engert, F., & Granato, M. (2019a). Distributed Plasticity Drives Visual Habituation Learning in Larval Zebrafish. *Current Biology*, *29*(8), 1337-1345.e4. https://doi.org/10.1016/j.cub.2019.02.039

Randlett, O., Haesemeyer, M., Forkin, G., Shoenhard, H., Schier, A. F., Engert, F., & Granato, M. (2019b). Distributed Plasticity Drives Visual Habituation Learning in Larval Zebrafish. *Current Biology*, *29*(8), 1337-1345.e4. https://doi.org/10.1016/j.cub.2019.02.039

Rankin, C. H., Abrams, T., Barry, R. J., Bhatnagar, S., Clayton, D., Colombo, J., … Thompson, R. F. (2010). Habituation Revisited: An Updated and Revised Description of the Behavioral Characteristics of Habituation. *NIH Public Access*, *92*(2), 135–138. https://doi.org/10.1016/j.nlm.2008.09.012.Habituation

Rathje, M., Fang, H., Bachman, J. L., Anggono, V., Gether, U., Huganir, R. L., & Madsen, K. L.

(2013). AMPA receptor pHluorin-GluA2 reports NMDA receptor-induced intracellular acidification in hippocampal neurons. *Proceedings of the National Academy of Sciences*, *110*(35), 14426–14431. https://doi.org/10.1073/pnas.1312982110

Regehr, W. G., & Abbott, L. F. (2004). Synaptic computation. *Nature*, *431*(October), 796–803.

Repina, N. A., Rosenbloom, A., Mukherjee, A., Schaffer, D. V, & Kane, R. S. (2017). At Light Speed: Advances in Optogenetic Systems for Regulating Cell Signaling and Behavior. https://doi.org/10.1146/annurev-chembioeng

Richardson, R., Tracey-White, D., Webster, A., & Moosajee, M. (2017). The zebrafish eye-a paradigm for investigating human ocular genetics. *Eye (Basingstoke)*, *31*(1), 68–86. https://doi.org/10.1038/eye.2016.198

Rinner, O., Rick, J. M., & Neuhauss, S. C. F. (2005). Contrast sensitivity, spatial and temporal tuning of the larval zebrafish optokinetic response. *Investigative Ophthalmology and Visual Science*, *46*(1), 137–142. https://doi.org/10.1167/iovs.04-0682

Risner, M. L., Lemerise, E., Vukmanic, E. V., & Moore, A. (2006). Behavioral spectral sensitivity of the zebrafish (Danio rerio). *Vision Research*, *46*(17), 2625–2635. https://doi.org/10.1016/j.visres.2005.12.014

Rizzo, M. (2013). Measuring contrast sensitivity. *Annals of Neurology*, *20*(3), 374–374. https://doi.org/10.1002/ana.410200322

Roberts, A. C., Bill, B. R., & Glanzman, D. L. (2013). Learning and memory in zebrafish larvae. *Frontiers in Neural Circuits*, *7*. https://doi.org/10.3389/fncir.2013.00126

Robles, E., Fields, N. P., & Baier, H. (2020). The zebrafish visual system transmits dimming information via multiple segregated pathways. *Journal of Comparative Neurology*, *529*(3), 539–552. https://doi.org/10.1002/cne.24964

Robles, E., Filosa, A., & Baier, H. (2013). Precise lamination of retinal axons generates multiple parallel input pathways in the tectum. *Journal of Neuroscience*, *33*(11), 5027–5039. https://doi.org/10.1523/JNEUROSCI.4990-12.2013

Robles, E., Laurell, E., & Baier, H. (2014a). The retinal projectome reveals brain-area-specific visual representations generated by ganglion cell diversity. *Current Biology*, *24*(18), 2085–2096. https://doi.org/10.1016/j.cub.2014.07.080

Robles, E., Laurell, E., & Baier, H. (2014b). The Retinal Projectome Reveals Brain-Area-Specific Visual Representations Generated by Ganglion Cell Diversity. *Current Biology*, *24*, 2085–2096. https://doi.org/10.1016/j.cub.2014.07.080

Ruhl, T., Zeymer, M., & von der Emde, G. (2017). Cannabinoid modulation of zebrafish fear learning and its functional analysis investigated by c-Fos expression. *Pharmacology Biochemistry and Behavior*, *153*, 18–31. https://doi.org/10.1016/j.pbb.2016.12.005

Sadamitsu, K., Shigemitsu, L., Suzuki, M., Ito, D., Kashima, M., & Hirata, H. (2021). Characterization of zebrafish GABAA receptor subunits. *Scientific Reports*, *11*(1), 1–11. https://doi.org/10.1038/s41598-021-84646-3

Sajovic, P., & Levinthal, C. (1982). Visual cells of zebrafish optic tectum: Mapping with small spots. *Neuroscience*, *7*(10), 2407–2426. https://doi.org/10.1016/0306-4522(82)90204-4

Sanes, J. R., & Zipursky, S. L. (2010a). Design Principles of Insect and Vertebrate Visual Systems. *Neuron*, *66*(1), 15–36. https://doi.org/10.1016/j.neuron.2010.01.018

Sanes, J. R., & Zipursky, S. L. (2010b). Design Principles of Insect and Vertebrate Visual Systems. *Neuron*, *66*(1), 15–36. https://doi.org/10.1016/j.neuron.2010.01.018

Sannita, W. G., Narici, L., & Picozza, P. (2006). Positive visual phenomena in space: A scientific case and a safety issue in space travel. *Vision Research*, *46*(14), 2159–2165. https://doi.org/10.1016/j.visres.2005.12.002

Santon, M., Münch, T. A., & Michiels, N. K. (2019). The contrast sensitivity function of a small cryptobenthic marine fish. *Journal of Vision*, *19*(2), 1–10. https://doi.org/10.1167/19.2.1

Schall, J. D., Ault, S. J., Vitek, D. J., & Leventhal, A. G. (1988). Experimental induction of an abnormal ipsilateral visual field representation in the geniculocortical pathway of normally pigmented cats. *Journal of Neuroscience*, *8*(6), 2039–2048. https://doi.org/10.1523/jneurosci.08-06-02039.1988

Schmitt, E. A., & Dowling, J. E. (1999). Early retinal development in the zebrafish, Danio rerio: light and electron microscopic analyses. *The Journal of Comparative Neurology*, *404*(4), 515–536. Retrieved from http://www.ncbi.nlm.nih.gov/pubmed/9987995

Schröder, C., Oesterle, J., Berens, P., & Yoshimatsu, T. (n.d.). Distinct Synaptic Transfer Functions in Same-Type Photoreceptors 1 2. https://doi.org/10.1101/2021.02.24.432674

Schröder, C., Oesterle, J., Berens, P., & Yoshimatsu, T. (2021). Distinct Synaptic Transfer Functions in Same-Type Photoreceptors 1 2. *BioRxiv*, 28. https://doi.org/10.1101/2021.02.24.432674

Schröder, C., Oesterle, J., Berens, P., Yoshimatsu, T., & Baden, T. (2021). Eye-Region Specific Ribbon Tuning Supports Distinct Modes of Synaptic Transmission in Same-Type Cone-Photoreceptors. *BioRxiv*, 2021.02.24.432674.

Schroeder, C., Oesterle, J., Berens, P., Yoshimatsu, T., & Baden, T. (2021). Distinct Synaptic Transfer Functions in Same-Type Photoreceptors. *ELife*, *10*, 28. https://doi.org/10.7554/eLife.67851

Sgritta, M., Locatelli, F., Soda, T., Prestori, F., & D'Angelo, E. U. (2017). Hebbian Spike-Timing Dependent Plasticity at the Cerebellar Input Stage. *The Journal of Neuroscience*, *37*(11), 2809–2823. https://doi.org/10.1523/JNEUROSCI.2079-16.2016

Sherman, S. M., & Koch, C. (1986). The control of retinogeniculate transmission in the mammalian lateral geniculate nucleus. *Experimental Brain Research*, *63*(1). https://doi.org/10.1007/BF00235642

Sherrington, C. S. (1906). Observations on the scratch-reflex in the spinal dog. *The Journal of Physiology*, *34*(1–2), 1–50.

https://doi.org/10.1113/jphysiol.1906.sp001139

Siniaia, M. S., Young, D. L., & Poon, C. S. (2000). Habituation and desensitization of the Hering-Breuer reflex in rat. *Journal of Physiology*, *523*(2), 479–491. https://doi.org/10.1111/j.1469-7793.2000.t01-1-00479.x

Sliney, D. H. (2016). What is light? the visible spectrum and beyond. *Eye (Basingstoke)*, *30*(2), 222–229. https://doi.org/10.1038/eye.2015.252

Sokolov, E N, VIinogradova, O. S. (1955). Extinction of vascular component of orientation reaction. *Zhurnal Vysshei Nervnoi Deiatelnosti Imeni I P Pavlova*, *5*(3), 344–350. Retrieved from http://www.ncbi.nlm.nih.gov/pubmed/13257872

Solomon, S. G., & Kohn, A. (2014). Moving Sensory Adaptation beyond Suppressive Effects in Single Neurons. *Current Biology*, *24*(20), R1012–R1022. https://doi.org/10.1016/j.cub.2014.09.001

Sovrano, V. A., & Andrew, R. J. (2006). Eye use during viewing a reflection: Behavioural lateralisation in zebrafish larvae. *Behavioural Brain Research*, *167*(2), 226–231. https://doi.org/10.1016/j.bbr.2005.09.021

Staubli, U., & Scafidi, J. (1997). Studies on long-term depression in area CA1 of the anesthetized and freely moving rat. *The Journal of Neuroscience : The Official Journal of the Society for Neuroscience*, *17*(12), 4820–4828. Retrieved from http://www.ncbi.nlm.nih.gov/pubmed/9169540

Sundquist, S. J., & Nisenbaum, L. K. (2005). Fast Fos: Rapid protocols for single- and double-labeling c-Fos immunohistochemistry in fresh frozen brain sections. *Journal of Neuroscience Methods*, *141*(1), 9–20. https://doi.org/10.1016/j.jneumeth.2004.05.007

Sundquist, S. J., Nisenbaum, L. K., & Sarah J. Sundquist, L. K. N. (2005). Fast Fos: Rapid protocols for single- and double-labeling c-Fos immunohistochemistry in fresh frozen brain sections. *Journal of Neuroscience Methods*, *141*(1), 9–20. https://doi.org/10.1016/j.jneumeth.2004.05.007

Tappeiner et al. (2012). Visual Acuity and Contrast Sensitivity of Adult zebrafish. In *Frontiers in Zoology* (Vol. 1, pp. 300–306). Elsevier. https://doi.org/10.1016/B978-1-4557-0737-9.00011-4

Thevenaz, P., Ruttimann, U. E., & Unser, M. (1998). A pyramid approach to subpixel registration based on intensity. *IEEE Transactions on Image Processing*, *7*(1), 27–41. https://doi.org/10.1109/83.650848

Thisse, C., & Thisse, B. (2008a). High-resolution in situ hybridization to whole-mount zebrafish embryos. *Nature Protocols*, *3*(1), 59–69. https://doi.org/10.1038/nprot.2007.514

Thisse, C., & Thisse, B. (2008b). High-resolution in situ hybridization to whole-mount zebrafish embryos. *Nature Protocols*, *3*(1), 59–69. https://doi.org/10.1038/nprot.2007.514

Thompson, R. (2001). Habituation. In *International Encyclopedia of the Social & Behavioral Sciences* (pp. 6458–6462). Elsevier. https://doi.org/10.1016/B0-08-043076-7/03639-1

Thompson, R. F., & Spencer, W. A. (1966). Habituation: A model phenomenon for the study of neuronal substrates of behavior. *Psychological Review*, *73*(1), 16–43. https://doi.org/10.1037/h0022681

Tien, N. W., Pearson, J. T., Heller, C. R., Demas, J., & Kerschensteiner, D. (2015). Genetically identified suppressed-by-contrast retinal ganglion cells reliably signal self-generated visual stimuli. *Journal of Neuroscience*, *35*(30), 10815–10820. https://doi.org/10.1523/JNEUROSCI.1521-15.2015

Trampel, R., Ott, D. V. M., & Turner, R. (2011). Do the congenitally blind have a stria of gennari? first intracortical insights in vivo. *Cerebral Cortex*, *21*(9), 2075–2081. https://doi.org/10.1093/cercor/bhq282

Trenholm, S., & Krishnaswamy, A. (2020). An annotated journey through modern visual neuroscience. *Journal of Neuroscience*, *40*(1), 44–53. https://doi.org/10.1523/JNEUROSCI.1061-19.2019

Turatto, M., Bonetti, F., & Pascucci, D. (2018). Filtering visual onsets via habituation: A context-specific long-term memory of irrelevant stimuli. *Psychonomic Bulletin and Review*, *25*(3), 1028–1034. https://doi.org/10.3758/s13423-017-1320-x

Ueda, K., Sekoguchi, T., & Yanagisawa, H. (2021). How predictability affects habituation to novelty. *PLoS ONE*, *16*(6 June), 1–15. https://doi.org/10.1371/journal.pone.0237278

Vigouroux, R. J., Duroure, K., Vougny, J., Albadri, S., Kozulin, P., Herrera, E., … Chédotal, A. (2021). Bilateral visual projections exist in non-teleost bony fish and predate the emergence of tetrapods. *Science*, *372*(6538), 150–156. https://doi.org/10.1126/science.abe7790

Wager, M. G. T. and J. F. S. (2011). The Visual System of Zebrafish and its Use to Model Human Ocular Diseases Gaia. *NIH Public Access*, *23*(1), 1–7. https://doi.org/10.1002/dneu.20919.The

Waldman, B. (1982). Quantitative and Developmental Analyses of the Alarm Reaction in the Zebra Danio, Brachydanio rerio. *Nature*, *139*(3528), 1014–1014. https://doi.org/10.1038/1391014a0

Walker, A. S., Burrone, J., & Meyer, M. P. (2013a). Functional imaging in the zebrafish retinotectal system using RGECO. *Frontiers in Neural Circuits*, *7*. https://doi.org/10.3389/fncir.2013.00034

Walker, A. S., Burrone, J., & Meyer, M. P. (2013b). Functional imaging in the zebrafish retinotectal system using RGECO. *Frontiers in Neural Circuits*, *7*(March), 1–10. https://doi.org/10.3389/fncir.2013.00034

Walston, S. T., Chow, R. H., & Weiland, J. D. (2018). Direct measurement of bipolar cell responses to electrical stimulation in wholemount mouse retina. *Journal of Neural Engineering*, *15*(4). https://doi.org/10.1088/1741-2552/aab4ed

Wan, J., & Goldman, D. (2016). Retina regeneration in zebrafish. https://doi.org/10.1016/j.gde.2016.05.009

Wang, K., Hinz, J., Haikala, V., Reiff, D. F., & Arrenberg, A. B. (2019). Selective processing of all rotational and translational optic flow directions in the zebrafish pretectum

and tectum. *BMC Biology*, *17*(1), 1–18. https://doi.org/10.1186/s12915-019-0648-2

Wark, B., Lundstrom, B. N., & Fairhall, A. (2007). Sensory adaptation. *Current Opinion in Neurobiology*, *17*(4), 423–429. https://doi.org/10.1016/j.conb.2007.07.001

Webster, M. A. (1996). Human colour perception and its adaptation. *Network: Computation in Neural Systems*, *7*(4), 587–634. https://doi.org/10.1088/0954-898X_7_4_002

Westergard, L., Christensen, H. M., & Harris, D. A. (2007). The cellular prion protein (PrPC): Its physiological function and role in disease. *Biochimica et Biophysica Acta - Molecular Basis of Disease*, *1772*(6), 629–644. https://doi.org/10.1016/j.bbadis.2007.02.011

Wiedenmann, B., & Franke, W. W. (1985). Identification and localization of synaptophysin, an integral membrane glycoprotein of Mr 38,000 characteristic of presynaptic vesicles. *Cell*, *41*(3), 1017–1028.

Wright, A., & Vissel, B. (2012). The essential role of AMPA receptor GluR2 subunit RNA editing in the normal and diseased brain. *Frontiers in Molecular Neuroscience*, *5*. https://doi.org/10.3389/fnmol.2012.00034

Wu, W., Luo, B., & Xiao, Z. (2018). An optimized protocol for whole mount in situ hybridization of mouse brain. *Int J Clin Exp*, *11*(3), 2313–2318.

Xi, Y., Noble, S., & Ekker, M. (2011). Modeling neurodegeneration in zebrafish. *Current Neurology and Neuroscience Reports*, *11*(3), 274–282. https://doi.org/10.1007/s11910-011-0182-2

Xiao, T., & Baier, H. (2007). Lamina-specific axonal projections in the zebrafish tectum require the type IV collagen Dragnet. *Nature Neuroscience*, *10*(12), 1529–1537. https://doi.org/10.1038/nn2002

Xie, J., Jusuf, P. R., Bui, B. V., & Goodbourn, P. T. (2019). Experience-dependent development of visual sensitivity in larval zebrafish. *Scientific Reports*, *9*(1), 1–11. https://doi.org/10.1038/s41598-019-54958-6

Ye, L., Haroon, M. A., Salinas, A., & Paukert, M. (2017). Comparison of GCaMP3 and GCaMP6f for studying astrocyte Ca2+ dynamics in the awake mouse brain. *PLoS ONE*, *12*(7), 1–17. https://doi.org/10.1371/journal.pone.0181113

Yin, C., Li, X., & Du, J. (2019a). Optic tectal superficial interneurons detect motion in larval zebrafish. *Protein and Cell*, *10*(4), 238–248. https://doi.org/10.1007/s13238-018-0587-7

Yin, C., Li, X., & Du, J. (2019b). Optic tectal superficial interneurons detect motion in larval zebrafish. *Protein and Cell*, *10*(4), 238–248. https://doi.org/10.1007/s13238-018-0587-7

Zahl, I. H., Samuelsen, O., & Kiessling, A. (2012). Anaesthesia of farmed fish: Implications for welfare. *Fish Physiology and Biochemistry*, *38*(1), 201–218. https://doi.org/10.1007/s10695-011-9565-1

Zariwala, H. A., Madisen, L., Ahrens, K. F., Bernard, A., Lein, E. S., Jones, A. R., & Zeng, H.

(2011). Visual tuning properties of genetically identified layer 2/3 neuronal types in the primary visual cortex of Cre-transgenic mice. *Frontiers in Systems Neuroscience*, *4*(JANUARY 2011), 1–16. https://doi.org/10.3389/fnsys.2010.00162

Zhang, C., Kolodkin, A. L., Wong, R. O., & James, R. E. (2017a). Establishing Wiring Specificity in Visual System Circuits: From the Retina to the Brain. *Annual Review of Neuroscience*, *40*(1), 395–424. https://doi.org/10.1146/annurev-neuro-072116-031607

Zhang, C., Kolodkin, A. L., Wong, R. O., & James, R. E. (2017b). Establishing Wiring Specificity in Visual System Circuits: From the Retina to the Brain. *Annual Review of Neuroscience*, *40*(1), 395–424. https://doi.org/10.1146/annurev-neuro-072116-031607

Zhang, R. W., Li, X. Q., Kawakami, K., & Du, J. L. (2016). Stereotyped initiation of retinal waves by bipolar cells via presynaptic NMDA autoreceptors. *Nature Communications*, *7*, 1–12. https://doi.org/10.1038/ncomms12650

Zhou, M., Bear, J., Roberts, P., Janiak, F., Semmelhack, J., Yoshimatsu, T., & Baden, T. (2020). What the Zebrafish's Eye Tells the Zebrafish's Brain: Retinal Ganglion Cells for Prey Capture and Colour Vision. *SSRN Electronic Journal*, 1–38. https://doi.org/10.2139/ssrn.3535700

Zhu, S., & Gouaux, E. (2017a). Structure and symmetry inform gating principles of ionotropic glutamate receptors. *Neuropharmacology*, *112*, 11–15. https://doi.org/10.1016/j.neuropharm.2016.08.034

Zhu, S., & Gouaux, E. (2017b, January 1). Structure and symmetry inform gating principles of ionotropic glutamate receptors. *Neuropharmacology*. Elsevier Ltd. https://doi.org/10.1016/j.neuropharm.2016.08.034

Zhu, S., Stein, R. A., Yoshioka, C., Lee, C. H., Goehring, A., McHaourab, H. S., & Gouaux, E. (2016). Mechanism of NMDA Receptor Inhibition and Activation. *Cell*, *165*(3), 704–714. https://doi.org/10.1016/j.cell.2016.03.028

Zhuo, M. (2016, December 3). Contribution of synaptic plasticity in the insular cortex to chronic pain. *Neuroscience*. Elsevier Ltd. https://doi.org/10.1016/j.neuroscience.2016.08.014

Zimmermann, M. J. Y., Nevala, N. E., Yoshimatsu, T., Osorio, D., Nilsson, D. E., Berens, P., & Baden, T. (2018). Zebrafish Differentially Process Color across Visual Space to Match Natural Scenes. *Current Biology*, *28*(13), 2018-2032.e5. https://doi.org/10.1016/j.cub.2018.04.075

Zylberberg, J., & Strowbridge, B. W. (2017). Mechanisms of Persistent Activity in Cortical Circuits: Possible Neural Substrates for Working Memory. *Annual Review of Neuroscience*, *40*(1), 603–627. https://doi.org/10.1146/annurev-neuro-070815-014006